AD A995072

WT-371 (EX)

EXTRACTED VERSION

OPERATION JANGLE

Particle Studies

Armed Forces Special Weapons Project
Washington, D.C.

July 1952

Nevada Proving Grounds
October—November 1951

NOTICE

This is an extract of Wt-371, Operation JANGLE, Particle Studies, which remains classified Secret/Restricted Data as of this date.

DTIC
ELECTE
S JAN8 1981 D
D

Extract version prepared for:
Director
DEFENSE NUCLEAR AGENCY
Washington, D.C. 20305

1 October 1979

Approved for public release; distribution unlimited.

80 10 3 037

DDC FILE COPY

DISCLAIMER NOTICE

THIS DOCUMENT IS BEST QUALITY PRACTICABLE. THE COPY FURNISHED TO DTIC CONTAINED A SIGNIFICANT NUMBER OF PAGES WHICH DO NOT REPRODUCE LEGIBLY.

PAGES _____

ARE

MISSING

IN

ORIGINAL

DOCUMENT

(18) DOE

Unclassified

SECURITY CLASSIFICATION OF THIS PAGE (When Data Entered)

REPORT DOCUMENTATION PAGE	READ INSTRUCTIONS BEFORE COMPLETING FORM
1. REPORT NUMBER (19) WT-371 (EX)	2. GOVT ACCESSION NO. AD-A995072
3. RECIPIENT'S CATALOG NUMBER	
4. TITLE (and Subtitle) (4) Operation JANGLE • Particle Studies • Projects 2.5a-1, 2.5a-2, 2.5a-3, 2.8	5. TYPE OF REPORT & PERIOD COVERED
	6. PERFORMING ORG. REPORT NUMBER WT-371 (EX)
7. AUTHOR(S) (10) Charles Robbines ~~et al~~ Hugh R. Lenman David R. Powers ↓ James I. Wilcox I. G. Poppoff	8. CONTRACT OR GRANT NUMBER(s) (15) DNA001-79-C-0455
9. PERFORMING ORGANIZATION NAME AND ADDRESS Armed Forces Special Weapons Project Washington, D. C.	10. PROGRAM ELEMENT, PROJECT, TASK AREA & WORK UNIT NUMBERS (12) 1383
11. CONTROLLING OFFICE NAME AND ADDRESS (11) 1 Oct 79	12. REPORT DATE July 1952
	13. NUMBER OF PAGES 417
14. MONITORING AGENCY NAME & ADDRESS (if different from Controlling Office)	15. SECURITY CLASS. (of this report) Unclassified
	15a. DECLASSIFICATION/DOWNGRADING SCHEDULE

16. DISTRIBUTION STATEMENT (of this Report)

Approved for public release; unlimited distribution.

17. DISTRIBUTION STATEMENT (of the abstract entered in Block 20, if different from Report)

18. SUPPLEMENTARY NOTES

This report has had the classified information removed and has been republished in unclassified form for public release. This work was performed by the General Electric Company-TEMPO under contract DNA001-79-C-0455 with the close cooperation of the Classification Management Division of the Defense Nuclear Agency.

19. KEY WORDS (Continue on reverse side if necessary and identify by block number)

JANGLE
Desert Rock
Nuclear Atmospheric Test
Radioactivity Measurements
Airborne Particles
Fallout Analyses
Aerosol Sampling
Fallout Distribution
Radiochemical Studies
Radioactivity Affects on Soil

20. ABSTRACT (Continue on reverse side if necessary and identify by block number)

The object of this study was to obtain data relative to the close-in ground level airborne and fallout hazard associated with each detonation in Operation JANGLE. For this purpose samples of the aerosol and fallout were obtained from 46 stations located between 4000 feet upwind and 50,000 feet downwind. The airborne particle studies reported herein were undertaken by the Chemical Corps to answer questions which were raised regarding the internal hazard due to the radioactive particulate matter associated with the cloud and base surge produced by a surface and underground detonation of an atomic weapon. It is believed that the data developed from this study will assist in

DD FORM 1 JAN 73 1473 EDITION OF 1 NOV 65 IS OBSOLETE

Unclassified

SECURITY CLASSIFICATION OF THIS PAGE (When Data Entered)

Abstract (Continued)

evaluating the relative importance of the internal hazard which can result from such a detonation.

This is a consolidation of material in WT-394, Airborne Particle Studies; WT-395, Fallout Particle Studies; WT-333, Radiochemical Studies of Large Particles; WT-335, Analysis of Test Site and Fallout Material.

Accession For
NTIS GRA&I X
DTIC TAB ☐
Unannounced ☐
Justification
By
Distribution/
Availability Codes
Dist | Avail and/or Special
A | 23

Released

DTIC
ELECTE
JAN8 1981
S D
D

UNANNOUNCED

FOREWORD

This report has had classified material removed in order to make the information available on an unclassified, open publication basis, to any interested parties. This effort to declassify this report has been accomplished specifically to support the Department of Defense Nuclear Test Personnel Review (NTPR) Program. The objective is to facilitate studies of the low levels of radiation received by some individuals during the atmospheric nuclear test program by making as much information as possible available to all interested parties.

The material which has been deleted is all currently classified as Restricted Data or Formerly Restricted Data under the provision of the Atomic Energy Act of 1954, (as amended) or is National Security Information.

This report has been reproduced directly from available copies of the original material. The locations from which material has been deleted is generally obvious by the spacings and "holes" in the text. Thus the context of the material deleted identified to assist the reader in the determination of whether the deleted information is germane to his study.

It is the belief of the individuals who have participated in preparing this report by deleting the classified material and of the Defense Nuclear Agency that the report accurately portrays the contents of the original and that the deleted material is of little or no significance to studies into the amounts or types of radiation received by any individuals during the atmospheric nuclear test program.

WT-394

OPERATION JANGLE

Project 2.5a-1

AIRBORNE PARTICLE STUDIES

by

Lt. Col. Charles Robbins
Chemical Corps

Major Hugh R. Lehman
U. S. Air Force

David R. Powers
Chemical Corps

James D. Wilcox
Chemical Corps

July 1952

CHEMICAL AND RADIOLOGICAL LABORATORIES
Army Chemical Center, Maryland

PROJECT 2.5a-1

ABSTRACT

The object of this study was to obtain data relative to the close-in ground level airborne and fall-out hazard associated with each detonation in Operation JANGLE. For this purpose samples of the aerosol and fall-cut were obtained from 46 stations located between 4000 feet upwind and 50,000 feet downwind. Several types of instruments were used in this study; filter samplers, cascade impactors, conifuges, particle separators, electrostatic precipitators, Brookhaven continuous air monitors, Tracerlab continuous air monitors and fall-out trays.

The concentration of beta activity in the cloud near ground zero a few minutes after the shot was found to be approximately 10^{-3} and 10^{-1} microcuries per cubic centimeter for the surface and underground shots respectively. The number median diameters of the particles in the surface and underground shots were 1.0 and 1.5 microns respectively at stations 4000 ft. downwind, decreasing in both cases to less than 0.1 microns at 50,000 ft. Data were also obtained on the variation of activity with particle size, as well as the percentage of the number of particles which were radioactive for both the aerosol and the fall-out. In addition, a study of fractionation and its manifestations was made.

PROJECT 2.5a-1

PREFACE

The airborne particle studies reported herein were undertaken by the Chemical Corps to answer questions which were raised regarding the internal hazard due to the radioactive particulate matter associated with the cloud and base surge produced by a surface and underground detonation of an atomic weapon. It is believed that the data developed from this study will assist in evaluating the relative importance of the internal hazard which can result from such a detonation.

ACKNOWLEDGMENT

The authors wish to make the following acknowledgments:

Lt Cdr Walter F. V. Bennett, USN, who made valuable contributions in planning for this test and in reducing the data obtained from the samples. In the early stage of preparation of this report, Lt Cdr Bennett was transferred to sea duty and his services were lost to our organization.

Mr. Curt L. Zitza, of CRL Engineering Division, for the design of equipment.

Mr. Robert C. Tompkins, of CRL Radiological Division, for the radiochemical analysis of samples and results on isotopic content.

Miss Phyllis Beamer for activity measurements.

Mr. Walter R. Van Antwerp, of CRL Test Division, for the sampling, analysis, and results of the cascade impactor.

CONTENTS

PROJECT 2.5a-1

ILLUSTRATIONS

PROJECT 2.5a-1

TABLES

CHAPTER 1

INTRODUCTION

1.1 OBJECTIVE

The primary objective of Project 2.5a was to conduct a study of the airborne particulate matter resulting from a surface and underground detonation of a nuclear weapon and to determine the following:

1. Concentration of radioactivity in the aerosol and its variation with distance from ground zero.

2. Variation of radioactivity with particle-size.

3. The variation of the particle-size distribution with distance from the point of detonation.

4. Total particles which are radioactive as a function of particle size.

Secondary objectives of this project were to study similar factors for the fall-out (factors which are inseparable from the aerosol) and the phenomenon of fractionation [1] for both.

An indirect objective of the project was to evaluate the field performance of the several instruments employed.

1.2 HISTORICAL

Chemical Corps results from SANDSTONE[2] derived from the cascade impactor indicated a predominance of particulate matter in the range of 0.1 to 0.4 micron diameter, with some material in the range 1 to 10 microns. The long sampling period and the large integrated sample collected left doubt as to the accuracy of the particle size measurements

---

1 These and certain other terms used in this report are defined in Appendix A.

2 Bernard Siegel, Cdr H. L. Andrews, USPHS, and Raymond E. Murphy, Particle Size of Material in Cloud, Operation SANDSTONE, Task Group 7.6, Project Report, Project 7.1-17/RS(CC)-9, 30 June 1948.

of the active particulates. Tracerlab results from SANDSTONE [3], derived from filters, indicated that in the frequency vs. particle size graph the mode occurred between 4 and 6 microns for particles in the range of 2 to 10 mocron diameter. The limit of resolution of the technique was approximately 1 micron, thus no observations were made on particles less than one micron diameter.

Chemical Corps results from Operation GREENHOUSE [4] derived from the cascade impactor indicated that cloud samples taken at 16,000-25,000 feet had a median size of approximately 0.3 micron. The results from the U. S. Naval Radiological Defense Laboratory derived from the electrostatic precipitator on this same Operation indicated a median particle size of 0.15 microns.

In June, 1950, the Joint Chiefs of Staff directed the test of an underground and surface nuclear detonation. The Armed Forces Special Weapons Project requested the Chemical Corps to submit proposals for participation in the test. As a result, Project 2.5a was developed to conduct airborne particle studies on the aerosol resulting from these bursts. Because of the large amount of ground contamination expected, these tests provided an opportunity to determine whether there is a correlation between particle size, isotopic content and decay rate, and to evaluate the internal hazard associated with these types of detonations.

1.3 AEROSOL SAMPLING

It may be safely said that the sampling of particulate aerosols is a field characterized by instrument design difficulties. And this is particularly true of sampling aerosols containing large particles; a condition which is produced by the detonation of atomic weapons near to or under the surface of the ground.

The difficulties, roughly, are two-fold. First, is the problem of introducing the particles into the sampling apparatus without prejudice with respect to particle size. This is the problem of obtaining isokinetic flow into the sampler. The second problem is to remove the particles from the air, again, without selecting for or against different sized particles. This problem is usually aggravated by the desire to remove the particles in such a manner that they may subsequently be subjected to size measurements or other types of analysis.

---

3 Report on Analysis Results and Conclusions Relating to Test Joe, December 1950, Department of the Air Force Contracts with Tracerlab, Inc., 130 High St., Boston, Mass.

4 GREENHOUSE 6.1 Report. Unpublished.

At the time of planning of this project there were a number of sampling instruments in existence, none of which satisfied the first criteria, but which partially satisfied the second criteria in a number of ways which were suitable to the types of measurements desired. For example, a filter sampler, in common use in the Chemical Corps, would collect all particle sizes to be encountered with better than 99.9 per cent efficiency, and would be excellent for the measurements necessary to determine activity concentration data.

Due to the cost and lack of time adjudged to be necessary to redesign all desired instruments for isokinetic flow, it was deemed necessary either to reduce the number and type of sampling instruments, or to use all instruments as they were, even though sampling was not isokinetic. A decision in favor of the latter course was made at an early stage of planning. The crux of this matter was the extent to which non-isokinetic sampling would affect the data obtained by the instruments. Unfortunately, only a qualitative discussion of this point can be made at the present time.

Anderson[5], working with cement dust less than 50 microns in diameter, reported dust concentrations of 150 to 180 per cent of the true concentrations in the samples taken at one-half of the stream velocity and concentrations of 80 per cent of the true value for samples taken at 140 per cent of stream velocity.

Figure 1.1 illustrates isokinetic flow. The streamlines enter the sampling tube without distortion. Any other condition results in deflection of the streamlines in the vicinity of the orifice, giving samples which are either too low or too high, depending upon whether the ratio of sampling speed to wind speed is less than or greater than one respectively. Figure 1.2 illustrates the sampling speed to wind speed ratio of one-half. In this case the sample will favor the larger particles. Figure 1.3 illustrates the sampling speed to wind speed ratio of two. In this case the sample will favor the smaller particles.

Table 1.1 indicates the deviations of the samplers from isokinetic flow, assuming the intake orifice is pointed into the wind. (Not the case in actual use) The average wind speed at the Nevada Test Site was approximately 5 miles per hour, or 1.34×10^4 cm/min. A value of one for the ratio sampling speed:wind speed, represents isokinetic flow.

5 Evald Anderson, "On the Qualitative Determination of Industrial Gas Dispersoids." Transactions of the American Inst. of Chemical Engineers, 34, 589. (1938)

PROJECT 2.5a-1

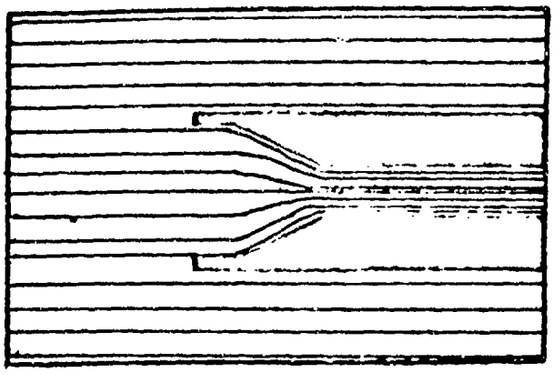

Fig. 1.1 Isokinetic Flow

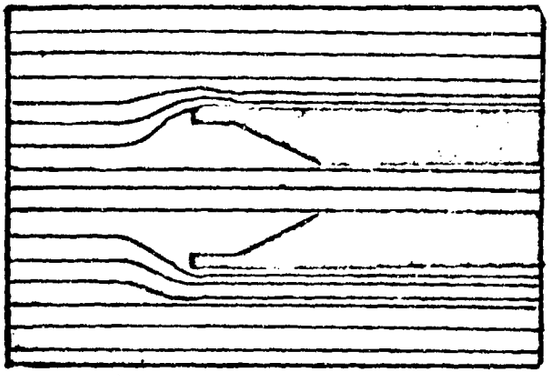

Fig. 1.2 Ratio of Sampling Speed to Wind Speed is 1/2

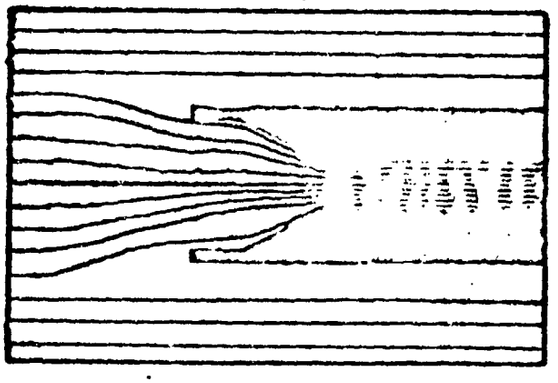

Fig. 1.3 Ratio of Sampling Speed to Wind Speed is 2

PROJECT 2.5a-1

TABLE 1.1

Air Sampling Speed Data

Instrument	Volume Flow Rate cm/min	Sampling Area cm	Sampling Speed cm/min	Sampling Speed / Wind Speed
Filter Sampler	3.4×10^4	100	3.41×10^2	2.54×10^{-2}
Cascade Impactor	1.25×10^4	10	1.2×10^3	8.95×10^{-2}
Centrifuge at 6000 RPM	2.2×10^2	0.18	1.2×10^3	8.95×10^{-2}
Tracerlab Continuous Air Monitor	7.4×10^4	13.2	5.6×10^3	4.18×10^{-1}
Brookhaven Continuous Air Monitor	9.6×10^4	10.4	9.25×10^3	6.90×10^{-1}
Particle Separator	2.83×10^4	52.8	5.38×10^2	4.02×10^{-2}
Radiological Air Sampler	5.0×10^2	0.6	7.94×10^2	5.94×10^{-2}
Electrostatic Precipitator	3.3×10^4	22	1.5×10^3	1.12×10^{-1}

It must be reemphasized that the values given in Table 1.1 are applicable only for the case of the instrument facing continually into the wind i.e. as a weather cock. Actually the filter samplers were mounted perpendicularly to the radii from the zero point so that in general on the "hot" legs they sampled broadside to the wind stream. This and the presence of the sheet metal hood (see Fig. 2.1), tended to make this instrument favor the smaller particles. The cascade impactors were oriented down the axis of radii from the zero point and on the "hot" legs were non-isokinetic to approximately the degree indicated in Table 1.1. All of the other instruments were oriented in the vertical direction and therefore were sampling broadside to the wind and in a manner comparable to the filter sampler, except that they favored the very largest particles which had a Stoke's fall velocity greater than the horizontal wind velocity.

1.4 RADIOACTIVITY MEASUREMENTS

While in any investigation of this nature all three kinds of nuclear radiation can be of interest, the hazard caused by the in-

halation of fission products is predominantly due to beta radiation.[6] For this reason, as well as the heavy counting load caused by the large number of samples, only beta counting was performed in this project. In order to report such quantities as concentration of activity in the aerosol, it was necessary to determine absolute beta disintegration rates, a difficult goal. An uncertainty of the order of 20% can be expected in the reported beta activity data.[7,8] Unless otherwise indicated, corrections for coincidence, sample covering, air path, and tube window were applied to all counting data, in addition to the usual geometry correction. No corrections for self scattering and self absorption or back scattering were made.

1.5 ORGANIZATION

Figure 1.4 shows the organization employed to prosecute this project, and Table 1.2 shows the assignment of stations to personnel.

6 See, for example, The Effects of Atomic Weapons, (U. S. Gov. Printing Office, Sept 1950), p. 257.

7 G. Friedlander and J. W. Kennedy, Introduction to Radiochemistry, (New York: John Wiley and Sons, 1949), p. 228

8 L. R. Zumwalt, "Absolute Beta Counting Using End-Window Geiger-Mueller Counter Tubes" MDDC -1346, (Oak Ridge: Technical Information Division, 1947) p. 1

FIGURE 1.4

ORGANIZATION OF PROJECT 2.5a

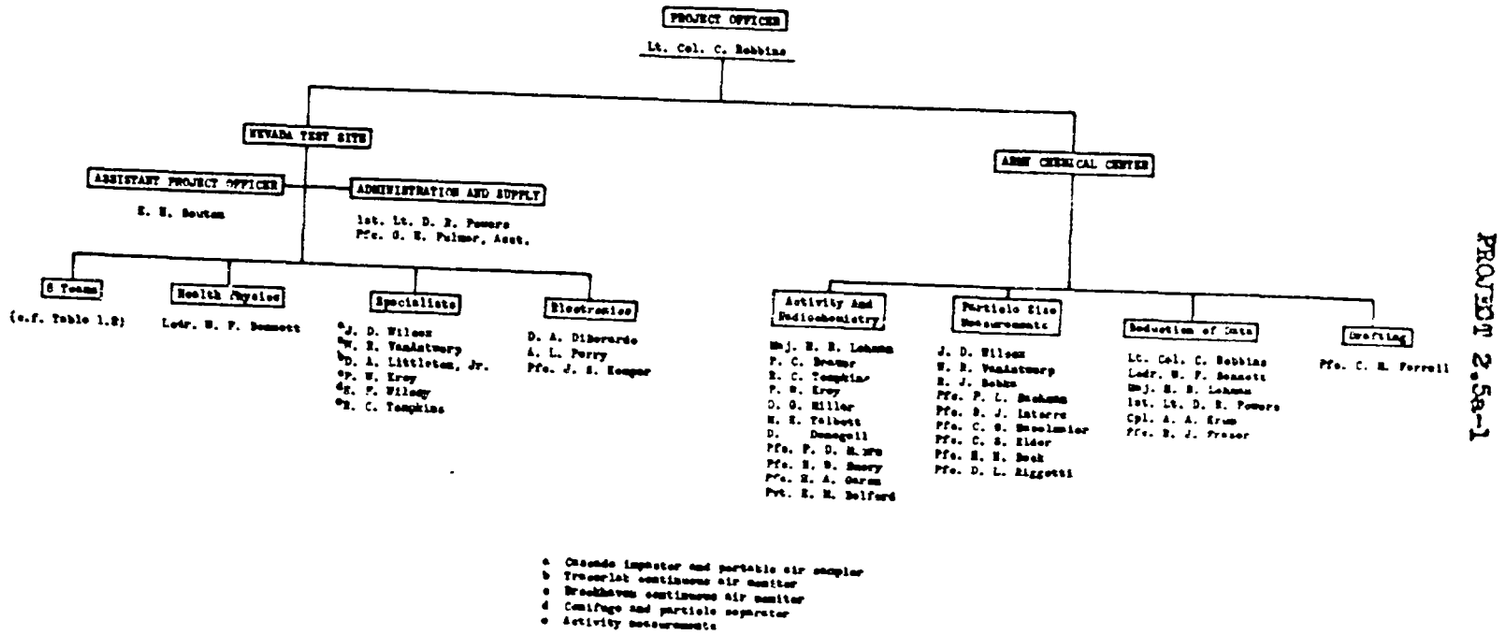

a Cascade impactor and portable air sampler
b Tracerlat continuous air monitor
c Brookhaven continuous air monitor
d Centrifuge and particle separator
e Activity measurements

Fig. 1.4 Organization of Project 2.5a

TABLE 1.2

Station Assignments to Personnel

Team No.	Group Leader	Organization	Asst. Group Leader	Organization	Station Nos Assigned
1	D. A. Littleton, Jr.	C&RL, ACC	Pfc. D. B. Sullivan	Technical Escort Det. Army Chemical Center	1,7,13,19
2	P. W. Krey	C&RL, ACC	J. L. Lindwarm	Research & Engineering Command, ACC	2,8,14,20 23,27
3	E. P. Sawyer	CmlC Board ACC	Pfc. R. W. Sullivan	Technical Escort Det. Army Chemical Center	3,9,15,21 24,28
4	M. J. Schumchyk	C&RL, ACC	Pvt. R. R. Weber	Technical Escort Det. Army Chemical Center	29,33,36,39
5	E. F. Wilsey	C&RL, ACC	Pvt. S. Wallace	Technical Escort Det. Army Chemical Center	4,10,16,22 26,46
6	J. R. Hendrickson	C&RL, ACC	Pvt. R. Lyons	Technical Escort Det. Army Chemical Center	30,34,37,40
7	E. H. Bouton	C&RL, ACC	A. Owyang	Dugway Proving Ground Tooele, Utah	5,6,11,12 17,18,42,43
8	Capt. G. G. Cannity	CmlC Training Comd.	Pvt. F. N. Gray	Technical Escort Det. Army Chemical Center	31,35,38,41

CHAPTER 2

INSTRUMENTS

2.1 FILTER SAMPLER

The purpose of this instrument was to filter the particulate matter from a known volume of the aerosol. By measuring the activity on the filter paper and volume of air filtered, the average concentration of activity in the cloud could be estimated.

2.1.1 Design

The filter samplers used in the tests (see Fig. 2.1) consisted of a motor driven suction pump drawing air through a filter paper sampling area of 100 cm^2.

2.1.2 Calibration

All filter samplers were calibrated at the test site with a dry flow-rate meter. For the surface shot the flow rates of several samplers were measured before and after the detonation. The results, given in Table 2.1, show that for the quantity of material filtered there was no appreciable change in resistance of the paper before and after the test. It was therefore considered reasonable to assume that the flow-rate remained constant during the sampling period.

The following code was used in describing the various filter samplers listed in Table 2.1. (For location of the stations, see Figs. 3.1 and 3.2.)

X Consisted of 1 sheet Chemical Corps No. 6 paper and 2 sheets of No. 5 paper. This type was used on all stations at distances greater than 4000 feet from zero. The sampler was located 7 feet above ground.

X_1 Consisted of 1 sheet Cml C No. 6 paper, 2 sheets of Cml C No. 5 paper backed up by 5 sheets of No. 6 paper. The 5 sheets of No. 6 paper served to cut down the flow of air approximately to 1 cubic foot per minute while the filter sampler was operating at full (24 volts) battery voltage. This type of sampler was used on all stations up to and including distances of 4000 feet from ground zero. The sampler was located 7 feet above ground.

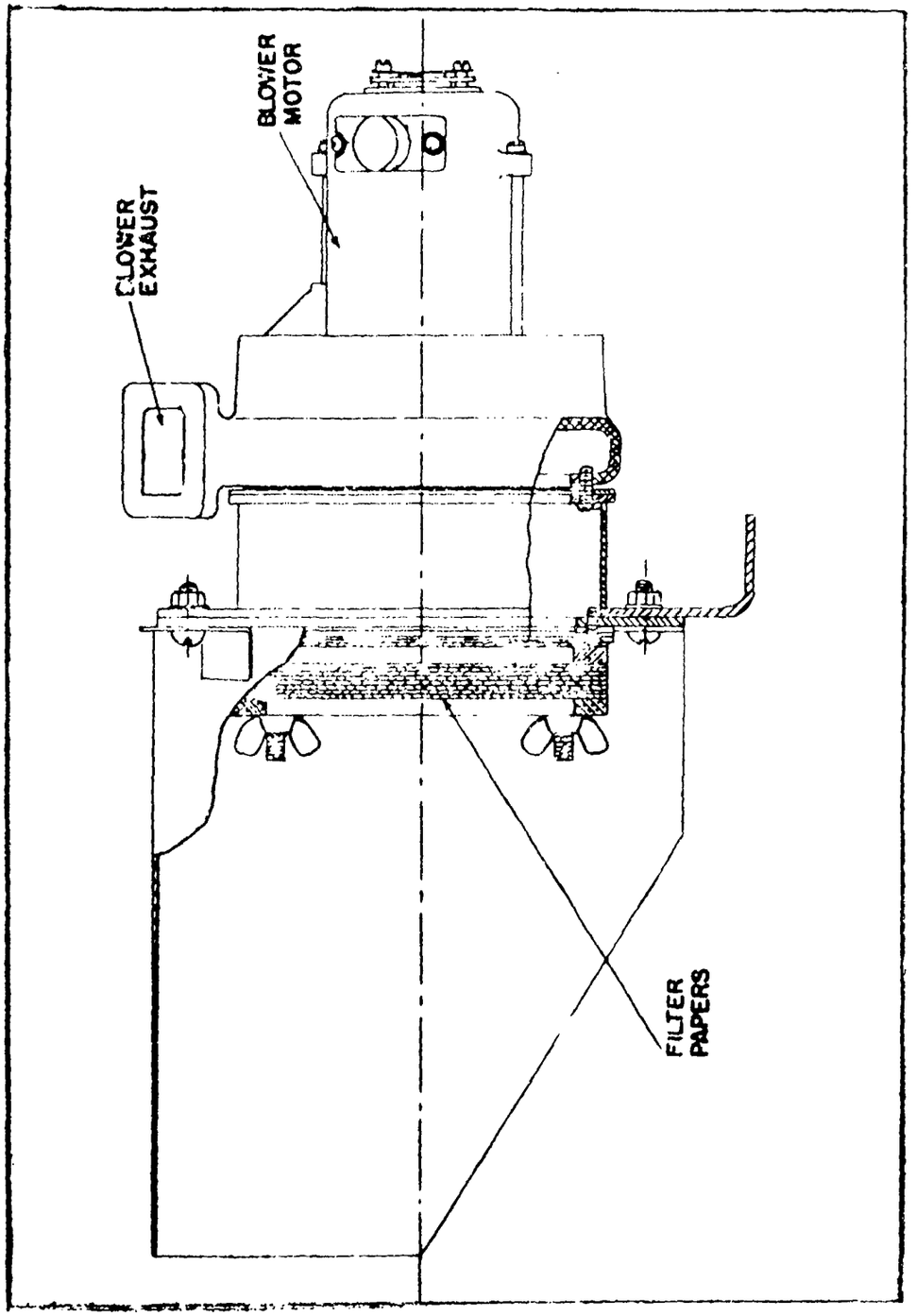

Fig. 2.1 Filter Sampler Assembly

PROJECT 2.5a-1

TABLE 2.1

Filter Sampler Data

Station Number	Location and Type Paper	Flow Rate (cu.ft/min) Before Surface Shot	Flow Rate (cu.ft/min) After Surface Shot	Purpose of Sample	Agency Performing Analysis
1	X_1	1.18	-	activity, decay	NIH, TL
2	X_1	1.36	damaged by blast	activity, decay	NIH, ACC
3	X_1	1.32	-	activity, autoradiograph	NIH, LASL, ACC
4	X_1	0.75	-	activity	NIH, TL
5	X_1	0.83	-	activity	NIH, ACC
6	X_1	1.36	-	activity	NIH, ACC
7	X_1	1.24	-	activity	NIH, TL
8	X_1	1.43	1.43	activity	NIH, TL
9	X_1	1.28	-	activity	NIH, TL
10	X_1	0.59	-	activity	NIH, TL
11	X_1	1.23	-	activity	NIH, ACC
12	X_1	1.38	-	activity	NIH, ACC
13	X_1	1.13	-	activity	NIH, ACC
14	X_1	1.21	1.20	activity	NIH, ACC
	G_1	0.65	0.87	activity	NIH
	L	4.28	4.00	radiochemistry	TL
	L_1	4.06	3.75	radiochemistry	ACC
	A	4.14	3.75	radiochemistry	NIH
15	G_1	0.77	-	activity	NIH
	A	4.28	-	radiochemistry	NIH
	L	4.14	-	radiochemistry	TL
	L_1	3.90	-	radiochemistry	ACC
16	X_1	0.90	-	activity, decay	NIH, TL
	G_1	0.86	-	activity, decay	NIH
	L	4.11	-	radiochemistry	TL
	L_1	4.29	-	radiochemistry	ACC
17	X_1	1.25	-	activity	NIH, ACC
18	X_1	1.32	-	activity	NIH, ACC
19	X	3.30	-	activity	NIH
	G	3.30	-	activity, decay	NIH
20	X	2.86	2.86	activity, decay	NIH, ACC
	G	3.12	3.16	activity	NIH
21	G	3.30	-	activity	NIH
22	X	3.45	-	activity, decay	NIH, TL

PROJECT 2.5a-1

TABLE 2.1 (cont'd)

Filter Sampler Data

Station Number	Location and Type Paper	Flow Rate (cu.ft/min) Before Surface Shot	Flow Rate (cu.ft/min) After Surface Shot	Purpose of Sample	Agency Performing Analysis
23	X	3.16	3.16	activity	NIH,TL
24	X	2.73	-	activity	NIH,TL
25	X	2.83	-	activity,decay autoradiograph	NIH,LASL,ACC
26	X	3.67	-	activity,autoradiograph	NIH,LASL
27	X	3.43	3.40	activity,decay	NIH,TL
28	X*		-	activity,autoradiograph	NIH,LASL
29	X	3.33	-	activity	NIH,TL
	M	3.09	-	activity,particle size	TL
30	X	2.26	-	activity,autoradiograph	NIH,LASL,ACC
	M	3.90	-	activity,particle size	TL
31	X	2.63	-	activity	NIH,TL
	M	3.57	-	activity,particle size	TL
32	X	3.53	-	activity,decay	
	M	4.29	-	activity,particle size	NIH,decay
33	X	3.20	-	activity,autoradiograph	NIH,LASL
34	X	3.00	-	activity,decay autoradiograph	NIH,LASL,ACC
35	X	3.12	-	activity,autoradiograph	NIH,LASL
36	X	3.51	-	activity,autoradiograph	NIH,LASL
37	X	3.63	-	activity,autoradiograph	NIH,LASL
38	X	2.62	-	activity,autoradiograph	NIH,LASL
39	X	3.12	-	activity,autoradiograph	NIH,LASL
40	X	2.46	-	activity,autoradiograph	NIH,LASL
41	X	3.0	-	activity,autoradiograph	NIH,LASL
42	X	2.65	-	activity,autoradiograph	NIH,LASL
43	X	2.38	-	activity,autoradiograph	NIH,LASL
44	X	2.46	-	activity,autoradiograph	NIH,LASL,ACC
45	X	3.37	-	activity,autoradiograph	NIH,LASL
46	X	3.00	-	activity,autoradiograph	NIH,LASL

*plus molecular filter adapter.

G — Same as X in all respects except that the filter sampler was located 2 feet above ground.

L, L_1, A — Consisted of 4 sheets of Chemical Corps No. 5 paper. This is an "open" paper and the purpose is to obtain a large sample for radiochemical analysis. The various letters designate the receiving agencies.

M — Consisted of 4 sheets of polyfiber paper (Air Force) paper. This is an "open" paper and the purpose is to obtain a large sample for radiochemical analysis.

Equipment at stations of the surface shot (1 through 46) was transferred to the corresponding stations of the underground shot (101 through 146). The handling of samples and analytical work for samples collected from the underground shot tests was the same as the surface shot, except that time did not permit the preparation of autoradiographs by the Los Alamos Scientific Laboratory.

The abbreviations of the receiving agencies are as follows:

ACC - Army Chemical Center
NIH - National Institute of Health
TL - Tracerlab, Inc., Boston, Massachusetts
LASL - Los Alamos Scientific Laboratory

2.2 THE CASCADE IMPACTOR

To determine the size-distribution of any heterogeneous cloud, a size-grading sampling method is desirable. It is also desirable to subject the particles to a minimum amount of physical strain as they are collected. The cascade impactor, first developed and described in detail by May[1], is particularly suited to these requirements. It size-grades particles in a manner suitable for analysis with light and/or electron microscopes and also collects the larger particles present (these being the most likely to shatter) at low velocities. The predominate disadvantage of the impactor is that it is not an absolute instrument, i.e., below a certain size, depending on the geometry of the last jet and the physical properties of the particle involved, the probability of collection decreases in a rather complex manner (but presumably monotonic with respect to particle size).

[1] K. R. May, "The Cascade Impactor: An Instrument for Sampling Coarse Aerosols", Journal of Scientific Instruments, 22 (Oct 1945) 187

The performance of a jet in a cascade impactor is determined by the effects of the previous stages and the flow rate through it, as well as its own physical characteristics; thus the instrument must be designed as a unit, each stage being compatible with both the preceding and the following ones. Since the impactor is to sample efficiently an extended particle size range (0.2-100 microns), five stages were considered necessary for suitable size-grading. The effectiveness of each stage, and therefore of the complete instrument will vary with flow rate. Thus it is necessary to maintain a suitable and constant flow rate.

Although narrower jets will impinge smaller particles efficiently, one might readily assume that the narrowest possible jet should be used for the fifth stage; however, supersonic flow cannot be obtained in a jet of this type. Thus, the flow rate cannot exceed a maximum value, which occurs when sonic velocity is reached in the smallest jet. In actual practice, this feature was used to control the flow rate in the cascade impactor. If a narrower jet had been used, the flow rate would have been reduced correspondingly, thereby reducing the sampling volume.

2.2.1 Design

A theory of impaction is necessarily based on the trajectories of small particles in a moving fluid and extensive studies of the factors effecting particle trajectories have been made by many investigators[2,3,4]. An approximate theory of impaction, by Baurmash[5] et al, is quite flexible, allowing immediate comparison of the efficiencies of various jet widths and velocities. This relation may be derived by considering a jet from which a fluid of density ρ , viscosity

---

[2] Ibid

[3] Johnstone and Roberts, "Deposition of Aerosol Particles from Moving Gas Streams", Industrial and Engineering Chemistry, 32 (1940) 650

[4] Lapple and Shepard, "Calculation of Particle Trajectories", Industrial and Engineering Chemistry, 32

[5] Baurmash, "Development of Continuous Jet Impactor Methods", UCLA 13, AnCU-206.

η , slit velocity V, is flowing in an approximately circular path of mean radius of curvature R, as shown in Fig. 2.2. It takes any particle roughly a time equal to

$$t = \frac{\pi R}{2V} \qquad (2.1$$

to traverse the quarter-circle arc. In this time it will have drifted radially outward a distance x equal to

$$x = ut \qquad (2.2)$$

where u is the Stokes velocity

$$u = \frac{D^2 \rho a}{18 \eta} \qquad (2.3)$$

D is the particle diameter and a is the radial acceleration and equal to V^2/R.

If it is assumed that the criterion for impaction is that the radial drift distance x is equal to half the jet width d, then it is possible to calculate the minimum particle diameter D_{min}, which will be impacted. Substituting and solving for D results in

$$D_{min} = 1 \frac{36 \eta d}{\pi \rho V} \qquad (2.4)$$

To check the validity of this formula, the experimental values obtained by May, Johnstone[6], and Casella[7] were compared with

[6] Memo Report, University of Ill., High Velocity Impactor for Sampling Aerosols, 15 March 1949.

[7] C. F. Casella & Co. Ltd., Cascade Impactor, Leaflet 72J, Regent House, Fitzroy Sq. London W. I.

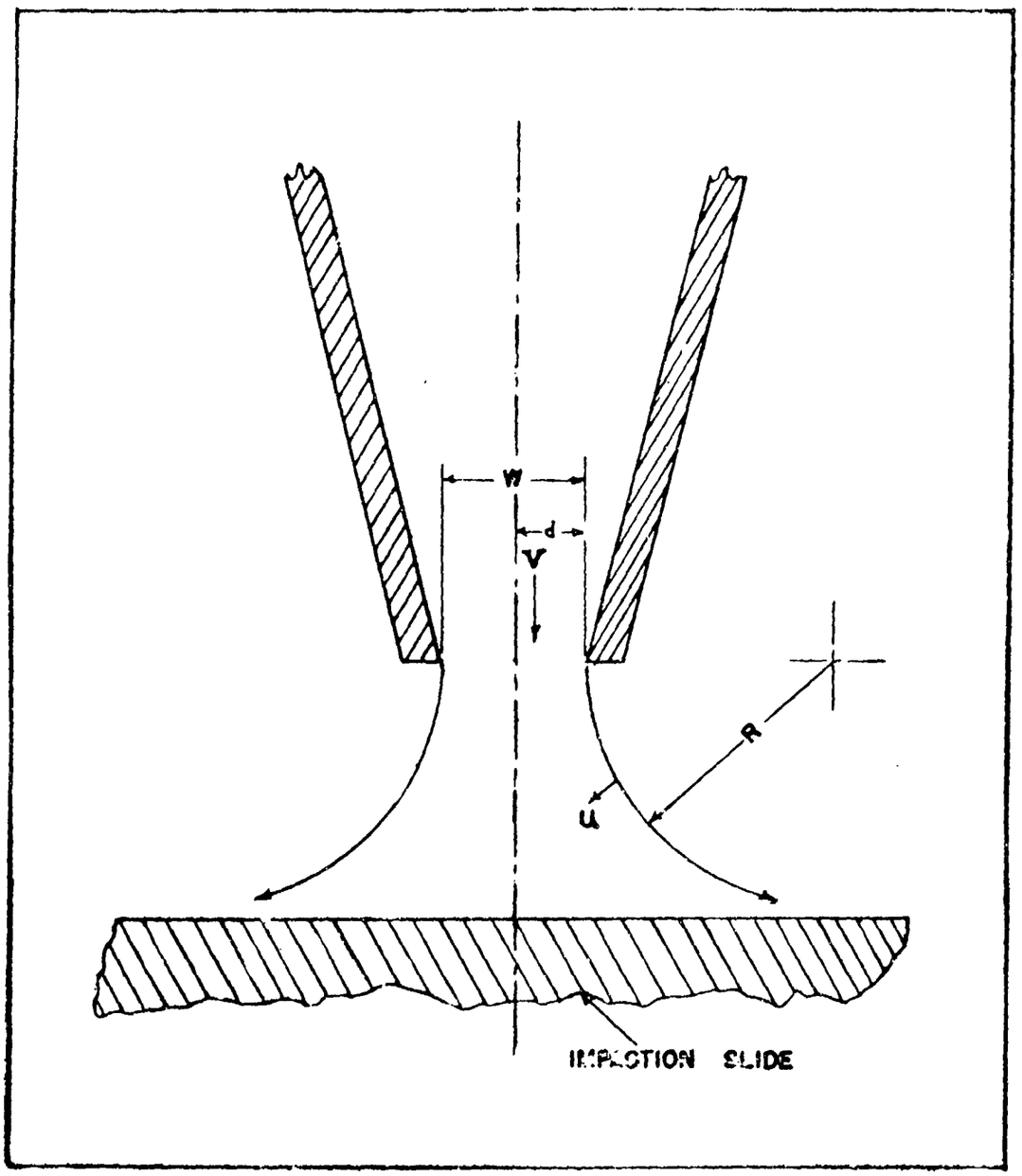

Fig. 2.2 Schematic Drawing of the Idealized Flow From a Cascade Impactor Slit. The slit length (into the paper) is assumed to be much greater than the width w.

those predicted by theory. The results were in excellent agreement.

The impactor described by Voegltin and Hodge[8] was found to be the most sturdy impactor available and since it was designed so that the jets could readily be interchanged it was decided to modify the Hodges model to fit requirements for sampling at Operation JANGLE. After some consideration it was decided to use the 1st, 2nd, and 4th jets of the original Hodge impactor for the first, second, and third jets of the new model and then to design two new jets. The development and performance of this modified Hodges-type impactor as well as refinements to eq. 2.4 have been previously described in detail[9].

A further important modification in this instrument was the inclusion of slides with electron microscope specimen screens set in recesses[10]. As a result, a slide assembly well suited for field use was developed.

2.2.2 Calibration

Critical flow rates of the cascade impactors used are shown in Table 2.2. The critical flow rates were determined using a previously calibrated Dry Test Meter and a vacuum gauge. To be reasonably certain that critical flow was attained, a vacuum of 18.0 inches of mercury was required for critical flow.

Table 2.3 gives the calculated sizes of particles efficiently removed for the modified instrument. Calibration of cascade impactors for actual efficiency for various particle sizes was not necessary for this work due to the heterogeneous density of aerosols expected. The samples were analyzed by direct methods, i.e., measuring and counting of each particle in a known representative area.

---

[8] Voegtlin & Hodge, Pharmocology and Toxicology of Uranium Compounds, Vol. FI-1, p. 483, McGraw-Hill, 1949.

[9] J. D. Wilcox, Design and Development of a New Five Stage Impactor, CRLIR 92, ACC, Md.

[10] J. D. Wilcox, A New Sampling Technique, CRLIR 70, ACC, Md.

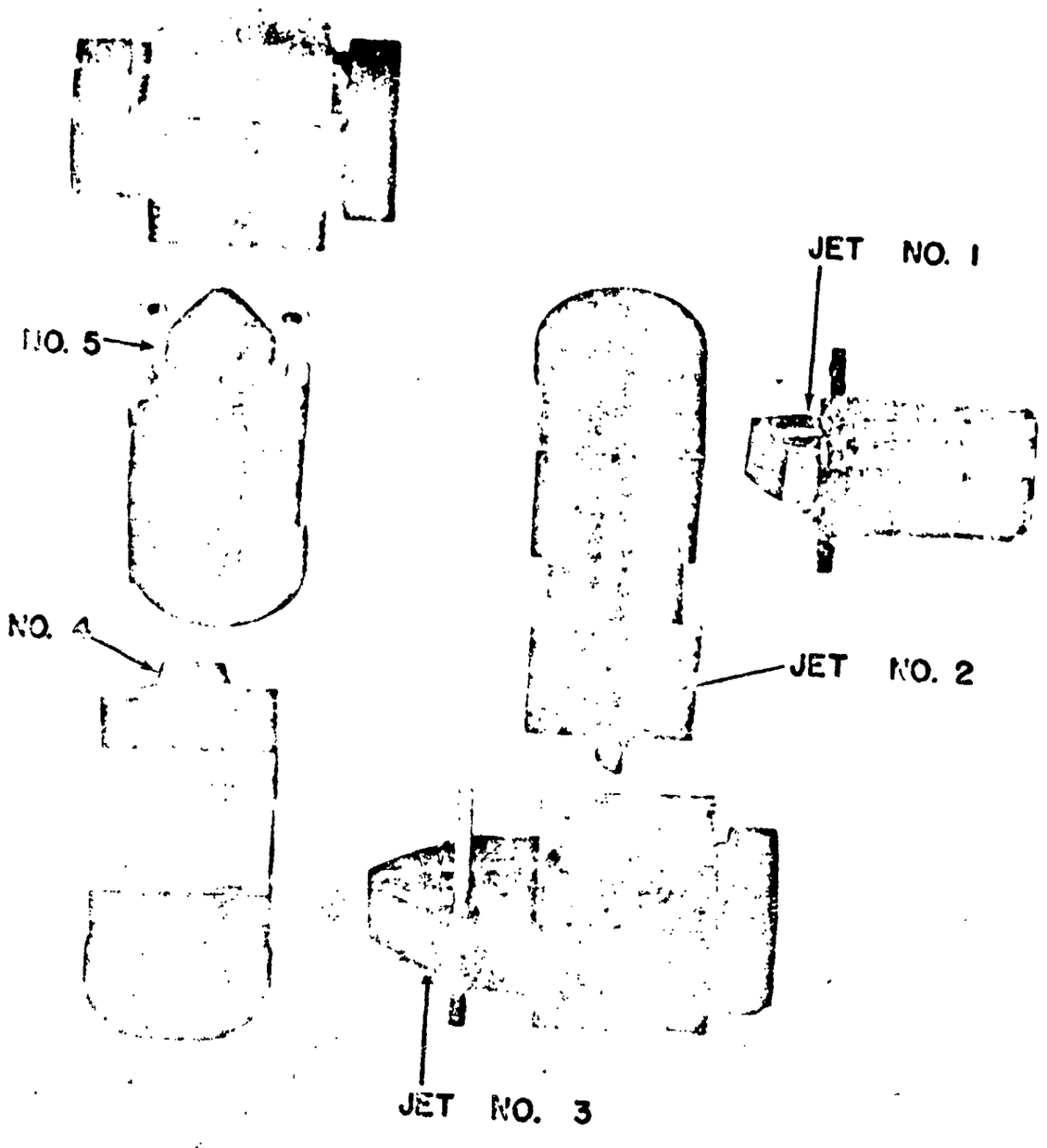

Fig. 2.3 The Jets of the Cascade Impactor in Exploded Arrangement.

TABLE 2.2

Cascade Impactor Critical Flow Rates

Impactor Identification	Flow Rate (liters per min.	Vacuum Between & Pump (inches of Mercury)	Impactor Identification	Flow Rate (liters per min.	Vacuum Between & Pump (inches of Mercury)
A	13.4	18.0	I	12.2	19.0
B	12.1	20.0	J	12.6	19.5
C	13.0	19.0	K	13.6	18.5
D	13.4	18.5	L	12.5	19.5
E	12.9	19.0	M	12.6	19.5
F	12.5	19.5	N	13.1	18.5
G	13.4	18.0	O	12.1	19.5
H	12.6	19.0	PT	12.2	20.0

TABLE 2.3

Cascade Impactor Jet Data[a]

Jet No.	Jet Length	Jet Width	Velocity at Orifice	Minimum Particle Diameter Impacted (D_{min}) microns			
				$\rho = 1$	$\rho = 2$	$\rho = 4$	$\rho = 7.5$
1	13.90mm	5.30 mm	2.83×10^{2} cm/sec	18.0	11.0	7.4	6.2
2	14.35mm	1.38 mm	1.05×10^{3} cm/sec	4.2	2.84	1.98	1.56
3	13.85mm	0.575mm	2.62×10^{3} cm/sec	1.77	1.17	0.84	0.63
4	9.15mm	0.395mm	5.76×10^{3} cm/sec	0.95	0.65	0.47	0.347
5	4.05mm	0.290mm	1.77×10^{4} cm/sec	0.47	0.32	0.224	0.168

[a] Flow rate of 12.6 l/min

2.3 CONIFUGE

The purpose of the conifuge was to provide a size-graded sample of the particulates in the aerosol.

2.3.1 Design

The conifuge consists of a conical head centrifuge formed by an inner and outer cone, arranged co-axially and separated by a narrow annular space through which a steady stream of aerosol is drawn by the self-pumping action of the cones, which are driven by a motor at high rpm. The cloud sample is introduced as a thin film into the annular space through a small tube at the apex of the inner cone. Since the particles are influenced by the transverse velocity of the air stream and the centrifugal velocity of the rotating cones, they follow a trajectory based upon their mass and terminal velocity. The particles pass between the two cones and deposit as a spectrum of particle sizes on the surface of the outer cone which is made of polystyrene plastic with two rows of six evenly spaced screws which carry electron microscope screens.

The thin filament of sampled cloud passing across the gap between the end of the sampling tube and the apex of the inner cone is in unstable equilibrium and is easily displaced by an inequality in the spacing of the two cones. The result is an uneven distribution of the samples on the outer cone. Precise workmanship is therefore essential in the construction of the centrifugal chamber and in the alignment of the whole apparatus. The design must also be robust enough for this adjustment to be retained after dismantling for cleaning and reassembly. Good seals must be obtained around the base of the two cones and around the base of the container. Poor seals give rise to leakage which alter flow rates and destroy regularity of the size separation. For a similar reason, the housing packing must be kept well oiled to prevent leakage through the bearings. To maintain the designed sampling rate, both the sampling inlet and exhaust jet must be subjected to the same external pressure. Figures 2.4 and 2.5 show photographs of the conifuge employed at Operation JANGLE.

The disadvantages of the present instrument are (1) low flow rate and vertical orientation which precludes approximating isokinetic conditions and (2) separation is dependent upon the density of particulates which is likely to be heterogeneous in the aerosol. According to Sawyer[11], "The depositing efficiency of the conifuge is 100

[11] K. F. Sawyer, Porton Technical Paper, No. 86, (Porton, U. K., 14 Dec. 1948)

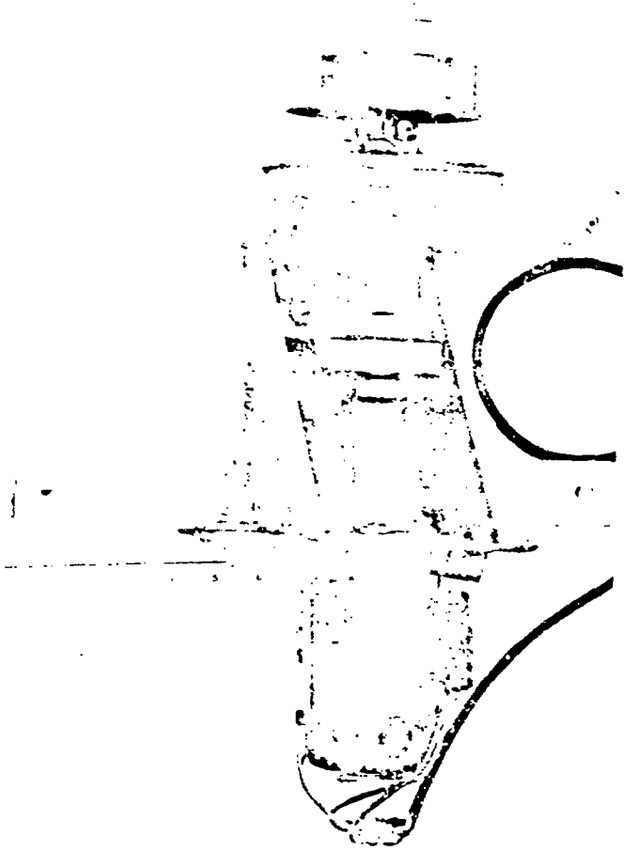

Fig. 2.4 Conifuge with Outer Cover Removed Showing Plastic Collecting Cone

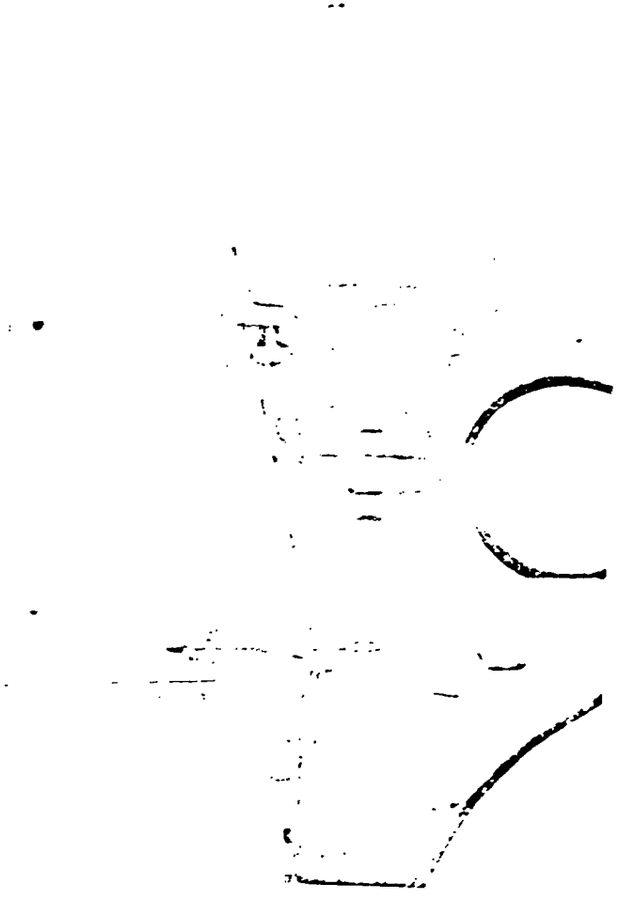

Fig. 2.5 Assembled Conifuge Showing Outer Cover in Place

per cent under all conditions for all particles which do not encounter the walls of the sampling tube on entry or impact upon the inner cone. Re-circulated particles would, if present, show no size separation and form a heterogeneous background to the main deposit".

2.3.2 Calibration

Recent laboratory testing of the conifuge has shown that the rate of sample flow is greater than was first assumed. Flow calibration data was obtained by filling a bottle full of ammonium chloride smoke and drawing the smoke through a 1.17 cm inside diameter glass tubing by the self-pumping action of the conifuge. The point of the smoke was then timed as it flowed through 50 and 100 cm lengths of the glass tubing and into the conifuge inlet tubing. The flow rates shown in Table 2.4 were obtained by the use of a "pipe coefficient" of 0.5 as suggested by Vennard[12] for laminar flow (Re = 380).

TABLE 2.4

Conifuge Flow Calibration

RPM	Corrected Flow Rate (cc/min)
8000	315
7000	265
6000	218
5000	173
4000	130
3000	90

Operating the conifuge at 5000 rpm gives a sampling rate of 173 cc/min with about 3460 cc/min of excess air recycled. The low sampling rate is a serious limitation. For good size separation, the sampling rate must not exceed about five per cent of the total flow rate (total volume circulating between the cones). The design of the Chemical Corps conifuge limited the speed to 8000 rpm when operating at extended periods of time (2-3 hours). For shorter operating times (20-30 min.) the conifuge can be operated at 10,000 rpm. A calibration curve of rpm vs voltage was used to obtain required speeds in the field.

[12] J. K. Vennard, Elementary Fluid Mechanics, (2nd ed) New York: Wiley and Sons, 1947. 7, p. 163.

PROJECT 2.5a-1

Test runs were made on the conifuge using a steel outer cone which had two slits covered by plastic slides along the slant height of the cone. An aerosol containing spherical glass particles was generated into a sampling chamber. Samples were taken with the conifuge, and the particle size distribution was determined with a microscope. Table 2.5 gives data obtained at a speed of 5000 rpm, a sampling time of 6 minutes, and an air flow of approximately 170 cc/min.

TABLE 2.5

Conifuge Particle Size Calibration

Distance From Top Edge	Particle Size (microns)
16 mm	12 -6
20	6 -4
24	4 -2.5
28	2.5-1.8
32	1.8-1.1
36	1.4-0.6
40	0.6-0.4
44	under .4

2.4 PARTICLE SEPARATOR

The purpose of the particle separator was to sample and fractionate the aerosol and fall-out particulate material into size ranges by means of a vertically oriented sifting device.

2.4.1 Design

Each particle separator consisted of:

1. Eleven bronze wire screen sieves which were to fractionate particles into class intervals of 37-43, 44-52, 53-61, 62-73, 74-88, 88-104, 105-124, 125-148, 149-176, 177-209 microns.

2. A porous stainless steel filter to retain particles larger than 1 micron.

3. A molecular filter to separate all the particles which pass through the porous stainless steel disk.

PROJECT 2.5a-1

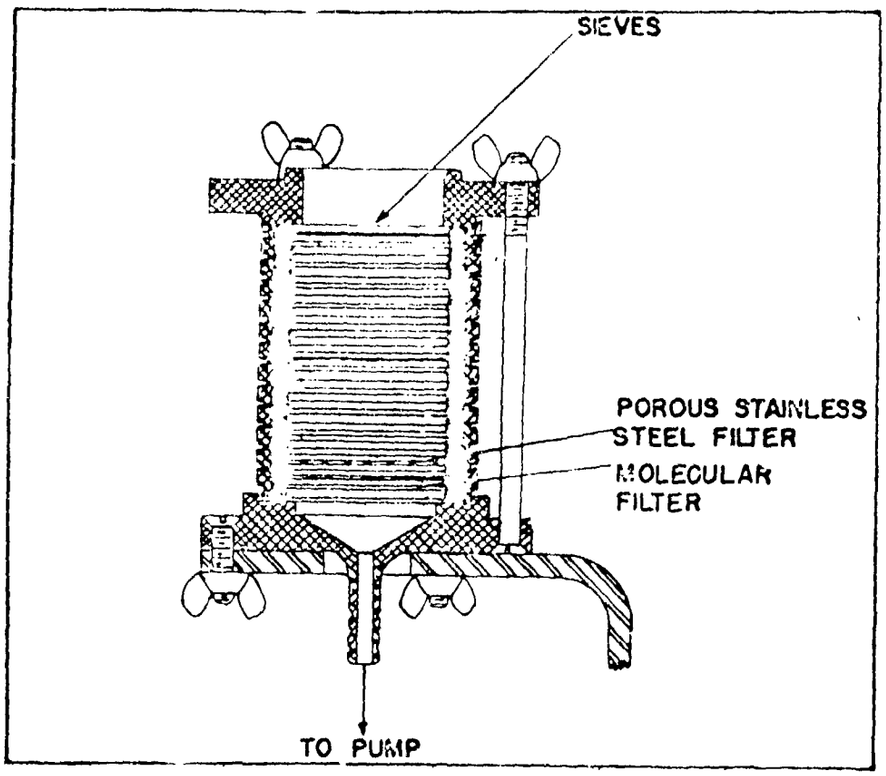

Fig. 2.6 Cross-sectional Drawing of a Particle Separator

TABLE 2.6

Particle Separator Calibration

Station Number	Flow Rate (cu.ft/min)		
	Before Surface Shot	After Surface Shot	After Underground Shot
8	0.89	0.87	0.88
9	0.62	-	0.45
14	0.83	0.90	0.79
15	0.82	-	0.81
20	0.88	0.83	0.92
21	0.89	-	0.85
23	0.89	0.86	1.00
24	0.93	-	0.94
28	0.95	-	0.94
29	0.98	-	1.02
30	0.82	-	0.90

4. A rotary type vacuum pump and hose connection to the particle separator to draw the particles through the apparatus. Air was drawn through the pump at the rate of approximately 1 cubic foot per minute.

The detailed design of the particle separator is shown in Fig. 2.6.

2.4.2 Calibration

Table 2.6 indicates the flow rate through the various filter samplers before and after each test. The results show that no appreciable change in resistance occurred in the particle separators during the test and the rate of flow through the particle separator was constant.

2.5 ELECTROSTATIC PRECIPITATOR

The purpose of the electrostatic precipitator was to sample the particulates. This instrument is not amenable to particle size determination unless microscope slides or screens are incorporated into the sampling cylinder.

2.5.1 Design

This instrument weighs about 50 pounds and consists of a metal cylinder through which air is drawn at the rate of 32 liters per minute at a speed of 25 cm/sec. An electrostatic potential of 300 volts was applied between an outside collecting cylinder and an inside central wire. The particulate matter is precipitated upon the outside cylindrical shell. A schematic diagram of the collecting cylinder is shown in Fig. 2.7.

2.6 CONTINUOUS AIR MONITORS

The purpose of the continuous air monitors was to measure the variation in the concentration of activity in the air with time.

2.6.1 Brookhaven Air Monitor

A filter paper feed system traveling at 4 inches per hour combined with a vacuum pump (3.5 cu ft/min) was employed to collect particulates from the air. A strip of filter paper 3 inches wide moves continuously at a predetermined rate over a rectangular sampling port. (1 in. x 1-3/4 in.) The particulate material in the aerosol was filtered onto the paper which passes under a shielded scintillation counter where

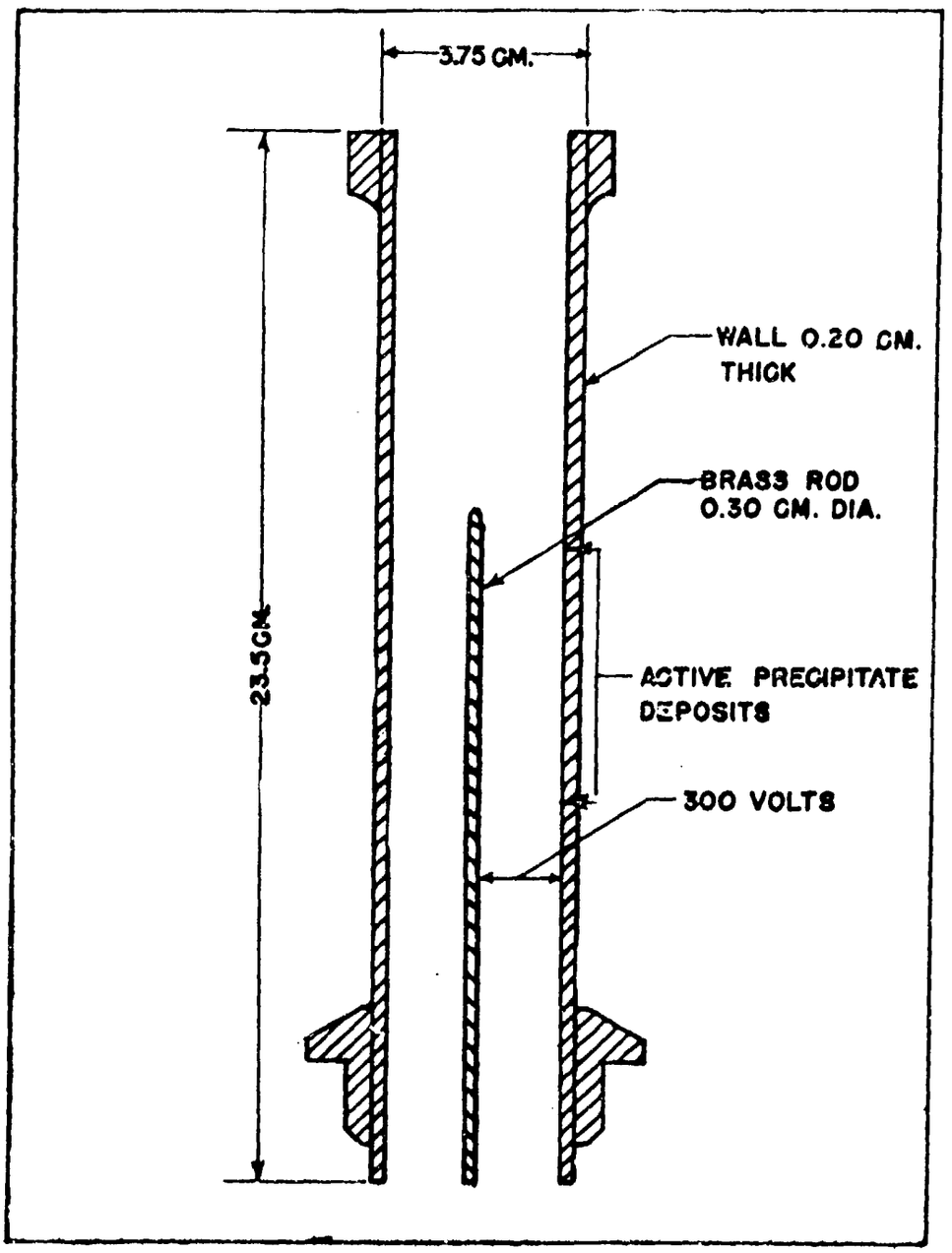

Fig. 2.7 Cross-sectional Drawing of the Electrostatic Precipitator Cylinder.

the activity was measured and a record made on an Esterline-Angus recorder. See Fig. 2.8.

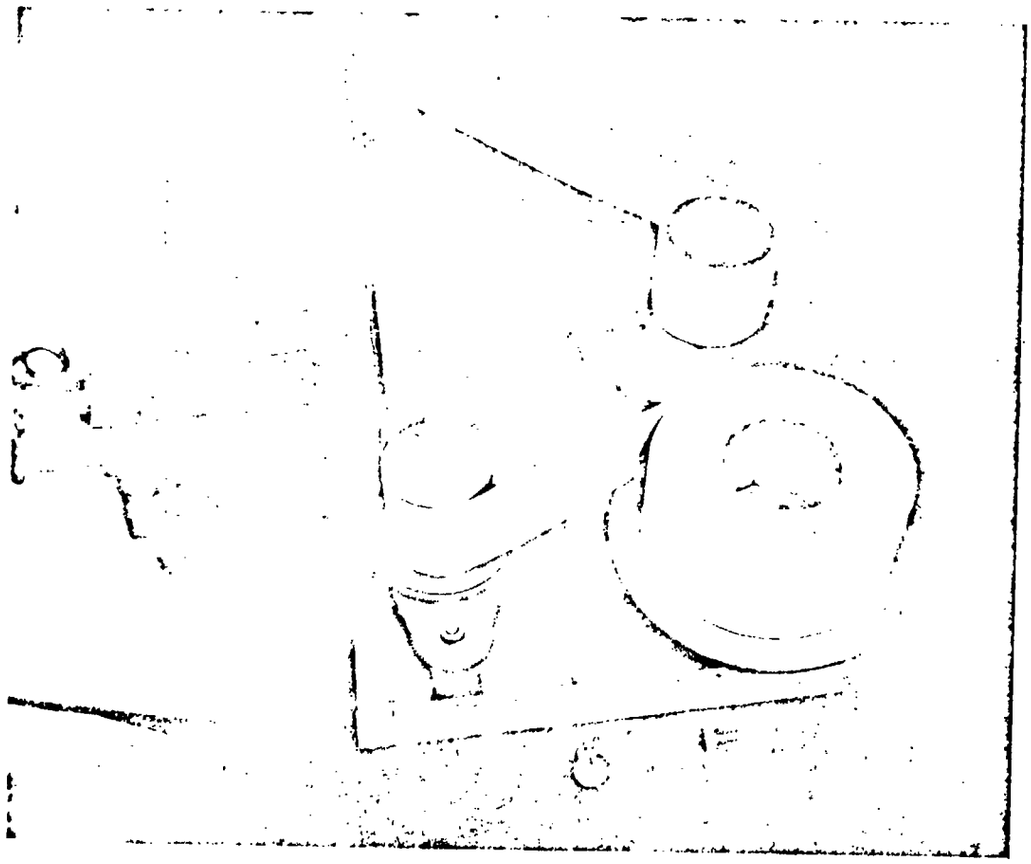

Fig. 2.8 Brookhaven Continuous Air Monitor.
Count Rate Meters Omitted.

The rate-meter and recorder were housed in a shack while the air sampler and scintillation counter were situated in a four foot shelf outside. A plastic cover protected the sampler from fall-out, except at the sampling port. The purpose of this procedure was to sample the cloud and protect the air sampler as much as possible. Cellophane sheet was fed from a roll onto the re-wind spool of the air sampler between successive layers of filter paper to eliminate cross contamination so that the filter paper could be recounted in the event of rate-meter or recorder failure. Rubber foam mats were placed under the electronic equipment to reduce vibration. Electric power (110 volts, 60 cycle) was supplied by a generator driven by a 2-cylinder gasoline engine.

The important feature of this instrument is that the sample is continuously collected on an area 1 in. x 1-3/4 in., the activity measurement is made over a contaminated strip 1 inch in width, and the radiation detector tube off-set approximately 5 inches from the center of the sampling ports, which results in a 30 minute delay between sampling and significant counting. The total time required for a one square inch (the size of the counter face) of filter paper to travel the sampling port is 41.25 minutes. Therefore an estimate of the activity in a cloud is based upon this period of sampling which ends approximately 52.5 minutes prior to counting and recording. A detailed discussion of the calibration of this instrument is given in the Appendix.

2.6.2 Tracerlab Air Monitor

This instrument also employs an air pumping system (2.6 cu.ft/min) with filter paper 6 inches wide traveling at 7 inches per hour or multiples of 1/4, 1/2, 2, and 4 times this rate. Wax paper was fed between successive layers of filter paper to prevent cross contamination. A Tracerlab P-12 alpha scintillation probe and a lead shielded Tracerlab TGC-1 Geiger-Muller tube were employed to detect alpha, beta and gamma radiations. The output voltage from two linear count-rate meters was recorded on a two point chart recorder manufactured by the Brown Instrument Company. The entire unit was housed in a metal cabinet and located in a shack with two air intake pipes, 12 feet long, extending from the instrument through the roof of the shack into the atmosphere. See Figs. 2.9 and 2.10.

The important feature of this monitor was that the radiation detectors were located directly over the sampling ports (2.25 in. diameter) and the activity was measured over this circular area. Inasmuch as deposition of the aerosol and counting occurs simultaneously, no time lag occurs. However, it may be noted that the counter reading at the time of deposition is not the same as when the tape is replayed through the instrument at a later time, despite correction for radioactive decay. A detailed discussion of this and other problems of instrument calibration may be found in Appendix C.

2.7 RADIOLOGICAL AIR SAMPLER

The Radiological Air Sampler (RAS) was a modification, for Operation JANGLE of the Portable Air Sampler (PAS) used previously by Test Division, CRL and Dugway Proving Ground, Utah. Its purpose was to provide an intermittent type of sampler capable of collecting a radioactive

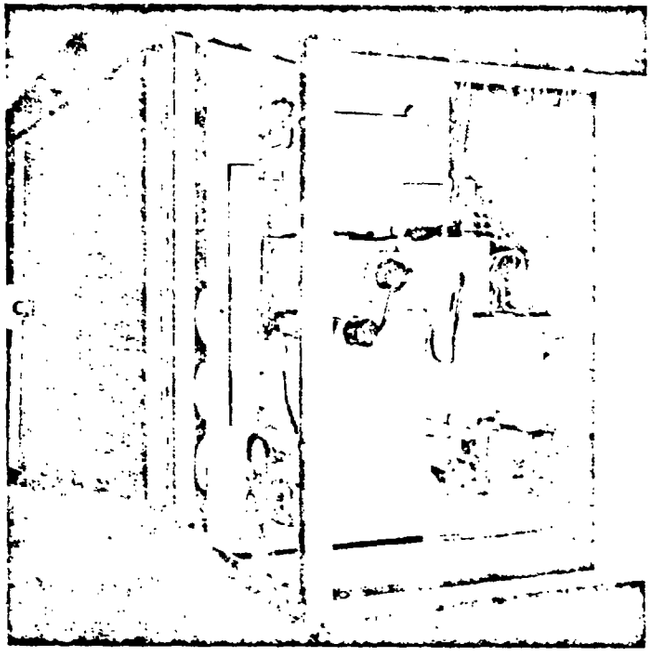

Fig. 2.9 Top View of the Tracerlab Air Monitor Showing the Counters and Filter Tape Transport System.

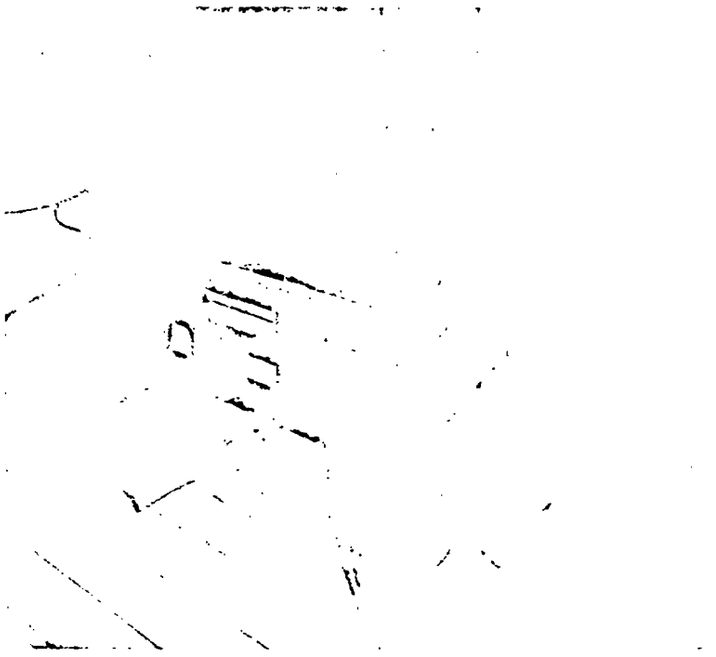

Fig. 2.10 Tracerlab Continuous Air Monitors as Installed, Showing the Two Air Intake Pipes.

aerosol as a function of time. As the sampler contains its own 6 volt DC power supply, the necessity of laying long power lines is avoided, thus simplifying its installation in the field.

2.7.1 Design

The general layout of the components of the RAS are best seen in Fig. 2.11. This instrument was surmounted by twelve plastic "molecular" filter[13] assemblies through which air was pumped successively for ten minutes by means of a rotary solenoid air valve controlled by a cyclin mechanism. The sampler was started five minutes prior to shot time by a signal which closed a 24 volt DC latching relay. Each filter in turn sampled the air for ten minutes and then the instrument automatically turned itself off. The complete design details of the RAS have been given previously[14].

2.7.2 Calibration

Calibrations of the instruments at the test site were made by using a molecular filter assembly in the line of flow. The flow calibration data was obtained using a Dry Test Meter and is shown in Table 2.7.

TABLE 2.7

Radiological Air Sampler Flow Calibration

RAS Code	Flow Rate Liters/Minute
A	0.380
B	0.385
C	0.445
D	0.445
E	0.440
F	0.440
H	0.445
I	0.450
K	0.440

[13] Alexander Goetz, "Molecular Filters", Report of Symposium III, Aerosols, Chemical Corps Technical Command, Army Chemical Center, Md. 4 April 1950.

[14] J. D. Wilcox, W. R. Van Antwerp, C. S. Elder. A Radiological Air Sampler - A Modification of a Portable Air Sampler. CRL Interim Rpt. 103 ACC, Md. 12 Apr 52.

Fig. 2.11 Radiological Air Sampler, Showing Filter Heads, Rotary Air Valve, Pump, Timing Mechanism, and Battery.

2.8 FALL-OUT TRAYS

The purpose of the fall-out trays was to collect samples of the fall-out for particle size distribution, activity measurements and radiochemical analysis.

2.8.1 Design

Wooden trays 23x36x2 in. with an effective exposure area of 21x34 in. were lined with thin sheets of polyethylene plastic approximately 0.001 in. thick. The trays were located on top of 7 feet high towers and 8 feet high shacks and covered until approximately 12 hours

before the test when all covers were removed. Several trays were located on the ground wherever shacks were not available or the NRDL thermal precipitator occupied the top of the tower. After the test the trays were covered, returned by truck to the rear area, and several hot particles removed for microscopic analysis at the test site by personnel of the Army Medical Center[15]. The remainder of the sample was bagged, crated, and returned by air to the ACC for particle size analysis and radiochemistry.

A possible disadvantage of the fall-out tray was the uncertainty of the amount of material blown out of or into the tray. Three trays were exposed to atmospheric conditions in the test area for several days and the amount of dust accumulated was too small to be weighed on a torsion balance. On this basis it was reasonable to assume that under normal conditions at the test site, insignificant amounts of material were blown into the trays. Figure 2.12 shows a fall-out tray in position at a typical station.

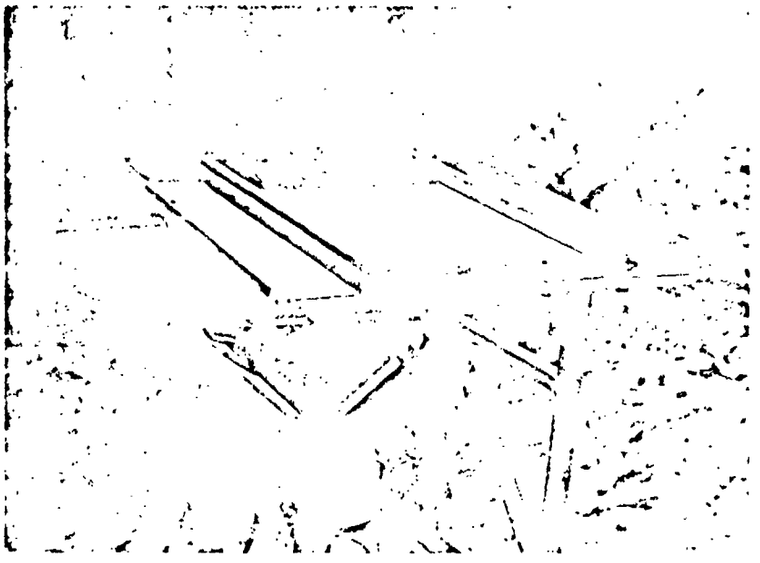

Fig. 2.12 Fall-out Tray Installed at a Typical Station. A filter sampler and a particle separator can also be seen.

[15]Roy D. Maxwell, Radiochemical Studies of Large Particles, Project 2.5a, Operation JANGLE, Army Medical Graduate School, Washington, D.C.

CHAPTER 3

EXPERIMENTAL PROCEDURE

3.1 STATION LAYOUT

On the basis of pre-shot meteorological data accumulated at the test site, 46 sampling stations were located for each shot as shown in Fig. 3.1 and 3.2. The general layout for each shot was the same, however minor changes in position were made to take advantage of differences in ground elevation. Equipment was secured to steel towers which were bolted to concrete foundations (this considerable overdesign of equipment was the result of the change from Operation WINDSTORM to JANGLE) within 4000 feet and wooden foundations beyond 4000 feet of the zero point. Sampling was done at 7 feet and 2 feet above the ground. Figures 2.11 and 3.3 illustrate the appearance of typical stations of this project.

3.2 DISTRIBUTION OF SAMPLING EQUIPMENT

The following items of sampling equipment were used:

1. Filter sampler
2. Cascade impactor
3. Conifuge
4. Particle separator
5. Electrostatic precipitator
6. Continuous air monitor
7. Portable air sampler
8. Fall-out tray

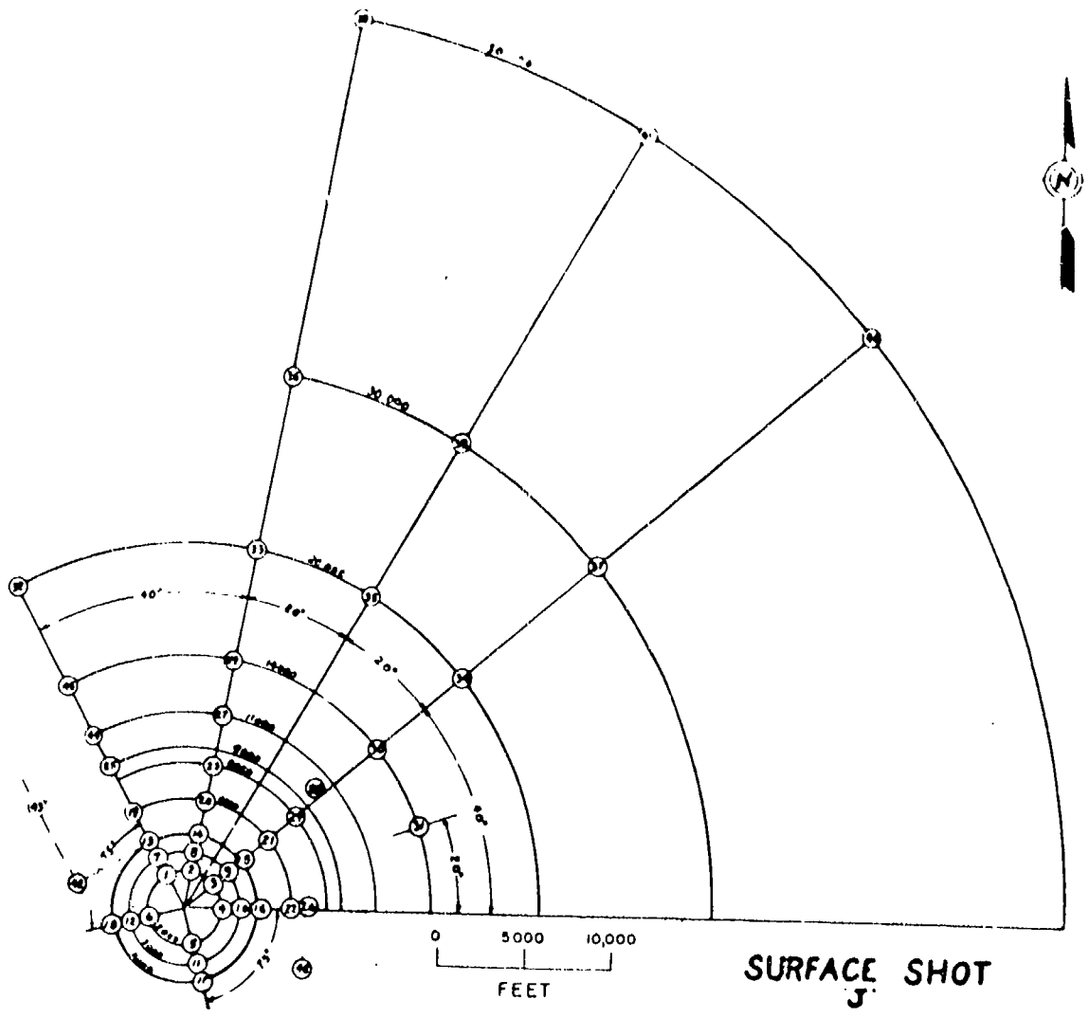

Fig. 3.1 Surface Shot Station Layout

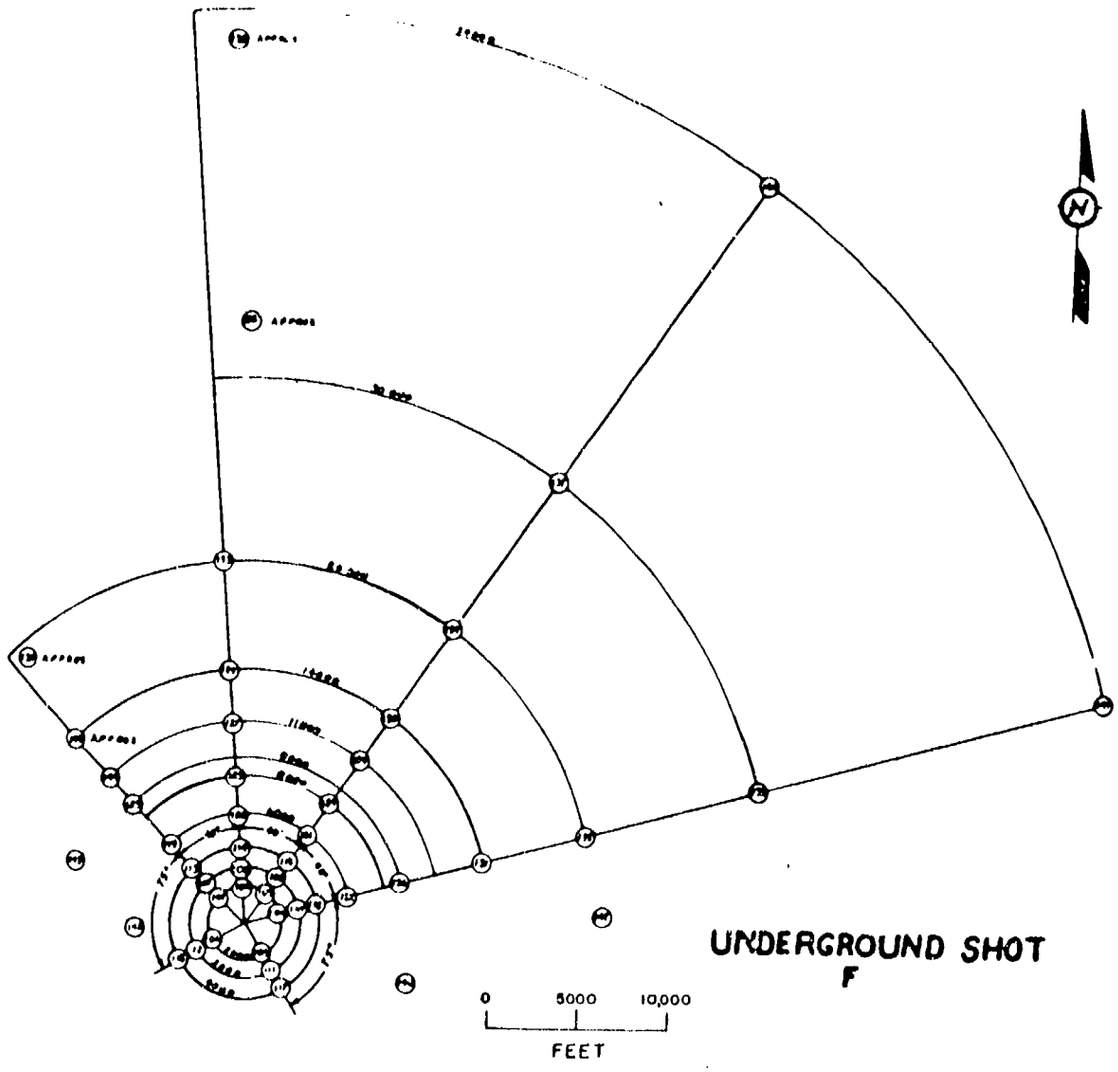

Fig. 3.2 Underground Shot Station Layout

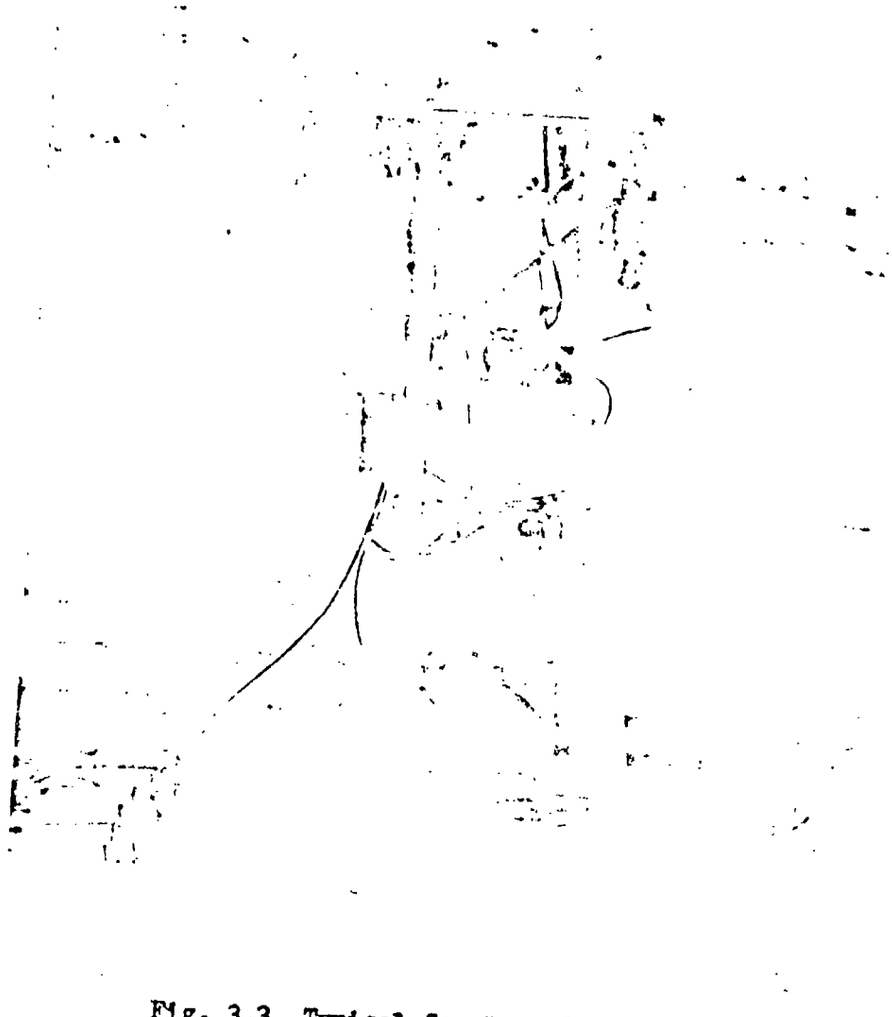

Fig. 3.3 Typical Sampling Station and Equipment. Ground Zero Can Be Seen.

TABLE 3.1

Location of Equipment

Instrument	Station Location
Filter Sampler	All stations; see Table 2.1
Cascade Impactor	13 14[a] 15 19 23 24 25 26 30 32 35[b] 40
Conifuge	13 14 15 19 22 23 24 25 26 30 32 35
Tracerlab Continuous Air Monitor	29 30 31 39 40 41
Brookhaven Continuous Air Monitor	36 37 38
Particle Separator	8 9 14 15 20 21 23 24 28 29 30
Electrostatic Preicpitator	33 34 129 130
Portable Air Sampler	14 20 21 27 28 33 36 39 119[b] 120[b] 121[b] 122
Fall-out Tray	1 2 3 4 7 10 14 15 16 19 21 22 23 24 27 29 30 31 33 34 36 37

(a) 3 instruments located here

(b) 2 instruments located here

Table 3.1 shows the manner in which the equipment was distributed. This distribution was based on a prior study of the weather, and the number of samplers available.

3.2.1 A Typical Station

The following instruments represent a typical tower installation; filter sampler, cascade impactor, conifuge, and particle separator. One 24 volt battery rated for 35 ampere hours was placed at each station for each piece of equipment requiring a 24-volt motor. Each motor required 10 ampere hours. One hundred and ten volt AC generators, rated at 3 KW were used at stations which required continuous air monitors, electrostatic precipitators or AC motors.

3.2.2 Triggering

At shot time minus 5 minutes a relay was closed by a signal which activated the clock relay and turned on the power supply.

It is of interest to discuss briefly the clock which controlled the sampling period of the instruments. Figure 3.6 shows the 8 day clock mechanism employed. It is of a type which can be set to open or close a relay for any hour of a particular day. Since shot time could not be accurately forecast, the following modifications were made to allow flexibility in the time of firing. One end of a rigid wire was fastened to the closing latch of a relay and the other end was inserted in the balance wheel of the mechanical clock; the clock was then wound and set so that the micro switches were closed and the relay was open. When the relay was closed at shot time minus five minutes, the rigid wire attached to the closing latch was pulled away from the balance wheel and the clock was started.

At shot time plus one hour and fifty-five minutes the clock mechanism opened the micro switch and caused the relay to open, disconnected the power supply, and stopped the sampling apparatus. Figure 3.5 gives the details of these circuits.

The cascade impactor required a separate timing device because it was necessary to sample for 1 minute when the cloud had arrived at the station. See Fig. 3.6. A longer sampling period would have provided excessive sample which could not be analyzed microscopically for particle size distribution.

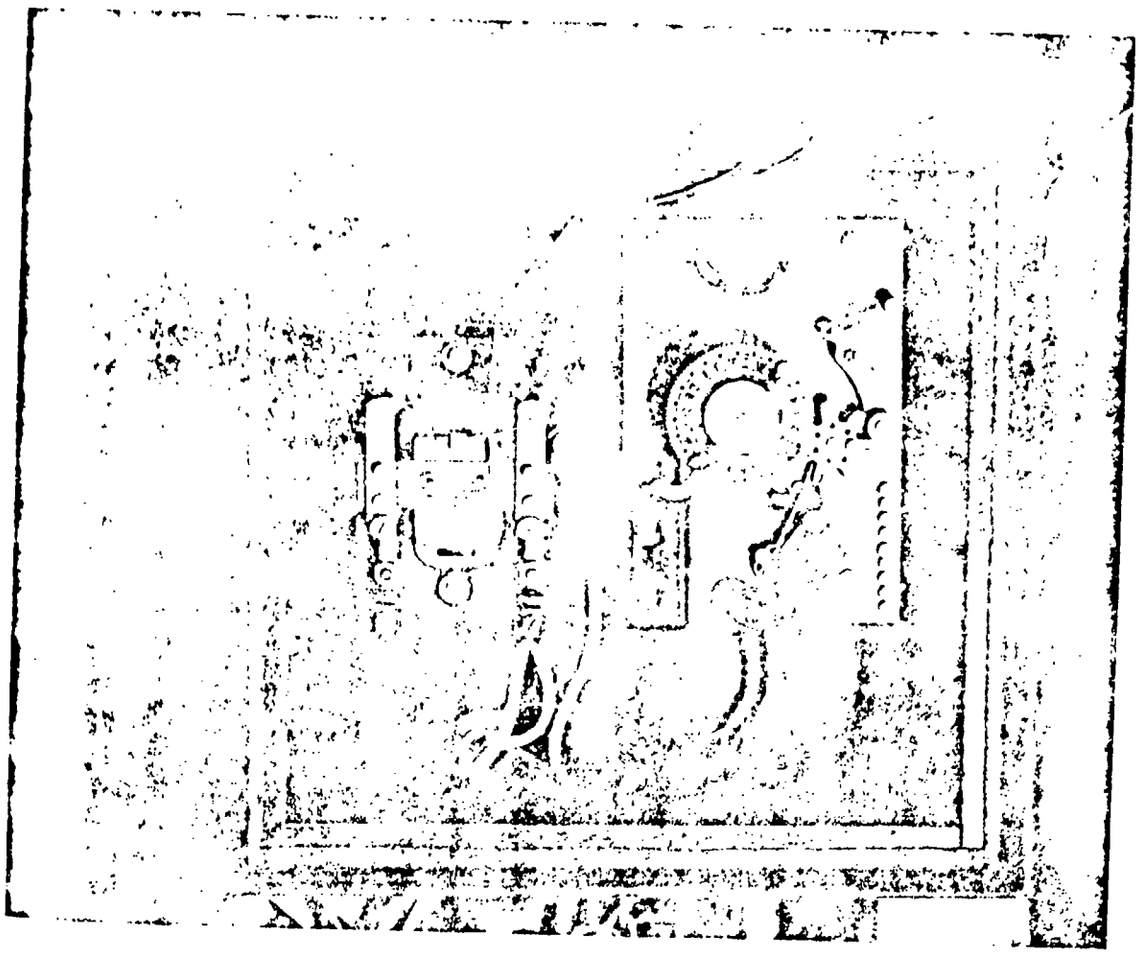

Fig. 3.4 Clock and Triggering Mechanism. The Rigid Wire Leads From the Relay to the Balance Wheel. When the Relay is Closed the Wire Was Withdrawn From the Balance Wheel, Starting the Timing of Equipment. The Outside Dimensions of the Box Are 10-1/2 by 10-1/2 Inches.

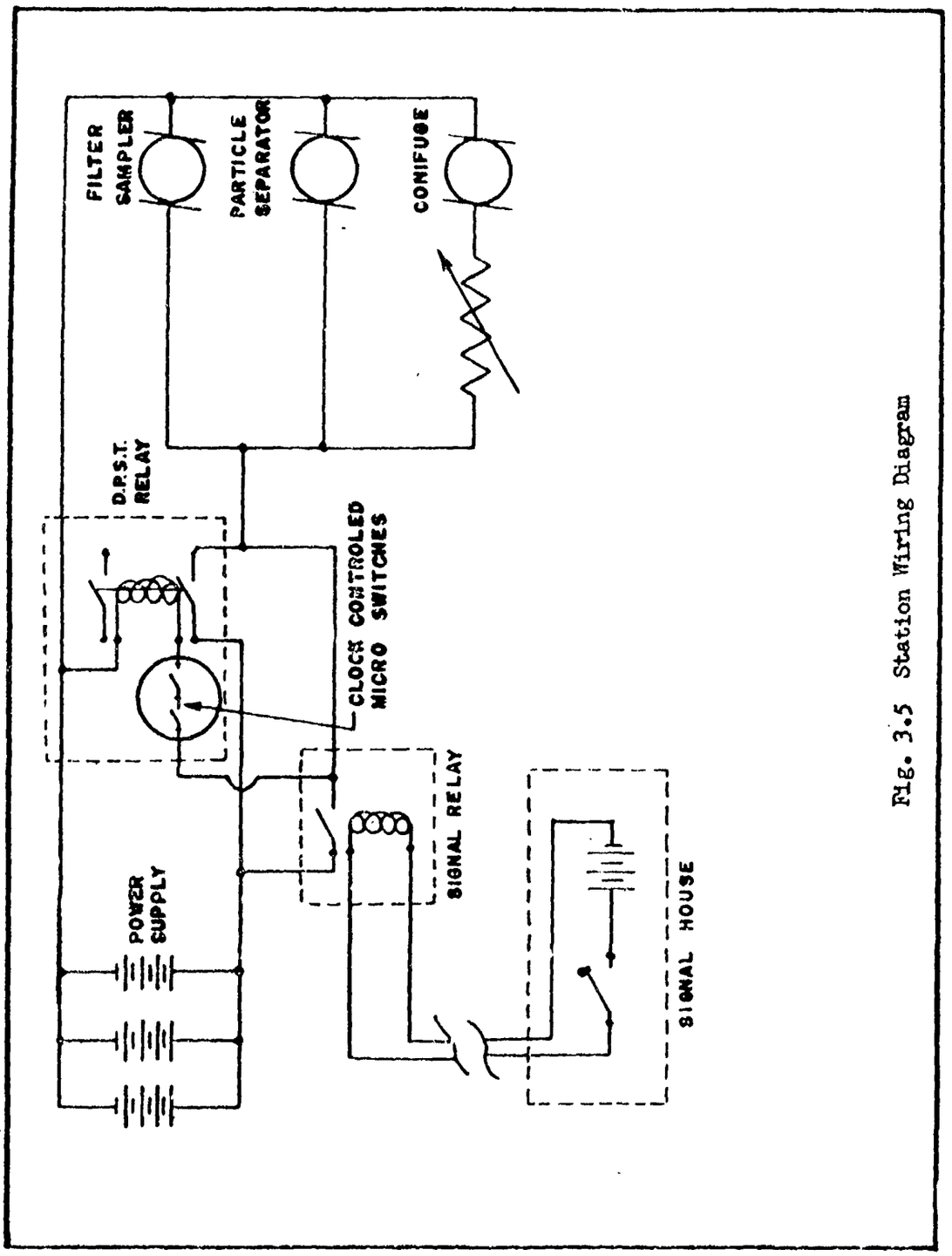

Fig. 3.5 Station Wiring Diagram

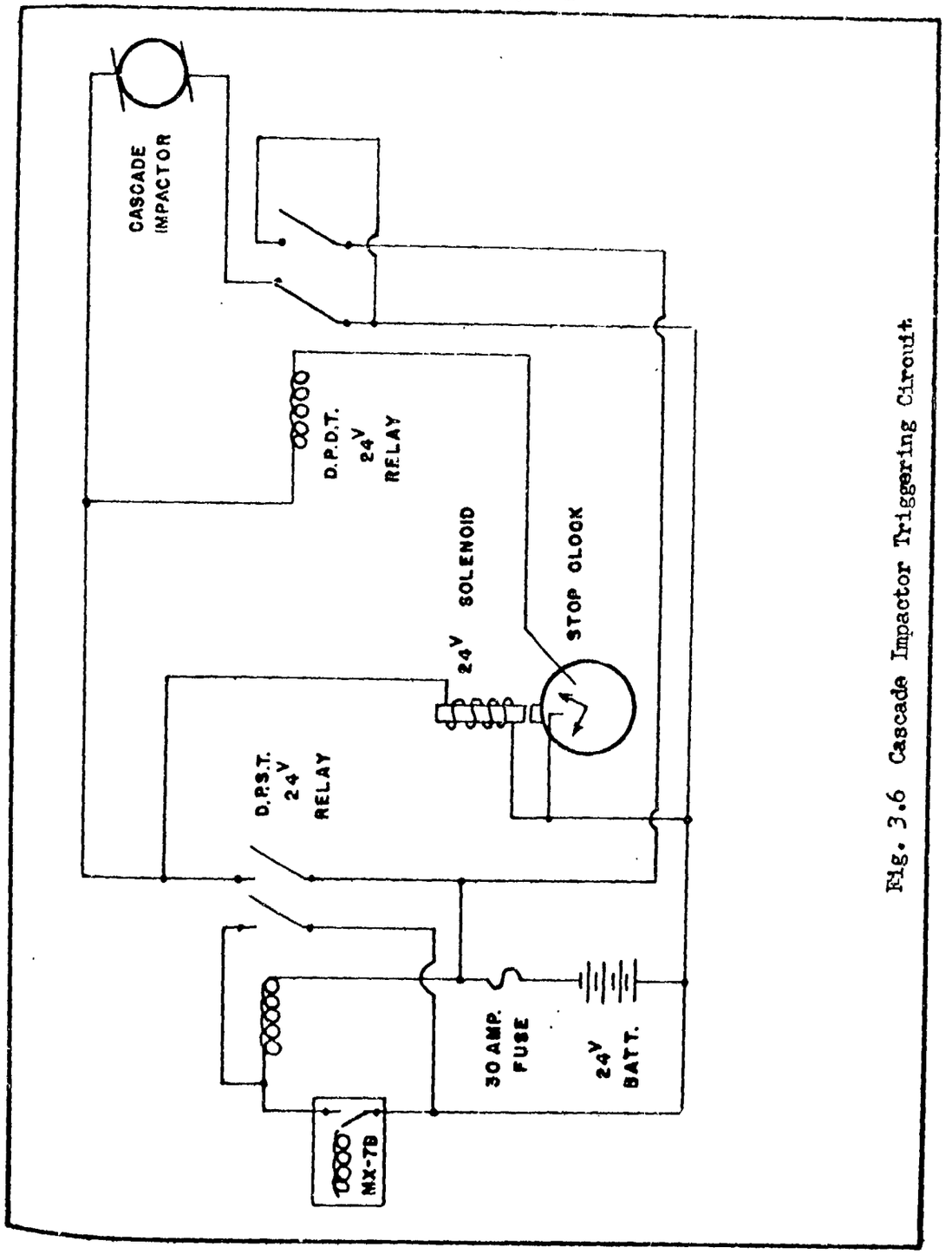

Fig. 3.6 Cascade Impactor Triggering Circuit

The triggering device was a Beckman MX-7B radiation detection alarm that was 50 per cent discharged and modified so that it would close a micro switch after being exposed to 50 milliroentgens. The alarm was placed on top of a tower and shielded in a well of lead brick, 8 inches thick and open at the top, thus it would presumably only be discharged by the radiation from the cloud.

After the cloud radiation discharged the MX-7B and closed the micro switch, the power relay was closed and supplied power from the 24 volt battery. The left pole of the relay upon closing shunted the MX-7B micro switch out of the circuit thus eliminating the possibility of its opening due to low current capacity and causing the circuit to function improperly. The right pole of the relay performed two functions upon closing; it connected one side of the battery to the cascade impactor motor and started the cascade impactor since the other side of the battery was connected to the motor through the left pole of the relay, and it also placed the clock solenoid coil across the battery. When this solenoid was placed across the battery it drove the plunger against the start button of the mechanical stop clock and started the clock. The sweep hand of the clock was arranged so that after one minute it came in contact with a terminal connected to one side of the battery and thus placed the coil of the relay across the battery through the sweep hand and threw the relay to the position opposite of that shown in Fig. 3.6. This action opened the cascade impactor circuit and at the same time shorted the terminals of the battery across the 30 ampere fuse; the fuse blew, and the battery was removed from the circuit eliminating the chance of the circuit recycling.

3.3 COLLECTION AND SHIPMENT OF SAMPLES

3.3.1 Surface Shot

Sample collections started after 4 hours and were completed within 30 hours after detonation. Rapid collection was possible due to the fact that all stations were lightly contaminated with the exception of those stations in the north-north east sector. Collections along these "legs" were deferred for approximately 20 hours to permit the area to "cool off". No pick-up team accumulated more than a 1 roentgen for the test; the maximum allowable dose for each test being 3 roentgens.

The collection of samples was accomplished by 8 groups; each consisting of a group leader, assistant, and a radiological safety

monitor; and each responsible for approximately 6 stations. Individuals wore protective clothing furnished by the radiological safety organization at the test site. This consisted of cotton-khaki coveralls, white skull cap, gloves, booties, respirator, and masking tape to seal the trouser-bootie opening. Personnel handled the sampling instruments with gloves. Filter sampler papers and portable air samplers were placed in wooden boxes and returned to the project office at the test site. The National Institute of Health (NIH) laboratory at the test site started activity measurements on filter sampler papers approximately 12 hours after shot time and completed measurements within approximately 48 hours.

Cascade impactors, conifuges, and particle separators were removed from the towers and the impactor slides and conifuge liners were removed in a dust-free room.

All samples were shipped in wooden boxes by military air to either the Army Chemical Center, Md. or Tracerlab, Inc., Boston, Mass., and analytical work was started approximately 5 days after shot time.

3.3.2 Underground Shot

Sample collections were started 6 hours after shot time and were completed 4 days later. Slow collection was necessitated by the fact that many stations were heavily contaminated. As in the surface shot, the heaviest contamination occurred in the north-north east sector, and entry into this area was delayed about 4 days.

The procedure of handling samples on this test was similar to the surface shot. Activity measurements were started 12 hours after detonation.

3.4 TREATMENT OF SAMPLES AT ACC

Shipments received at the Army Chemical Center were opened, disassembled, and distributed for analysis among the various groups in the Chemical and Radiological Laboratories according to a prearranged plan. Cascade impactor plates and conifuge cones were removed in a dust-free room and alalyzed for activity and particle size. Laboratory analysis started approximately 8 hours after the receipt of samples at the ACC.

Page 44, blank

CHAPTER 4

DATA AND RESULTS

4.1 CONCENTRATION OF ACTIVITY IN THE AEROSOL

4.1.1 Filter Sampler

Approximately 46 filter samplers were employed in each shot of Operation JANGLE to obtain samples of the aerosol from which activity concentration data could be derived. As described in paragraph 2.1, these instruments sampled for a period of from 5 minutes before to 115 minutes after shot time, and yielded basic data in the form of filter papers upon which was deposited a measurable amount of radioactivity.

The average concentration of activity at each station over the interval H/0 to H/115 minutes could be computed by dividing the measured activity (corrected for decay) by the volume of air sampled in 115 minutes. However, in order to obtain the concentration of activity in the cloud, it was necessary to know when and how long the instrument actually sampled the cloud, information not obtainable from the filter sampler itself. It was originally planned to determine these quantities by an examination of aerial photographs and the NBS gamma intensity data (Project 2.1a), but after careful study of records from both these sources the conclusion was reached that this determination would be possible for only five stations, all in the Underground shot. The difficulty arose in defining the "edge" of the complicated cloud structure either visually, or in terms of the gamma intensity. This was particularly true for times later than about 15 minutes after either shot, and for directions other than downwind. For example, from the photographs, it appeared that many crosswind stations never sampled the cloud, even though fair amounts of radioactivity were found on the filter papers from these stations.

To estimate the concentration of activity in the cloud, then, it was first necessary to estimate when and how long each filter sampler sampled the cloud proper. This has been done by assuming a reasonable model of the cloud, based upon the data obtained from aerial photographs, and calculating when this cloud arrived and departed from each station. The elapsed time and length of sampling time were then calculated and compared with the figures used to calculate the 115 minute concentrations, resulting in factors which could be applied to the latter to give the concentration in the cloud

proper. These factors were employed in order to emphasize the effect of these calculations. It should be noted that the cloud model, because of the restrictive assumptions regarding its size, was applied only to the downwind stations.

The following is a description of the cloud model:

At zero time a cloud of diameter d_o is rapidly created. This cloud drifts downwind in a straight line, the velocity of the center of the cloud V being a constant 5 mph, or 440 feet per minute. The subsequent cloud diameter d increases with time, and hence with distance from ground zero r according to the equation:

$$d = d_o + 0.1(r)$$

The arrival time of the front edge of the cloud at station whose distance from ground zero is r is:

$$t_1 = \frac{r - d/2}{V}$$

and the arrival time of the rear edge of the cloud

$$t_2 = \frac{r + d/2}{V}$$

The length of time of sampling is

$$t_2 - t_1 = \frac{d}{V}$$

The elapsed time between zero time and the time at which this sampling took place has been chosen as

$$H + \sqrt{t_1 t_2}$$

The observed initial diameter of the cloud was:

Surface Shot = 880'
Underground Shot = 3750'

Table 4.1 presents the results of these calculations for the appropriate distances from ground zero. The factor f_1 in column 5 is the ratio of the 115 minute sampling period to the sampling period determined on the basis of the model:

$$f_1 = \frac{115}{t_2 - t_1}$$

The factor f_2 in column 7 is the activity correction that must be applied to correct the activity from H/60 min. (see next paragraph) to $H / \sqrt{t_1 t_2}$ minutes. The product $f_1 f_2$, therefore, is the correction factor that must be applied to the 115 minute concentration data to obtain the approximate concentration on the cloud proper. Table 4.1 also gives the arrival of the front and rear edges, respectively, of the cloud at the only stations where these could be observed from the aerial photographs.

Tables 4.2 and 4.3 present the average concentration of activity over the 115 minute sampling period, (col. 3) together with the data required for this determination (Cols. 1 and 2). It will be noted that the selection of H/60 minutes as the time to which the activity for all stations is corrected is an arbitrary selection. The 115 minute concentrations have been plotted on a station layout in Figs. 4.1 and 4.2. From these plots stations were selected at which the concentration of the activity in the cloud was calculated. The latter concentrations and the factors which produced them are listed in cols. 4 and 5 in Tables 4.2 and 4.3.

Activity measurements were made on Chemical Corps type 6 filter paper initially by NIH at the Nevada Test Site within 100 hours after each shot, using a Model PC-1 proportional counter made by the Nuclear Measurement Corporation. Second and third papers were radioautographed in many cases and found to be free from activity. In the few cases where activity was observed, it was attributed to leakage through the edges of the filter paper package since the filter paper is 99.97 per cent efficient for 0.3 micron particles at a flow rate of 32 liters per minute through 100 square centimeters area.

TABLE 4.1

Calculation of Sampling Interval and Elapsed Time
on the Basis of Cloud Model

r (feet)	t_1 (min)	t_2 (min)	t_2-t_1 (min)	f_1	$\sqrt{t_1 t_2}$ (min)	f_2	$f_1 f_2$
			Surface Shot				
2,000	3.3	5.8	2.5	46	4.3	24	1.1×10^3
3,000	5.5	8.2	2.7	43	6.7	14	6.0×10^2
4,000	7.6	10.5	2.9	39	8.9	10	3.9×10^2
6,000	11.9	15.3	3.4	34	13.5	6.1	2.1×10^2
8,000	16.3	20.1	3.8	30	18.1	4.2	1.3×10^2
11,000	22.8	27.3	4.5	26	25.0	2.9	7.5×10^1
14,000	29.2	34.4	5.2	22	31.7	2.2	4.8×10^1
20,000	42.1	48.7	6.6	17	45.4	1.4	2.4×10^1
30,000	63.7	72.5	8.8	13	68.0	.86	1.1×10^1
50,000	107.	120.	13.	8.8	113.0	.45	3.9
			Underground Shot				
2,000	.9*	9.2*	8.3	13.9	3.0	37	5.2×10^2
3,000	2.3 2.1*	11.4* 11.5	9.1	12.6	5.1	19	2.4×10^2
4,000	4.4 4.1*	13.7 13.7*	9.3	12.4	7.8	12	1.5×10^2
6,000	8.8 8.5*	18.5 18.3*	9.7	11.8	12.8	6.5	7.7×10^1
8,000	13.1	23.3	10.2	11.3	17.5	4.4	5.0×10^1
11,000	19.6	30.5	10.9	10.5	24.5	2.9	3.0×10^1
14,000	26.0	37.6	11.6	9.9	31.3	2.2	2.2×10^1
20,000	39.0	51.9	12.9	8.9	45.0	1.4	1.2×10^1
30,000	Y60.6	75.7	15.1	7.6	67.8	.86	6.5
50,000	102.	123.	21.0	5.5	112.0	.47	2.6

* Values observed from aerial photographs.

TABLE 4.2

Filter Sampler Concentration of Activity, Surface Shot

Station	Activity at H + 60 minutes μc	Volume Sampled Between Zero and H + 115 min. $cm^3 \times 10^6$	Average Conc. of Activity over 115 min. $\frac{\mu c}{cm^3}$	Factor $f_1 f_2$	Conc. of Activity in Cloud $\frac{\mu c}{cm^3}$
1	4.3×10^{-1}	4.1	1.0×10^{-7}	1.1×10^{3}	1×10^{-2}
2*	8.1	4.6	1.7×10^{-6}	1.1×10^{3}	2×10^{-3}
3	2.1	4.4	4.4×10^{-7}		
4*	1.0	2.5	4.1×10^{-7}		
5	7.8×10^{-3}	2.8	2.7×10^{-9}		
6*	1.9×10^{-2}	4.6	4.2×10^{-9}		
7	3.3	4.2	7.9×10^{-7}	6.0×10^{2}	5×10^{-4}
8	2.5	4.8	5.2×10^{-7}	6.0×10^{2}	3×10^{-4}
9	5.6×10^{-1}	4.3	1.3×10^{-7}		
10	5.6×10^{-1}	2.0	2.7×10^{-7}		
11	6.9×10^{-4}	4.1	1.6×10^{-10}		
12	1.2×10^{-3}	4.7	2.7×10^{-10}		
13		3.8		3.9×10^{2}	
14	2.2	4.1	5.3×10^{-7}	3.9×10^{2}	2×10^{-4}
15*	9.9×10^{-1}	4.0	2.5×10^{-7}		
16	9.1×10^{-1}	3.1	3.0×10^{-7}		
17	0	4.3	0		
18	4.9×10^{-4}	4.5	1.1×10^{-10}		
19	1.6	11.1	1.4×10^{-7}		
20		9.7		2.1×10^{2}	
21	4.4	11.0	3.9×10^{-7}		
22	4.8	11.7	4.1×10^{-7}		
23	1.4×10^{1}	10.6	1.4×10^{-6}	1.3×10^{2}	2×10^{-4}
24	4.7	9.3	5.1×10^{-7}		
25*	1.3×10^{-1}	9.6	1.4×10^{-8}		
26	4.1	12.1	3.4×10^{-7}		
27	1.6×10^{-1}	11.6	1.4×10^{-6}	7.5×10^{1}	1×10^{-4}
28	6.6×10^{-3}	11.0	6.0×10^{-10}		
29	2.6×10^{1}	11.3	2.3×10^{-6}	4.8×10^{1}	1×10^{-4}
30	4.7	7.7	6.1×10^{-7}		
31*	6.6×10^{-3}	8.9	7.4×10^{-10}		
32	7.8×10^{-3}	12.0	6.5×10^{-10}		
33		11.9			
34	3.6	10.2	3.5×10^{-7}		
35	4.5	10.6	4.3×10^{-7}		
36	4.7	11.9	3.9×10^{-7}	1.1×10^{1}	4×10^{-6}
37*	2.6×10^{-1}	12.0	2.2×10^{-8}		

* Instrument did not function properly.

TABLE 4.2 (Contd)

Station	Activity at H + 60 minutes μc	Volume Sampled Between Zero and H + 115 min. $cm^3 \times 10^6$	Average Conc. of Activity over 115 min. $\frac{\mu c}{cm^3}$	Factor $f_1 f_2$	Conc. of Activity in Cloud $\frac{\mu c}{cm^3}$
38	1.8	8.6	2.1×10^{-7}		
39	4.1	10.6	3.8×10^{-7}	3.9	1×10^{-6}
40	1.3	8.3	1.6×10^{-7}		
41*	2.8×10^{-2}	10.2	2.7×10^{-9}		
42	5.1×10^{-1}	9.0	5.7×10^{-8}		
43	0	8.1	0		
44	4.7×10^{-3}	8.2	5.7×10^{-10}		
45	3.2×10^{-3}	11.4	2.8×10^{-10}		
46	2.8×10^{-1}	10.2	2.8×10^{-8}		

* Instrument did not function properly.

TABLE 4.3

Filter Sampler Concentration of Activity, Underground Shot

Station	Activity at H + 60 minutes μc	Volume Sampled Between Zero & H + 60 Min $cm^3 \times 10^6$	Average Conc. of Activity over 115 min. $\frac{\mu c}{cm^3}$	Factor $f_1 f_2$	Conc. of Activity in Cloud $\frac{\mu c}{cm^3}$
101				5.2×102	
102	3.6×10^2	4.6	7.7×10^{-5}	5.2×102	4×10^{-2}
103		4.4			
104	5.5×10^{-1}	2.5	2.1×10^{-7}		
105	8.5×10^{-1}	2.8	3.0×10^{-7}		
106	4.0	4.6	8.6×10^{-7}		
107	4.4×10^2	4.2	1.0×10^{-4}	2.4×10^2	2×10^{-2}
108	4.6×10^3	4.8	9.5×10^{-4}	2.4×10^2	2×10^{-1}
109	2.9×10^2	4.3	6.8×10^{-5}		
110	5.2×10^{-1}	2.0	2.5×10^{-7}		
111	1.2×10^2	4.0	2.9×10^{-5}		
112	2.8	4.6	6.1×10^{-7}		
113		3.8		1.5×10^2	
114	1.1×10^2	4.1	2.8×10^{-5}	1.5×10^2	4×10^{-3}

TABLE 4.3 (Contd)

Station	Activity at H + 60 minutes μc	Volume Sampled Between Zero & H + 60 Min $cm^3 \times 10^6$	Average Conc. of Activity over 115 min. $\frac{\mu c}{cm^3}$	Factor $f_1 f_2$	Conc. of Activity in Cloud $\frac{\mu c}{cm^3}$
115	6.7×10^{1}	4.0	1.6×10^{-5}		
116	7.3×10^{-2}	3.0	2.4×10^{-8}		
117	2.2	4.2	5.3×10^{-7}		
118	1.2	4.4	2.6×10^{-7}		
119	1.2×10^{1}	11.1	1.1×10^{-6}		
120	4.5×10^{2}	9.7	4.7×10^{-5}	7.7×10^{1}	4×10^{-3}
121	4.3×10^{2}	11.0	3.9×10^{-5}		
122	2.6×10^{-2}	11.7	2.2×10^{-9}		
123	1.1×10^{4}	10.6	1.0×10^{-3}	$50. \times 10^{-1}$	5×10^{-2}
124	4.0×10^{2}	9.2	4.3×10^{-5}		
125	2.9×10^{1}	9.6	3.0×10^{-6}		
126		12.1			
127	7.4×10^{3}	11.6	6.4×10^{-4}	3.0×10^{1}	2×10^{-2}
128	1.4×10^{2}	11.0	1.3×10^{-5}		
129	8.8×10^{3}	11.3	7.8×10^{-4}	2.2×10^{1}	2×10^{-2}
130	7.5×10^{1}	7.6	9.8×10^{-6}		
131		8.9			
132	2.8	12.0	2.3×10^{-7}		
133		11.8		1.2×10^{1}	
134	2.9	10.1	2.8×10^{-7}		
135		10.6			
136		11.9		6.5	
137	4.6	12.0	3.8×10^{-7}		
138		8.5			
139	1.0×10^{2}	10.6	9.9×10^{-6}	2.6	3×10^{-5}
140	9.2	8.2	1.1×10^{-6}		
141		10.1			
142	2.1	9.0	2.4×10^{-7}		
143	7.9	8.0	9.8×10^{-7}		
144	2.2×10^{1}	8.2	2.6×10^{-6}		
145	3.7×10^{-1}	11.4	3.2×10^{-8}		
146	9.6×10^{-3}	10.1	9.4×10^{-10}		
147	9.9×10^{-1}	11.0	9.0×10^{-8}		

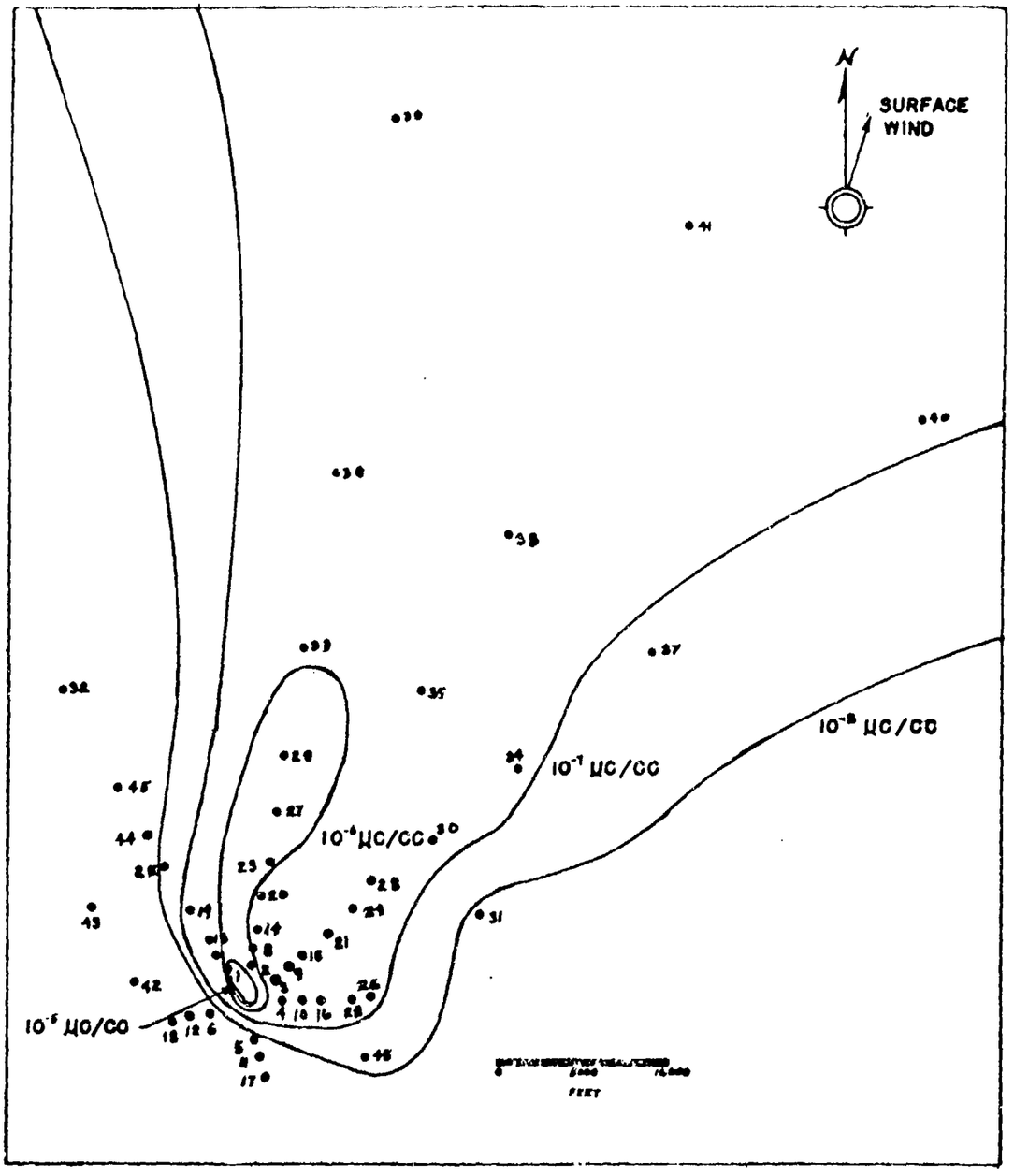

Fig. 4.1 Lines of Fqual Concentration of Activity, Surface Shot Activity Corrected to H + 1 Hours, Sampling Time 115 Minutes.

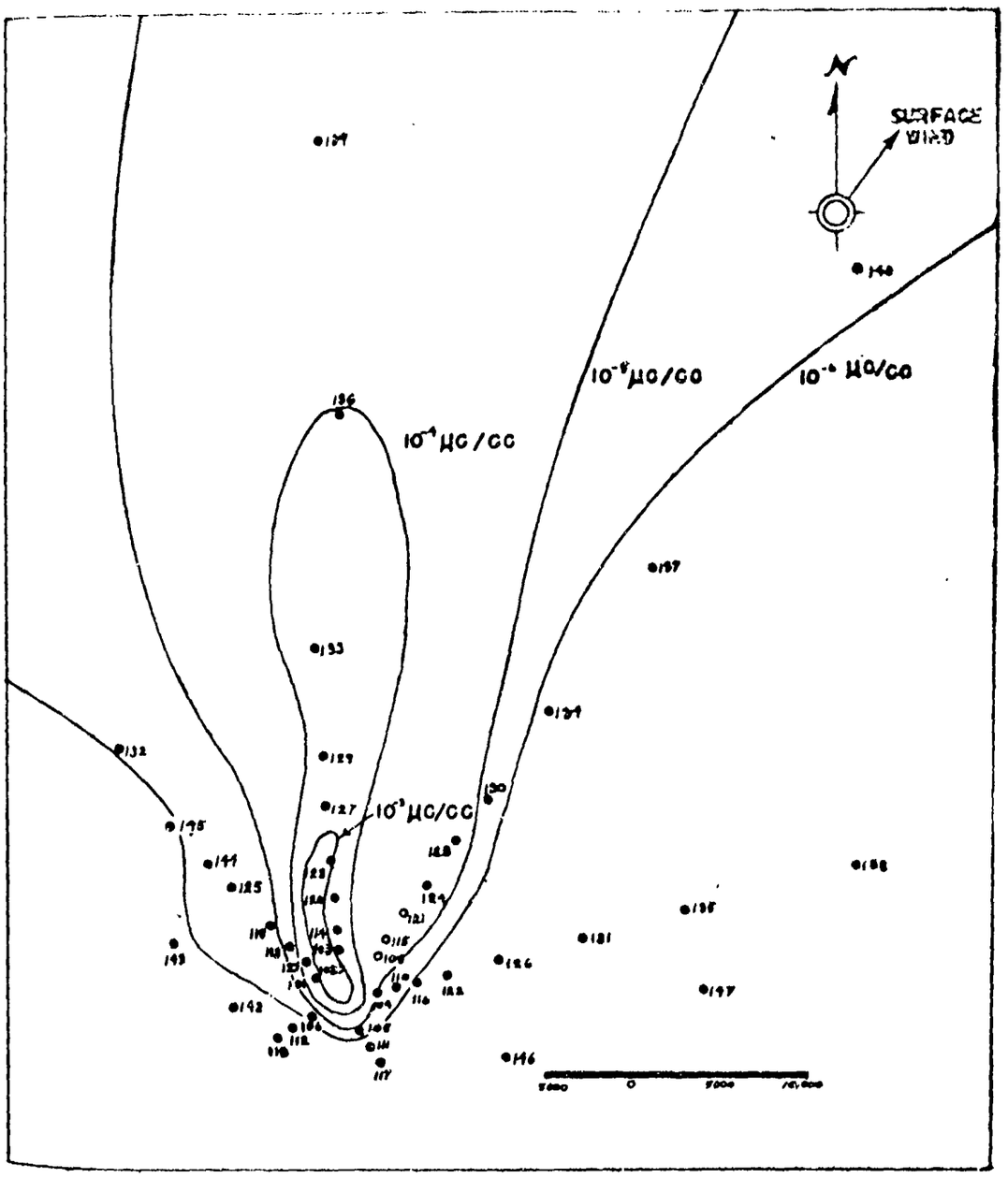

Fig. 4.2 Lines of Equal Concentration of Activity, Underground Shot. Activity Corrected to H + 1 Hours, Sampling Time 115 Minutes.

PROJECT 2.5a-1

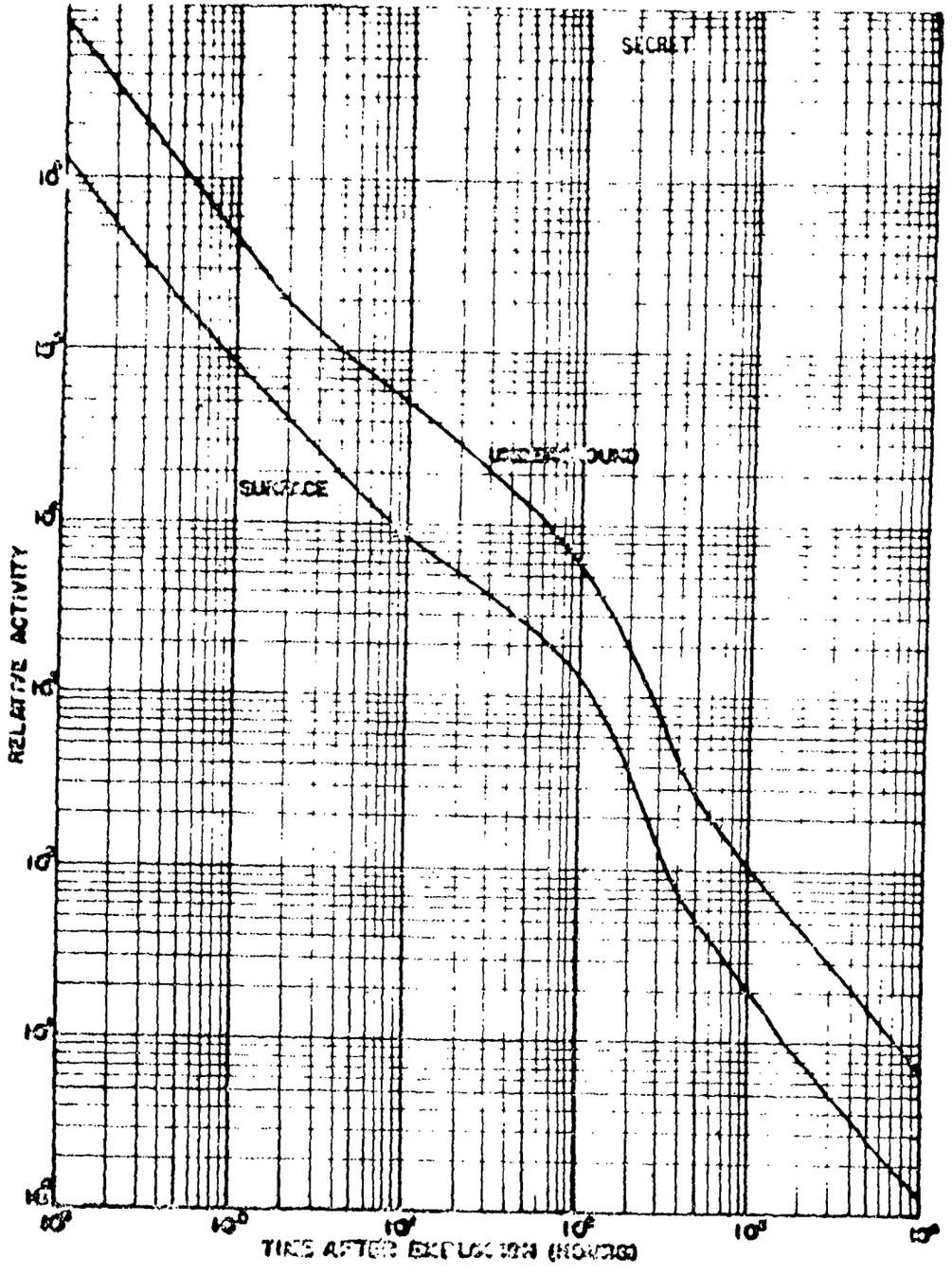

Fig. 4.3 Beta Decay Curves Obtained By NIH From Crater Lip Samples.

All activities were corrected to a common time by means of a decay curve obtained from a single station. Unfortunately approximately 40 per cent of the filter papers from both shots were too active to be counted by NIH; these were sent by military aircraft either to Tracerlab or to ACC, where they were counted between 120 and 600 hours after the shot. At these two laboratories activity measurements were corrected to a common time (ACC, H/400 hours, Tracerlab, H/600 hours) by means of the decay curves from the individual filter samplers.

Extrapolation of activity data back to very early times, was accomplished by use of the decay curves obtained by NIH[1] from crater and lip samples. These are presented in Fig. 4.3. The experimental data from which these curves were derived began at approximately H/4 hours and continued to about H/2000 hours. Extrapolations have been made to H/0.1 and H/10,000 hours.

Wherever possible the decay slopes from these "master" curves were compared with the decay slopes obtained at various time intervals from several filter samplers and various other equipment and agreement was considered satisfactory. Exact agreement is not achieved because of fractionation (See Par. 4.5.3) which influences the decay slope of samples taken at various distances from ground zero. The use of a single decay curve for all the filter sampler data thus introduces an error in the extrapolated activities.

4.1.2 Air Monitors

Three Brookhaven continuous air monitors (BCAM) and six Tracerlab continuous air monitors (TCAM) were employed to measure the radioactivity of the aerosol for both shots of Operation JANGLE. Table 4.4 summarizes their operation. It can be seen that a large number of failures occurred which were attributed either to failure of the 110 volt motor generator set[2], or mechanical failures of the instruments themselves. These latter difficulties were largely due to the delicate nature of the monitors under the severe conditions of the Nevada Test Site and the receipt of the TCAMs only a week prior to the surface shot.

For the surface shot, the BCAM at station 38 (30,000 ft. NE and defiladed by a ridge from the zero point) furnishes an interesting record as shown in the "raw" data plotted in Fig. 4.4. Of particular interest is the occurrence of a "pip" approximately 5 minutes after

[1] Letter from NIH, dated 7 February 1952.

[2] The large quantities of fine dust at the Test Site tended to rapidly foul the spark plugs.

TABLE 4.4

Air Monitor Operation for Surface and Underground Shots

Station Number	Instrument	Operation
36	BCAM	Defective rate meter prior to test
37	BCAM	Motor generator failure
38	BCAM	Vacuum leak, qualitative data
29	TCAM	Satisfactory
30	TCAM	Shear pin failure, data obtained
31	TCAM	Motor generator failure
39	TCAM	Satisfactory although off scale
40	TCAM	Mechanical failure
41	TCAM	Motor generator failure
136	BCAM	Motor generator failure
137	BCAM	Capstan frozen to sampling port
138	BCAM	Imperfect filter paper
129	TCAM	Mechanical failure
130	TCAM	" "
131	TCAM	" "
139	TCAM	Recorder broken, replay data obtained
140	TCAM	Satisfactory
141	TCAM	Satisfactory but low concentration

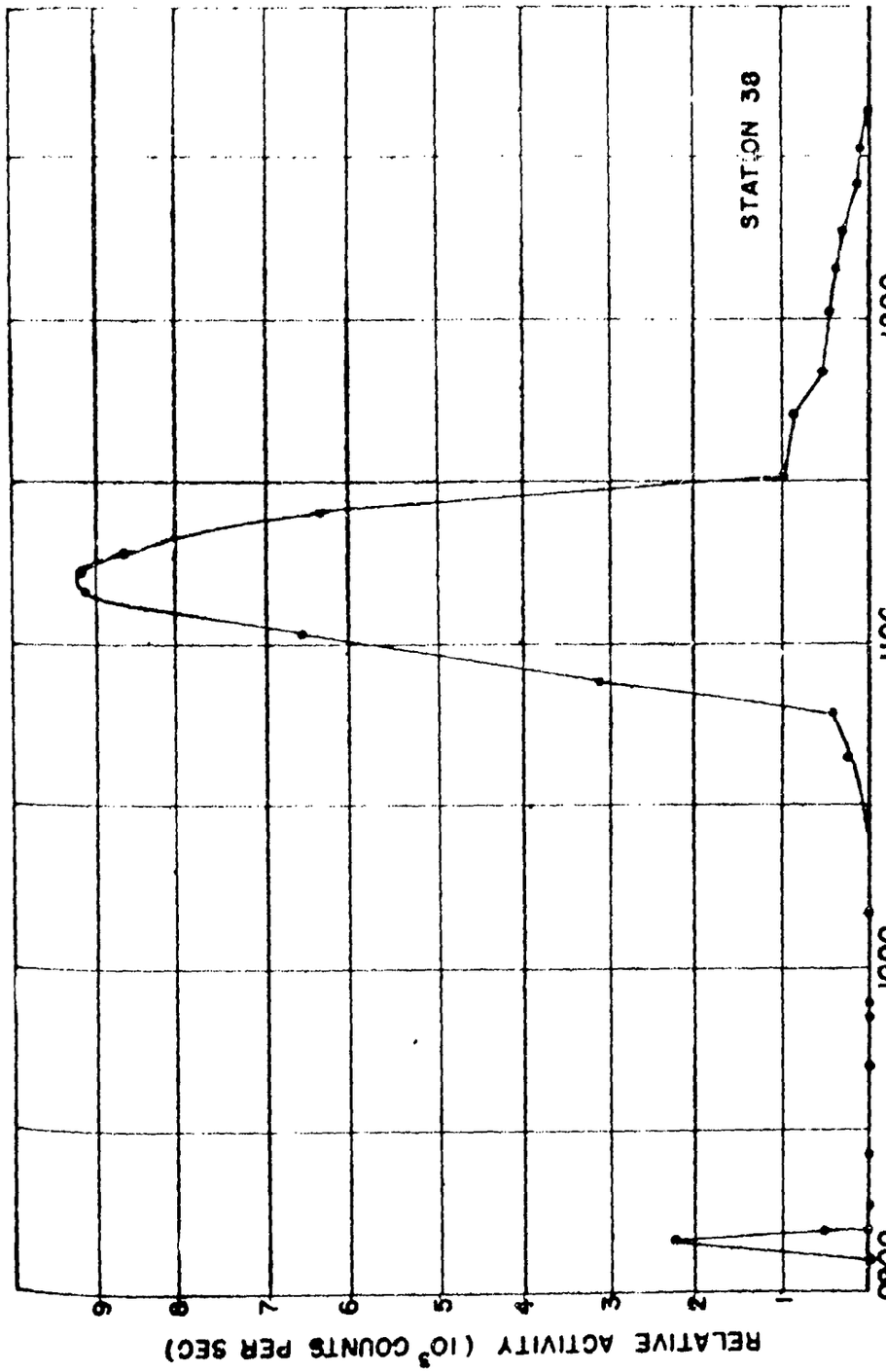

Fig. 4.4 Raw Counting Data from a BCAM at Station 38.

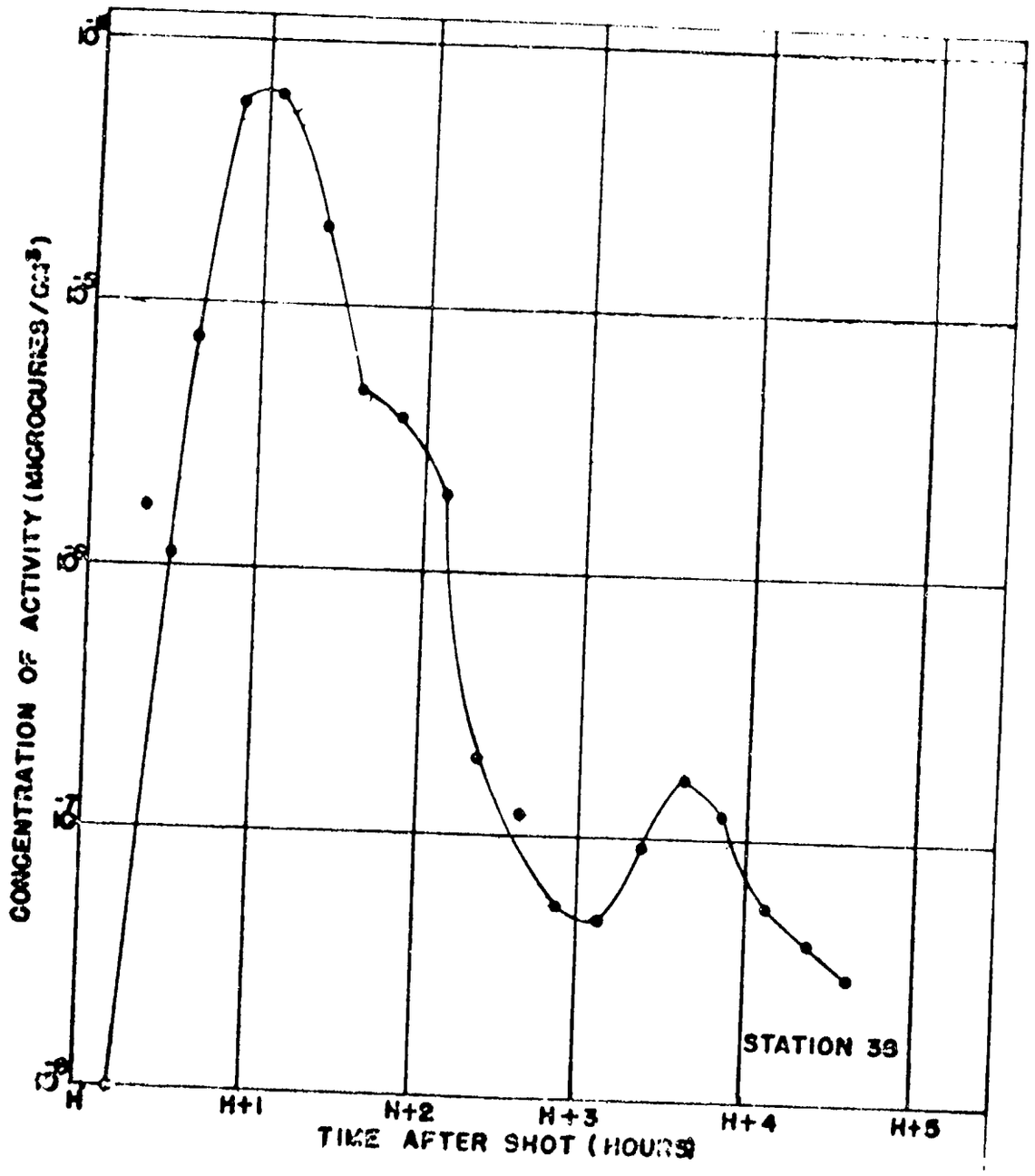

Fig. 4.5 Approximate Concentration of Activity at Station 38.

zero time (0900 hours PST). This "pip" appears to be identifiable only as external gamma radiation from an overhead cloud whose average speed was about 20 mph[3]. Fig. 4.5 presents the same data converted to microcuries per cubic centimeter by the methods described in Appendix B together with appropriate allowances to instrument time lag. The maximum at 1000 hours corresponds to a ground-level cloud speed of about 5 mph. Unfortunately the exact flow rate through the instrument is in doubt due to damage to the vacuum line right angle bend which could not be repaired prior to the zero hour so that the data of Fig. 4.5 must be regarded as approximate. It is interesting to note that the rate of change of the ground-level cloud activity concentration appears to have been as rapid as the BCAM was able to measure. It would thus appear that the BCAM in its present form is not well suited to monitor such rapidly changing concentrations.

For the surface shot, the Tracerlab Continuous Air Monitor (TCAM) at station 29 furnished a record of events which are plotted in Fig. 4.6. The cloud apparently arrived about an hour after shot time and either remained there for a number of hours, or as appears more likely, gamma radiation from local fall-out contributed a significant count rate to the instrument.

The TCAM at station 30 failed when a shear pin in the paper drive mechanisms broke, causing the monitor to sample on one spot of filter paper. However, the beta activity concentrations were readily obtained by graphical differentiations[4] of the recorded counts per minute, dividing by the volumetric flow rate, and applying the efficiency factor for a uniformly contaminated tape as derived in Appendix C. This record is presented in Fig. 4.7. The sharp changes of activity concentrations in the ground-level cloud can be especially well seen here since no instrument time lag or averaging error exists for these data.

Due to a pre-shot estimate that the 20,000 c/m beta scale was most desirable for a distant station, the TCAM at surface shot station 39 went off scale ($> 44 \times 10^{-7}$ uc/cc) at about H/1.5 hours and remained there until the record was retrieved by the pick-up crew on 20 November. The count rate record obtained is shown in Fig. 4.8. Of especial interest

---

[3] A ground-level cloud could not have been sampled on the tape and register as early as 0915. See paragraph 2.6.2 for time lag discussion.

[4] It may be noted that while a moving air monitor filter tape furnishes an averaged concentration directly, the derivative of the record obtained from a stationary tape gives instantaneous concentrations.

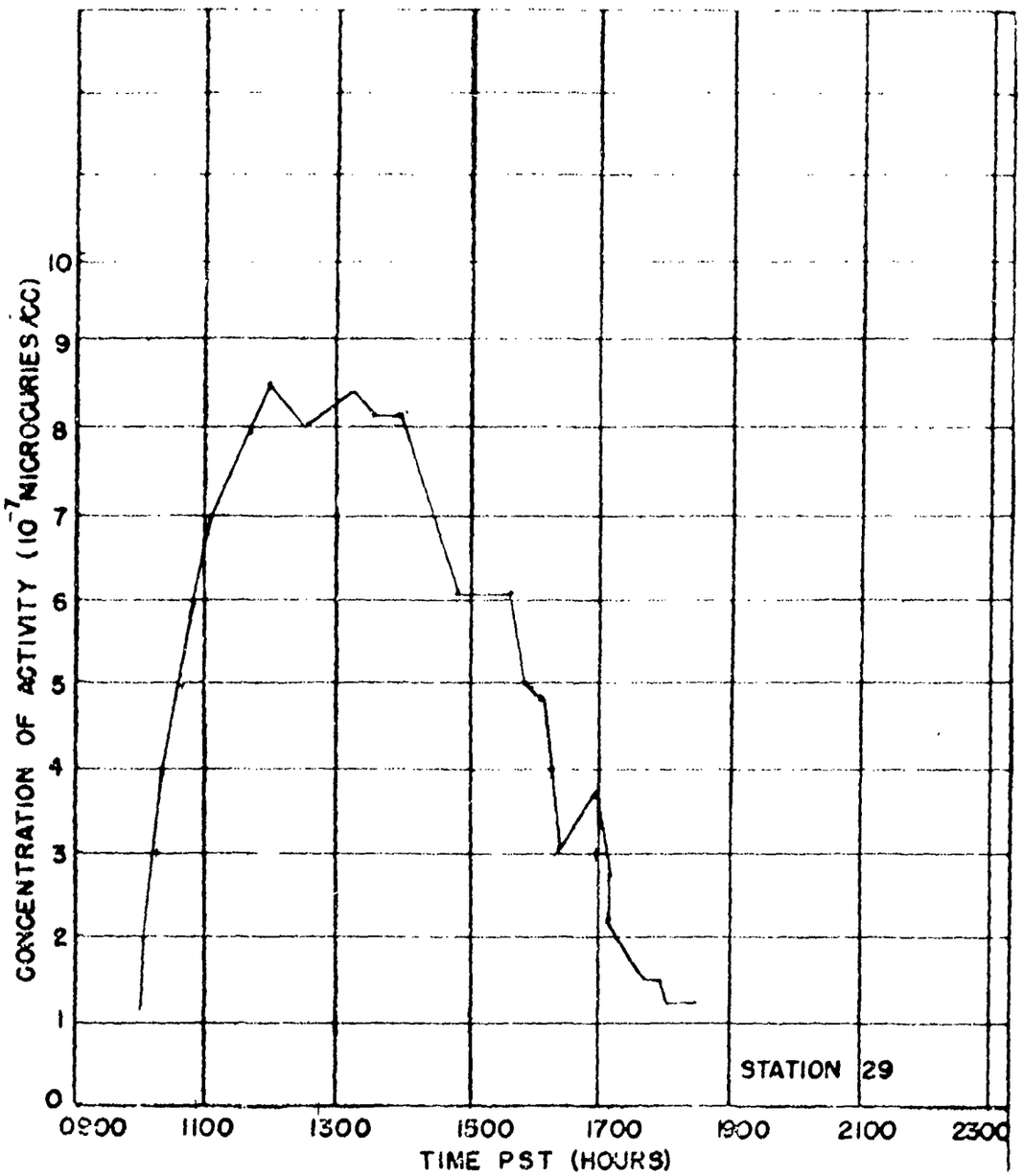

Fig. 4.6 Concentration of Activity at Station 29, Surface Shot, TCAM Data.

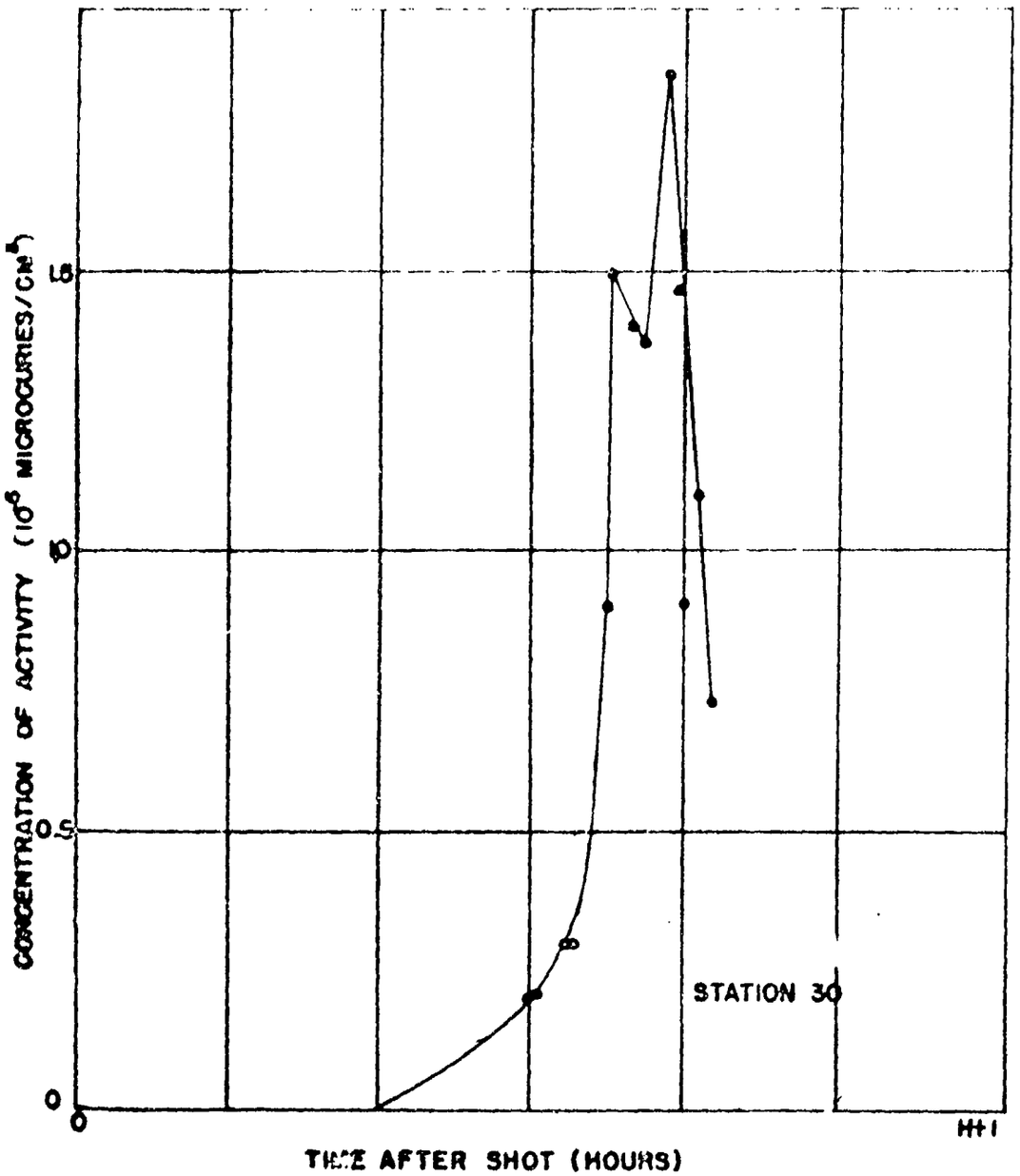

Fig. 4.7 Concentration of Activity at Station 30, Surface Shot, TCAM Data.

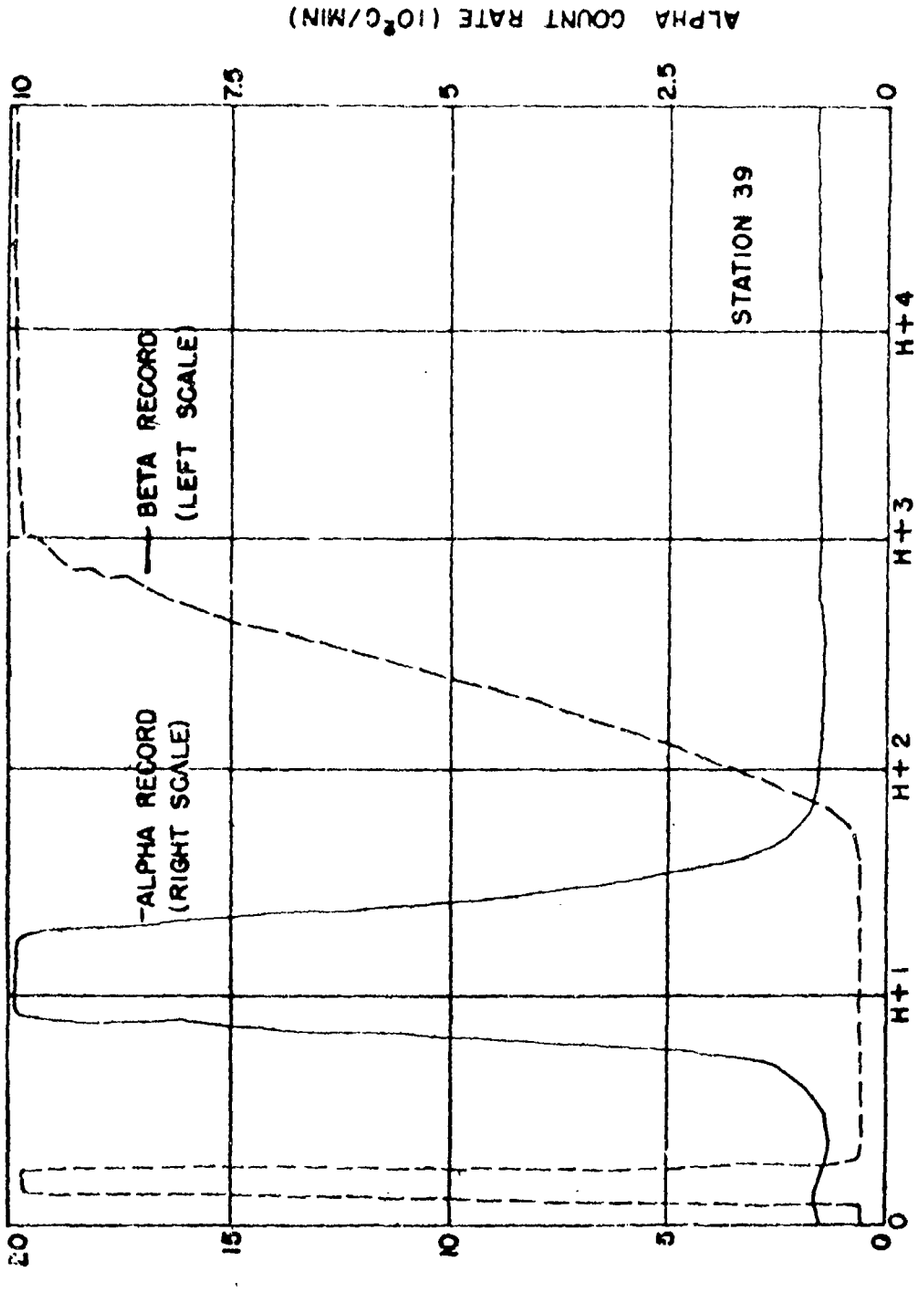

Fig. 4.8 Relative Activity Record Obtained from TCAM at Station 39, Surface Shot

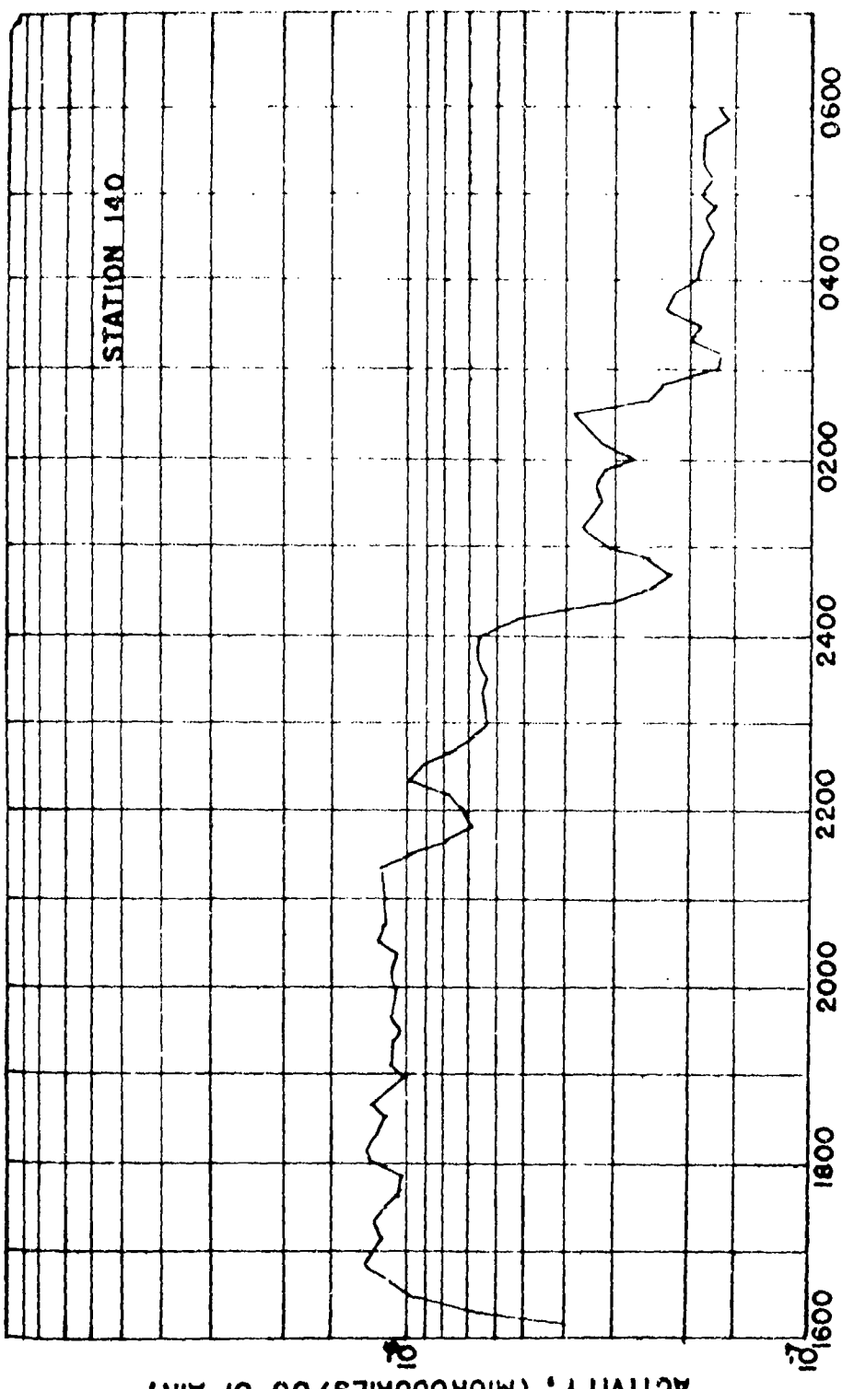

Fig. 4.9 Concentration of Activity at Station 140, Underground Shot, TCAU Data

is the alpha count rate pip which occurred at about H/2 hours. This pip occurred after cessation of a shot time beta pip (see discussion of BCAM 38) and prior to the hump due to the ground-level cloud. Since the beta record at this time shows nothing it is difficult to explain this effect.

A more regular record was obtained from the TCAM at station 140, in the Underground Shot. Fig. 4.9 presents the concentration of activity derived from the instrument at this station.

4.1.3 Particle Separator

Concentration data were obtained from particle separators used in each shot of Operation JANGLE by summing the activities measured on all the sampling elements of the particle separator, correcting for decay, and dividing by the volume of air sampled in the 115 minute sampling time. These data, of course, represent the average concentration in the air over the 115 minute sampling time. Concentration of activity in the cloud was computed using the sampling time and elapsed time as determined from the cloud model described in paragraph 4.1.1, for selected particle separators. These data are presented in Table 4.5.

The eleven screens, the metal disc, and the molecular filter of each particle separator were counted in a Nuclear Measurement Corporation PC-1 proportional counter. It was necessary to use two rings, one plastic and one aluminum, to prevent excessive contamination, hold the screen in place in the chamber, and yet insure suitable contact with the piston. In counting the surface shot samples it was found that the screens, metal disc, and molecular filters caused disturbances in the counting chamber; namely, the counting rate of any individual sample decreased with time. The surface shot samples had essentially no loose particles so colloidal graphite was sprayed on each sample before counting. After this treatment, reproducible measurements were obtained. The underground shot samples presented a more difficult problem since there was a large deposit of loose granular particles on most of the screens except the molecular filters. These screens were covered on both the influent and effluent sides with scotch tape. In this way it was possible to achieve reproducible results without seriously effecting the beta counting rates.

These activity measurements were made between 150 and 400 hours after the Surface Shot, and in two series, 400 to 800 hours and 1000 and 1200 hours after the underground shot, due to the extremely high activities encountered. Decay corrections were made to H/200, 400, and 1000 hours respectively by means of the individual decay curves for each

TABLE 4.5

Particle Separator Concentration of Activity

Station	Activity Corrected to H + 60 min. (μc)	Volume of Air Sampled in 115 minutes ($cm^3 \times 10^6$)	Average Conc. of Activity Over 115 min. $\mu c/cm^3$	Factor $f_1 f_2$	Conc. of Activity in Cloud $\mu c/cm^3$
			Surface Shot		
8	6.1	3.0	2.0×10^{-6}	6.0×10^{2}	1×10^{-3}
9	1.1	2.1	5.3×10^{-7}		
14	10.2	2.8	3.6×10^{-6}	3.9×10^{2}	1×10^{-3}
15	0.64	2.8	2.3×10^{-7}		
20	4.6	2.9	1.5×10^{-6}	2.1×10^{2}	3×10^{-4}
21	2.4	3.0	8.1×10^{-7}		
23	4.2	3.0	1.4×10^{-6}	1.3×10^{2}	2×10^{-4}
24	1.6	3.2	4.9×10^{-7}		
28	0.91	3.2	2.8×10^{-7}		
29	0.93	3.3	2.8×10^{-7}	4.8×10^{1}	1×10^{-5}
			Underground Shot		
108	1.6×10^{3}	3.0	5.5×10^{-4}	2.4×10^{2}	1×10^{-1}
109	4.2×10^{2}	1.5	2.7×10^{-4}		
114	2.7×10^{3}	2.7	1.0×10^{-3}	1.5×10^{2}	2×10^{-1}
115	6.9×10^{1}	2.7	2.5×10^{-5}		
120	3.3×10^{3}	3.1	1.2×10^{-3}	7.7×10^{1}	9×10^{-1}
121	3.8×10^{2}	2.9	1.3×10^{-4}		
123	3.8×10^{3}	3.4	1.1×10^{-3}	5.0×10^{1}	6×10^{-2}
124	4.4×10^{2}	3.2	1.4×10^{-4}		
128	4.2×10^{2}	3.2	1.3×10^{-4}		
129	2.9×10^{2}	3.5	8.6×10^{-5}	2.2×10^{1}	2×10^{-3}
130	2.9×10^{2}	3.1	9.7×10^{-5}		

sampling screen. The NIH decay curves (Fig. 4.3) were used to correct all activities to earlier times.

4.1.4 Cascade Impactor

Concentration data was also obtained from seven cascade impactors in the surface shot and ten cascade impactors in the underground shot. As discussed in paragraph 2.2.1, these instruments contained five slides and a molecular filter. By summing the measured activities on these elements, correcting for decay, and dividing by the volume sampled, the concentration of activity was determined. Since some of these instruments sampled for only a minute, and were initiated by a radiation alarm upon arrival of the cloud, the concentrations derived from these instruments should represent the concentration of activity in the cloud proper. The balance of the cascade impactors sampled for the usual 115 minutes, and their concentration data should represent the average concentration over that interval. The data from selected impactors of this latter group have been corrected by the methods described in paragraph 4.1.1 to produce the concentration of activity in the cloud. The entire data are presented in Table 4.6.

The measurements of activity on the cascade impactor slides were made in a gas flow proportional counter (Nuclear Measurements Model PC-1) in which the brass piston forming the base of the counting chamber was milled out in such a manner that the surface of the slide was flush with the surface of the piston. Calibration was accomplished with a UXIIB standard mounted with the same geometry as the sample geometry. No corrections were made for absorption or scattering. The measurements were completed by about H/200 hours and were corrected to H/100 hours by means of individual decay curves. Use was made of the NIH decay curves (Fig. 4.3) to connect back to H/1 hours.

4.1.5 Radiological Air Sampler

The Radiological Air Sampler which consisted basically of twelve small filter samplers sampling in succession, was designed to produce concentration data as a function of time. The decision to use these instruments was made a short time prior to Operation Jangle, and was based upon a desire to evaluate the instrument. Although time did not allow construction of a device to afford protection of the filter assembly, it was planned that the first filter assembly, which sampled from H-5 minutes to H/5 minutes, be used as a control for the balance of the filter assemblies. The assumption was made that the fall-out would uniformly contaminate all the filter assemblies, and that the first assembly, which had ceased sampling before the arrival of the cloud, would contain only fall-out activity. This activity would be subtracted from the activities on succeeding assemblies.

PROJECT 2.5a-1

TABLE 4.6

Cascade Impactor Concentration of Activity

Station	Activity at H + 60 min. (μc)	Sampling Interval (mins)	Volume Sampled (cm^3)	Concentration of Activity ($\mu c/cm^3$)	Factor f_2	Conc. of Act in Cloud ($\mu c/cm^3$)
Surface Shot						
13	2.8×10^{-3}	1	1.3×10^{4}	2.1×10^{-7}	10	2×10^{-6}
23	1.9×10^{-3}	1	1.3×10^{4}	1.5×10^{-7}	4.2	6×10^{-7}
25	2.1×10^{-4}	115	1.6×10^{6}	1.3×10^{-10}		
26	1.1×10^{-2}	115	1.5×10^{6}	7.2×10^{-9}		
30	2.9×10^{-2}	115	1.5×10^{6}	1.9×10^{-8}		
35	2.5×10^{-2}	115	1.6×10^{6}	1.6×10^{-8}		
40	6.0×10^{-3}	115	1.5×10^{6}	4.1×10^{-9}		
Underground Shot						
113	1.7×10^{-3}	1	1.3×10^{4}	1.3×10^{-7}	12	2×10^{-6}
114	7.5×10^{-3}	1	1.2×10^{4}	6.2×10^{-7}	12	7×10^{-6}
115	3.5×10^{-3}	1	1.3×10^{4}	2.7×10^{-7}		
119	1.8×10^{-3}	1	1.3×10^{4}	1.3×10^{-7}		
124	1.8×10^{-3}	115	1.5×10^{6}	1.2×10^{-9}		
125	1.1×10^{-3}	115	1.6×10^{6}	7.0×10^{-10}		
126	5.6×10^{-4}	115	1.5×10^{6}	3.7×10^{-10}		
132	8.0×10^{-5}	115	1.5×10^{6}	5.3×10^{-11}		
135	3.8×10^{-4}	115	1.6×10^{6}	2.4×10^{-10}		
140	2.3×10^{-3}	115	1.5×10^{6}	1.6×10^{-9}		

However, it was found that the activities on the various filter assemblies varied widely; in many cases there was more activity on the first filter assembly than on succeeding assemblies. A particularly good example of this variability was afforded by the two RAS at station 120. Both instruments failed to be initiated, and consequently all 24 filter assemblies were subjected only to fallout. On one of these instruments the most active filter assembly was more than three times as active as the least active filter assembly, and the standard deviation, percentagewise, of the 24 from the mean activity (computed by summing the activities and dividing by the number of filter assemblies) was found to be 25 per cent. Probably a reasonable explanation for this effect is that the small filter assembly offers a poor target, statistically, for large highly radioactive particles, or that in the various stages of transportation of the samples, these particles were lost.

Since the variability in fall-out activity was sufficiently large to mask the activity due to the sampled aerosol, it has not been possible to determine the concentration of activity in the aerosol with this instrument.

4.3 PARTICLE SIZE DISTRIBUTION

4.2.1 Cascade Impactor

The slides of twelve cascade impactors in each shot were examined by optical and electron microscopic methods to determine the size distribution of particles in the aerosol. A summary of the data from each shot is presented in Tables 4.7 and 4.8. The measuring and computing methods by which these data were obtained are described in the following paragraphs.

The particles on the first and second jets were counted and measured by examining the projected image of 1000 diameters from a light microscope. The particles on the 3rd and 4th jets were examined from projected images of 50,000 diameters. All measurements were made with transparent rules with millimeter divisions. Particles which measured between 14 and 15 mm were recorded as 15 mm, particles which measured between 15 and 16 mm were recorded as 16 etc. An attempt was made to measure the equivalent diameter of each particle (i.e., the diameters of a circle of area equal to the area of the particle). Since most of the particles had a rather circular projection, little difficulty was encountered. In most cases, the 2nd, 3rd, and 4th jet samples were relatively homogeneous and a particle count of 300-600 particles appeared satisfactory. The 1st and 5th jet samples were rather heterogeneous and particle counts of 400-1000 were made. The area represented

PROJECT 2.5a-1

TABLE 4.7

Cascade Impactor Particle Size Distribution
Surface Shot

	NMD (μ)	D^2MD (μ)	MMD (μ)	σ_g	Dav σ (μ)	Total No.	Total Surface	Total Mass
Cascade Impactor 13								
Jet 1	2.02	17.0	41.5	2.97	4.45	1.61×10^5	7.73×10^6	1.34×10^8
Jet 2	0.67	11.4	51.8	3.99	2.19	1.18×10^5	1.47×10^6	3.17×10^7
Jet 3	0.458	1.39	4.04	2.36	0.72	1.72×10^5	1.85×10^5	5.87×10^5
Jet 4	0.335	2.94	8.18	2.98	0.68	9.40×10^5	1.17×10^5	4.78×10^5
Jet 5								
Comp. Imp.	0.998	17.1	47.7	3.28	2.15	5.45×10^5	1.02×10^7	1.87×10^8
Cascade Impactor 14								
Jet 1	0.71	11.8	42.0	3.59	2.14	1.25×10^5	1.63×10^7	3.46×10^8
Jet 2	0.87	25.7	101.3	4.20	2.82	6.72×10^5	3.07×10^7	4.22×10^8
Jet 3	0.91	16.0	66.0	3.79	2.27	2.30×10^5	4.11×10^6	4.58×10^8
Jet 4	0.83	7.45	8.80	2.23	2.72	4.39×10^4	6.48×10^5	5.11×10^6
Jet 5								
Comp. Imp.	0.75	15.6	75.5	3.63	2.42	2.2×10^6	5.31×10^7	1.88×10^9
Cascade Impactor 15								
Jet 1								
Jet 2								
Jet 3	Insufficient Sample.							
Jet 4								
Jet 5								
Comp. Imp.								
Cascade Impactor 19								
Jet 1	0.96	17.9	69.5	3.90	2.84	1.50×10^5	3.99×10^6	8.46×10^7
Jet 2	1.92	22.9	84.2	2.86	4.10	7.49×10^4	5.08×10^6	1.96×10^8
Jet 3								
Jet 4	Insufficient Sample.							
Jet 5								
Comp. Imp.								
Cascade Impactor 23								
Jet 1	0.19	9.90	59.50	1.96	1.84	4.56×10^5	3.71×10^7	5.23×10^8
Jet 2	1.65	39.0	42.0	3.96	8.35	3.24×10^4	8.12×10^6	3.27×10^8
Jet 3	2.07	5.30	7.50	1.88	2.53	1.40×10^5	1.90×10^5	1.38×10^6
Jet 4	1.13	3.69	9.18	2.26	2.07	2.81×10^4	1.97×10^5	1.52×10^6
Jet 5								
Comp. Imp.	0.605	7.65	31.6	3.47	1.93	4.63×10^6	4.87×10^7	9.35×10^8

PROJECT 2.5a-1

TABLE 4.7 (cont'd)

	NMD (μ)	D^2MD (μ)	MMD (μ)	σ_g	Davg (μ)	Total No.	Total Surface	Total Mass
Cascade Impactor 24								
Jet 1 Jet 2 Jet 3 Jet 4 Jet 5 Comp.Imp.	Insufficient Sample.							
Cascade Impactor 25								
Jet 1	2.72	15.3	31.2	2.50	5.03	2.09×10^{5}	1.09×10^{7}	1.49×10^{8}
Jet 2	2.17	5.35	8.40	2.05	3.26	2.11×10^{5}	5.28×10^{6}	2.34×10^{7}
Jet 3	.97	3.44	6.78	2.22	1.44	3.58×10^{5}	1.38×10^{6}	6.87×10^{6}
Jet 4	1.15	2.31	3.13	1.74	1.29	3.68×10^{5}	9.63×10^{5}	2.56×10^{6}
Jet 5	0.438	1.16	1.76	2.01	.50	8.45×10^{5}	4.12×10^{5}	5.41×10^{5}
Comp.Imp.	0.84	9.15	20.7	2.83	1.65	1.99×10^{8}	1.79×10^{7}	2.12×10^{8}
Cascade Impactor 26								
Jet 1	6.25	16.7	25.6	1.91	7.30	2.2×10^{4}	2.19×10^{5}	5.01×10^{7}
Jet 2	1.03	5.25	10.3	2.76	2.19	4.13×10^{5}	3.54×10^{6}	3.24×10^{7}
Jet 3	.495	2.19	4.03	2.40	.776	9.24×10^{5}	1.10×10^{6}	2.84×10^{6}
Jet 4	.519	1.48	2.25	1.98	.66	7.47×10^{5}	6.22×10^{5}	1.10×10^{6}
Jet 5	.095	.778	1.38	2.97	.182	1.88×10^{6}	1.49×10^{5}	1.05×10^{6}
Comp.Imp.	.302	6.00	19.4	3.44	.678	4.04×10^{6}	8.14×10^{6}	8.39×10^{7}
Cascade Impactor 30								
Jet 1	.94	6.0	18.7	2.67	2.18	1.29×10^{6}	1.29×10^{7}	1.65×10^{8}
Jet 2	1.41	3.83	6.2	2.13	2.29	1.05×10^{6}	8.62×10^{5}	4.28×10^{6}
Jet 3	1.01	1.87	2.32	1.62	1.10	4.59×10^{5}	8.21×10^{5}	1.70×10^{6}
Jet 4	.643	1.27	1.82	1.80	.798	3.34×10^{5}	3.00×10^{5}	5.14×10^{5}
Jet 5	.052	.362	.816	2.80	.099	4.80×10^{5}	1.10×10^{4}	4.00×10^{3}
Comp.Imp.	.89	6.11	8.75	2.50	1.50	2.67×10^{6}	1.56×10^{7}	8.05×10^{7}
Cascade Impactor 32								
Jet 1	1.97	9.85	21.0	2.64	3.61	1.26×10^{5}	3.27×10^{5}	4.07×10^{7}
Jet 2	1.70	3.72	5.15	1.94	2.44	6.67×10^{4}	4.05×10^{5}	1.93×10^{6}
Jet 3	.62	3.47	9.05	2.66	1.02	1.87×10^{5}	4.46×10^{5}	2.47×10^{6}
Jet 4	.495	1.07	1.57	1.88	.66	5.34×10^{5}	3.32×10^{5}	4.57×10^{5}
Jet 5	.216	.590	.967	2.11	.31	1.57×10^{6}	2.21×10^{5}	1.33×10^{5}
Comp.Imp.	.345	5.41	18.2	3.18	.67	2.47×10^{6}	4.98×10^{6}	4.99×10^{7}

TABLE 4.7 (cont'd)

	NMD (μ)	D^2MD (μ)	MMD (μ)	σ_g	Davg (μ)	Total No.	Total Surface	Total Mass
				Cascade Impactor 35				
Jet 1	3.75	11.6	18.4	2.11	5.32	3.46×10^{5}	1.76×10^{7}	2.57×10^{8}
Jet 2	2.08	5.85	9.20	2.14	3.23	1.88×10^{5}	3.14×10^{6}	2.31×10^{7}
Jet 3	1.44	2.90	3.79	1.70	1.42	2.61×10^{5}	9.43×10^{5}	3.34×10^{6}
Jet 4	.83	1.36	1.11	1.64	.97	4.82×10^{5}	5.91×10^{5}	9.37×10^{5}
Jet 5	.098	.308	.46	1.96	.072	1.14×10^{7}	1.72×10^{5}	6.44×10^{4}
Comp.Imp.	.592	12.5	31.4	3.82	1.44	2.42×10^{6}	2.43×10^{7}	3.16×10^{8}
				Cascade Impactor 40				
Jet 1	1.52	22.3	82.6	3.55	3.70	3.53×10^{4}	1.62×10^{6}	4.91×10^{7}
Jet 2	1.94	3.72	5.10	1.75	2.60	3.83×10^{4}	3.64×10^{5}	1.75×10^{6}
Jet 3	1.47	2.67	3.18	1.79	1.21	1.67×10^{5}	4.67×10^{5}	1.40×10^{6}
Jet 4	0.705	1.56	2.47	1.95	0.944	2.53×10^{5}	3.31×10^{5}	6.80×10^{5}
Jet 5	0.033	0.256	0.620	2.98	0.068	8.82×10^{6}	1.00×10^{5}	3.05×10^{4}
Comp.Imp.	0.030	9.25	81.5	5.36	0.138	9.31×10^{6}	3.09×10^{6}	5.63×10^{7}

TABLE 4.8

Cascade Impactor Particle Size Distribution
Underground Shot

				Cascade Impactor 113				
Jet 1	0.91	4.43	14.80	2.85	1.9	6.04×10^{5}	4.11×10^{6}	3.81×10^{7}
Jet 2	1.28	7.9	18.9	2.58	2.51	8.94×10^{3}	1.22×10^{5}	1.57×10^{6}
Jet 3								
Jet 4	Excessive Sample.							
Jet 5								
Comp.Imp.								
				Cascade Impactor 114				
Jet 1	1.68	12.6	30.9	2.80	3.43	1.94×10^{5}	5.41×10^{6}	8.89×10^{7}
Jet 2	1.42	4.75	8.58	2.22	2.44	1.40×10^{4}	1.50×10^{5}	1.02×10^{6}
Jet 3	1.04	2.21	2.90	1.88	1.85	3.80×10^{4}	1.68×10^{5}	4.95×10^{5}
Jet 4	0.74	4.37	7.55	2.57	1.76	1.38×10^{4}	7.69×10^{4}	4.34×10^{5}
Jet 5								
Comp.Imp.	1.41	12.3	31.5	2.99	3.15	2.61×10^{5}	6.32×10^{6}	1.02×10^{8}

TABLE 4.8 (Cont'd)

	NMD (μ)	D^2MD (μ)	WMD (μ)	σ_g	D_{avg} (μ)	Total No.	Total Surface	Total Mass
Cascade Impactor 115								
Jet 1	3.30	27.2	73.0	2.61	5.98	9.35×10^3	1.24×10^6	4.38×10^6
Jet 2	1.72	58.0	102.16	3.90	4.61	2.3×10^3	2.55×10^5	1.78×10^7
Jet 3								
Jet 4	Excessive Sample.							
Jet 5								
Comp.Imp.								
Cascade Impactor 119								
Jet 1	1.13	10.5	25.6	3.10	2.72	1.67×10^5	3.07×10^6	4.18×10^7
Jet 2	1.00	10.8	25.7	3.60	2.52	4.78×10^3	7.93×10^4	1.09×10^6
Jet 3								
Jet 4	Excessive Sample.							
Jet 5								
Comp.Imp.								
Cascade Impactor 123								
Jet 1	0.46	5.70	18.0	3.35	1.54	7.61×10^6	3.87×10^7	3.52×10^8
Jet 2	3.35	8.35	11.5	1.90	4.33	1.20×10^4	3.37×10^5	3.44×10^6
Jet 3	1.05	5.75	13.0	2.75	2.12	3.00×10^4	2.52×10^5	2.11×10^6
Jet 4	0.5	5.99	14.5	3.40	1.00	2.42×10^5	6.19×10^5	2.42×10^6
Jet 5	0.88	1.77	2.53	1.61	1.15	1.03×10^5	1.28×10^5	4.22×10^5
Comp.Imp.	0.473	5.65	20.4	3.47	1.28	8.00×10^6	4.26×10^7	4.15×10^8
Cascade Impactor 124								
Jet 1	0.81	2.17	96	3.83	2.53	4.13×10^3	1.01×10^5	3.68×10^6
Jet 2	1.23	8.00	19.5	2.67	2.45	3.9×10^3	5.42×10^4	6.94×10^5
Jet 3								
Jet 4	Excessive Sample.							
Jet 5								
Comp.Imp.								
Cascade Impactor 125								
Jet 1	1.95	5.90	9.90	2.10	2.80	1.56×10^5	2.27×10^7	1.86×10^8
Jet 2	0.68	5.50	11.80	2.96	1.76	3.73×10^4	2.32×10^5	1.79×10^6
Jet 3								
Jet 4	Excessive Sample.							
Jet 5								
Comp.Imp.								

PROJECT 2.5a-1

TABLE 4.8 (Cont'd)

	NMD (μ)	D^2_{MD} (μ)	MMD (μ)	σ_g	D_{avg} (μ)	Total No.	Total Surface	Total Mass
Cascade Impactor 126								
Jet 1 Jet 2 Jet 3 Jet 4 Jet 5 Comp.Imp.	Excessive Sample.							
Cascade Impactor 130								
Jet 1	2.34	9.15	16.20	2.31	3.81	2.23×10^5	6.14×10^6	7.97×10^7
Jet 2	1.46	4.30	6.75	2.19	2.41	3.78×10^5	3.44×10^6	1.87×10^7
Jet 3	1.48	4.35	6.80	2.16	2.41	2.14×10^5	1.96×10^6	1.15×10^7
Jet 4	0.85	1.89	2.84	2.00	1.57	3.32×10^5	1.11×10^6	3.15×10^7
Jet 5	0.058	0.196	0.328	2.28	0.098	1.75×10^6	2.92×10^4	7.08×10^3
Comp.Imp.	0.120	8.25	20.7	3.67	0.726	2.89×10^6	1.02×10^7	1.10×10^8
Cascade Impactor 132								
Jet 1	2.5	10.5	20.5	2.44	4.10	2.35×10^4	7.51×10^5	9.57×10^5
Jet 2	1.38	4.15	5.85	2.21	2.33	1.64×10^4	1.41×10^5	7.52×10^5
Jet 3	1.55	2.41	3.01	1.62	2.08	3.05×10^4	1.68×10^5	5.44×10^5
Jet 4	0.343	1.41	2.44	2.28	0.476	1.30×10^5	7.03×10^4	1.20×10^5
Jet 5	0.18	0.304	0.376	1.63	0.201	1.62×10^6	8.72×10^4	2.94×10^4
Comp.Imp.	0.203	7.95	29.3	3.25	0.350	1.82×10^6	1.19×10^4	1.38×10^4
Cascade Impactor 135								
Jet 1	0.49	2.72	7.50	3.06	1.42	5.05×10^5	1.63×10^5	7.95×10^5
Jet 2	0.70	4.20	11.30	2.99	1.79	2.93×10^4	1.71×10^5	1.26×10^6
Jet 3	1.12	2.55	4.65	1.96	1.93	3.44×10^4	1.78×10^5	8.06×10^5
Jet 4	0.139	1.08	2.25	2.76	0.283	5.20×10^5	9.93×10^4	1.35×10^5
Jet 5	0.053	0.20	0.41	2.30	0.086	2.12×10^6	5.80×10^4	8.56×10^3
Comp.Imp.	0.104	2.39	11.7	4.04	0.339	3.37×10^6	2.34×10^5	1.15×10^7
Cascade Impactor 140								
Jet 1	1.26	7.55	19.5	2.78	2.54	1.24×10^5	1.70×10^5	2.14×10^7
Jet 2	0.81	3.72	9.40	2.74	1.84	5.34×10^4	3.10×10^5	1.87×10^6
Jet 3	0.73	1.75	2.17	2.22	1.50	1.04×10^5	3.00×10^5	8.84×10^5
Jet 4	0.184	1.44	3.17	3.10	0.31	4.02×10^5	1.43×10^5	2.01×10^5
Jet 5	0.12	0.24	0.36	1.33	0.14	3.34×10^6	7.40×10^4	2.15×10^4
Comp.Imp.	0.094	2.39	11.7	4.04	0.339	3.37×10^6	2.34×10^5	1.15×10^7

by the count was measured and recorded. Also the total impaction area was measured for each sample with the light microscope using scattered light.

A table of data and calculations was made for each jet, the completed table being similar in form to Table 4.9.

TABLE 4.9

Sample Cascade Impactor Data and Calculation Sheet

Diameter Microns	Number	Per Cent by No.	$n_i D_i^2$	Per Cent by Surface	Cum. Per Cent by Area	$n_i D_i^3$	Per Cent by Mass	Cum. Per Cent by Mass

It will be noticed that to obtain the percent by surface and percent by mass only the relative surface area and mass were computed.

Three sets of points representing cumulative per cent less than stated size by number, by surface, and by mass, were plotted on log-probability paper. Straight lines were drawn to represent the sets of points by inspection, using the following criteria:

A. The slope in best agreement with all three sets of points was used for all three lines. (If the distribution is assumed to be log-normal then this procedure is indicated by theory[5,6,7].

[5]Hatch & Choate, "Statistical Description of the Size Properties of Non-Uniform Particulate Substances", J. Franklin Inst., 207, (1929), 369

[6]T. Hatch, "Determination of Average Particle Size From the Screen Analysis of Non-Uniform Particulate Substances", J. Franklin Inst., 215, (1933), 27

[7]C. E. Lappel, "Mist and Dust", Heating and Air Cond., 18, (1946)

Also, this method gives a single average measure of the degree of homogeneity of the sample.)

B. The slope being already determined, the lines were positioned to best fit the points in the 10-90 per cent range.

C. Known difficulties in analysis, such as measuring the smallest particles, were allowed some consideration. The following parameters were obtained from the lines:

NMD = Number Median Diameter = D(50%) from No. line.

D^2MD = Surface Median Diameter = D(50%) from surface line.

MMD = Mass Median Diameter = D(50%) from mass line.

σ_g = Geometric Standard Deviation = $\frac{D(84.13\%)}{D(50\%)}$

Other values obtained are:

D_{avg} = Average Diameter = $\frac{n_i D_i}{n_i}$

Total No. of Particles Collected
Total Surface (Relative)
Total Mass (Relative)

There are many good arguments against the use of log-probability plots to represent sub-samples such as those from the jets of a cascade impactor[8,9]. However, the method is expedient and gives parameters that represent the sample to a reasonable accuracy. There are several analytic methods of curve fitting[8,9], but they would be

[8] F. Kottler, "The Distribution of Particle Sizes", Parts I and II, J. Franklin Inst., 250 (Oct & Nov, 1950), 339 and 419.

[9] F. Kottler, "The Goodness of Fit and Distribution of Particle Sizes", Parts I and II, J. Franklin Inst., 251, (May and June 1951) 499 and 617.

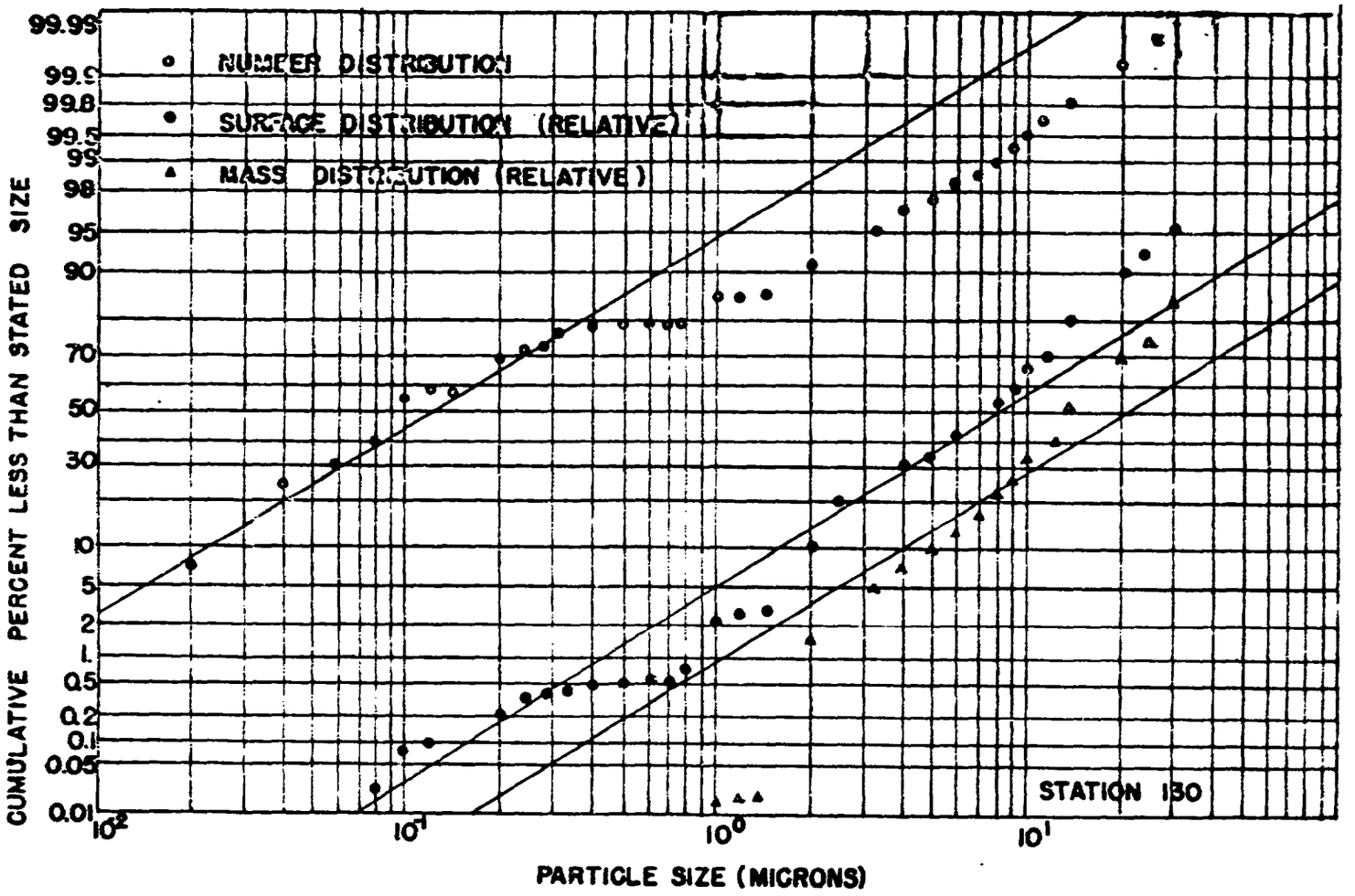

PROJECT 2.5a-1

Fig. 4.10 Particle Size Distribution in the Aerosol at Station 130, Cascade Impactor Data

very difficult to use considering the large number of points involved and the fact that parallel lines are to be drawn.

Having obtained sufficient information about the individual jet samples, it was necessary to combine the data from each set of 5 jets to obtain the size distribution of the cloud. An area correction factor was obtained for each jet by dividing the impaction area of the jet by the area counted. The number of particles in each size group (class interval) was multiplied by the area factor and the resulting number represented the total number of particles in each class interval collected by the jet. An integrated set of fifth class intervals covering the entire size range studied (0.02-100 microns) had been formulated, and the individual jet data were fit to these class intervals on a sub-size basis. The number falling in each class interval was found by adding the contributions from each jet; a table of data and calculations similar to those for the individual jets was made. From the data thus obtained, four cycle log-probability plots for the entire cascade impactor were constructed, from which the parameters tabulated tabulated in Table 4.7 and 4.8 were taken. Fig. 4.10 is an example of such a graph. It should be noted that the parameters listed in the tables permit reconstruction of the straight lines in any desired plot.

4.2.2 Filter Sampler

The filter papers from the filter samplers at stations 29,30 and 129,130 were analyzed by Tracerlab for particle size distributions. The results are reported in Appendix E.

4.2.3 Fall-out Tray

Of the twenty fall-out trays employed in each shot, one tray in the surface shot and twenty in the underground shot collected a weighable sample of the fall-out material. The former and eight of the latter contained sufficient material to permit a sieve analysis, while four of the latter passed sufficient material through the last (37 micron) sieve to permit further separation by means of a Roller Analyzer. Fig. 4.11 shows the mass of the material collected on the trays plotted against distance grom ground zero, while Figs. 4.12 through 4.15 show the particle size distributions obtained from the four stations that were put through the sieve analysis and Roller Analyzer.

The sieve analysis consisted of sifting the samples through a column of U. S. standard sieves shaken by a Rotap machine. This machine was operated for 5 minutes on fractions greater than 1410 microns, and for ten minutes on smaller size fractions. In the case of four stations where more than grams of material was found to pass the last screen,

PROJECT 2.5a-1

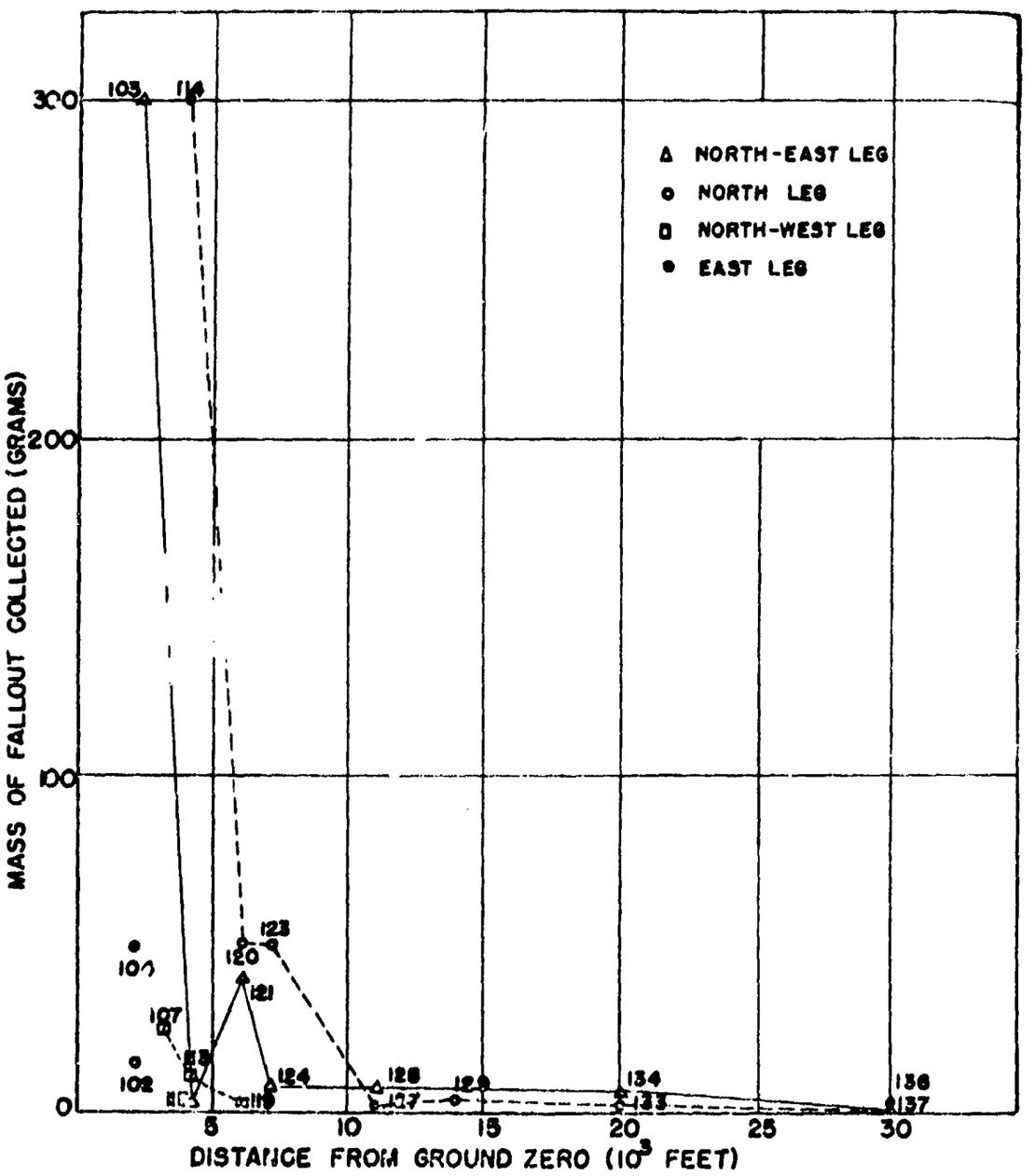

Fig. 4.11 Mass of Material Collected by the Fall-out Trays

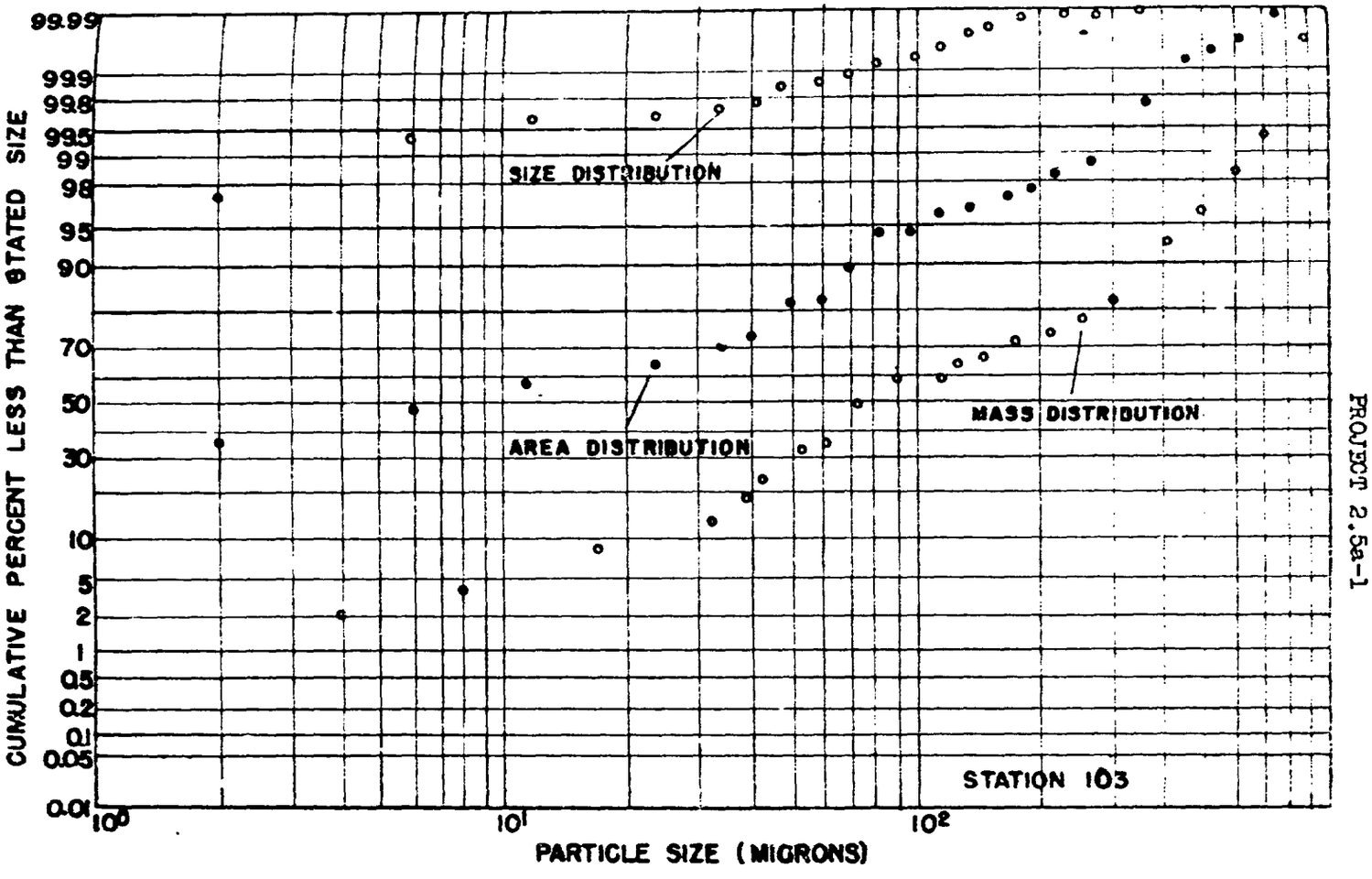

Fig. 4.12 Particle Size Distribution of Fall-out, Underground Shot, Station 103

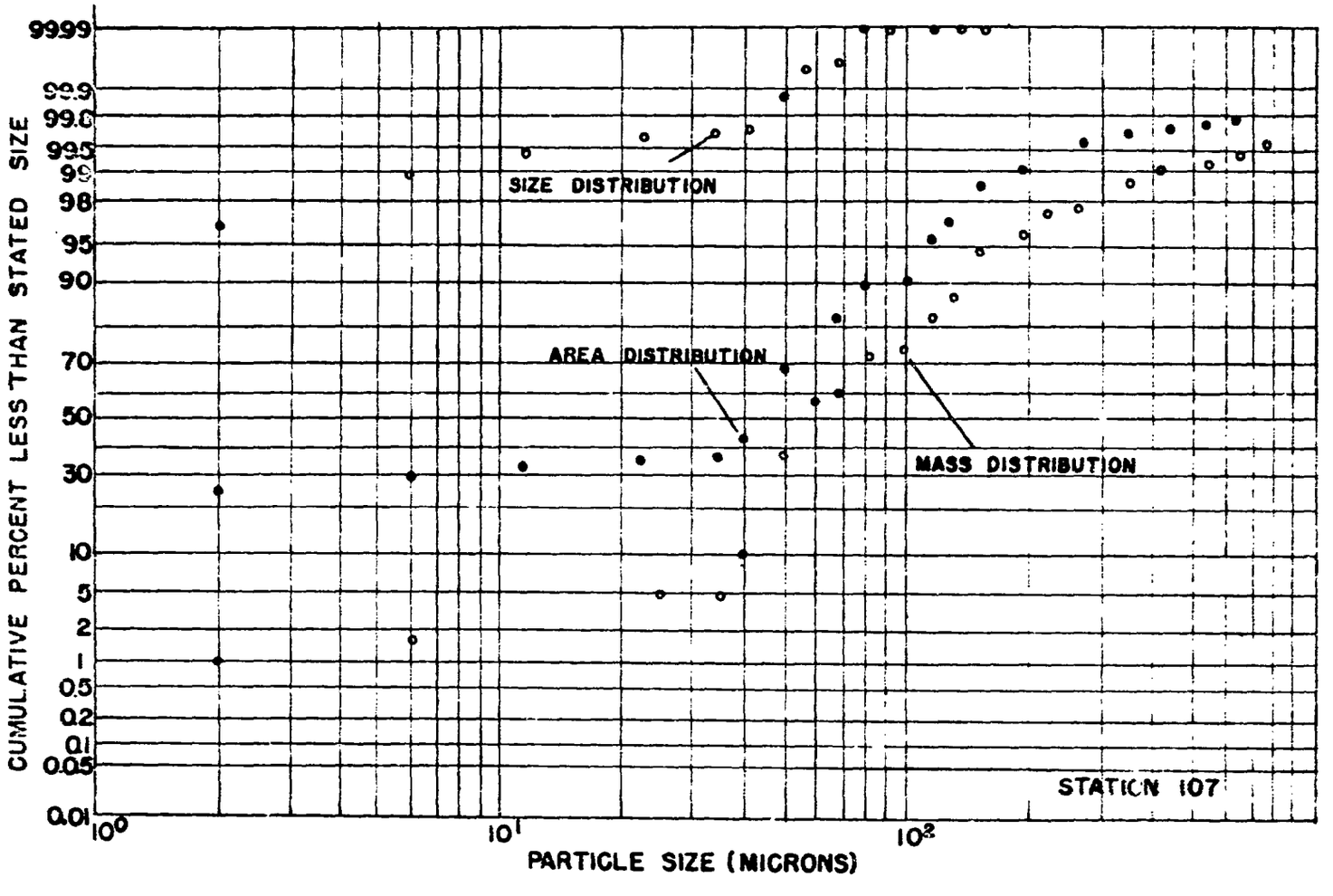

Fig. 4.13 Particle Size Distribution of Fall-out Station 107, Underground Shot

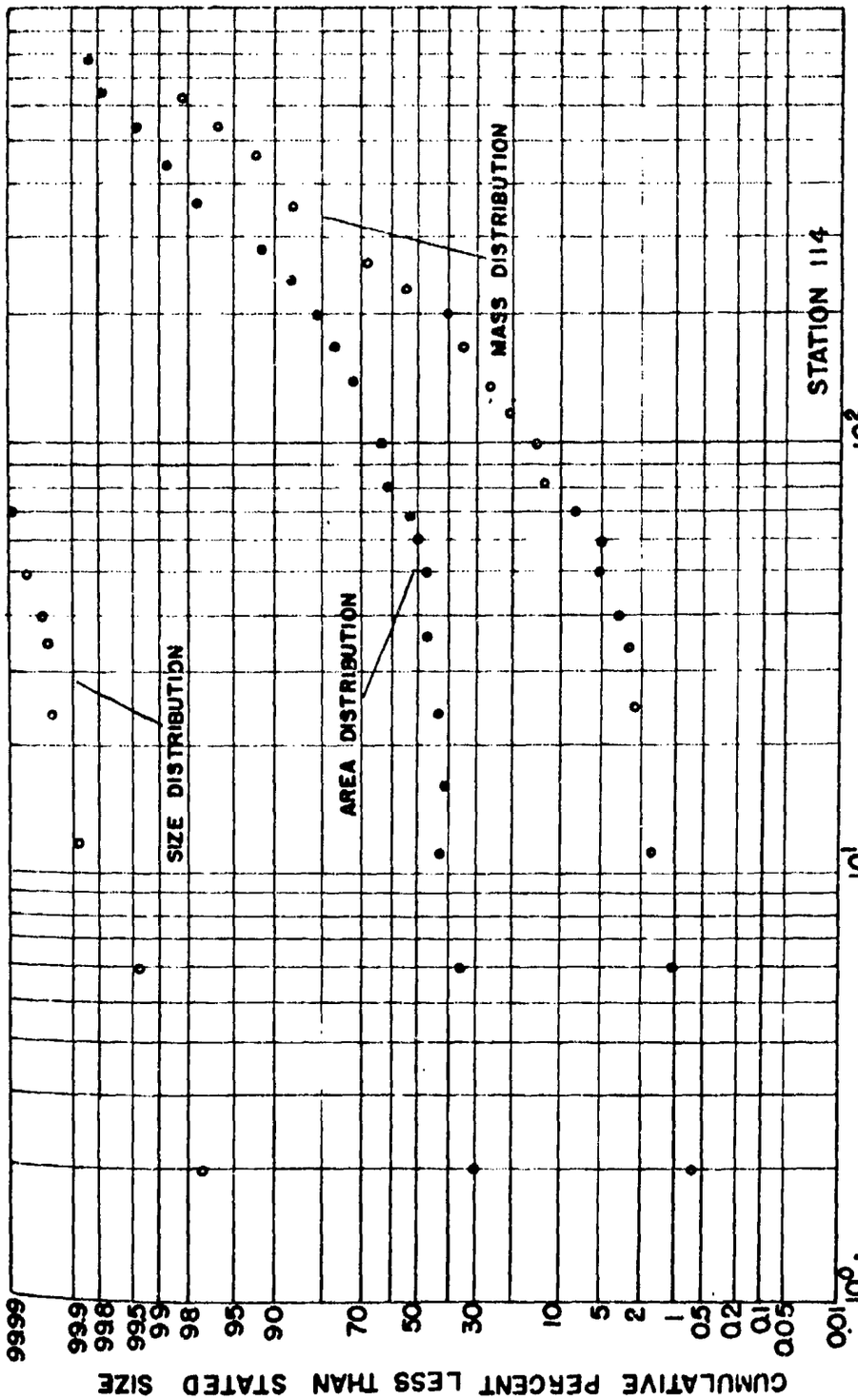

Fig. 4.14 Particle Size Distribution of Fall-out, Station 114, Underground Shot

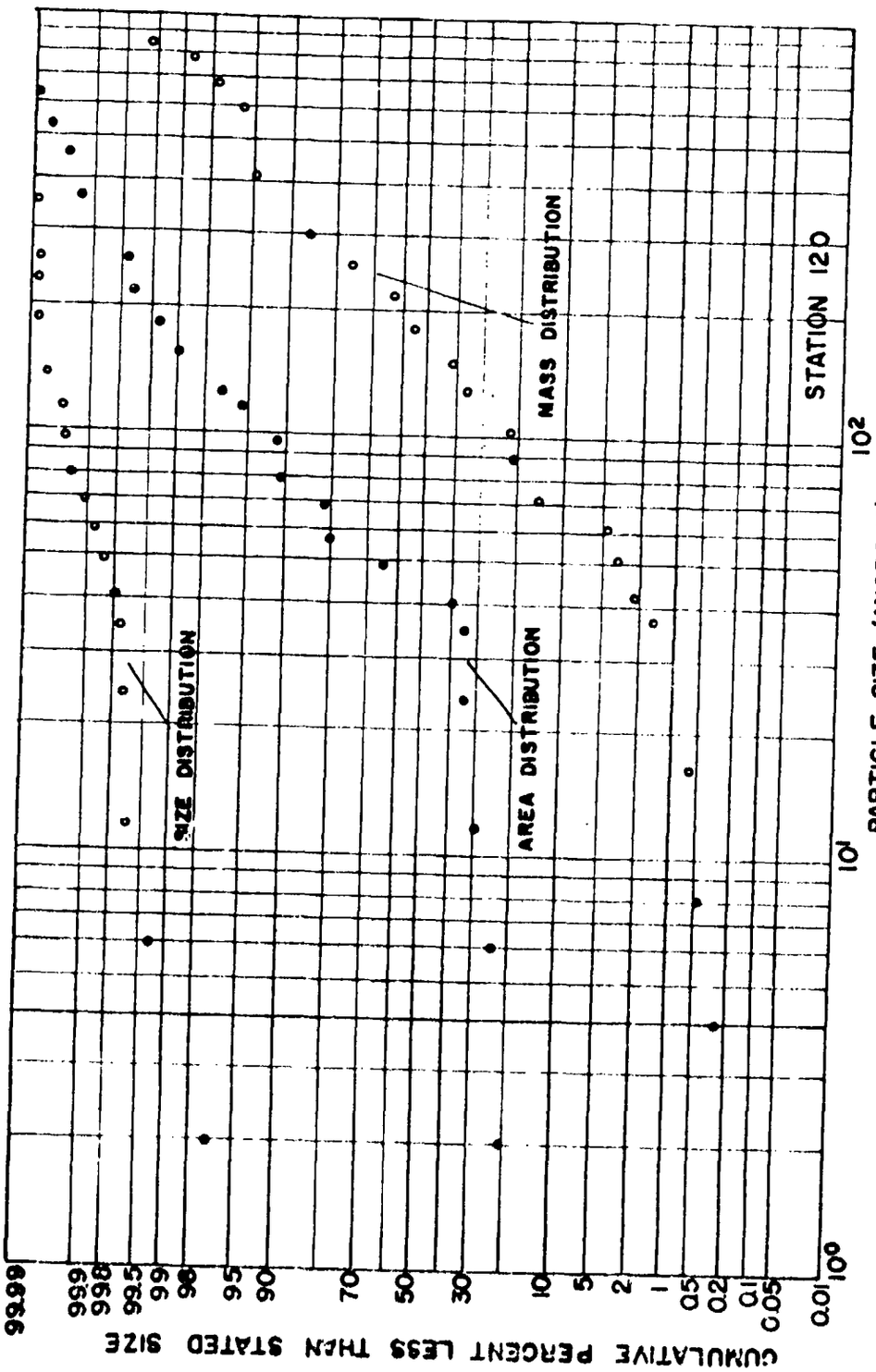

Fig. 4.15 Particle Size Distribution of Fall-out, Station 120, Underground Shot

further fractionation was accomplished with the Roller Analyzer. This machine separated the remaining sieve material into the size fractions 0-4, 4-8, 8-16, and 16-37 microns and the fractions were weighed on an analytical balance.

The basic data obtained in this technique, then, is the weight associated with the various particle size fractions, which may be termed the weight distribution of the fall-out sample. A specific gravity of 2.7 was assumed for all particles, and from the weight distribution the area distribution as well as the size distribution has been computed. It was also assumed that all particles on a given sieve were of a size equal to the average pore size of that sieve and the next higher. All particles were treated as spheres in the calculations.

4.2.4 Pre-Shot Soil Analysis

The particle size distribution of the soil at the test site was determined on six samples taken at five foot depth intervals from a location near the underground shot zero point. These samples were analyzed by the method described in par. 4.2.3; the data are presented in Figs. 4.16 and 4.17.

4.3 RADIOACTIVITY AS A FUNCTION OF PARTICLE SIZE

4.3.1 Cascade Impactor

The activity in the aerosol as a function of particle size was determined from the cascade impactors by measuring the activity on each slide and plotting these data against the particle size impacted on the slide.

The data are tabulated in Tables 4.10 and 4.11 for the surface and underground shots respectively. The activity on each slide, corrected to H/1 hours, is shown in column 4, while the NMD, the measure of the size of particles on that slide, is shown in column 3. The latter data were taken from Tables 4.7 and 4.8. Column 7 shows the specific activity of the particles on each slide as computed by dividing the activity on the slide by the mass of particles on that slide. The latter were obtained by multiplying the "total mass" on each jet in Tables 4.7 and 4.8 by $\pi \rho / 6$, where $\rho = 2.7 \times 10^{-12}$ grams per cubic micron.

A description of the procedures used in making the activity measurements is given in par. 4.1.4.

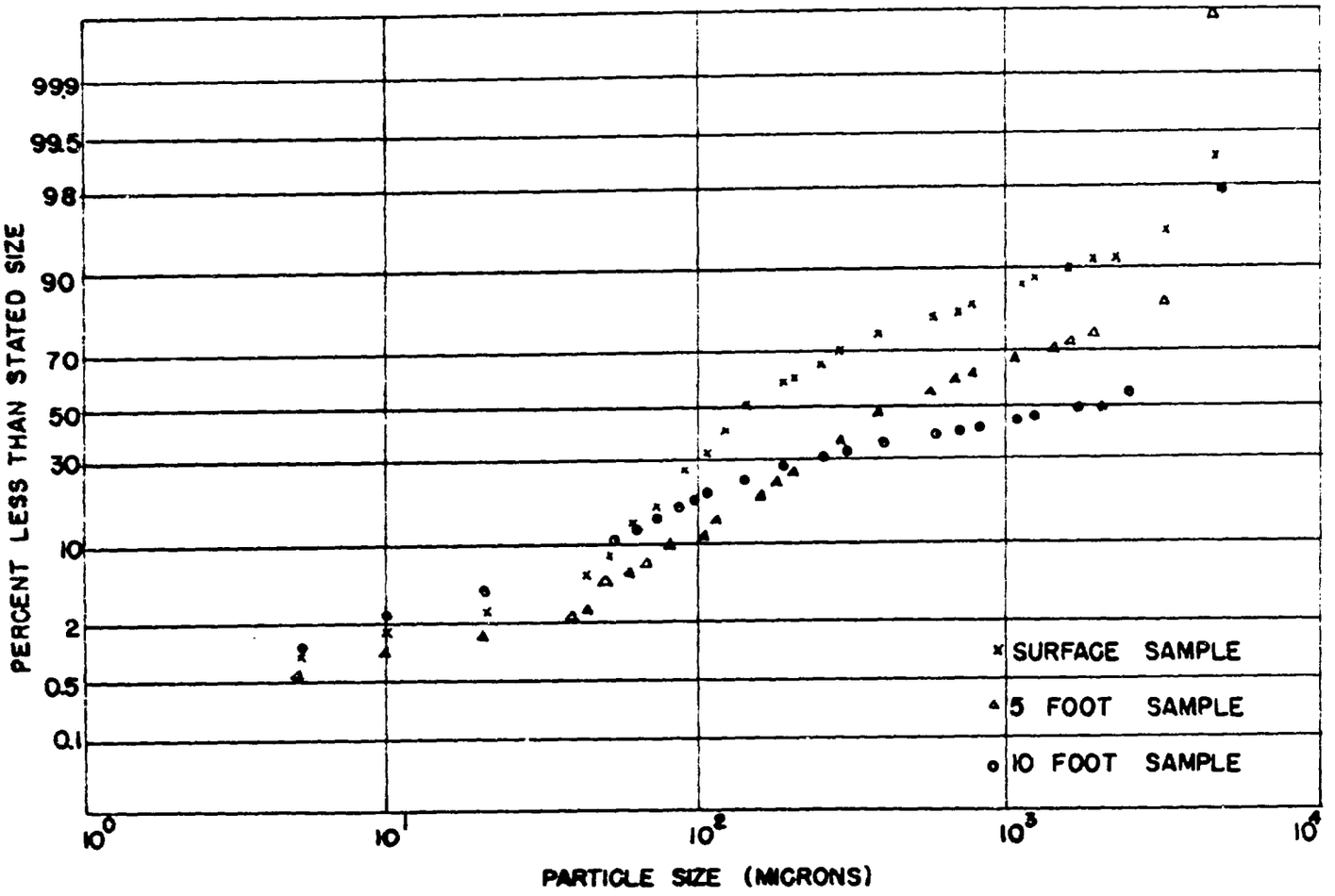

Fig. 4.16 Particle Size Distribution of Pre-shot Soil, Surface, Five and Ten Foot Depths.

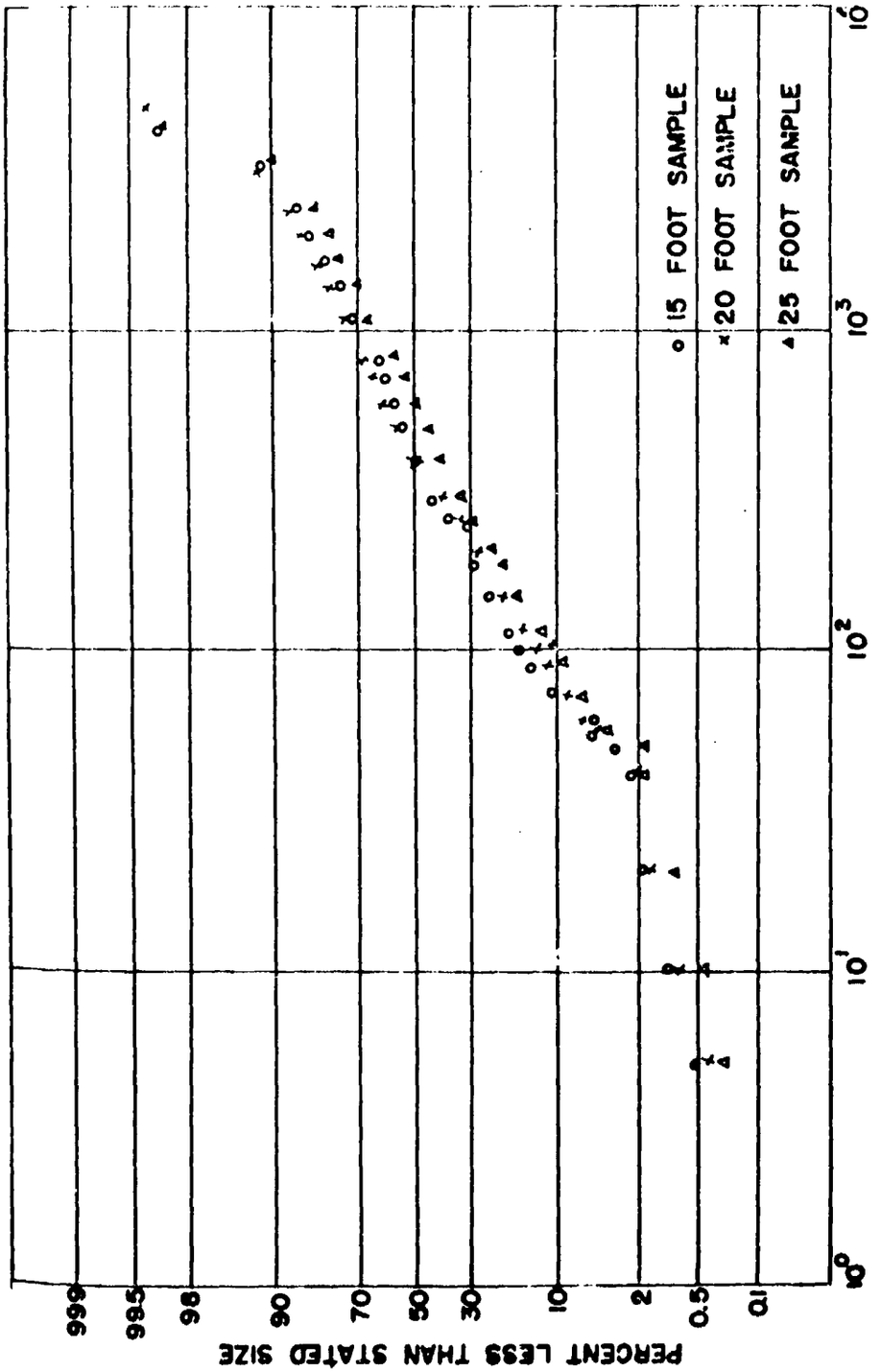

Fig. 4.17 Particle Size Distribution of Pre-shot Soil, Fifteen, Twenty, and Twenty-five Foot Depths

PROJECT 2.5a-1

TABLE 4.10

Surface Shot Activity Measurements on the Cascade Impactor

Station No.	Jet No.	Number Median Diameter (microns)	Activity on Jet at H + 1 Hrs. (μc)	Percentage of Total Cas. Imp. Activity	Mass of Particles on Jet (grams)	Specific Activity $\frac{\mu c}{gram}$
13	1	2.0	3.7×10^{-4}	13.	1.9×10^{-4}	1.9
13	2	0.67	2.2×10^{-3}	80.		
13	3	0.45	1.9×10^{-4}	7.	8.3×10^{-7}	2.3×10^{2}
23	1	0.19	7.5×10^{-4}	40.	7.4×10^{-4}	1.0
23	2	1.6	1.1×10^{-3}	59.	4.6×10^{-4}	2.4
23	4	2.1	2.5×10^{-5}	1.	2.1×10^{-6}	1.2×10^{1}
25	1	2.7	1.1×10^{-4}	51.	2.1×10^{-4}	5.2×10^{-1}
25	2	2.2	6.7×10^{-5}	32.	3.3×10^{-5}	2.1
25	5	0.44	3.6×10^{-5}	16.	7.6×10^{-7}	4.7×10^{1}
26	1	6.3	2.7×10^{-4}	3.	7.1×10^{-5}	3.8
26	2	1.0	4.4×10^{-3}	41.	3.2×10^{-5}	1.4×10^{2}
26	3	0.50	4.8×10^{-3}	44.	4.0×10^{-6}	1.2×10^{3}
26	4	0.52	7.0×10^{-4}	6.	1.6×10^{-6}	4.5×10^{2}
26	5	0.09	6.3×10^{-4}	6.	1.5×10^{-7}	4.3×10^{3}
30	1	0.94	7.0×10^{-4}	2.	2.3×10^{-4}	3.0
30	2	1.4	9.0×10^{-3}	32.	6.7×10^{-6}	1.3×10^{3}
30	3	1.0	1.4×10^{-2}	48.	2.4×10^{-6}	5.7×10^{3}
30	4	0.64	3.2×10^{-3}	11.	7.3×10^{-7}	4.4×10^{3}
30	5	0.05	1.9×10^{-3}	7.	5.6×10^{-9}	3.4×10^{5}
35	1	3.8	1.6×10^{-3}	6.	3.6×10^{-4}	4.4
35	2	2.1	5.5×10^{-3}	22.	3.3×10^{-5}	1.7×10^{2}
35	3	1.4	1.2×10^{-2}	48.	4.7×10^{-6}	2.6×10^{3}
35	4	0.83	5.2×10^{-3}	21.	1.3×10^{-6}	3.9×10^{3}
35	5	0.10	7.0×10^{-4}	3.	9.1×10^{-8}	7.7×10^{3}
40	1	1.5	1.8×10^{-4}	3.	6.9×10^{-5}	2.6
40	2	1.9	2.1×10^{-3}	35.	2.5×10^{-6}	8.5×10^{2}
40	3	1.5	1.8×10^{-3}	30.	1.9×10^{-6}	9.1×10^{2}
40	4	0.71	1.2×10^{-3}	20.	9.7×10^{-7}	1.2×10^{3}
40	5	0.03	7.0×10^{-4}	12.	1.4×10^{-8}	1.6×10^{4}

PROJECT 2.5a-1

TABLE 4.11

Underground Shot Activity Measurements on the Cascade Impactor

Station No.	Jet No.	Number Median Diameter (microns)	Activity on Jet at H +1Hrs. (μc)	Percentage of Total Cas. Imp. Activity	Mass of Particles on Jet (grams)	Specific Activity $\frac{\mu c}{gram}$
113	1	0.91	1.4×10^{-4}	8.	5.4×10^{-5}	2.6
113	2	1.3	5.4×10^{-4}	32.	2.2×10^{-6}	2.4×10^{2}
113	3		3.5×10^{-4}	20.		
113	4		3.5×10^{-4}	20.		
113	5		3.4×10^{-4}	20.		
114	1	1.7	9.9×10^{-4}	13.	1.3×10^{-4}	7.9
114	2	1.4	2.9×10^{-3}	39.	1.4×10^{-6}	2.0×10^{3}
114	3	1.0	1.5×10^{-3}	19.	6.9×10^{-7}	2.1×10^{3}
114	4	0.74	1.3×10^{-3}	17.	6.1×10^{-7}	2.1×10^{3}
114	5		8.5×10^{-4}	12.		
115	1	3.3	2.8×10^{-3}	78.	6.2×10^{-6}	4.4×10^{2}
115	2	1.7	2.3×10^{-4}	7.	2.5×10^{-5}	9.1
115	3		1.2×10^{-4}	3.		
115	4		1.7×10^{-4}	5.		
115	5		2.5×10^{-4}	7.		
119	1	1.1	7.8×10^{-4}	44.	5.9×10^{-5}	1.3×10^{1}
119	2	1.0	2.8×10^{-4}	16.	1.5×10^{-6}	1.8×10^{2}
119	3		4.4×10^{-4}	24.		
119	4		2.2×10^{-4}	12.		
119	5		7.0×10^{-5}	4.		
124	1	0.81	1.7×10^{-4}	9.	5.2×10^{-6}	3.3×10^{1}
124	2	1.2	8.5×10^{-4}	46.	9.3×10^{-7}	8.7×10^{2}
124	3		6.2×10^{-4}	34.		
124	4		1.9×10^{-4}	10.		
124	5		2.2×10^{-5}	1.		

TABLE 4.11

Underground Shot Activity Measurements on the Cascade Impactor
(Contd)

Station No.	Jet No.	Number Median Diameter (microns)	Activity on Jet at H + 1 Hrs. (μc)	Percentage of Total Cas. Imp. Activity	Mass of Particles on Jet (grams)	Specific Activity $\frac{\mu c}{gram}$
125	1	1.9	5.6×10^{-4}	50.	2.6×10^{-4}	2.1
125	2	0.68	9.5×10^{-5}	8.	2.5×10^{-6}	3.8×10^{1}
125	3		6.7×10^{-5}	6.		
125	4		3.2×10^{-4}	29.		
125	5		8.3×10^{-5}	7.		
126	1		3.1×10^{-5}	5.		
126	2		3.2×10^{-5}	6.		
126	3		7.7×10^{-5}	14.		
126	4		7.2×10^{-5}	13.		
126	5		3.5×10^{-4}	62.		
132	1	2.5	1.9×10^{-5}	24.	1.3×10^{-5}	1.4
132	2	1.4	1.8×10^{-5}	22.	1.1×10^{-6}	1.7×10^{1}
132	5	0.18	4.3×10^{-5}	54.	4.2×10^{-8}	1.0×10^{3}
135	1	0.49	9.5×10^{-5}	25.	1.1×10^{-5}	8.5
135	2	0.70	6.1×10^{-5}	16.	1.8×10^{-6}	3.4×10^{1}
135	3	1.12	1.8×10^{-5}	5.	1.1×10^{-6}	1.6×10^{1}
135	4	0.14	1.5×10^{-4}	39.	1.9×10^{-7}	7.8×10^{2}
135	5	0.053	6.0×10^{-5}	15.	1.2×10^{-8}	5.0×10^{3}
140	1	1.26	1.7×10^{-4}	7.	3.0×10^{-5}	5.6
140	2	0.81	9.5×10^{-5}	4.	2.6×10^{-6}	3.6×10^{1}
140	3	0.73	1.4×10^{-3}	60.	1.2×10^{-6}	1.1×10^{3}
140	4	0.18	4.9×10^{-4}	22.	2.8×10^{-7}	1.7×10^{3}
140	5	0.12	1.6×10^{-4}	7.	3.0×10^{-8}	5.3×10^{3}

4.3.2 Conifuge

By means of a radioautograph technique, it was possible to determine the activity in the aerosol as a function of particle size (subject to the limitations of the conifuge). Unfortunately, of all the conifuge cones employed, only the one from station 133, located 20,000 feet north of the underground zero point, exhibited what could be considered a good radioautograph pattern. The majority were not sufficiently active to produce a definite film darkening while most of those that were sufficiently active produced irregular patterns, indicating improper operation of the instrument.

The technique consisted of placing the plastic conifuge cone over a matching conical mandrel upon which was fitted a fan-shaped piece of DuPont dosimeter film, type 552. After an exposure of approximately one month, the cones were removed and the film processed. This radioautograph (Fig. 4.18) was scanned along several radii with an Ansco optical densitometer (after standardizing on the clear film) at a number of distances from the inner edge of the fan shaped film. The averaged optical densities were plotted versus r, the distance from the inner edge of the film. This plot was graphically integrated and normalized to a fractional density and plotted versus r as shown in Fig. 4.19. Assuming that the density of the film was proportional to the radioactivity deposited upon the conifuge cone, and the density of the aerosol was similar to glass, the percent activity of the aerosol as a function of particle size can be obtained by use of the data of Table 2.5. In addition, these data were plotted on log probability paper as shown in Fig. 4.20.

Upon the basis of the results from this conifuge, it may be concluded that the median radioactive particle size of the aerosol at station 133 was of the order of two microns.

4.3.3 Particle Separator

Although a determination of the activity of the aerosol as a function of particle size from the particle separator would have been a relatively easy matter and, indeed, the necessary activity measurements were made, no results are reported because the instrument failed to separate particles satisfactorily according to their size.

Microscopic examination of the particle separator screens revealed that the larger screens collected a considerable amount of fine ($< 37\ \mu$) airborne particles while the larger material ($> 37\ \mu$) behaved normally in passing through the various meshed screens. This effect can be seen by examination of Figs. 4.21 and 4.22, which are photomicrographs of the first screen of the particle separator at station 123, taken at different magnifications. Figure 4.21 shows the large particles which

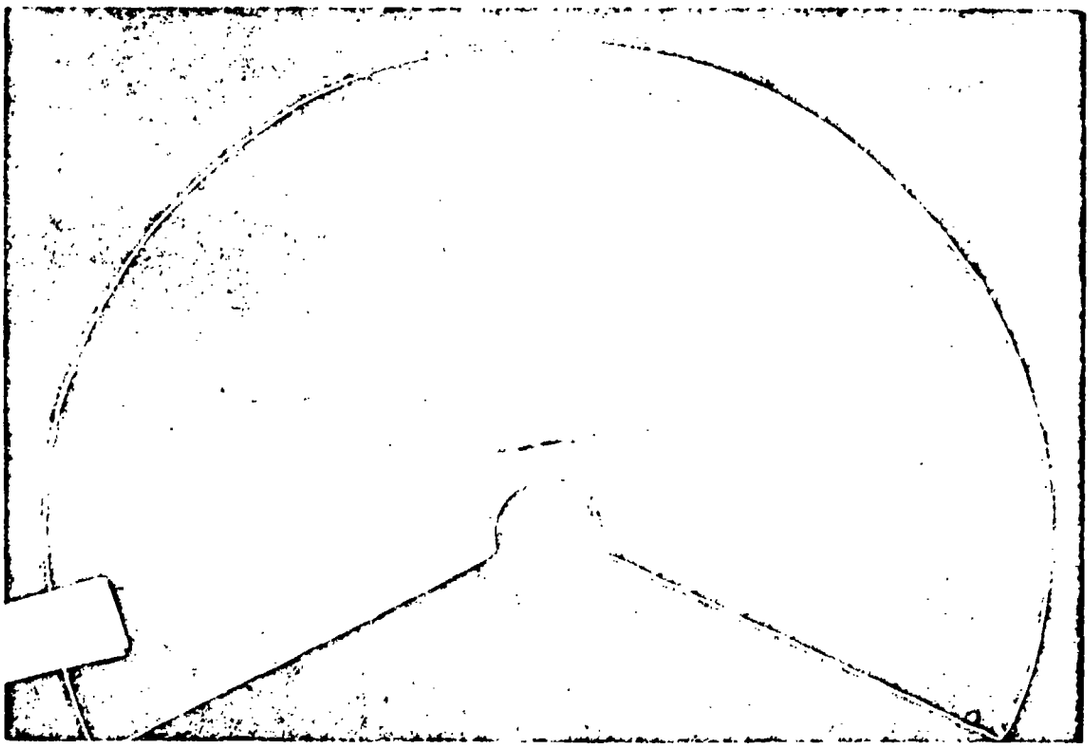

Fig. 4.18 Radioautograph of Conifuge Cone, Station 133, Underground Shot. This is Actually a Positive Print. The Dark Radial Lines Were Caused By the Use of Scotch Tape to Obtain Samples of the Collected Particles. The Dark Dots Were Caused By the Electron Microscope Screens.

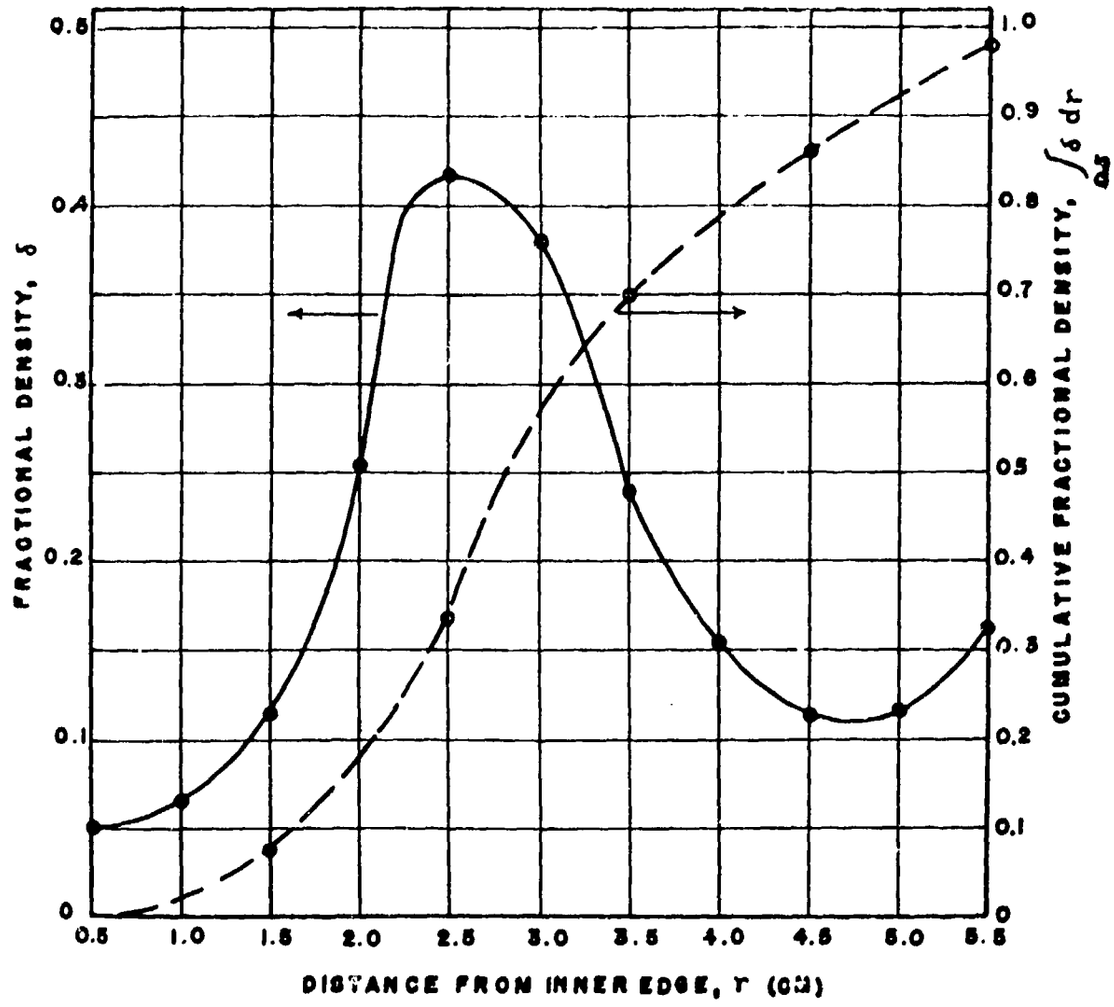

Fig. 4.19 Fractional Density and its Integral, Station 133, Underground Shot, Conifuge Data.

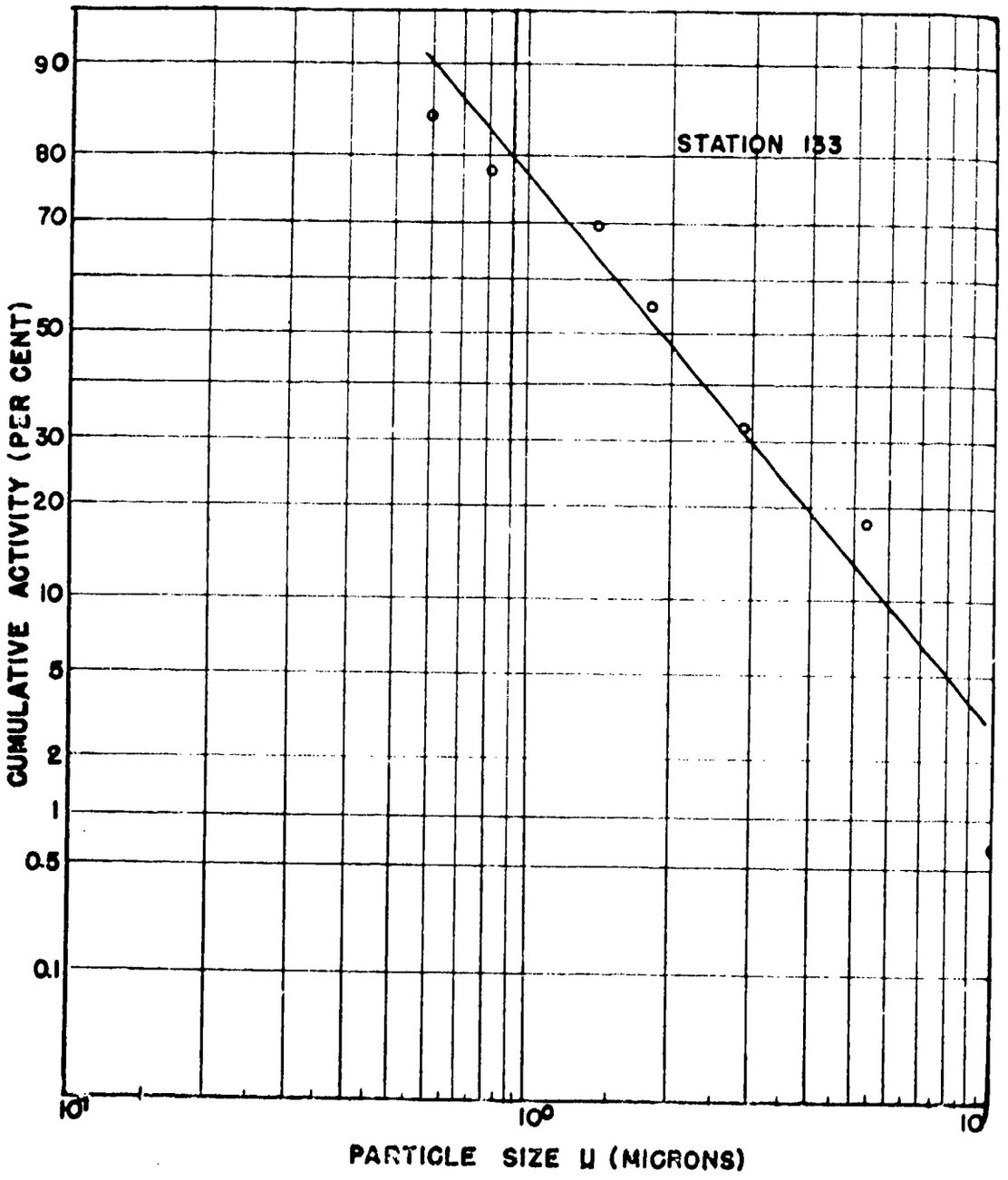

Fig. 4.20 Cumulative Percent Activity as a Function of Particle Size, Station 133, Underground Shot, Conifuge Data.

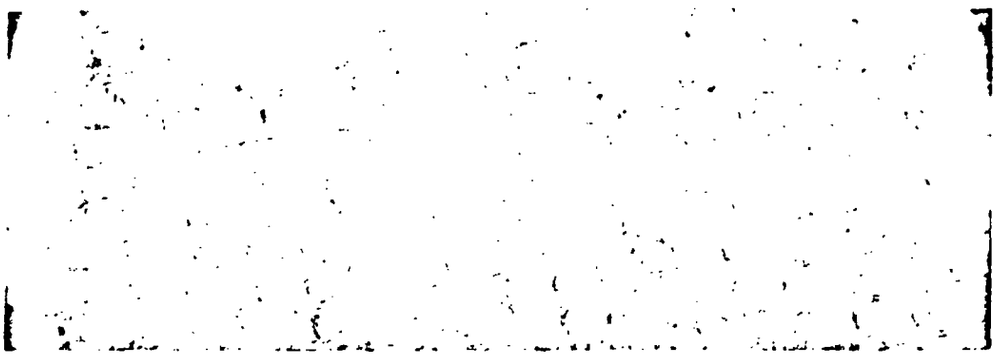

Fig. 4.21 Photomicrograph of the First Screen of the Particle Separator at Station 123, at 20x Magnification. The Large Particles are Apparent.

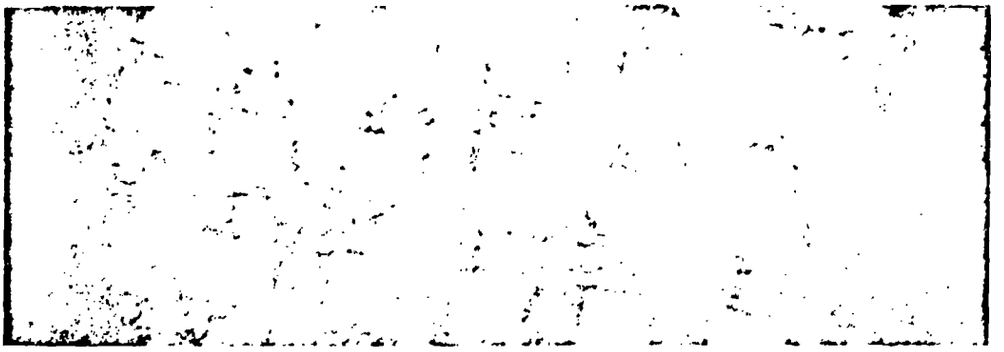

Fig. 4.22 Photomicrograph of the First Screen of the Particle Separator at Station 123, at 50x Magnification. The Small Particles May be Seen Adhering to the Screen Wires.

Fig. 4.23 Photomicrograph of a Clean Particle Separator Screen.

were stopped by the screen, while Fig. 4.22 shows the small particles that also adhered to the screen. For comparison purposes a photomicrograph of a clean screen has been included in Fig. 4.23. It was noted that the large mesh screens were densely covered, front and rear, by a layer of the order of one to ten microns, while the smaller mesh screens were almost entirely free of particulate matter. Activity measurements and microscopic examination of the porous stainless steel back-up filters indicated, however, that a considerable number of particles passed all screens.

The only plausible explanation of this anomaly so far advanced is that the air passing through the screens builds up an electrostatic charge on the well insulated metal screens sufficient to attract and remove from the air stream those particles with suitable charge and inertia values while permitting the neutral and oppositely charged particles to pass through the screens until mechanically stopped by the back-up filter.

In order to test this hypothesis, attempts were made in this laboratory to measure electrostatic charge built up by the particle separator screens while air passed through at the correct rate. A charge of the order of a volt was indicated by an oscilloscope after several minutes of air flow. While it is conceivable that in the drier climate at the Nevada Test Site a somewhat higher electrostatic potential might be attained, it would appear that the electrostatic theory is untenable unless the particulate matter in the JANGLE aerosols was highly charged.

4.3.4 Fall-out Tray

Activity measurements were made on the particle size fractions obtained in the sieve analysis (see par. 4.2.3) of one fall-out tray from the surface shot and eight trays from the underground shot, and from these data the activity of the fall-out as a function of particle size has been determined. Figs. 4.24 through 4.29 show in cumulative fashion the percentage of activity associated with each particle size fraction, the data from stations at the same radial distance being shown on the same graph. Table 4.12 shows the specific activity, corrected to H/1 hour, of the particle size fractions of four stations from the underground shot.

The activity measurements were made by means of a Tracerlab SC-6a automatic sample changer and associated equipment. Aliquots of each particle size fraction were transferred to the counting planchets and coated with collodion to prevent loss in handling. A Tracerlab TBC-1 Geiger tube having a window thickness of 2.48 mg/cm^2 was

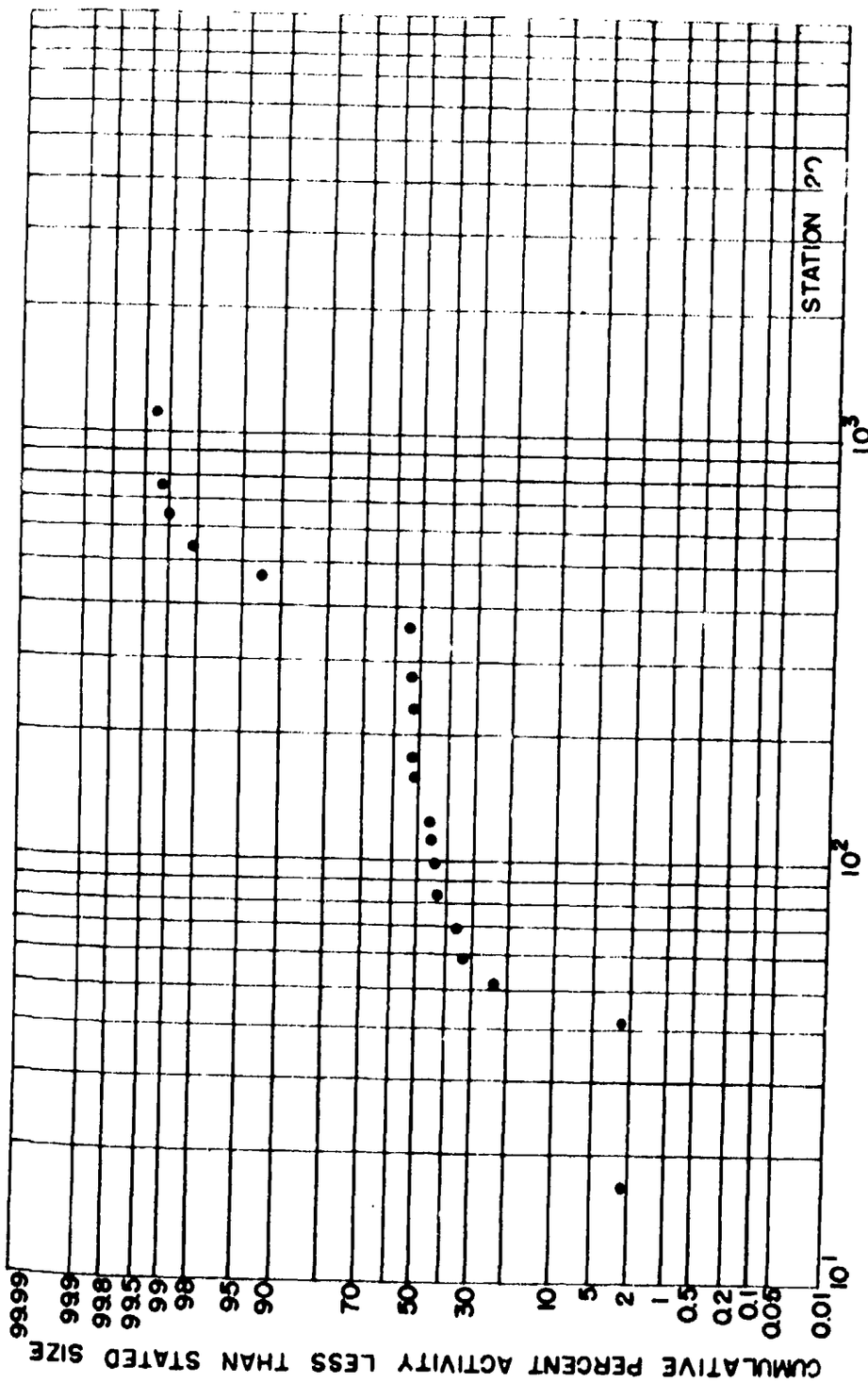

Fig. 2.24 Fall-out Activity as a Function of Particle Size, Station 20, Surface Shot.

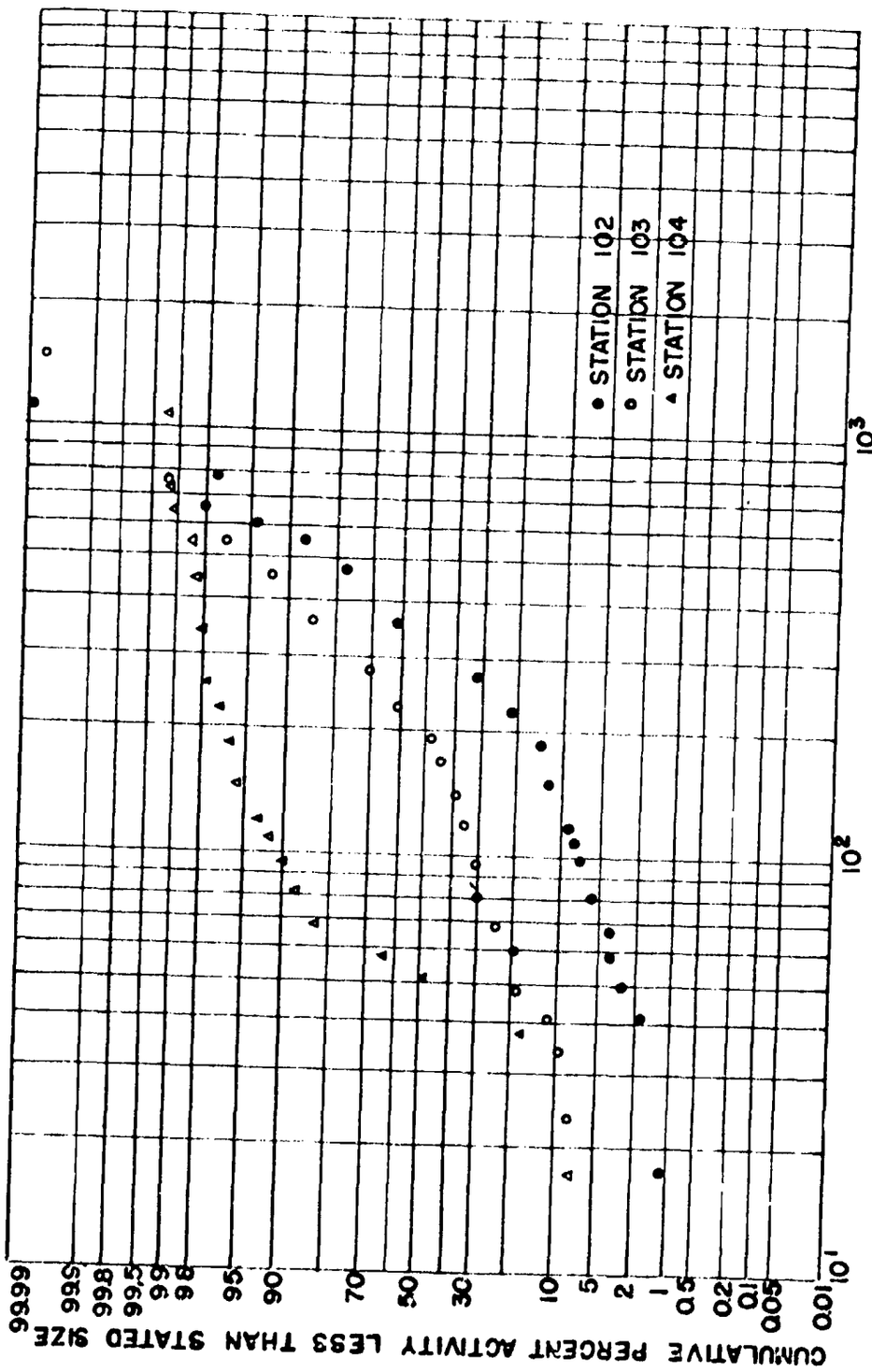

Fig. 4.25 Fall-out Activity as a Function of Particle Size, 2000 Foot Radius, Underground Shot.

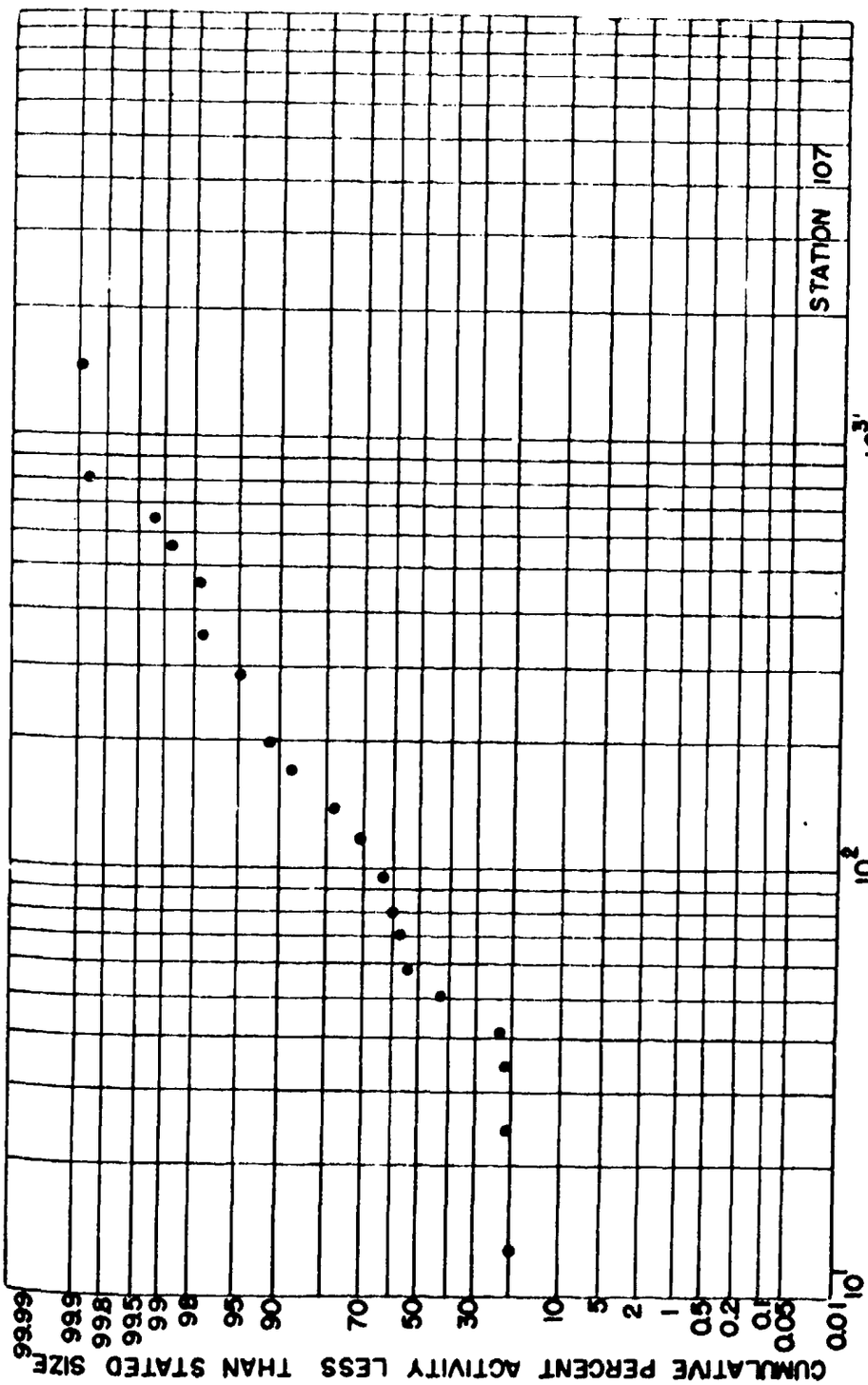

Fig. 4.26 Fall-out Activity as a Function of Particle Size, 3000 Foot Radius, Underground Shot.

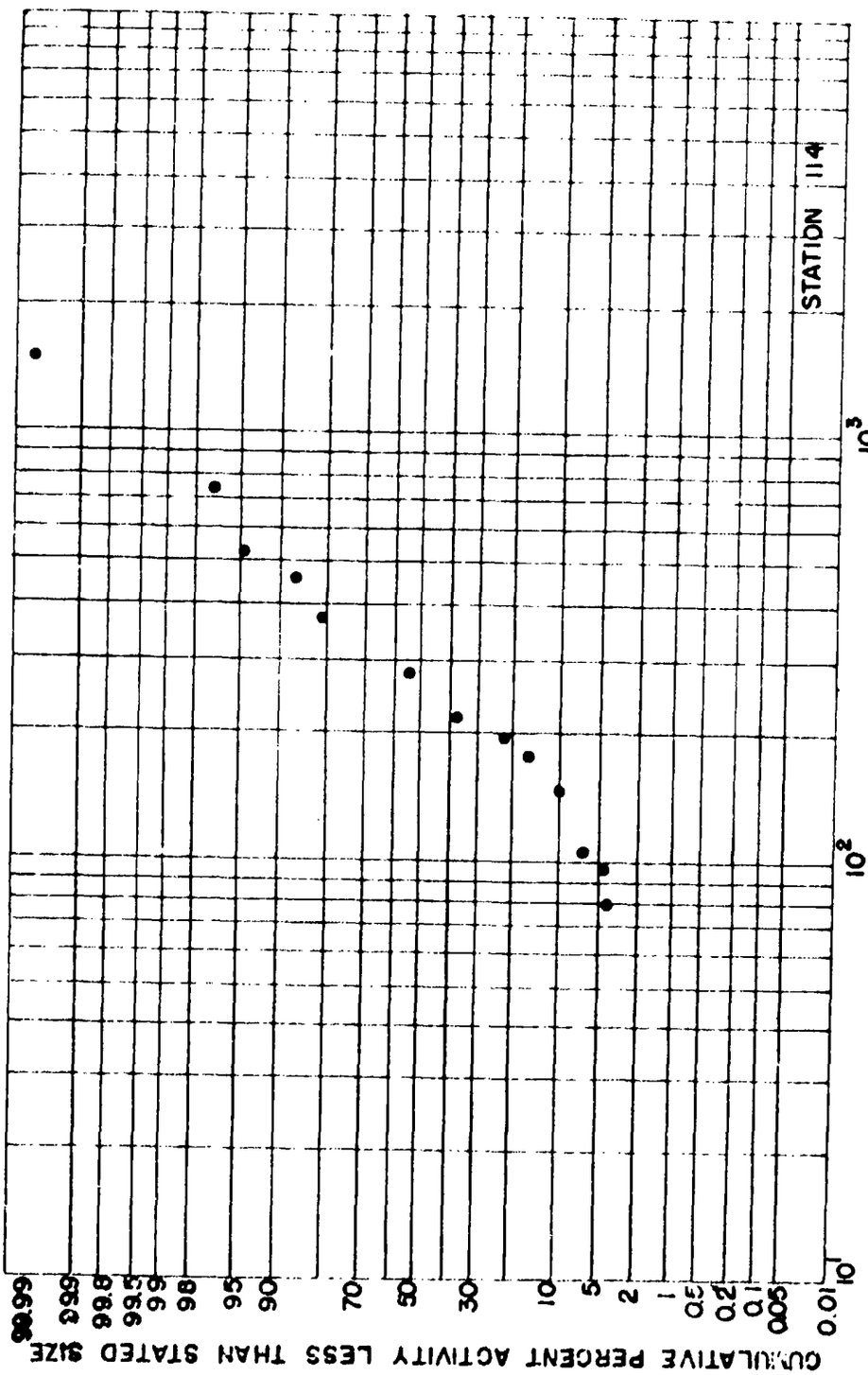

Fig. 2.27 Fall-out Activity as a Function of Particle Size, 4000 Foot Radius, Underground Shot.

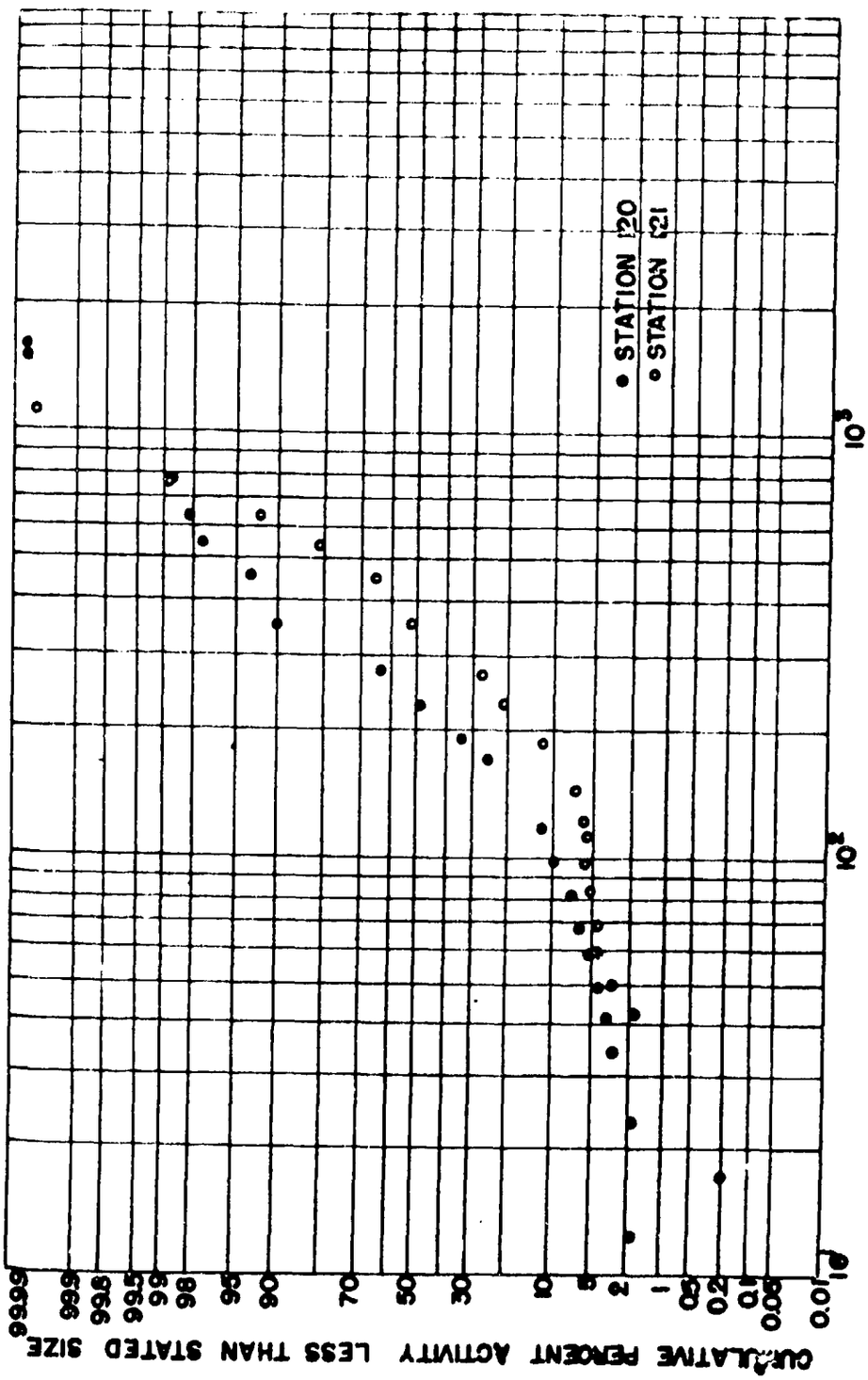

Fig. 4.28 Fall-out Activity as a Function of Particle Size, 6000 Foot Radius, Underground Shot.

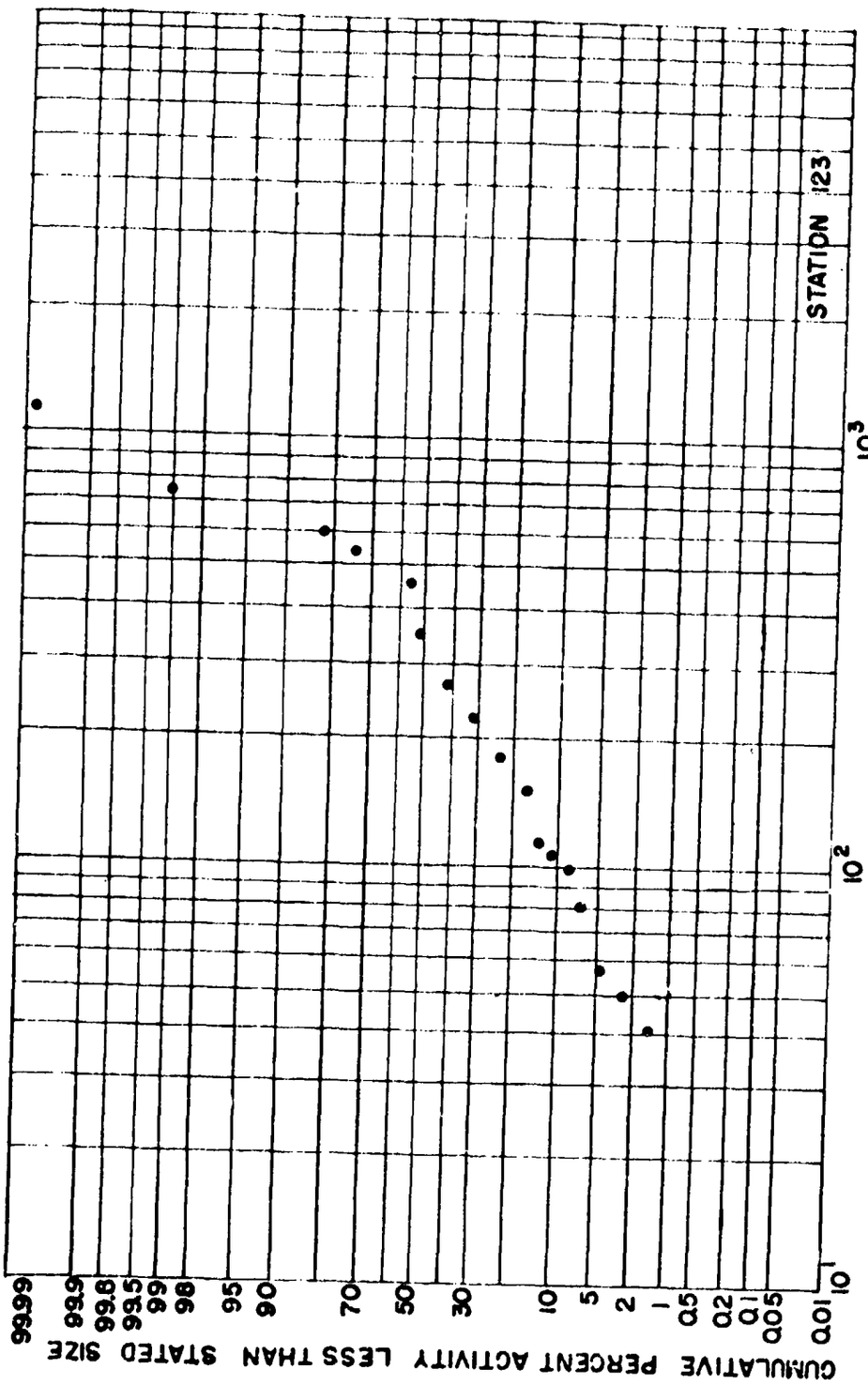

Fig. 4.29 Fall-out Activity as a Function of Particle Size, 8000 Foot Radius, Underground Shot.

PROJECT 2.5a-1

TABLE 4.12

Specific Activity Corrected to H+1, of Fall-out.
Underground Shot

Particle Size (microns)	Station 103 (10^{-1} uc/gm)	Station 107 (10^{-1} uc/gm)	Station 114 (10^{-1} uc/gm)	Station 120 (10^{-1} uc/gm)
2	51.	36.	28.	48.
6	30.	26.	19.	24.
12	14.	19.	10.	19.
24	10.	12.	8.5	17.
34	7.5	8.7	8.6	11.
40	16.	10.	12.	16.
48	17.	10.	8.8	11.
58	24.	8.4	6.2	11.
68	12.	9.1	7.6	8.3
81	13.	7.2	7.8	5.7
96	11.	15.	1.0	6.5
115	26.	13.	13.	11.
137	42.	17.	22.	14.
163	44.	23.	22.	16.
194	48.	25.	32.	19.
230	48.	27.	34.	30.
274	71.	115.	35.	32.
358	77.	33.	41.	39.
460	43.	32.	39.	22.
545	69.	43.	46.	30.
650	80.	64.	40.	43.
775	38.	72.	44.	52.
1500	360.	18×10^{-2}	51.	25.

employed, and the scaler was preset for a cumulative count of 4096 for each sample. A Tracerlab R-11a simulated P^{32} source was used as a reference standard for absolute beta counting. Range curves in aluminum were run for the standard and several fall-out samples to determine correction factors for air path and window losses. Back scattering and possible collodion absorption corrections were not attempted. All activity measurements were made between 1000 and 2000 hours after the shot and were corrected to H-1000 by means of individual decay curves obtained on each sample. The NIH decay curves described in par. 4.1.1 were used to correct all fractions from H/1000 hours to H/1 hour.

4.4 PERCENTAGE OF RADIOACTIVE PARTICLES

4.4.1 Cascade Impactor

The number of active particles on each of the five slides from the cascade impactors at stations 123 and 130 was determined by means of a radioautograph technique. Since the particle size analysis of the cascade impactors (par. 4.2.1) yielded the total number of particles per slide, the percentage of radioactive particles could be determined. The data are presented in Figure 4.30.

The radioautographs were made after the particle size measurements were completed since the emulsion on the slides would have interfered with the electron microscope particle size analysis. Eastman Kodak Company type NTB stripping film was cut to size and cemented over the sample area of the slide. Development of the film was carried out as recommended by Eastman Kodak Company. The radioautographs were then examined by means of a microscope to determine the number of particles with associated activity. The slides from station 123 were exposed from H/1704 to H/2208 hours; station 130 slides from H/1704 to H/2016. Although other slides were exposed for an even greater length of time, too few of the particles on each slide were sufficiently active to provide reliable results.

4.4.2 Fall-out Tray

The size fractions of the fall-out from stations 103 and 120 of the underground shot were analyzed by a radioautograph technique to determine the percentage of radioactive particles. The data are presented in Fig. 4.31. The size fractions were obtained from the sieve analysis described in par. 4.2.3, and the radioautograph technique is described below.

PROJECT 2.5a-1

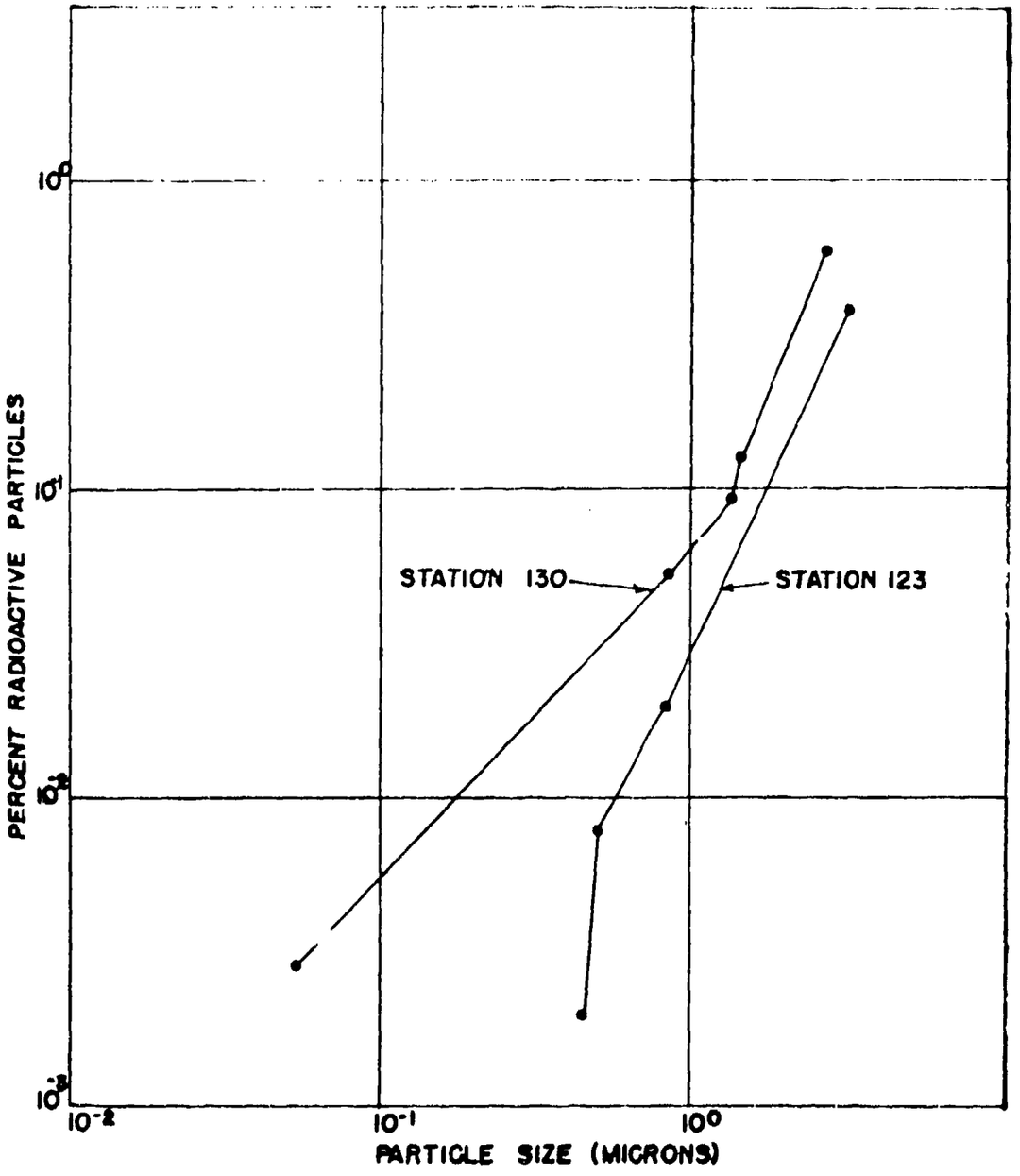

Fig. 4.30 Percentage of Active Particles in the Aerosol as a Function of Particle Size, Underground Shot, Cascade Impactor Data.

PROJECT 2.5a-1

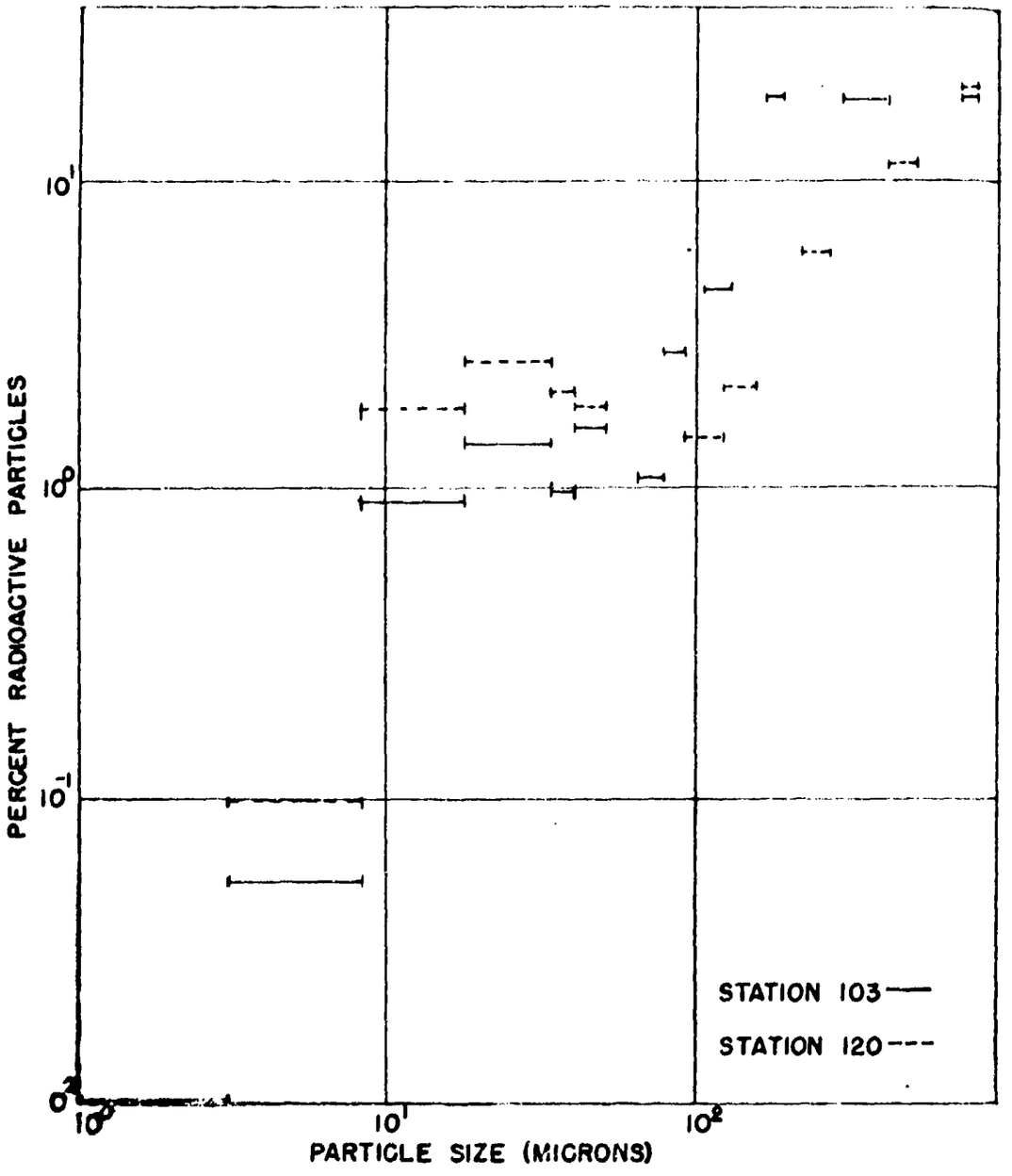

Fig. 4.31 Percentage of Active Particles in the Fall-out as a Function of Particle Size, Underground Shot.

After some experimentation, a number of procedures for determining the percentages of radioactive particles were developed[10] for various size ranges. These were as follows: Method No. 1 approximately 150 to 850 microns. In this method, Kodak NTB Autoradiographic Stripping Film was employed to distinguish active particles. This emulsion was stripped from its cellulose backing, relaid emulsion side down on its backing and lightly fastened to it with strips of tape. The fractionated sample was distributed over the back side of the emulsion by means of a spatula and the particles were affixed by covering with a Duco cement solution (one volume of cement to four of acetone). After drying, the strip film was reversed and retaped to the support. The film was stored in a light-tight box for a three to four day exposure. The exposed film was developed with DuPont x-ray developer, fixed, washed, and dried and again removed from its support and fastened to a clean glass slide over millimeter graph paper for examination and counting with a stereomicroscope. Black areas were observed above each radioactive particle while the inactive ones did not effect the emulsion. The intensity of blackening appeared somewhat variable and occasional difficulty was experienced when only a small spot was evident or when only a portion of the particle appeared to be active or when the emulsion appeared fogged or grey rather than intense black. In doubtful cases the particle was considered to be radioactive. A number of these "doubtful" active particles were picked up and were found in every case to be radioactive when held in front of the window of a G-M tube counter. Thus the assumption that all "doubtful" particles were active appears to be justified. Considerable wrinkling of the strip film was experienced but this does not interfere with the method. Below approximately 150 microns the method becomes impractical due to difficulties in ascertaining the nature of many particles.

Method No. 2, approximately 16 to 150 microns. Kodak NTB Nuclear Track plates softened for 10 to 15 seconds in warm water (50 C) were utilized in this procedure. The size-fractionated particles were distributed over the moist plates in the same manner as in the first method and the plates with their adhering particles were allowed to dry and expose for two to three days in a light-tight box. The plates were developed with careful agitation so as to avoid displacement of the imbedded particles. Examination of the plate with a stereomicroscope revealed the radioactive particles over their associated darkened area on the film. (See Fig. 4.32)

---

[10] Malcolm G. Gordon and Benjamin J. Intorre, "Some Techniques Applicable to the Study of ABD Fall-out", CRL Interim Report No. 137, 14 Mar 1952.

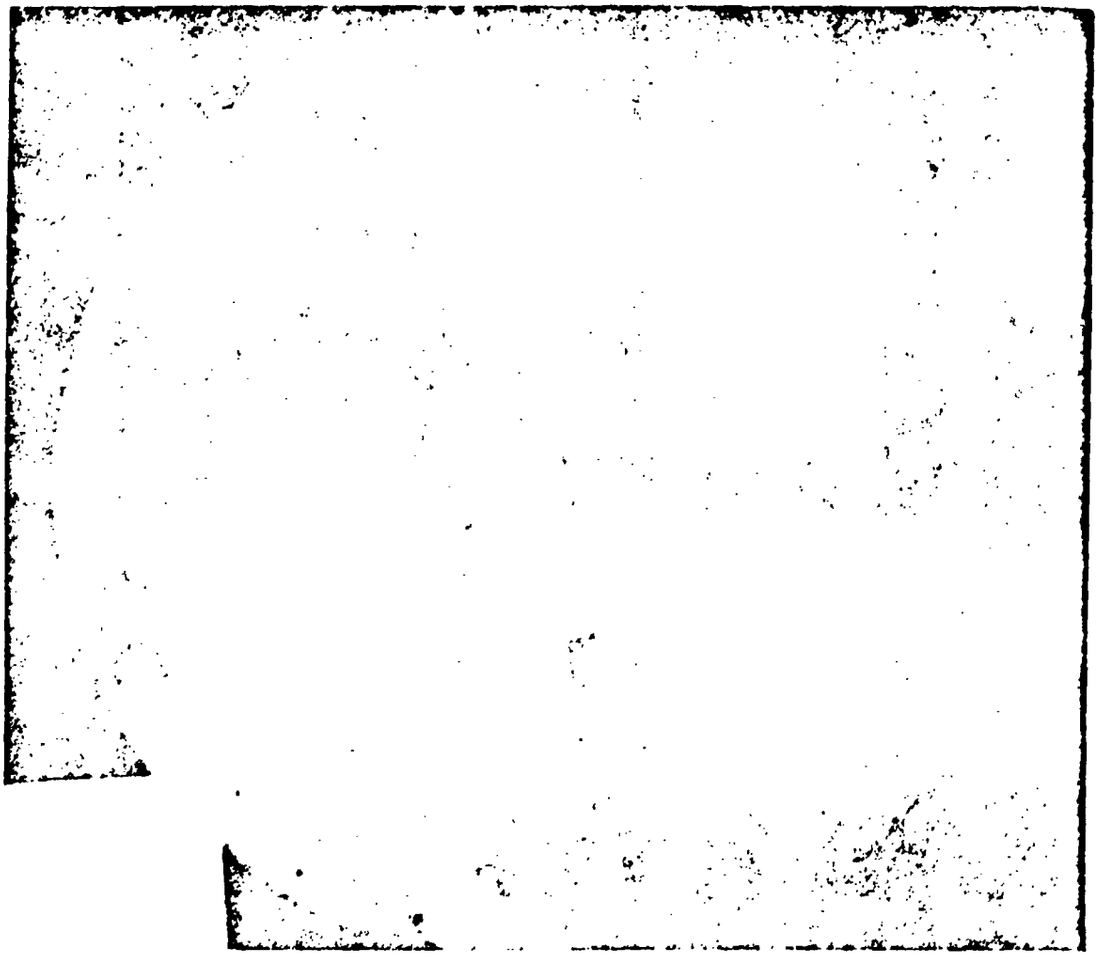

Fig. 4.32 Station 103 Fall-out Particles (74-88 u) on an NTB plate showing the film darkening around two radioactive particles.

As a check upon the agreement of the two methods, the percentage of radioactive particles in a 240 to 420 micron range sample was determined. Results of 16.7 and 17.7 per cent were obtained for the strip-film and the plate methods respectively.

Method No. 3, approximately 8 to 40 microns. Inasmuch as the smaller particles tended to agglomerate, the second method was modified for the lowest particle size ranges so that the sample was dropped into a swirling inch of hot water (50°C) in a battery jar. After suspension of the particles an NTB plate was submerged and after approximately 30 seconds removed, dried, exposed for four or five days and then processed in the usual manner. Particle counting was most easily accomplished in the range of 8 to 40 microns by visually counting the radioactive particles in a given area with a light background and then photographing the same area with a dark background. The total number of particles could be conveniently counted on the print.

4.5 STUDY OF FRACTIONATION

4.5.1 Radiochemistry

The study of fractionation included radiochemical analysis of many JANGLE samples obtained from various types of instruments which were located at a number of different stations. Sr^{89}, Zr^{95}, Mo^{99}, Ag^{111}, Cd^{115}, Ba^{140}, Ce^{141}, and Ce^{144}, were determined on four filter papers from the underground shot, and Zr^{95} and Mo^{99} were determined on a horizontal ointment plate from the surface shot. These data are tabulated in Table 4.13 as counting rate ratios (at zero time) with respect to Mo^{99} (an allegedly non-fractionating nuclide). Ag^{111}/Ba^{140} and Ag^{111}/Cd^{115} ratios have also been tabulated because of their special interest.

In addition, the large quantities of fall-out collected from the underground shot at Operation JANGLE provided a unique opportunity to perform radiochemical analyses upon size-graded particles. Sr^{89}, Zr^{95}, Ba^{140}, and Ce^{144} were determined on a number of different particle size fractions of fall-out collected at stations 103, 107, 114, and 120. These data are tabulated in Table 4.14. Mo^{99} was not determined because the decision to make the fall-out analysis was not made until some weeks after the shot. The nuclide activity per unit mass of radioactive material was calculated by dividing the nuclide activity by the mass of active particles in each fraction. The latter was determined by applying the data of par. 4.3.3 to the measured mass of each fraction. These data are tabulated in Table 4.15 and will be used in the discussion in par. 5.5.

Pages 108, 109, 110 blank

PROJECT 2.5a-1

The fission products separations were carried out essentially by the methods compiled by Coryell and Sugarman[11] as modified by J-11 Group, Los Alamos Scientific Laboratory. The only important modification was the determination of silver as iodate rather than iodide. The fall-out samples were run in duplicate, the others in quadruplicate.

In order to provide a basis for comparison with other laboratories, radiochemical analyses were performed on an irradiated U^{235} sample for each of the fission products listed above with the exception of Cd^{115} and Ce^{141}. The sample consisted of 14.8 milligrams of enriched uranium foil irradiated to 9.3×10^{13} fissions in the Brookhaven pile.

Filter paper samples were digested by treatment with fuming nitric, perchloric, and hydrofluoric acids by the procedure described by Spence and Bowman[12]. The M-5 ointment was removed from the aluminum plate with facial tissue and digested by the same procedure. It was necessary to repeat the digestion to effect complete solution. The fall-out samples were fumed successively with perchloric and hydrofluoric acids and taken up with hydrochloric acid.

Samples were mounted in a reproducible geometry system on 3-1/4x2-1/2x1/16 inch aluminum cards. In the case of Mo, Cd, Ag, Ba, and Sr the final precipitation was carried out by the glass chimney and Hirsch funnel technique, which confined the precipitate to a defined area on the filter paper. Ce and Zr precipitates were tapped out of the ignition crucibles into counter ores in the aluminum cards. Samples were covered with either 3.8 mg/cm^2 of cellophane or 0.45 mg/cm^2 of rubber hydrochloride. Ce^{144} was counted face down and hence through 217 mg/cm of aluminum.

Each mounted sample was counted for decay with a thin mica end-window G-M tube and conventional scaler unit until a satisfactory curve was obtained or the activity became too low, whichever occurred first. The counting rates were measured to 0.95 errors[13] of 2-5% for the

---

[11] C. D. Coryell and N. Sugarman, Radiochemical Studies: The Fission Products, McGraw-Hill Book Co., New York, N. Y. 1951

[12] R. W. Spence and M. G. Bowman, "Radiochemical Efficiency Results of Operation SANDSTONE", SANDSTONE Report 10, Appendix A, Los Alamos Scientific Laboratory, March 25, 1949

[13] i.e., We are 95% certain that the statistical error in counting is not greater than the listed per cent.

plate. Spreads[14] for repeated analyses on the size-graded fall-out were within 5% for the Ba^{140} and Sr^{89} and from 10-20% for Ce^{144} and Zr^{95}. The spreads for the filter paper and ointment plate work were also 10-20%

The activity was read from the smoothed decay curve at an arbitrary time and corrected to zero time. Four different G-M tubes, cross-calibrated with samples of each fission product, were used, and all data were corrected to the same tube. Data were further corrected to 100% chemical yield, first shelf and zero added absorber. No corrections for coincidence were required nor were corrections made for self-absorption and self-scattering since time did not permit preparation of correction curves. This error was insignificant except in the case of some strontium samples where the chemical yields were extremely high. The correction even here would be less than 5%. The aluminum mounting cards provided saturation backscattering. Corrections to zero added absorber were based on absorption curves in Coryell and Sugarman[15]. Barium activities were corrected for growth of lanthanum activity as indicated by Finkle and Sugarman[16].

4.5.2 Activity of the Radioactive Particles as a Function of Particle Size

In the study of fractionation it is of interest to determine the activity of the radioactive particles as a function of their size, surface area, and mass. The analysis of the size-graded fall-out samples at stations 103 and 120 of the underground shot for activity and per cent active particles offered an opportunity to determine these quantities indirectly. The results are presented in Figures 4.33 through 4.35.

The following procedure was employed: The percent active particle data (par. 4.4.2) in each fraction were applied to the

[14]The spread was obtained by dividing the difference between the extremes by the mean.

[15]Coryell and Sugarman, op. cit., Book 2

[16]Ibid., p. 1123

PROJECT 2.5a-1

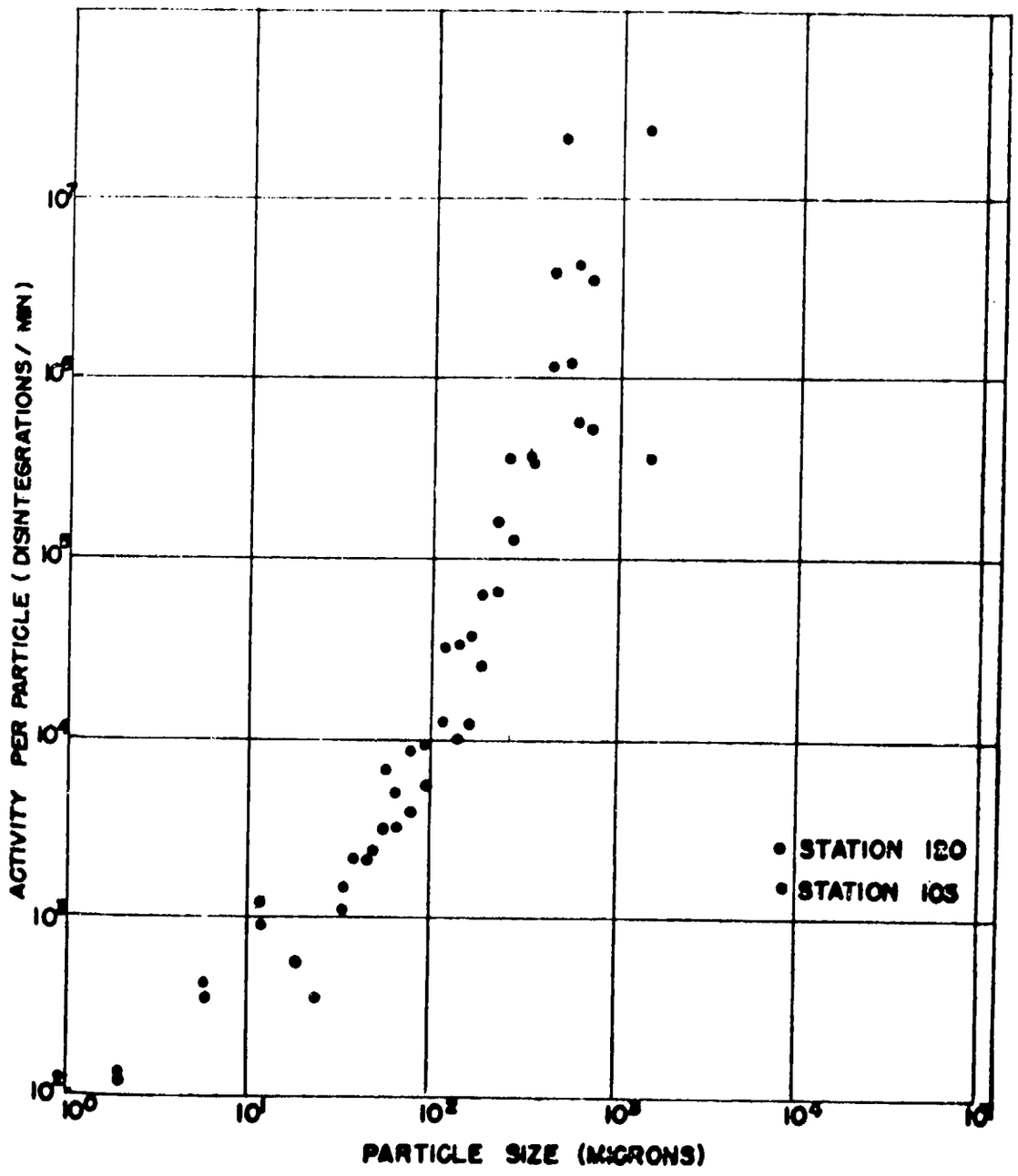

Fig. 4.33 Activity per Radioactive Particle as a Function of Particle Size.

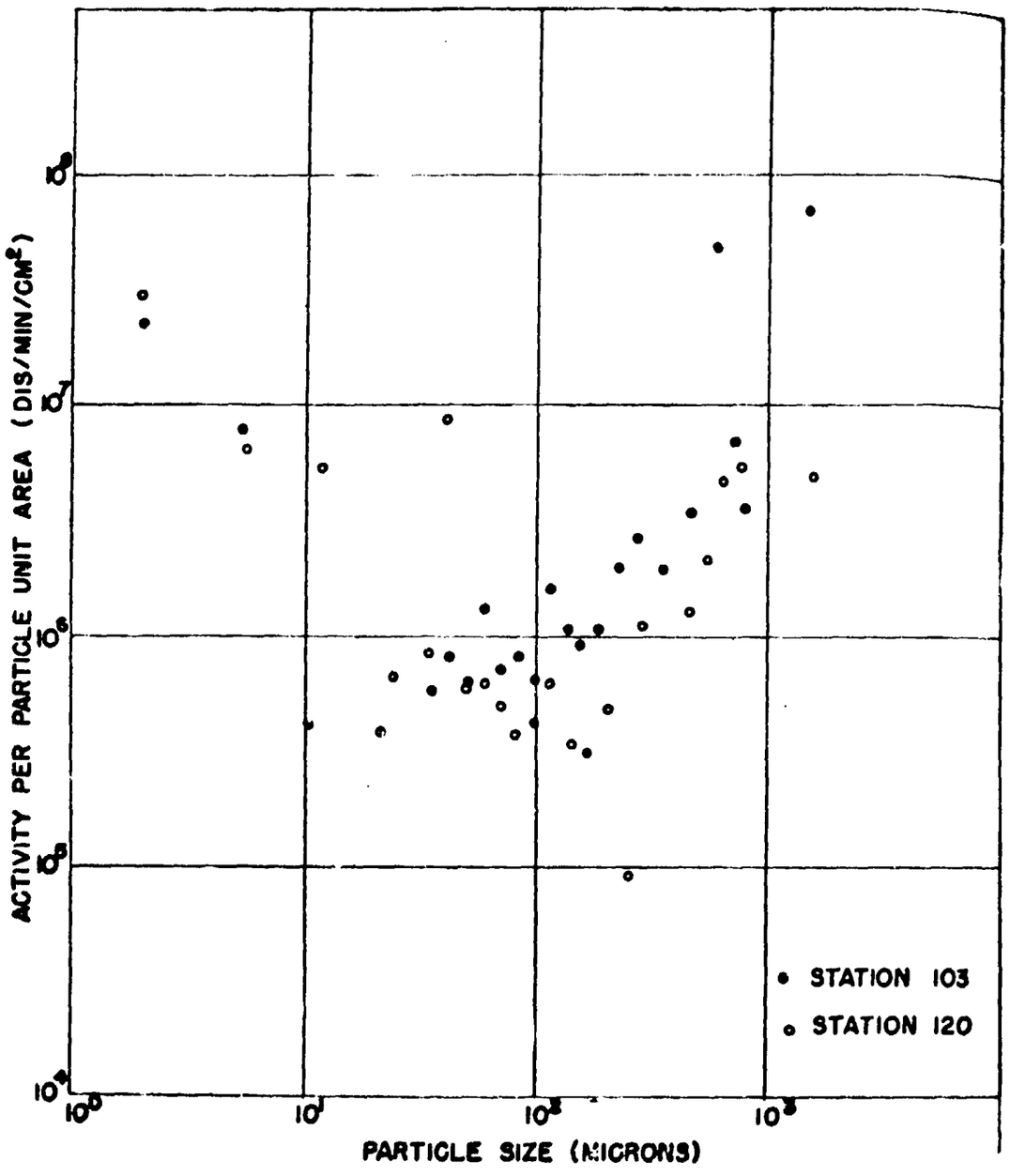

Fig. 4.34 Activity per Unit Area of Radioactive Particles as a Function of Particle Size.

PROJECT 2.5a-1

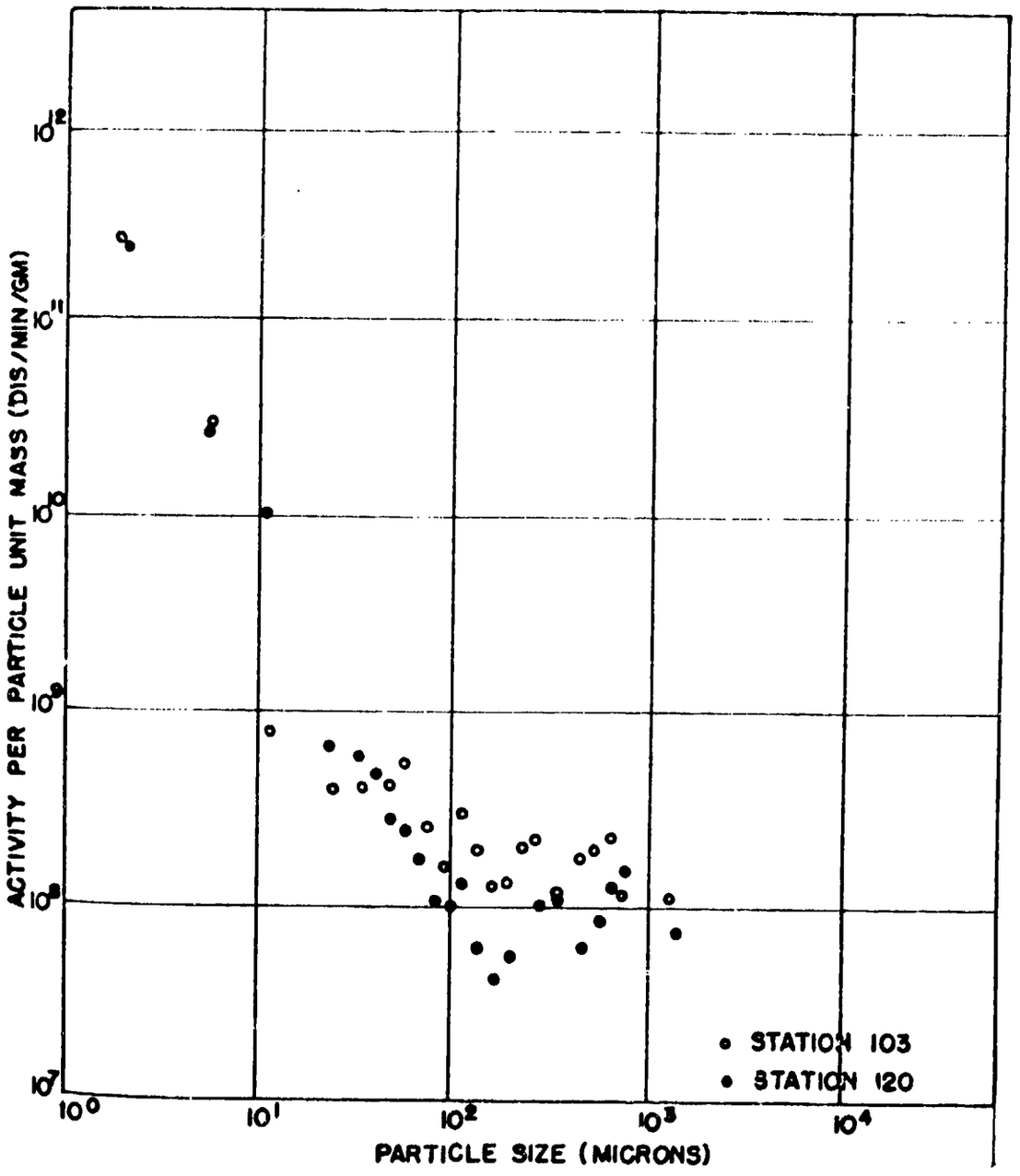

Fig. 4.35 Activity per Unit Mass of Radioactive Particles as a Function of Particle Size.

specific activity of that fraction (par. 4.3.4), giving the specific activity of the active particles of the fraction (assuming all particles in the fraction had the same weight). Making the further assumption that all particles in the fraction had the same density and shape, the activity per unit active particle surface area, and the activity per active particle were calculated. A specific gravity of 2.7 was assumed, and all particles were assumed to be spherical in shape. The size of particles in a given size fraction was taken to be the average of the pore size of the sieve on which the particles were found and the pore size of the sieve directly above.

4.5.3 Decay Rates

It was expected that fractionation would manifest itself by a variation in decay rate with particle size. To investigate this possibility, the activity measurements on the size fractions of fallout at stations 103,107,114, and 120 were continued from about H/1000 hours to approximately H/2000 hours. The resulting activities were plotted as a function of time on log-log paper and a straight line was fitted to them by the method of least squares. The slopes of these lines are presented in Table 4.16. The data for station 120 is presented in graphical form in Figure 4.36.

TABLE 4.16

Decay Slopes (Between H/1000 and 2000 Hours) of Size Graded Fall-out Samples

Particle Diameter (microns)	Decay Slope*			
	Station 103	Station 107	Station 114	Station 120
1500	-1.110	/0.127	-1.217	-1.225
775	-1.238	-0.448	-1.205	-1.124
650	-1.291	-1.417	-1.058	-1.221
545	-1.162	-0.613	-1.177	-1.203
460	-1.424	-0.587	-1.165	-1.105
358	-1.128	-1.252	-1.247	-1.066
274	-1.284	-0.796	-1.241	-1.154
230	-1.244	-0.878	-1.241	-1.279
194	-1.308	-0.943	-1.229	-1.140
163	-1.349	-0.913	-1.253	-1.165
137	-1.302	-0.687	-1.241	-1.211
115	-1.331	-0.856	-1.329	-1.228
96	-1.354	-0.883	-1.288	-1.229
81	-1.331	-1.204	-1.247	-1.186
68	-1.430	-0.987	-1.300	-1.244
58	-1.337	-0.843	-1.215	-1.321
48	-1.436	-1.170	-1.312	-1.261
40	-1.343	-0.836	-1.394	-1.294
18	-1.424	-0.738	-1.429	-1.331

*The decay slope is defined as n in the equation

$$A = kt^n$$

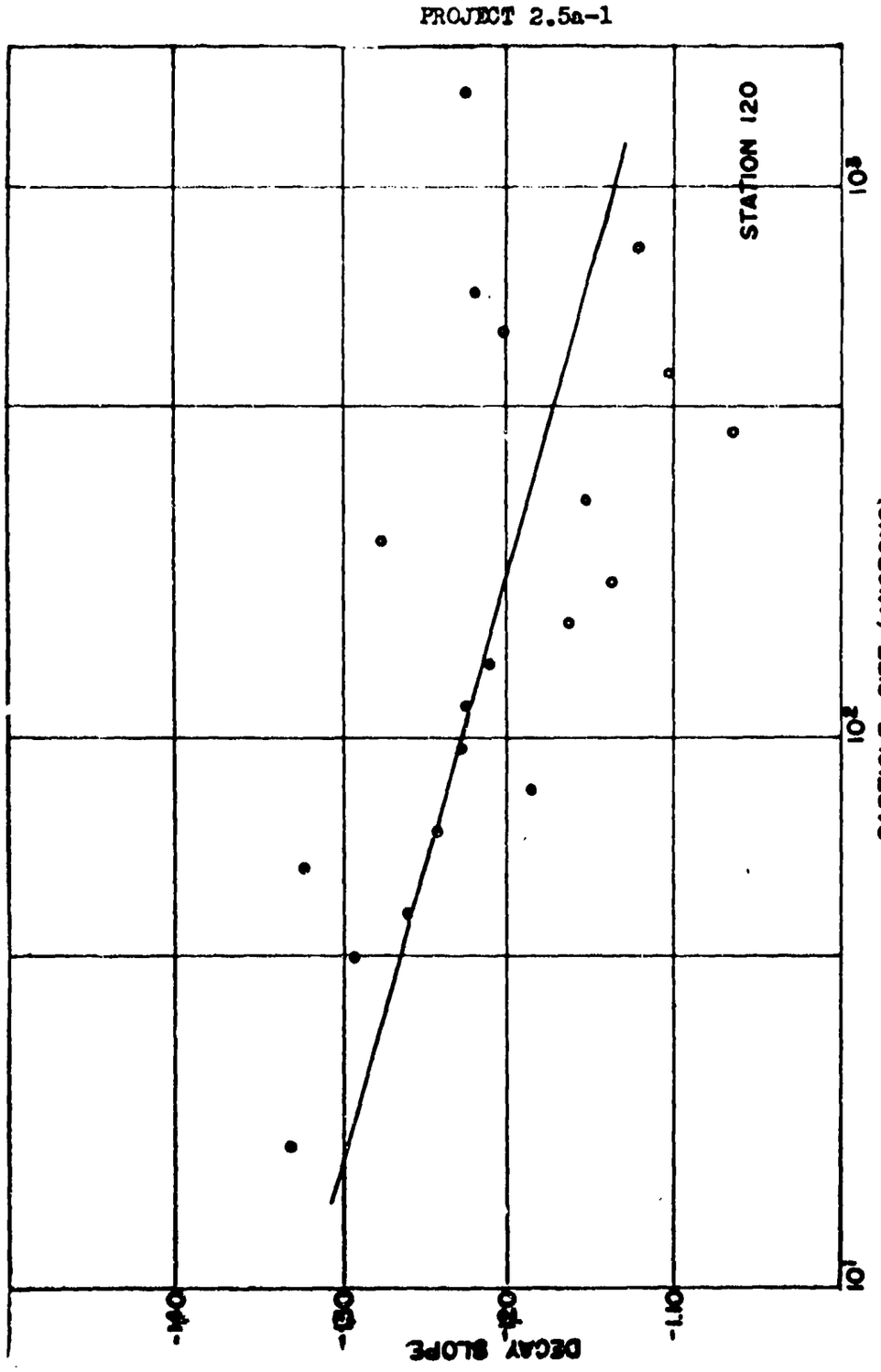

Fig. 4.36 Decay Slope vs Fall-out Particle Size, Station 120, Underground Shot

CHAPTER 5

DISCUSSION

5.1 CONCENTRATION OF ACTIVITY IN THE AEROSOL

Before proceeding to a discussion of some of the details of the activity concentration data, it is well to compare the data obtained by the four types of instruments which were employed. Such a comparison is made in Table 5.1, in which the ratios of the concentrations obtained from the particle separator, cascade impactor, and continuous air monitor, to those obtained from the filter sampler have been computed. The table illustrates, for one thing, the extremely large variations that may be expected in measurements of this sort made with existing sampling equipment. It is apparent that the data obtained by the particle separator varied from one tenth to ten times that of the filter sampler. There is apparent disagreement between the cascade impactor and the filter sampler, the former being smaller than the latter by a factor of the order of a several hundred. The case of this disagreement is thought to be due to the fact that the cascade impactor, in obtaining a relatively small sample, is more susceptible to the loss of large particles, because collection of the particles is made on a glass slide, rather than on filter paper. Comparison between the continuous air monitor and the filter sampler suffers from the lack of data from the former, together with a contradiction on two of the four records obtained, that is, apparently the cloud did not reach the station until after the 115 min filter sampler sampling period was over. One of the remaining two records indicated the continuous air monitor data was ten times, the other one tenth as large than the filter sampler data. Probably the only conclusion that can be reached from this comparison is that the filter sampler concentration data is in systematic disagreement with the cascade impactor data, but is not in systematic disagreement with the particle separator or continuous air monitor data, although agreement in any particular case may be no better than plus or minus one order of magnitude.

It is possible that the comparison of the particle separator-filter sampler data may shed some light upon the question of the effect of non-isokinetic sampling upon the concentration data. It will be remembered that the particle separators were oriented with the axis of their sampling port in the vertical direction, while the filter samplers were oriented in the horizontal direction. Under these conditions one would expect that the particle separator, in collecting the largest particles

PROJECT 2.5a-1

TABLE 5.1

Comparison of Concentration of Activity Data

Station	Particle Separator[1] / Filter Sampler[1]	Cascade Impactor[2] / Filter Sampler[1]	Continuous Air Monitor[3] / Filter Sampler[1]
		Surface Shot	
8	3.8		
14	6.8		
15	9.2×10^{-1}		
21	2.5		
23	1.0	1.1×10^{-1}	
24	9.7×10^{-1}		
25		9.5×10^{-3}	
26		2.1×10^{-2}	
28	4.7×10^{2}		
29	1.2×10^{-1}		1.1×10^{-1}
30		3.2×10^{-2}	
35		3.6×10^{-2}	
38			9.6
40		2.6×10^{-2}	
		Underground Shot	
108	5.7×10^{-1}		
109	4.0		
114	3.5×10^{1}	2.1×10^{-2}	
115	1.5	1.6×10^{-2}	
119		1.2×10^{-1}	
120	2.6×10^{1}		
121	3.4		
123	1.0		
124	3.1	2.8×10^{-5}	
125		2.3×10^{-4}	
128	1.0×10^{1}		
129	1.1×10^{-1}		
130	1.1×10^{1}		
132		2.2×10^{-4}	
140		1.4×10^{-3}	

1 Average concentration over 115 minute sampling period.
2 Station numbers less than 25 and 125, concentration over 1 minute sampling period; greater than 25 and 125, over 115 minute sampling period.
3 Average concentration over 115 minutes computed from concentration vs. time curve.

would cause a systematic decrease in the particle separator-filter sampler concentration ratio with distance from ground zero. However, no such trend can be detected, and it is thought, therefore, that the effect due to non-isokinetic sampling, at least in the case of concentration data, may be masked by the spread already present in the data.

The question of the accuracy of the cloud model described in paragraph 4.1.1 is open to some conjecture. Certainly the records of the continuous air monitors indicate the cloud arrived later and stayed much longer at the most distant stations than is indicated by the cloud model. At the very close stations, the age of the cloud becomes extremely important because of the activity decay correction. At the stations of medium distance therefore, the cloud model can be expected to give the best results. The concentration of activity in the cloud proper, bases on the cloud model, has been plotted in Fig. 5.1 as a function of distance from ground zero. The data indicate the underground shot produced an aerosol 10 to 100 times as active as the surface shot.

5.2 PARTICLE SIZE DISTRIBUTION

As was indicated in Chapter 4, essentially only one instrument was employed to obtain the particle size distribution of the aerosol, the cascade impactor, and thus there can be no inter-instrument comparison of results. A discussion of the particle size distribution of the cloud, therefore becomes a discussion of the cascade impactor data. The most important fact to be emphasized is that sampling was non-isokinetic in the sense that the intake velocity was considerably less than the wind velocity, but that the intake throat was pointed toward ground zero, and therefore, generally speaking into the wind. Under these conditions the intake aerodynamics favor the large particles. However, as was indicated in paragraph 5.1, the impactor, though undoubtedly removing these particles from the airstream, must have shattered them, or else subsequently lost them, since no particles larger than about 40 microns were observed in the examination of the slides.

However, the tendency toward smaller particle sizes in the aerosol with increasing distance from ground zero was definitely observed in both shots. Figs. 5.2 and 5.3 illustrate this situation. It is apparent that the underground shot initially possessed a distribution containing larger particles than the surface shot, but that these particles rapidly fell out, leaving at distances of 20,000 feet a distribution containing smaller particles than the surface shot. This result may be explained by the fact that the underground shot cloud was

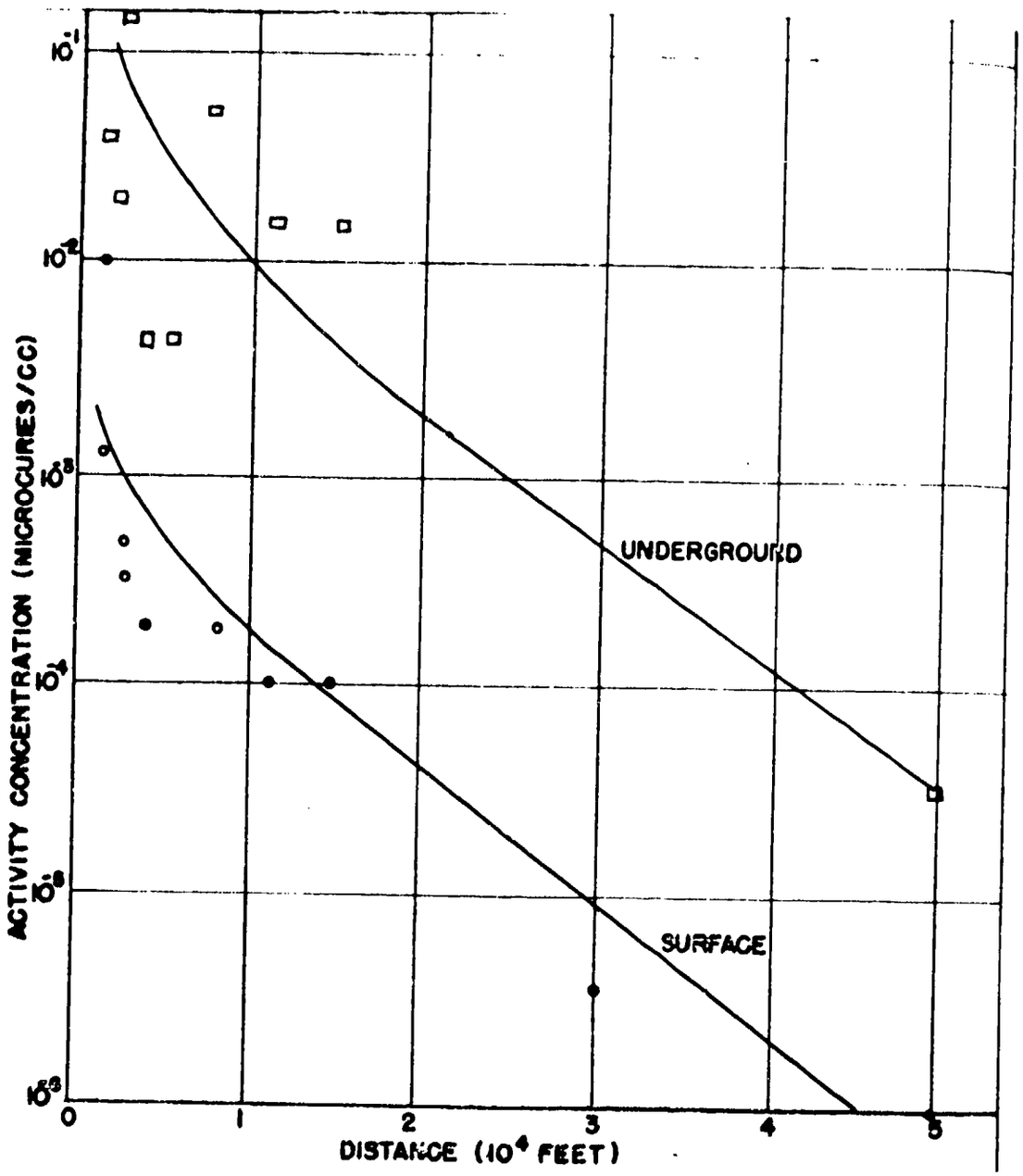

Figure 5.1 Concentration of Activity in the Cloud as a Function of Distance on the Downwind Leg. Filter Sampler Data. Activity was corrected to time at which cloud passed each station.

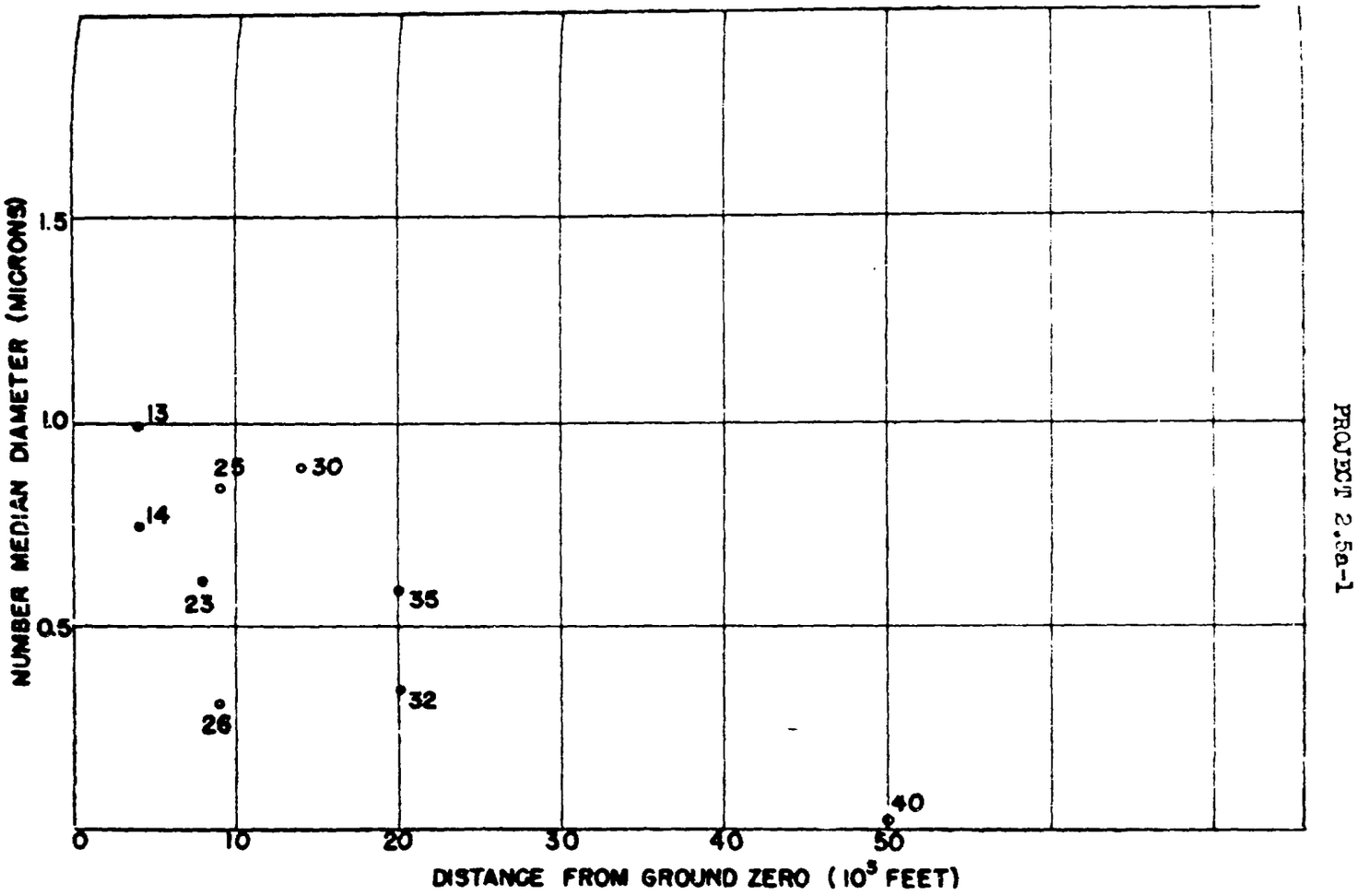

PROJECT 2.5a-1

Figure 5.2 Surface Shot Number Median Diameter of the Particles in the Aerosol as a Function of Distance from Ground Zero. Cascade Impactor Data.

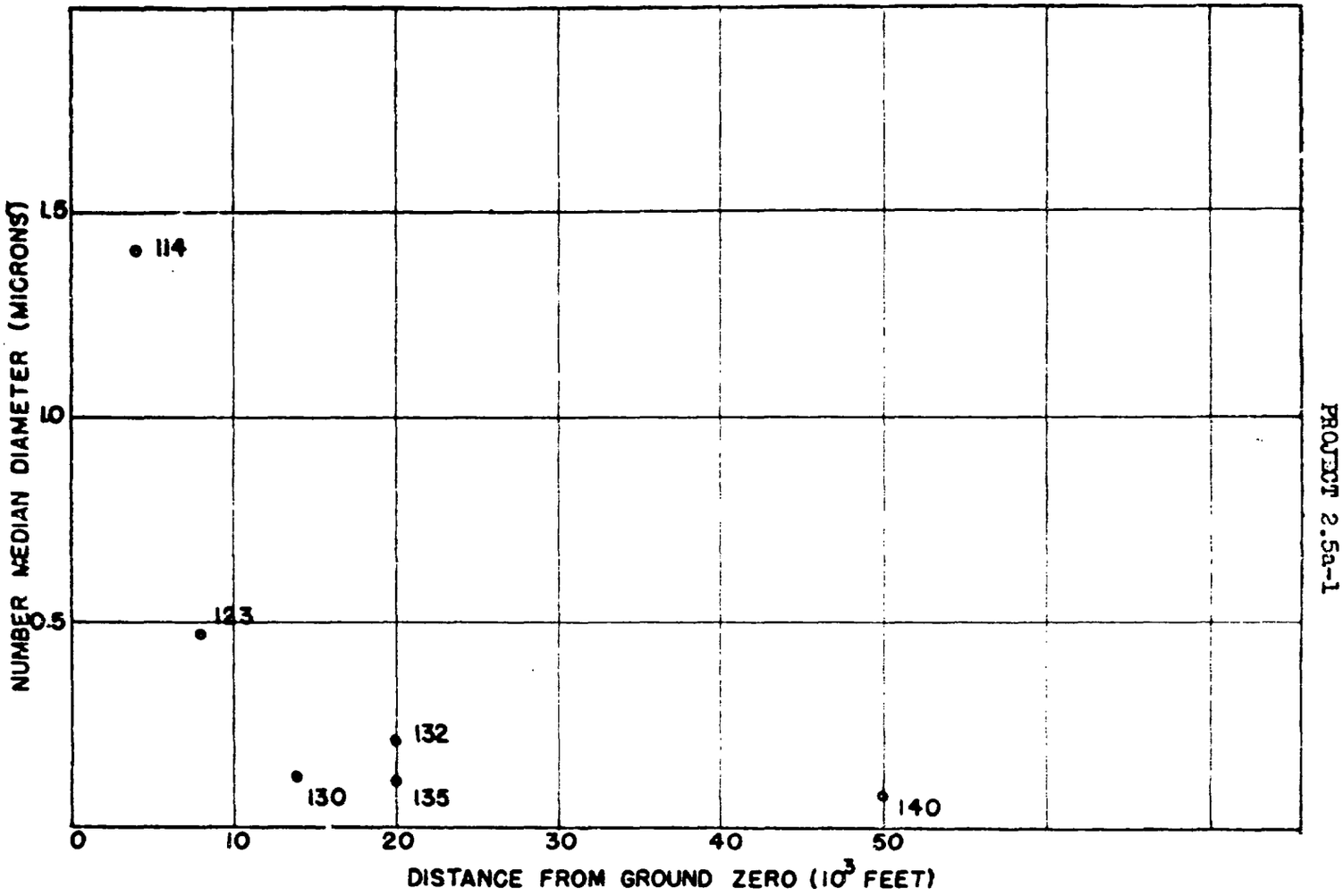

PROJECT 2.5a-1

Figure 5.3 Underground Shot Number Median Diameter of the Particles in the Aerosol as a Function of Distance from Ground Zero. Cascade Impactor Data.

lower than the surface shot cloud, giving the large particles less time in which to be carried by the wind out to the more distant stations. By the time both clouds reached 50,000 ft. the NMD of their distributions had reached a value of less than 0.1 micron.

The material on the fall-out tray was collected under favorable conditions in the sense that no appreciable wind sprang up between the time of the shot and the recovery of the trays, conditions under which very little material could have been removed or added as determined experimentally. The analysis of the material was carried out according to standard procedure and apparently no difficulties were encountered. Nonetheless the resulting distributions (see Figs. 4.12 through 4.15) indicated the fall-out had a very small NMD, less than one micron, a distinct anomaly inasmuch as the aerosol NMD apparently was about this size. In addition, the lines representing the size, area, and mass, distributions did not give a straight line trend. For these reasons, no attempt was made to fit straight lines to the data, with the result that convenient parameters describing the distribution were lacking, making a comparison of distributions difficult. It can be noted, however, that station 103, which is shown in the photographs as being in the base surge from the underground shot, had a noticeably larger percentage of particles less than 10 microns than the other four stations analyzed, giving wieght to the idea that the base surge was composed of small particles.

5.3 RADIOACTIVITY AS A FUNCTION OF PARTICLE SIZE

It was hoped that the cascade impactor would size grade particles sufficiently so that activity measurements made on the five slides would give an indication of the activity of the particles in the aerosol as a function of particle size. However, these data, which are contained in Tables 4.10 and 4.11, present such large scatter as to make such a correlation impossible. An example of this is easily seen by consideration of the percentage of activity on the first slide. One would expect that the first slides on the nearest impactors would contain a large percentage of the total activity of the impactor, while the first slides on the farther impactors would contain less, since there would be fewer of these very highly active particles present in the aerosol at the farther stations. Even this effect, which should be very pronounced, is not evident. A partially satisfactory explanation of this can be made by the fact that the cascade impactor, in its collection of particles, size grades them only by virtue of widely overlapping efficiency curves, and that a wide spectrum of particle sizes may be found on any one slide, although the NMD of the distribution varies from slide to slide.

This, of course, does not affect the particle size analysis by virtue of the way in which it is carried out, however, it might frustrate any work dependent upon size grading.

It is unfortunate that a larger number of conifuges did not give satisfactory data. Although all conifuge cones were radioautographed, only a few showed any darkening at all, and only one of these showed a smooth distribution of film density. The others had only splotches of activity, which probably indicated the presence of turbulence in the cone volume. The fact that most conifuge cones were not sufficiently active to produce radioautographs can be attributed to the small flow rate of the instrument.

The activity as a function of particle size data obtained from the fall-out trays appears to be satisfactory, except that a self-absorption correction, originally considered to be almost negligible, apparently is necessary for the large particle sizes. This question is discussed in more detail in paragraph 5.5.2.

It should be pointed out that the specific activity data from the fall-out, which indicates the relative activity of each particle size range, can be applied to the mass distribution of the aerosol as determined from the cascade impactor to yield the distribution of activity as a function of particle size of the aerosol. The assumption made is that, in any given particle size range at any given station, the specific activity of the aerosol is the same as that of the fall-out. If this is not the case, the implication is that there must be some selection on the basis of activity in determining which particle of a given size range will remain in the aerosol or will fall out.

5.4 PERCENTAGE OF ACTIVE PARTICLES

If the percentage of active particle data (paragraph 4.4) of the cascade impactor and the fall-out tray for the underground shot are combined, it appears that the percentage of active particles is a monotonic function of particle size over the range of particle sizes covered by the two types of data, i.e., from 10^{-1} to 10^{3} microns. In fact it appears that a straight line, with a slope of one, representing a linear function, fits the data well.

Since both the cascade impactor data and the fall-out tray depended upon a radioautographic method of differentiating the active from the inactive particles, it was thought that the exposure time of the radioautograph would affect the results. This was not borne out by results of the cascade impactor, since a number of radioautographs of different exposure times showed no apparent change in the percentage of active particles.

5.5 STUDY OF FRACTIONATION

5.5.1 Radiochemistry

The data concerning the nuclide activity per unit mass of active material as a function of particle size, which is contained in Table 4.15, provided a method of investigating the mechanism whereby particles acquire activity. The data for Sr^{89} and ZR^{95} have been plotted in Figs. 5.4 and 5.5. Referring to Fig. 5.4, it appears that a straight line with a slope of -1 may be fitted to the data, whereas this is not possible with the data in Fig. 5.5. Allowing for some over-simplification, it appears that the Sr^{89} activity is a function of particle surface, whereas that for Zr^{95} tends to be more of a volume function. Ba^{140} gives a plot similar to the Sr^{89} plot, while Ce^{144} is similar to Zr^{95}. Further study is being made of these data, particularly with respect to the question of whether the activity of Zr^{95} and Ce^{144} is concentrated in a shell rather than a volume. Examination of the decay chains of these four nuclides provides a plausible reason why there should be a difference in the mechanism for acquiring radioactivity. The decay chains are as follows[4]:

Kr^{89} —2.6m→ Rb^{89} —15.4m→ Sr^{89}

Kr^{95} —short→ Rb^{95} —short→ Sr^{95} —short→ Y^{95} —10.5m→ Zr^{95}

Xe —16s→ Cs —66s→ Ba^{140}

Xe^{144} —1s→ Cs^{144} —short→ Ba^{144} —short→ La^{144} —short→ Ce^{144}

It may be seen that Ba^{140} and Sr^{89} both have gaseous precursors that have half-lives long in comparison with the lifetime of the fireball. Since gases such as krypton and xenon are not significantly subject to adsorption above liquid air temperatures, it is logical to suppose that while the Zr^{95} and Ce^{144} chains passed the rare gas stage early enough to be adsorbed during the particle growth process, no appreciable amount of Kr^{89} and Xe^{140} decayed before the particles had ceased to grow. Hence the Sr^{89} and Ba^{140} activities were confine' to the outermost surfaces of the particles.

---

4 C. D. Coryell & N. Sugarman, op cit, pp. 1996-2001.

Pages 128, 129, blank

5.5.2 Activity of the Radioactive Particles

In order to investigate the mechanism whereby particles become radioactive, the data described in paragraph 4.5.2 activity of the radioactive particles as a function of their size, surface area, and mass were calculated. (The latter, it will be noted would be the sum of all the nuclide activities of the kind discussed in the paragraph immediately above if a radiochemical analysis could be performed on all the nuclide species.)

One of the questions that arose in the study of the data was the effect of self absorption and self scattering upon the measured activity of the different particle size fractions. The former is susceptible to quantitative treatment if the range curve for the activity is known, while the latter is as yet not well understood. The complexity of the combination can perhaps best be seen by examining the data of Nervik and Stevenson[5], who have plotted a self-scattering and self-absorption correction factor versus sample thickness, with beta energy as a parameter, for NaCl and $Pb(NO_3)_2$.

A simple calculation can be made to investigate the magnitude of the self-absorption. Assuming:

(1) The attenuation of beta particles is described by the equation

$$e^{-\frac{0.693}{T_{\frac{1}{2}}} w} \qquad (5.1)$$

where w is the path length in milligrams/cm^2, and $T_{\frac{1}{2}}$ is the half thickness of the particle for the fission product radiation. The latter was taken to be 20 mg/cm^2 in accordance with the data of paragraph 4.5.4.

---

[5] W. E. Nervik and P. C. Stevenson, "Self-Scattering and Self-Absorption of Betas by Moderately Thick Samples". Nucleonics, I, (1952), 19.

(2) The particles are cubical, so that the mean path length travelled by a beta in escaping from the particle is

$$\overline{l} = \frac{s}{2} \qquad (5.2)$$

where s is the side of the cube.

(3) The density of the particles is 2.7 grams/cm^3, making the thickness factor of the particle material equal to 2.7×10^{-1} mg/cm^2/micron. The relative self-absorption of a 1 micron particle is:

$$e^{-\frac{0.693}{20} \times 0.5 \times 2.7 \times 10^{-1}} = e^{-.0048} \approx 1 \qquad (5.3)$$

while that for a 1000 micron particle is:

$$e^{-\frac{0.693}{20} \times 500 \times 2.7 \times 10^{-1}} = e^{-4.8} \approx \frac{1}{120} \qquad (5.4)$$

Thus the correction factor for self-absorption for a 1000 micron particle is 120 times that for a 1 micron particle, and therefore is of great importance. Previous calculations had led to the belief that this correction was negligible.

No data is available to estimate the effect of self-scattering, but it is probable that it is negligible in comparison to the correction for self-absorption.

It has been suggested that the necessity for making these corrections could be side-stepped by crushing the large particles before measuring their activity. This is presently being carried out on some of the fractions that are still sufficiently active.

5.5.3 Decay Slopes

A study of the variation of decay slope with particle size (paragraph 4.5.3) has yielded no information other than further proof of fractionation.

Page 132 blank

CHAPTER 6

SUMMARY

It was expected that the considerable quantities of dirt thrown up by the Jangle explosions would trap a relatively large proportion of the fission products of the bomb, creating highly radioactive aerosols containing relatively large particles.

The concentration of beta activity in the aerosols was found to be 10^{-3} and 10^{-1} microcuries per cubic centimeter for the surface and underground shots respectively. These are based on filter sampler data taken from the nearest stations (2000 ft. to 4000 ft.) on the downwind leg, as modified by an estimation of the arrival and departure time of the cloud.

The number median diameters of the particles in the aerosols were 1.0 and 1.5 microns for the surface and underground shots respective-16, at stations 4000 ft. downwind, decreasing to less than 0.1 microns at 50,000 ft. for both shots. These figures were obtained from the cascade impactor. The particle size distribution of the fall-out was also determined at a number of stations of the underground shot.

No satisfactory data giving activity as a function of particle size in the aerosol were obtained due to unsatisfactory operation of the instruments designed to size grade aerosol particles during the sampling process. These data, however, were determined for the fall-out at a number of stations on the underground shot. The percentage of active particles in the surface shot aerosol was determined to be 0.01 per cent for particles approximately one micron in diameter. For the underground shot fall-out, this percentage was found to be 20 per cent for particles approximately 100 microns in diameter.

Data of the various consequences or manifestations of fractionation were made on size-graded particles of fall-out from the underground shot, and study of these data have made possible a number of interesting conjectures regarding the mechanism whereby particles become radioactive.

Page 134 Blank

APPENDIX A

DEFINITION AND ABBREVIATION OF TERMS

BCAM	- Brookhaven Continuous Air Monitor
BNL	- Brookhaven National Laboratory
CRL	- Chemical and Radiological Laboratories
Decay Slope	- the exponent in the decay equations $A = ct^n$
Fall-out	- particulate matter once a part of the aerosol that has precipitated to the ground
Fractionation	- any variation in the fission product nuclide abundance, usually applied to the variation as a function of particle size
Isokinetic	- actually "equal motion", but is generally applied to particulate sampling that is carried out so as not to be selective in any way
MF	- molecular filter
NIH	- National Institutes of Health
NRDL	- Naval Radiological Defense Laboratory
RAS	- Radiological Air Sampler
TCAM	- Tracerlab Continuous Air Monitor

Page 136, blank

APPENDIX B

CALIBRATION OF THE BROOKHAVEN CONTINUOUS AIR MONITOR

The counting efficiency of this instrument may be obtained by passing a small rectangle of filter tape of width w and length s (s is equal to w for the Brookhaven air monitor), see Fig. B.1, inserted into the center line of an uncontaminated filter tape. This small section of filter tape bears a uniformly distributed known beta activity, G of the same species as for which the calibration is desired. As the tape passes under the counter in the x direction, a count rate is recorded which may be converted into a plot of observed counts per unit time versus distance. Such a plot will have the appearance of the graph shown in Fig. B.2, and should be symmetrical about the origin. The maximum count rate at $x = 0$, C_o is the count rate when the counter face is exactly covered uniformly contaminated filter tape Cu is the finite summation of the rates obtained when the center of the standardising rectangle is at x position equal to 0, $\pm s$, $\pm 2s$, $\pm 3s$, etc. and is thus

$$C_u = c_o + \sum_{n=1}^{n=\infty} 2c_n \qquad \text{(B.1)}$$

Emperically it has been found that with counters positioned close to the tape that Eq. B.1 can be reduced to

$$C_u = c_o + 2c_1 + 2c_2 \qquad \text{(B.2)}$$

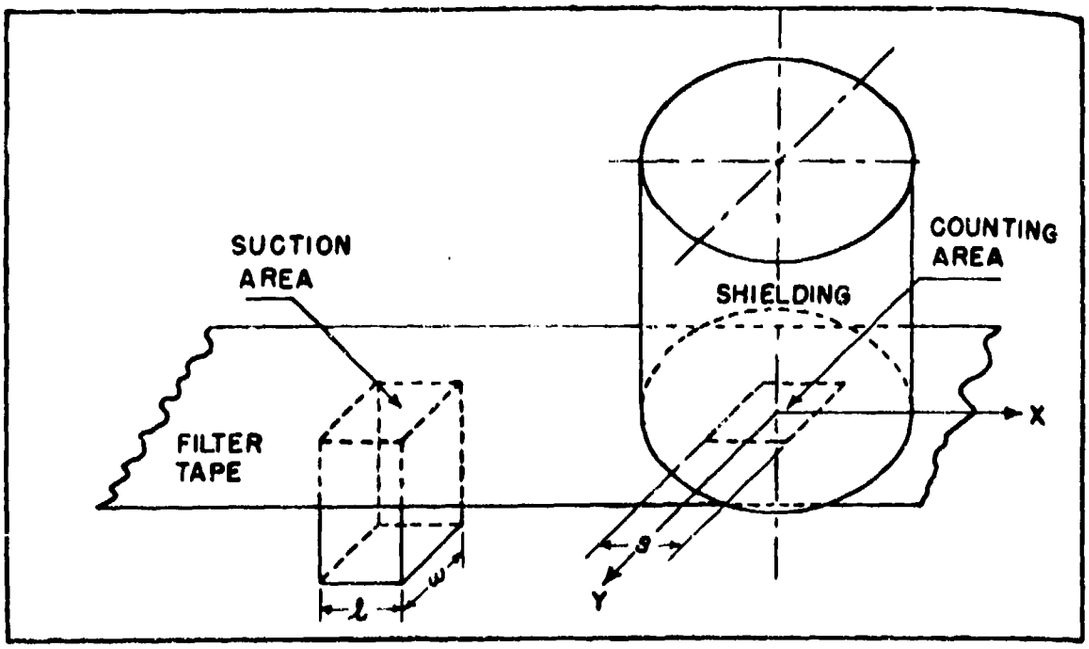

Fig. B.1 Schematic Drawing of the Brookhaven Continuous Air Monitor

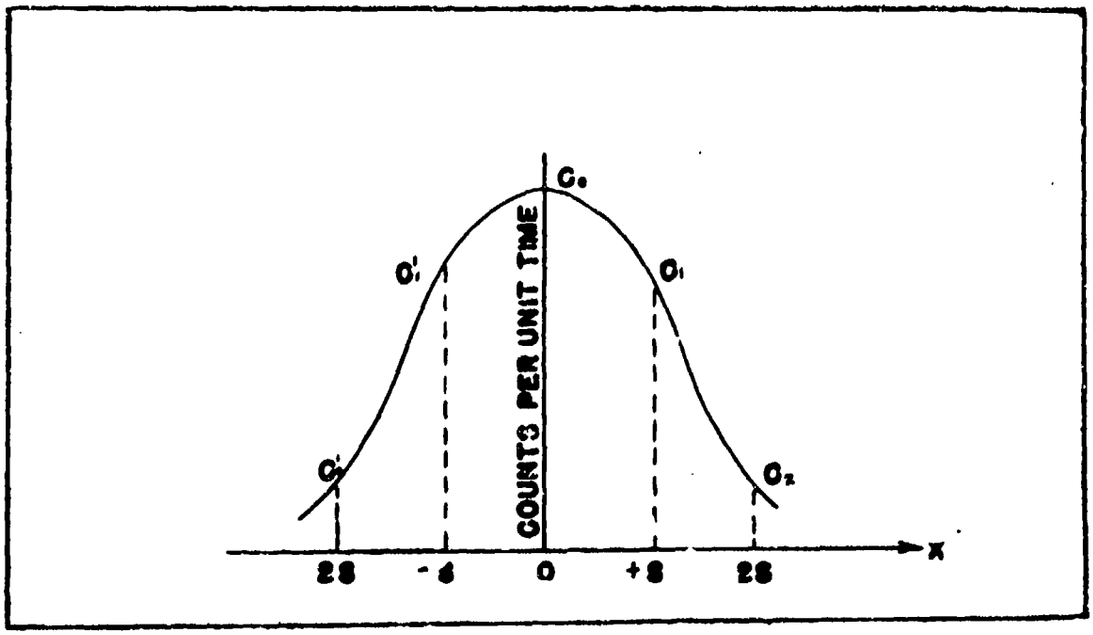

Fig. B.2 Count Rate as a Function of Displacement for the Brookhaven Continuous Air Monitor.

The fraction of the total counting rate contributed by the segment of width w and length S positioned directly in front of the tube is

$$\frac{\sigma_o}{\sigma + 2\sigma_1 + 2\sigma_2} = \frac{\sigma_o}{\sigma_u} = f \qquad (B.3)$$

The efficiency E of the segment in this position may be defined as

$$\sigma_o = C_u f = EG \qquad (B.4)$$

The activity per standard segment (width w and length s) is given by

$$G = aV \qquad (B.5)$$

where a = activity per unit volume of cloud; V = volume of air sampled through the standard segment. From Eq. B.4

$$C_u = E\,aV \qquad (B.6)$$

$$a = \frac{\sigma_u f}{EV}$$

This equation limits a to the average value of the time interval during which the unit segment of paper was contaminated. For the sake of clarity the midpoint of this time interval can be taken as the time corresponding to the value a.

To obtain an unknown activity concentration a from the instrument count rate meter readings C_u, it was necessary to determine the instrument constants E, f, and V. E and f were determined by the following procedure: With the center of the window as a reference point, the standard activity paper was moved one and two inches on either side and the

counting rates observed. The sum of the counting rates in all such positions gives the counting rate of a uniformly contaminated filter paper of infinite length. Proceeding in this manner the results shown in Table B.1 were obtained.

TABLE B.1

Efficiency Data for Brookhaven Monitor

Distance From Center of Window	Counts Per	Incremental Efficiency (per cent)
0	501	23
∕ 1 inch	35.5	1.61
∕ 2 inch	2.35	0.11
- 1 inch	58.9	2.67
- 2 inch	2.0	0.09
	Total 599.75 ≈ 600	

These results are plotted in Fig.B.3. The activity of the one square inch standard corresponded to 2.2×10^5 disintegrations per second. Thus

$$f = \frac{501}{600} = .83$$

$$E = \frac{5.01 \times 10^2}{2.2 \times 10^5} = .23$$

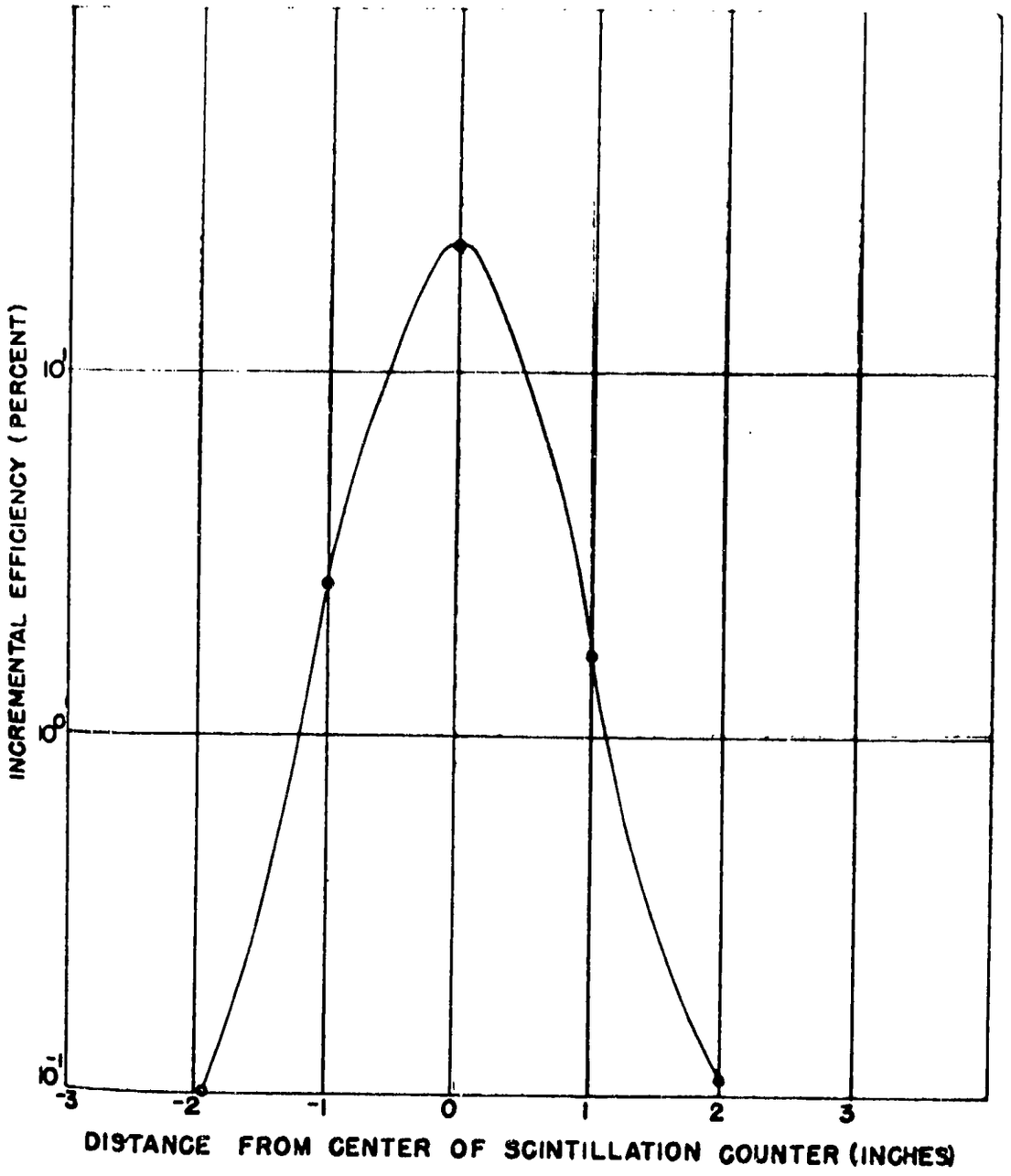

Fig. B.3 Incremental Efficiency as a Function of Distance for the Brookhaven Continuous Air Monitor

Since the sampling port measured 1 inch wide by 1.75 inches long, the filter tape transport velocity was 4 inches/hour and the flow rate through the sampling port was 3.5 cubic feet per minute, the value of V was found to be:

$$V = 1.5 \times 10^{6} \text{ cm}^3$$

Therefore, the counts per minute on the instrument count rate meter may be converted to microcuries per cubic centimeter by the equation:

$$\frac{\left(\frac{\mu c}{cm^3}\right)}{} \times 1.1 \times 10^{-12} \text{ (c/m)} \qquad \text{(B.8)}$$

APPENDIX C

CALIBRATION OF THE TRACERLAB CONTINUOUS AIR MONITOR

Interesting two dimensional counting geometry problems occur if a continuous air monitor is constructed with both circular suction and counting areas (of radii R and r respectively) as is the case for the Tracerlab continuous air monitor. (See Fig. C.1).

For simplicity in the following derivations, the steady-state conditions of an aerosol of constant beta activity per unit volume, a flowing at a constant volumetric flow rate, V depositing activity at a uniform rate, q (equal to $aV/\pi R^2$) per unit area on a filter tape moving at a constant velocity, u has been assumed. It is also convenient to consider first a previously contaminated filter tape being rerun through the monitor with the coordinate axes x,y and x', y' as shown in Fig. C.1.

It may be noted that the activity concentration, Z deposited upon the filter tape is proportional to the cord length of the suction circle in the x' direction and is given by the relation,

$$Z = \frac{2q}{u}\sqrt{R^2 - y^2} \qquad (C.1)$$

with the restriction that

$$-R \leq y \leq R$$

and Z can thus be represented graphically as the elliptic sheet, infinite in the x direction shown in Fig. C.2.

As the contaminated tape with its elliptical distribution of activity passes under the counter window, the counting efficiency of each differential area is a function of x and y (or O and in polar coordinates). This function can be determined experimentally by placing a small, known, uniformly contaminated filter paper standard in the filter tape and passing it under the counter in the x direction as was done to obtain the data shown in Fig. C.3. Inasmuch as the efficiency of the G-M counter should be symmetrical about its central axis, the entire function can be represented by a solid of revolution, the

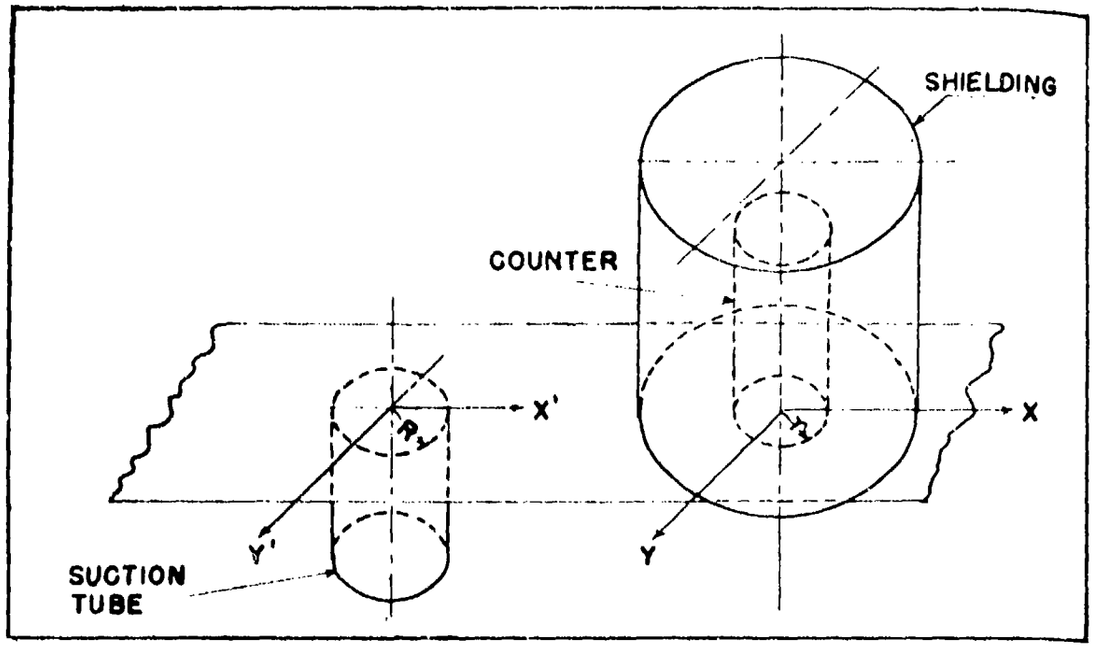

Fig. C.1 Schematic Drawing of the Tracerlab Continuous Air Monitor

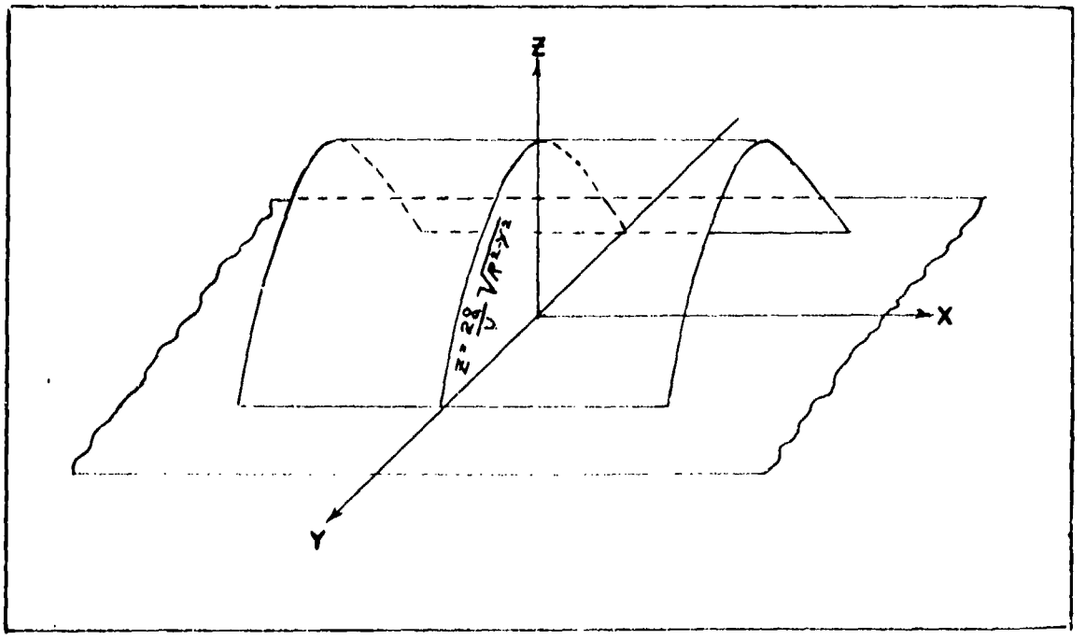

Fig. C.2 Activity Concentration as a Function of Tape Position for the Tracerlab Continuous Air Monitor

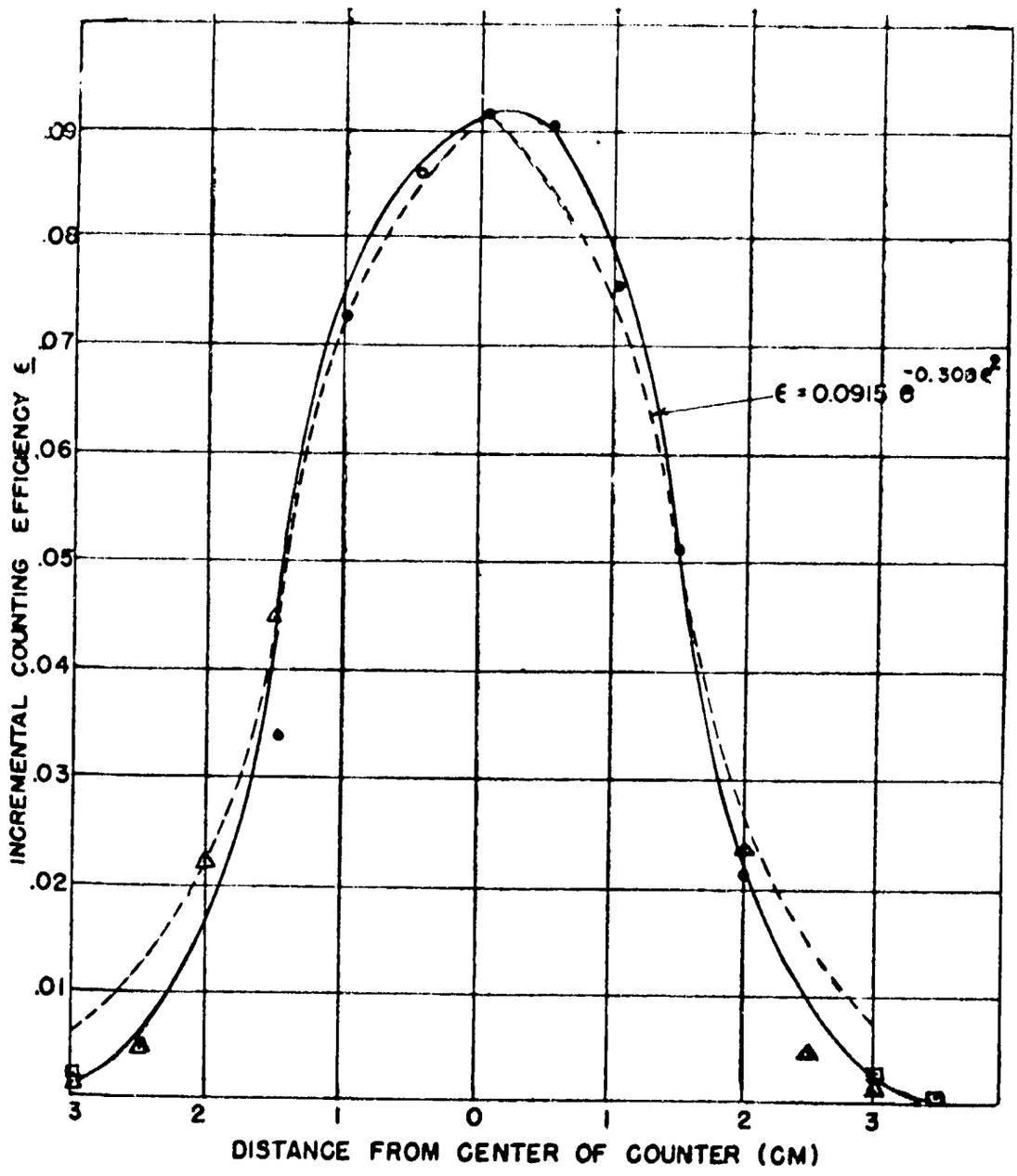

Fig. C.3 Variation of Counting Efficiency with Distance for the Tracerlab Air Monitor.

first quadrant of which is shown in Fig. C.4.

The differential count rate, z summed up by the G-M tube of the air monitor is the product of the activity concentration and the counting efficiency for each element of area of the x,y plane of the filter tape. Thus

$$z = \epsilon Z \qquad (C.2)$$

and can be represented by the solid sketched in the first quadrant of Fig. C.5.

The count rate, A finally recorded on the air monitor recorder is the volume between the surface described by the function z and the x,y plane in Figure C.5 and is approximately expressed by the definite double integral

$$A = 4 \int_0^R \int_0^{\sqrt{R^2 - y^2}} z \cdot dy \cdot dx \qquad (C.3)$$

or in the more convenient cylindrical coordinates by

$$A = 4 \int_0^R \int_0^{\frac{\pi}{2}} z \cdot \rho \cdot d\theta \cdot d\rho \qquad (C.4)$$

It may be noted that the upper limit of integration, R, for ρ introduces a small error due to the neglected volumes in the x direction

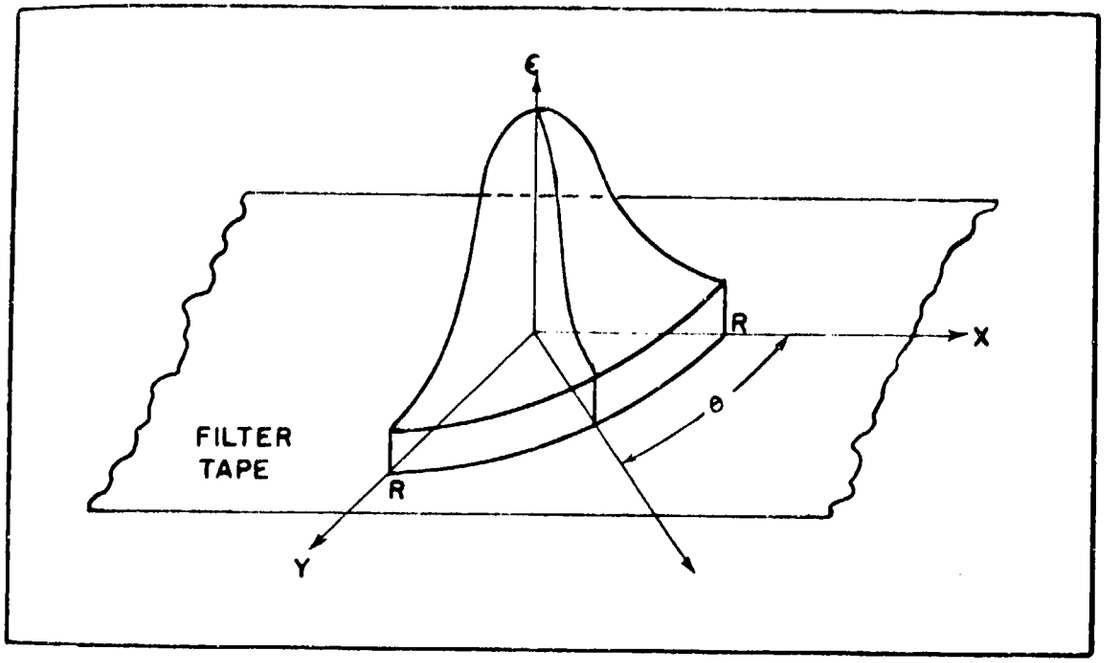

Fig. C.4 Differential Counting Efficiency as a Function of Tape Position for the Tracerlab Continuous Air Monitor

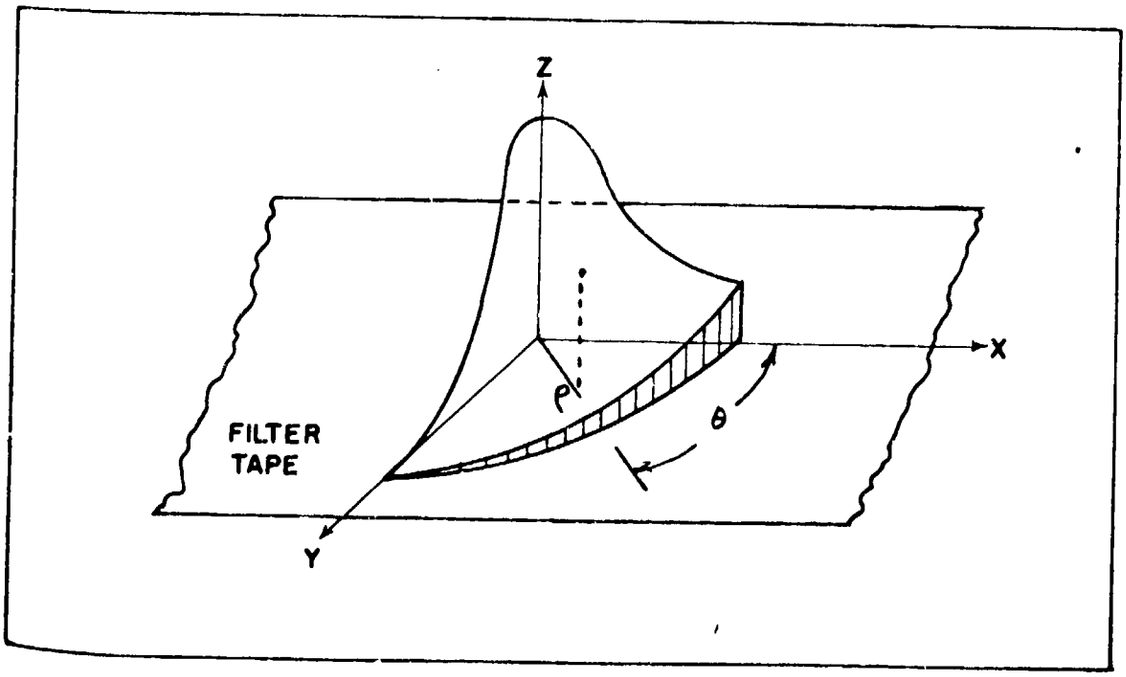

Fig. C.5 Differential Count Rate as a Function of Tape Position.

which should be trivial in the case of the well shielded Tracerlab air monitor.

The function

$$\epsilon = \alpha e^{-\beta\rho^2} \tag{C.5}$$

may be arbitrarily selected to represent the solid of Fig. C.4. Substitution of this and Eq. C.1 into Eq. C.4 after changing to cylindrical coordinates by the substitution

$$y = \rho \sin\theta$$

results in the relation

(C.6)

$$A = 4 \int_0^R \int_0^{\frac{\pi}{2}} e^{-\beta\rho^2} \cdot \rho \cdot \frac{2qR}{u} \sqrt{(1 - k^2 \sin^2\theta)} \, d\theta \, d\rho$$

in which the function, $\sqrt{1-k^2 \sin^2\theta}$ can be recognized as the elliptic integral of the second kind, $E(k,\theta)$. As the upper limit of the first integral is $\pi/2$, the complete elliptic integral, $E(k)$ can be obtained from tables [1] for various values of k where k is equal to ρ/R.
Equation C.6 thus becomes

$$A = \frac{8\alpha qR}{u} \int_0^R \rho \, e^{-\beta\rho^2} \cdot E(k) \cdot d\rho \tag{C.7}$$

[1] R. S. Burington, Handbook of Mathematical Tables (2nd ed; Sandusky, Ohio: Handbook Publishers, 1945) p.263.

and can be readily evaluated by graphical integration of a plot of the term within the integral sign versus ρ noting that k varies from 0 to 1 in the interval ρ = 0 to R. In terms of air concentration, Eq. C.7 becomes

$$\frac{uc}{cm^3}_{\text{Replay}} = \left[\frac{(1.77 \times 10^{-7})\ (u)\ (R)}{\alpha V \int_0^R \rho e^{-\beta \rho^2} E(k)\ .d\rho}\right] .A \qquad (C.8)$$

Thus the beta activity concentration of the sampled aerosol is a simple multiple of the recorded counting rate when the filter tape is played back through the Tracerlab air monitor.

A somewhat more complicated problem occurs during the build-up of activity upon the filter tape. Thus in Fig. C.1 the coordinate axes x,y and x',y' coincide. The deposition of activity upon the tape may be represented by the shape in Fig. C.6. Beyond ρ equal to R in the x direction, the surface becomes identical to the elliptic sheet of Fig. C.2 but within the region

$$0 \leq \rho \leq R$$

the activity concentration may be expressed by

$$Z = \frac{(q)}{u} \quad \frac{(R \neq x)}{R} \quad \sqrt{R^2 - y^2} \qquad (C.9)$$

which may be transformed to cylindrical coordinates by the substitutions

$$x = \rho \cos \theta \text{ and } y = \rho \sin \theta$$

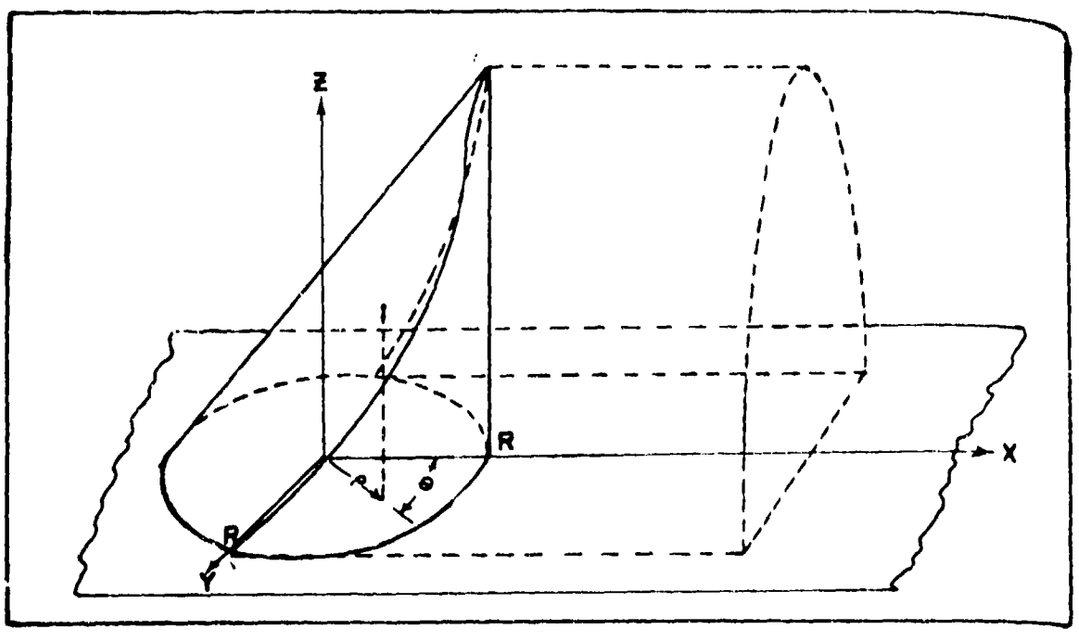

Fig. C.6 Activity Concentration During Deposition as a Function of Tape Position for the Tracerlab Continuous Air Monitor.

and Eq. C.9 becomes

$$Z = \frac{(qR)}{u} \quad (1 \pm k\cos\theta) \sqrt{1 - k^2 \sin^2\theta} \qquad (C.10)$$

Substitution of Eq. C.10, C.2 into Eq. C.4 for the first and second quadrants results in

$$A = 2 \int_0^R \int_0^{\pi} \alpha_o - \beta\rho^2 \cdot \rho \cdot \frac{(qR)}{u} \sqrt{(1 \pm k\cos\theta)\ 1 - k^2 \sin^2\theta}\ d\theta\, d\rho \qquad (C.11)$$

or (C.12)

$$A = \frac{2\pi qR}{u} \int_0^R \rho e^{-\beta\rho^2} \left[\int_0^{\pi} E(k,\theta)\, d\theta + k \int_0^{\pi} \sqrt{1 - k^2 \sin^2\theta} \cdot \cos\theta \right] . d\rho$$

As it can be easily seen that

$$\int_0^{\pi} 1 - k^2 \sin^2\theta \cdot \cos\theta = 0 \qquad (C.13)$$

and also since

$$\int_0^{\pi} E(k,\theta)\, d\theta = 2 \int_0^{\pi/2} E(k,\theta) \cdot d\theta \qquad (C.14)$$

Equation C.14 may be simplified to

$$A = \frac{4\pi qR}{u} \int_0^R e^{-\beta\rho^2} \cdot E(k) \cdot d\rho \qquad (C.15)$$

which gives the counting rate for the moving tape. It may be noted that this is half of Eq. C7 so that the graphical integration need be performed only once for both cases. By use of Eq. C.7 and C.15, the initial and several replay results may be combined to investigate the radioactive de-

cay characteristics of the aerosol sampled by the Tracerlab air monitor.

An experimental determination of the value of the constants in these equations was made by means of the following procedure: A standard activity sample was prepared by placing an aliquot of a fission product mixture on a small (5 x 5 mm) square of filter tape from the Tracerlab continuous air monitor. This mixture was selected because of its beta range curve was considered to approximate that of the fission products resulting from the surface and underground detonations. The standard square was calibrated for its absolute beta activity while on a 4 mg/cm cellophane additional backscatterer in order to duplicate the conditions under which the tape itself is counted. This was done by raising the G-M counter in its shield to a higher position and mounting the square and reference activity standards on cards positioned on the lower bracket. Range curves for the reference standards as well as the calibrating square were determined on another counter with a shorter air path and thinner G-M tube window. These data were combined after appropriate corrections for air path, aluminum absorber of the air monitor, and the tube window so that the absolute beta activity of the filter paper square was determined by the average of two Tracerlab simulated P^{32} and two I^{131} reference standards which were stated to be accurate to ten per cent.

The standardized square was placed in a 5 x 5 mm square hole (backed with a similar 4 mg/cm^2 backscatterer) in a movable strip of air monitor filter paper in such a manner that the center of the standard square approximately coincided with the central axis of the G-M counter. Activity measurements for this square were made by moving it along the center line of the path followed by the tape, stopping at half centimeter intervals beginning 3 cm before, and 5 cm after departure of the center point of the standard from the central axis of the differential counting efficiency are given in Table C.3 and are plotted in Fig. C.3. The slight asymmetry of the curve is apparently due to a one millimeter error in positioning the calibrating standard. For purposes of comparison, the Gaussian curve used to approximate this function has been sketched in as a dotted line.

The function

$$\epsilon = \alpha \, e^{-\beta\rho^2} \qquad (C.16)$$

was selected to represent the two dimensional efficiency of the Tracerlab air monitor G-M tube (See Fig. C.4). By use of the smooth curve of Fig. C.3 the constants and of Eq. C.5 were found to be 0.0915 and 0.308 respectively for Unit No. 1. The integral of Eq. C.7 was then evaluated by tabulation of the values of the function

$$\rho \, e^{-\beta\rho^2} \cdot E(k) \qquad (C.17)$$

as a function of ρ and k as shown in Table C.2 and plotted in Fig. C.7. This curve was graphically integrated by the method of Moore[2] between the limits zero and R with the result that

$$\int_0^R e^{-\beta\rho^2} \cdot E(k) \cdot d\rho = 2.14 \qquad (C.18)$$

Substitution of this value into Eq. C.8 and rearranging resulted in the relations

$$\frac{(uc)}{cm^3}_{\text{Initial}} = (2.2 \times 10^{-11})(A) \qquad (C.19)$$

and

$$\frac{(uc)}{cm^3}_{\text{Replay}} = (1.1 \times 10^{-11})(A) \qquad (C.20)$$

which gave the air beta activity concentration from the observed initial and replay counting rates from the Tracerlab continuous air monitor.

In order to confirm the validity of the equations derived above as well as the accuracy of the emperical constants α and β, the calculated overall counting efficiency, ϵ_{ov} of a large circular (2.25 in. in diameter) filter standard was compared with the experimentally determined efficiency of a comparable standard. The overall counting efficiency can be obtained by integration of the expression

$$\epsilon_{ov} = \frac{4}{\pi R^2} \int_0^R \int_0^{\pi/2} e^{-\beta\rho^2} \cdot \rho \cdot d\theta \cdot d\rho \qquad (C.21)$$

[2] A. D. Moore, Proceedings of the Society for the Advancement of Engineering Education, California Meeting, 48, 452, (1940).

PROJECT 2.5a-1

TABLE C.1

Tracerlab Air Monitor Efficiency as a Function of Distance, x

Distance From Center of Counter cm	Scale of Instrument	Counts Per Minute	Differential Counting[a] Efficiency
0	100	37,500	0.0915
0.5	100	37,000	0.0903
1.0	100	31,000	0.0757
1.5	100	21,150	0.0516
2.0	100	9,040	0.0221
2.0	20	9,800	0.0239
2.5	20	1,970	0.0048
3.0	20	600	0.00146
3.0	2	750	0.00183
3.5	2	350	0.00085
- 0.5	100	35,400	0.0863
- 1.0	100	29,800	0.0731
- 1.5	100	13,500	0.0329
- 1.5	20	18,300	0.0446
- 2.0	20	9,300	0.0227
- 2.5	20	2,170	0.0053
- 3.0	20	700	0.0017
- 3.0	2	760	0.0019

(a) The absolute beta activity of the 5 mm square standard was approximately 4.10×10^6 d/min after correction for absorbers, tube window and air.

TABLE C. 2

Tabulation of the Function $\rho e^{-\beta\rho^2} \cdot E(k)$

ρ	ρ^2	$K = \frac{\rho}{R}$	$\sin^{-1} K$	$E(K)^{(a)}$	$e^{-\beta\rho^2}$	$\rho e^{-\beta\rho^2}$	$\rho e^{-\beta\rho^2} \cdot E(K)$
0	0	0	0	1.57	1	0	0
0.5	0.25	0.174	10	1.559	0.926	0.463	0.724
1.0	1.0	0.348	20.5	1.52	0.735	0.735	1.12
1.2	1.44	0.417	24.5	1.50	0.642	0.771	1.16
1.44	2.07	0.5	30	1.468	0.530	0.764	1.12
1.5	2.25	0.521	31.4	1.457	0.500	0.750	1.094
1.6	2.56	0.556	33.8	1.44	0.455	0.728	1.05
1.7	2.89	0.59	36.1	1.425	0.411	0.698	0.995
2.0	4.0	0.695	44	1.36	0.293	0.586	0.797
2.2	4.84	0.764	49.8	1.306	0.225	0.495	0.646
2.4	5.76	0.834	56.5	1.23	0.170	0.408	0.502
2.6	5.76	0.834	56.5	1.23	0.170	0.408	0.502
2.88	8.3	1.0	90	1.0	0.078	0.224	0.224

(a) R. S. Burington, Handbook of Mathematical Tables (2nd edition; Sandusky, Ohio: Handbook Publishers, 1945) p. 263.

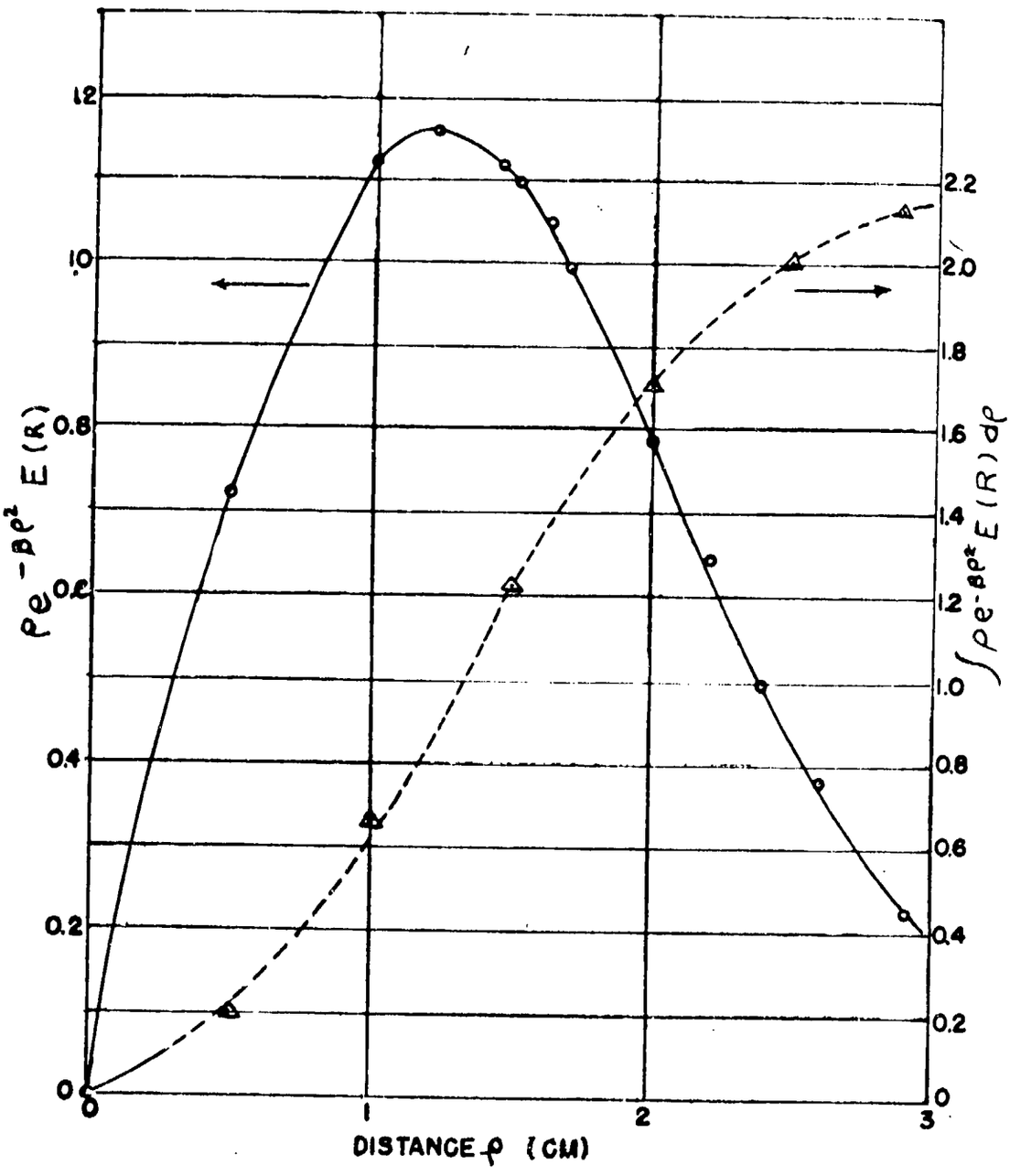

Fig. C.7 Plot of the Function of Table C.2 Versus ρ and Its Intergral Curve.

which may be derived by applying the same reasoning as used in Appendix B. Integration of Eq. C.21 results in

$$\epsilon_{ov} = \frac{\alpha}{\beta R^2} \left(1 - e^{-\beta R^2}\right) \qquad (C.22)$$

Substitution of the numerical values for α, β, and R into this equation results in

$$\epsilon_{ov} = 0.033$$

for the calculated counting efficiency of a uniformly contaminated standard 2.25 in. in diameter. For comparison, standard activity papers were prepared by spraying circular discs 2.25 in. in diameter with radioactive dust and calibrating them with a G-M counter of known geometry. The calibrated discs were placed under the G-M tube of the air monitor and the activity observed with the following results:

TABLE C.3

Efficiency Data for Tracerlab Air Monitor for Circular Uniformly Contaminated Area(a)

Standard	Activity d/min. Corrected for Window, Air and Absorber	Observed c/min	Efficiency
1	1.38×10^6	3.98×10^3	0.029
2	1.36×10^6	2.98×10^4	0.022
3	4.3×10^5	9.82×10^3	0.023
			Aver. = 0.025

(a) Data for Unit No. 1. Average value for units four and five were 0.024 and 0.032 respectively.

The agreement between the values presented in Table C.3 and the calculated value is considered to be sufficiently close to confirm the validity of the derived expressions and the constants employed, especially in view of the fact that completely uniform distribution of the radioactive dust over the filter paper discs was difficult to attain by the method employed. Due to the greater experimental simplicity, more direct approach, and the greater care exercised in its preparation and calibration, the small 5 x 5 mm square standard was used as the basis for the activity concentrations reported in paragraph 4.12.

APPENDIX D

EVALUATION OF INSTRUMENTS

D.1 INTRODUCTION

The evaluation of the hazard to personnel from an ABD cloud can be made from studies of data on activity and particle size of the generated aerosol. Such a study requires four types of information. These are:

(a) Properties of the cloud expressed as activity and mass per unit volume and time.

(b) Properties of fall-out expressed as activity and mass per unit time.

(c) Particle size distributions of (a) and (b) expressed as a function of time.

(d) Radiochemistry of (a) and (b) above.

Since the collection of these data is a field operation, laboratory accuracies should not be expected; even though laboratory equipment be employed.

A brief description has been prepared of each item of sampling equipment used for Operation JANGLE. It is intended to discuss the advantages and disadvantages associated with each instrument insofar as its ability to collect samples for the above data; this information should aid (1) the design of improved sampling instruments, and (2) the selection of instruments for use in future tests.

D.2 CONTINUOUS AIR MONITOR

In this instrument the aerosol is drawn through a moving strip of filter material which removes particulate matter. The activity of the collected particles is then measured by conventional alpha and beta counters as the strip is moved through the counting chambers.

Operation JANGLE employed two continuous air monitors - Brookhaven and Tracerlab. The Tracerlab instrument is a refinement of the Brookhaven model in that it is more compact. The Tracerlab measures activity at the same time as sampling. However, this may or may not be an advantage, since contamination of counting equipment is possible. The Brookhaven continuous air monitor measures activity shortly after collection.

The continuous air monitor furnishes a complete record of (1) alpha, and (2) beta plus gamma radiation for any desired period of time. This valuable record is not produced without great difficulty since the continuous air monitors are bulky, delicate, and complex from the viewpoint of field operation. They require a good AC power supply and must be protected from all so-called bad weather conditions. The instrument weighs about 500 pounds.

D.3 FILTER SAMPIER

The filter sampler is another cloud or aerosol sampling instrument which collects particulate matter on filter paper. The collection is made by pulling air through the paper at from 1 to 6 cfm. The paper is then removed and its activity determined by proper alpha and/or beta plus gamma counters.

The filter sampler may operate from battery or AC power generator and is rugged, light weight (about 20 pounds), and simple to operate. Data on ABD cloud activity collected with this instrument is difficult to interpret for two principal reasons: (1) The variation of activity with time cannot be obtained except by auxiliary apparatus, (2) the predetermined flow rate is subject to errors due to clogging of the collection paper. The exact clogging effect is difficult to determine except by visual operation of the instrument which is impossible in field operation.

D.4 INTERMITTENT AIR SAMPLER

The intermittent air sampler collects the cloud and/or fall-out particulate matter on each of twelve (12) filters so arranged that each filter is employed for a preset time of operation. The collected aerosol particles may be counted for alpha and beta plus gamma activities.

The resulting record will furnish data concerning the variation of activity with each time interval employed. Clogging effects will not be encountered for most cases, since the sampling time intervals may be kept short (say 10 minutes).

This instrument is light weight and is operated from batteries. The unit complete with batteries weighs about 25 pounds. Although the unit is compact, it is not rugged and requires shielding from rain and dust. The arrangement of the filters is such that they are unprotected from fall-out.

D.5 PARTICLE SEPARATOR

The particles separator is designed to fractionate particles from the ABD cloud. The fracionation is to be done at the time of sampling and is accomplished by a series of wire screen cloths with openings of 37, 44, 53, 61, 73, 88, 105, 125, 148, 177, and 210 microns. A molecular back up filter is employed for collection of particles less than 37 microns.

In theory, each screen is counted and the relationship between particle size and activity determined. It has been shown that small particles tend to stick to screen wires instead of being captured on their proper sized screen.

The separator is a small piece of equipment, but requires auxiliary vacuum and power supply. The separator weighs about 1 pound without vacuum pump.

D.6 CONIFUGE

The conifuge samples cloud aerosol for particle size analysis in range of 0.3 to 10 microns at the rate of about 170 cc per minute as air is drawn between two conical surfaces (rotating at 5000 rpm) which are separated approximately one-eighth inch apart. The particulate matter is centrifuged out with respect to mass. A section of the outside plastic conical surface is cut out and examined microscopically for particle size. Electron microscope screens are located on the plastic.

The conifuge is quite rugged but produces excessive vibration of auxiliary equipment. It requires a power supply which may be either generator or batteries. The instrument without power supply weighs about 30 pounds and is well protected from elements (weather) except for dust protection.

Particle size analysis of conifuge samples obtained in the field has not been entirely successful even though the theory is good. Since the surface area for collection of particles is large, the instrument is capable of long periods (1-2 hrs.) of operation for most field sampling duties.

There is no method for obtaining particle size vs. time of collection data.

Isokinetic sampling is not obtained.

D.7 CASCADE IMPACTOR

The cascade impactor is a cloud or aerosol sampling instrument, operated to obtain a sample for particle size analysis in range of 0.1 to 20 microns. Air at the rate of 12.5 liters per minute is drawn through a series of five jets with decreasing orifice diameter. The air stream from each jet impinges upon a glass plate which collects the particulate matter. The first plate, which is opposite the coarse stream, collects the largest particles while the last plate collects the smallest particles. The instrument weighs about 30 pounds including the vacuum pump, but not including AC or DC power supply.

The volume of sample is large but can be maintained for but a minute for most field sampling jobs, since the collecting area is small. It is difficult to predetermine exact sampling times desired and remote control or alarm control is complex.

The instrument is fairly rugged, and is well protected from elements although dust protection is not adequate.

When proper sampling time is used, an ideal sample is obtained and frantionation allows some approximation to be made of the relationship between particle size and activity.

D.8 THERMAL PRECIPITATOR

The thermal precipitator is an aerosol sampling instrument whereby particles are precipitated on a cold surface through their reaction from a hot filament. Particles from 0.02 to 10 microns are resolved as aerosol is sampled at the rate of approximately 7 cc/min.

The thermal precipitator has been used in the field and isokinetic sampling attempted. The instrument is bulky (weight 40 pounds) delicate, complex, and requires a large DC power supply. However, a good sample for particle size analysis can be obtained.

Except for dust, adequate weather protection is provided but no attempt has been ride to provide particle size vs. time data.

D.9 ELECTROSTATIC PRECIPITATOR

The electrostatic precipitator is an instrument which may be used to collect particles for particle size and/or activity measurements. Air is drawn through a metal cylinder between which and an inside electrode, there has been applied an electrical potential of several thousand volts. The sampling rate can be varied according to the design of the power supply.

The precipitator operates at high collection efficiency, has no clogging effects, and can be readily adapted for counting. However, no technique is available for obtaining activity vs. time data with the instrument.

Particle size analysis could be made of the collected sample, although no exact techniques are known. There is no fractionation of particles nor any particle size vs. time technique.

In general, the precipitator requires specialized auxiliary electronic equipment (power supply) and a good AC source. There is no information on its behavior under conditions of high humidity. The use of high voltages makes it a dangerous piece of equipment especially so in wet climates.

The precipitator complete with high voltage power supply and vacuum equipment weighs about 40 pounds.

D.10 DIFFERENTIAL FALL-OUT COLLECTOR

The differential fall-out collector is an improvement of the fall-out tray in that fall-out variation with time may be determined. The use of slides for particle size analysis makes this a desirable instrument. The collector is operated by a mechanical clock which rotates a disc beneath a slotted cover in such manner as to collect fall-out on the disc.

The instrument is light weight (5 pounds), fairly rugged, and complete except for minor design changes. There appears to be an improper seal on the cover which allows dust leakage. No information is available on the protection afforded against a wet, humid atmosphere.

D.11 CONCLUSIONS AND RECOMMENDATIONS

None of the sampling equipment discussed here is entirely satisfactory. Although some instruments approach the desired type, there is a need for sampling equipment to furnish the data listed in the introduction. In order to obtain such improved experimental results with greater efficiency and therefore economy, the following considerations should be incorporated into redesign of sampling equipment.

(1) Permit alpha and/or beta plus gamma activity measurements of cloud and fall-out samples.

(2) Approach 100 per cent sample collection efficiency.

(3) Simple and accurate flow calibration.

(4) Well adapted for high counting geometry with a minimum of manipulation.

(5) Keep field installation effort at minimum.

(6) Operation in wet, humid as well as hot, dry, or cold climates not affected by dust.

(7) Suitable for operation from stationary ground position as well as moving vehicle or aircraft.

(8) Prepared for remote control of starting and stopping mechanisms.

(9) Power requirements suitable for AC or DC circuits to be operated by battery or generator.

(10) Keep sample pick-up time short to allow rapid recovery of samples from highly radioactive fields.

(11) Allow quick removal of equipment from field, vehicle or aircraft.

(12) Permit replacement of sampling equipment as a unit- furnish with plug-in receptacles for electrical as well as air and vacuum connections.

(13) Reduce the need of tools in assembly, sample pick-up, and roll-up operations.

(14) Allow shipment via truck, express, or aircraft with a minimum of packing.

(15) Allow decontamination by washing with hot water and/or steam.

APPENDIX E

INTERIM REPORT, ARMY CHEMICAL CORPS, CONTRACT NO. DA-18-108-CML-2532 with Tracerlab, Inc., R.D. Epple, Project Director[1]

E.1 PREFACE

This Interim Report contains the experimental results of the work on JANGLE, together with the interpretations that can be made at this time. Each of the three parts of the report are independent units, and have therefore been assembled with this in mind. Each section consists of a short introduction that indicates the purpose of the work. This is followed by the experimental results and a discussion of the significance of the results.

It is anticipated that the final report will add to this report sufficient information to permit a thorough evaluation of the results. It will include considerable detailed information about the experimental procedures developed in this laboratory.

E.2 ACKNOWLEDGEMENT

This report has been written by the following members of the Tracerlab staff:

Charles Sherman	Counting Program and Decay Curves
James Shearer	Particle Size Distribution
Robert Epple	Radiochemistry

1. This report is reproduced here in its entirety, and is edited only with respect to format.

E.3 COUNTING PROGRAM

The object of the counting program was to measure the radioactivity contained on filter papers which sampled the cloud under certain known conditions of operation, and to determine the radioactivity as a function of time after time-zero. These two aspects of the program are necessary for the evaluation of the radiation hazard to personnel in the vicinity of an atomic explosion. Solution of the radiation hazard problem also requires knowledge of the distribution of sizes of the radioactive particles; this part of the problem is treated on Section E.4.

E.3.1 Filter Sampler Activity

Table E.1 and Table E.2 give the beta activity of each filter paper received. These activities were measured with a "wrap around" counter set up which used a Tracerlab TGC-5A tube. Each paper was wrapped around a cylindrical lead jig of such diameter that it just fit over the tube. The lead jig had an opening of 43^2cm which faced the thin-walled (30 mg/cm^2) portion of the tube. Thus the remaining part of the paper was shielded from the tube by the 1/8 inch thick wall of the lead jig, and the activity of 43 cm^2 from the central part of each paper was measured. Each paper was left in its plastic bag for counting to avoid contaminating the apparatus. The effective absorber thickness along radii of this cylindrical arrangement is then approximately 20 mg/cm^2 of plastic plus 30 mg/cm^2 of glass. A smaller area was measured for some of the most active papers.

In Tables E.1 and E.2 the time of each measurement is given in hours after time-zero in the second column. The activity of each paper (cpm) corrected for background is given in the third column. For purpose of comparison it is necessary to correct each activity measurement to some standard time after time-zero. 600 hours after time-zero has been used, and each activity measurement corrected to this time by use of the measured decay curves (see Figures E.1-E.5). Each corrected activity measurement has been multiplied by the appropriate area factor (100/43) (is the factor in most cases) giving the total beta activity of each paper at 600 hours; these results appear in the fourth column. This latter result was not calculated for those cases where the activity was extremely small. Blank spaces in the third column indicate that the observed counting rate was lower than the background rate.

Although the counting set-up described above has not been thoroughly calibrated, it is known that the disintegration rate is related to the counting rate by the following approximate equation:

$$\text{dpm} = 15\ (\text{cpm}).$$

PROJECT 2.6a-1

TABLE E.1

Filter Sampler Counting Data, Surface Shot

Sample	Time of Count After T_0 Hours	CPM	CPM For Whole Area at 600 Hours
S-1X-1 *	215	5013	3430
2 *	215	2.2	
3 *	215	2.9	
S-4X-1	not received	-	
2	602	2.5	
3	603	2.5	
S-7X-1	268	297	266
2	268	-	
3	268	2.6	
S-8X-1	266	225	202
2	266	0.9	
3	266	-	
S-9X-1	not received		
2	604	0.6	
3	605	5.7	
S-10X-1	194	71.3	43
2	194	-	
3	194	-	
S-15X-1	191	147.3	91
2	191	-	
3	191	0.5	
S-16X-1	196	155.6	95
2	196	-	
3	196	-	
S-21X-1	240	446.0	347
2	240	-	
3	240	0.6	

*These numbers refer in each case to the first, second and third filter papers collected at each station.

PROJECT 2.5a-1

TABLE E.1 (Cont'd)

Sample	Time of Count After T_o Hours	CPM	CPM For Whole Area at 600 Hours
S-22X-1	216	527	362
2	216	0.2	
3	216	0.8	
S-23X-1	265	1284	1150
2	265	0.9	
3	265	3.7	
S-24X-1	240	532	415
2	240	-	
3	240	-	
S-27X-1	218	1918	1310
2	218	0.2	
3	218	9.4	
S-29X-1	287	2022	2050
2	287	-	
3	288	4.1	
S-31X-1	244	-	
2	245	-	
3	263	0.8	

TABLE E.2

Filter Sampler Counting Data, Underground Shot

Sample	Time of Count After T_o Hours	CPM	CPM For Whole Area at 600 Hours
U-101X-1			
2	not received		
3			
U-104X-1	190	41.7	36
2	190	2.2	
3	190	5.9	5.1

PROJECT 2.5a-1

TABLE E.2 (Cont'd)

Sample	Time of Count After To Hours	CPM	CPM For Whole Area at 600 Hours
U-107X-1	1940	3540	33,100
2	144	40.4	29
3	144	34.9	25
U-108X-1	1940	3070	342,000
2	384	139	216
3	384	132	205
U-109X-1	1940	2343	21,900
2	169	34.7	27
3	169	43.7	34
U-110X-1	192	30.3	26
2	192	10.3	8.9
3	192	5.2	4.4
U-115X-1	165	6360	4940
2	165	10.4	8.2
3	165	17.1	13
U-116X-1			
2	not received		
3			
U-121X-1	1940	3474	32,400
2	168	62.3	49
3	168	95	74
U-122X-1	121	6.9	4.0
2	121	2.5	
3	121	-	
U-123X-1	1940	8635	842,000
2	433	389	650
3	433	1206	2010

TABLE E.2 (Cont'd)

Sample	Time of Count After T Hours	CPM	CPM For Whole Area at 600 Hours
U-124X-1	1940	3205	29,800
2	193	50.1	43
3	193	174	150
U-127X-1	1940	4940	551,000
2	360	625	910
3	360	1970	2870
U-129X-1	1940	6640	622,000
2	167	782	608
3	167	1280	995

Since our counting arrangement has a much higher efficiency for beta rays than gamma rays the activities listed in Tables E.1 and E.2 are essentially the beta activities; it is estimated that 1/2-1% of this is due to gamma activity.

In order to measure the alpha activity of these papers it is necessary to obtain a very thin sample (not more than 2-3 mg/cm^2). This has been done by dissolving a small portion of one of the most active papers from each shot, and evaporating the resulting solution on a platinum planchet until the maximum allowable thickness has been obtained. The beta and alpha activities of these samples will be measured and the alpha activity of each of the other papers estimated by using this beta: alpha ratio and the measured beta activities. Nuclear track plates will be used to measure the alpha activity since this has proven to be one of the most reliable methods of measuring alpha activity. This work is in progress although results are not available yet.

It can be seen from Tables E.1 and E.2 that the majority of the activity is present on the first paper in the series of three papers. In the cases of U-104X and U-110X, however, the activity of the last paper in the series (#3) is about 15% of the activity of the first paper (#1). It should be noted that these two sets of papers came from adjacent stations on one side of the station layout. The three papers from each of these two sets were radioautographed for 17 days beginning February 4, 1952, in an attempt to investigate further the nature of the radioactive particles which they contained. Although the activity of these papers was not great enough to permit any definite statements to be made from this type of in-

vestigation, it was found that the number of spots on the radiographs of the last papers in each series was less than 15% of the number of spots on the radiographs of the first papers. This is consistent with the hypothesis that the particles on the last papers of the series are smaller than the particles on the first papers.

E.3.2 Filter Sampler Activity Decay

Beta decay curves for the designated papers were obtained with the counting arrangement described previously and appear in Figures E.1 through E.7. Decay measurements were taken on the first paper in the series of three since this one had the majority of the activity. Paper U-122X was received and counted, but did not contain enough activity for decay measurements. In Figures E.1-E.7 counts per minute is given on dotted curve drawn through each set of experimental points represents a decay which is inversely proportional to the time; it is fitted to the data at 600 hours. This type of decay agrees with the Hunter and Ballou results for fission product decay for times between about 100 and 900 hours, and is seen to agree approximately with the data here. For times greater than about 900 hours, the data is seen to decay slightly faster than the dotted curve which is also in agreement with the Hunter and Ballou results. The data is given here up to about 1200 hours (50 days) after time-zero; further data is being taken and will be given in a future report.

E.3.3 Discussion

The data of Tables E.1 and E.2 when combined with the diagrams of the station layout show the spatial distribution of the activity with respect to ground-zero. It is seen that the majority of the activity covers only two arms of the four-armed station layout system, and that in some cases, more activity was collected on the distant papers than on the near ones. Figures E.1-E.7 give the activity as a function of time after time-zero. As we have seen, this data agrees well with the Hunter and Ballou results for fission product decay for the range of times under consideration. It would be desirable for the purposes of evaluating radiation hazards to know the shape of the decay curve for a wider range of time than has been possible here. The data is being extended to longer times in those cases where the activity is sufficient. Although measurements were begun as soon as the papers were received in this laboratory, the earliest data is between 100 and 200 hours after time-zero. Since we have good agreement with the Hunter and Ballou results for the range of time over which the measurements were made, it is reasonable to assume that our best approximation for earlier times is also the Hunter and Ballou results. One qualification must be made; when induced activities are present in appreciable amounts, the decay curve will differ from that of Hunter and Ballou results. Evidence of such activity is seen in some of the figures where the experimental curve differs from the dotted curve at early times.

We have presented data in this section which when combined with other known data (such as amount of air sampled per filter paper, position with respect to ground-zero, prevailing atmospheric and wind conditions, etc.) can be used to evaluate the radiation hazard to personnel in the vicinity of an atomic explosion at various times after the explosion.

E.4 PARTICLE SIZE DISTRIBUTIONS

E.4.1 Radioactive Particles

These particles were found by first dispersing the filter paper fibers with a needle in a layer of collodion on a glass slide, and then radioautographing the slide. The developed film was realigned with the slide and a search made under each "spot". If the field of view was too crowded, that area of collodion was redispersed and radioautographed again. Most of the particles were found to be spherical, but we found more irregular shapes on JANGLE than on previous tests. When a particle has been found, its diameter is measured, and its approximate color and shape are noted. The diameters of all the particles found are then classed into groups such that all particles of group i have diameters D such that:

$$D_i - \frac{\Delta D}{2} < D \leq D_i + \frac{\Delta D}{2} \qquad (E.1)$$

where the group width ΔD is 0.5 microns.

If N_i is the number of particles in the ith group, then the total number N is simply:

$$N = \sum^{i} N_i \cong \int_0^{\infty} \frac{dN}{dD}\, dD \qquad (E.2)$$

where we have made the assumption that the size distribution will approach a smooth curve as N becomes large.

The results for N_i vs D_i are shown in E.8 for the surface shot, Stations 29, and 30, and Fig. E.9 for the underground shot Stations 129 and 130.

There are several sources of error in our measurement. First, the radioautograph will not give a visible spot when the particle is weakly radioactive. This means that as the particle diameter becomes smaller, the efficiency of recovery decreases. Second, the difficulty of seeing a particle increases as the diameter decreases, further lowering the efficiency of recovery. Furthermore, it is not possible to correct for these effects in a quantitative way, since all the factors involved are not completely under our control. It is our feeling, based on past experience, that we can always recover particles of diameter $D > 4$ microns with 100% efficiency. In some special cases this limit can be decreased.

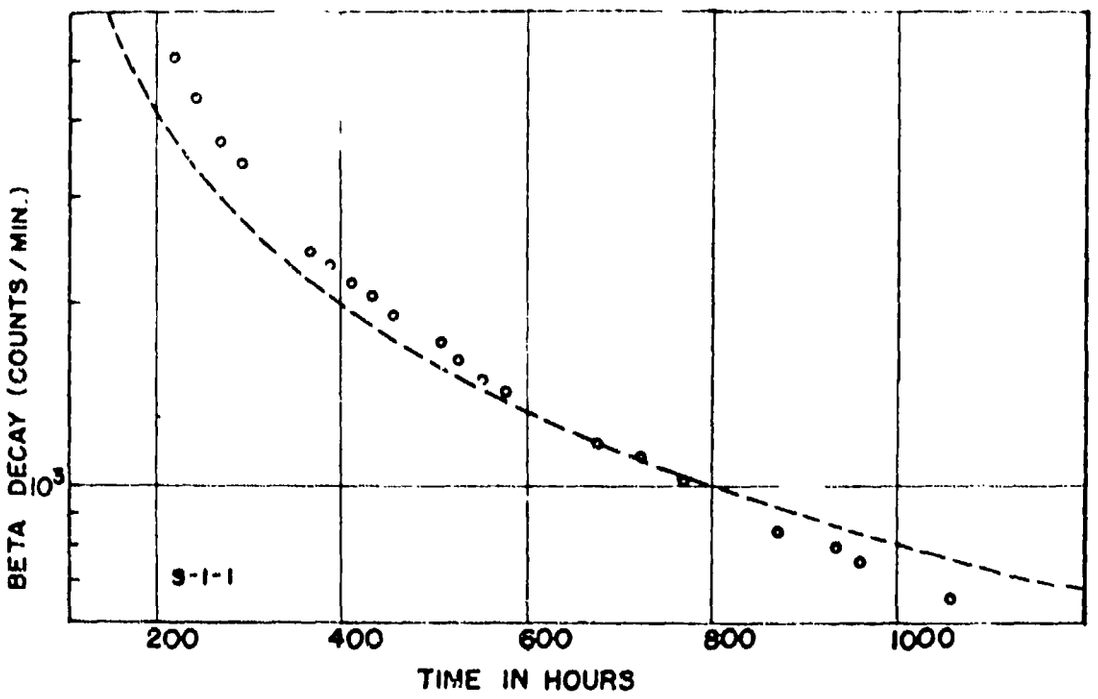

Fig. E.1 Beta Decay Curve, First Filter Paper of Filter Sampler at Station 1, Surface Shot.

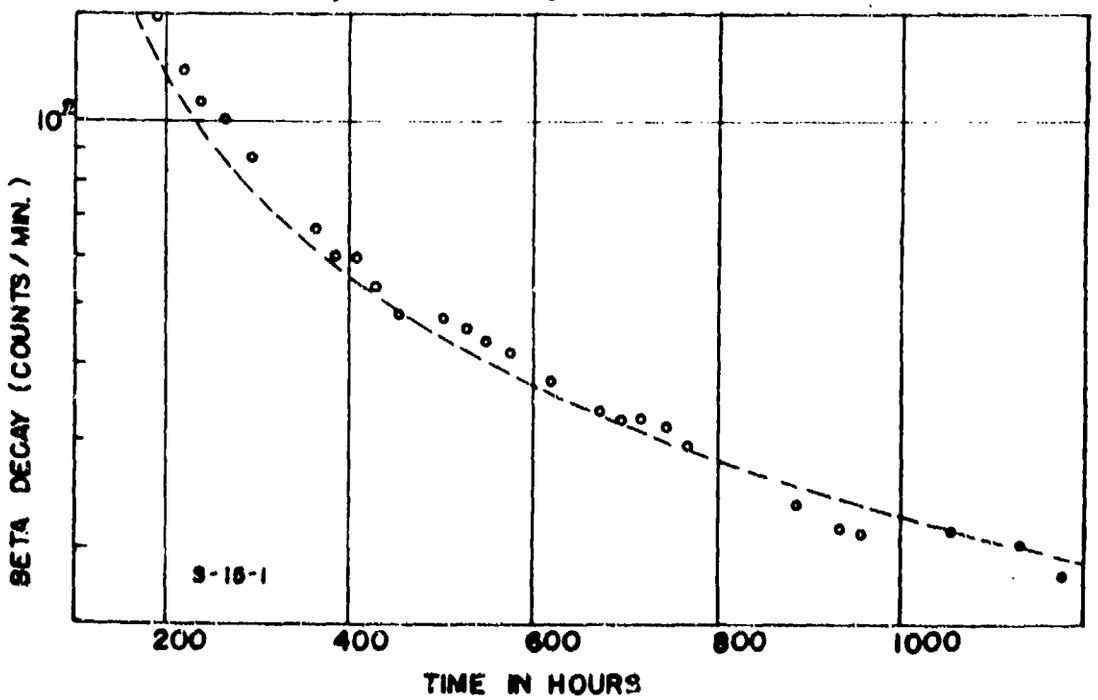

Fig. E.2 Beta Decay Curve, First Filter Paper of Filter Sampler at Station 15, Surface Shot.

PROJECT 2.5a-1

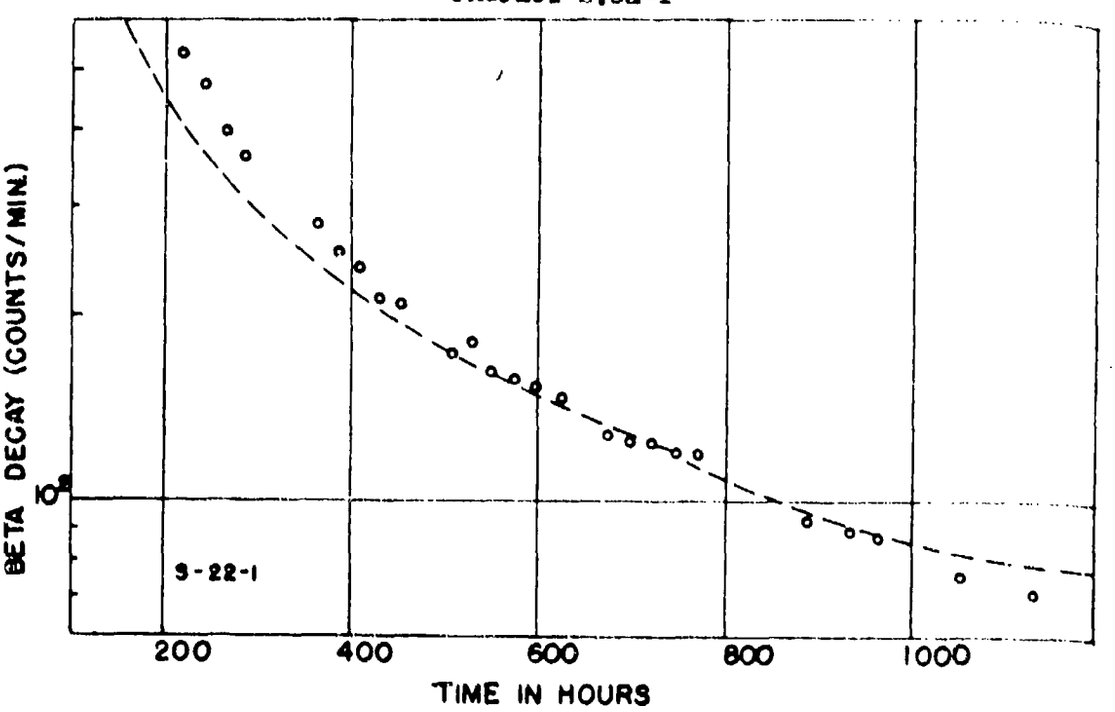

Fig. E.3 Beta Decay Curve, First Filter Paper of Filter Sampler at Station 16, Surface Shot.

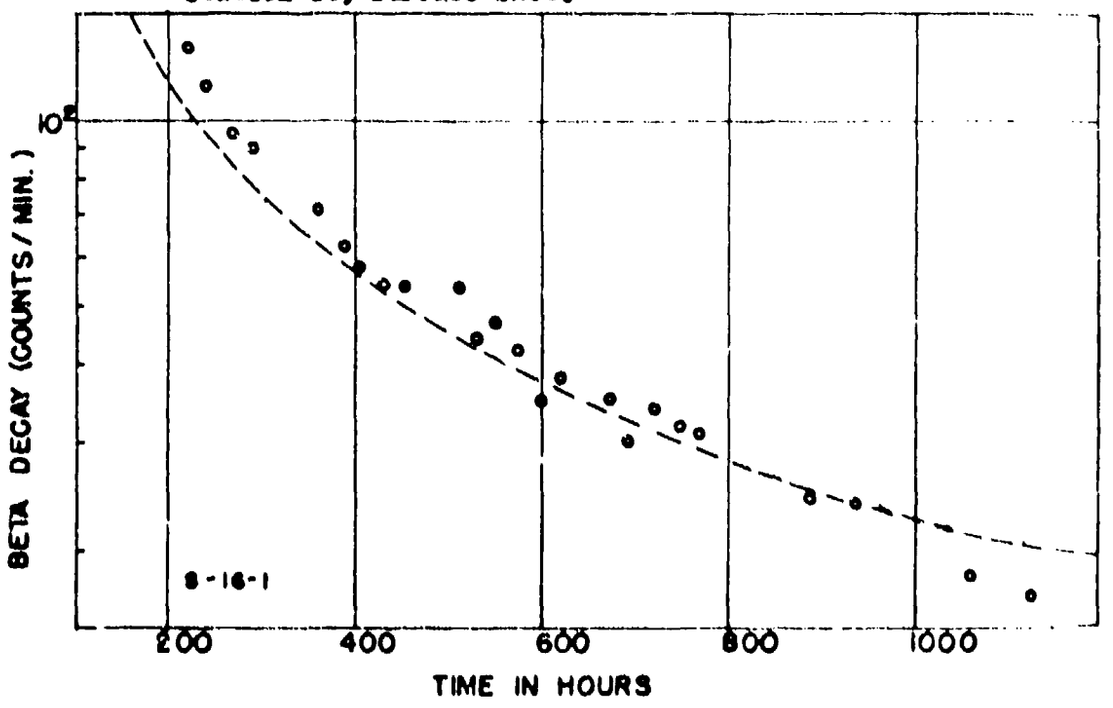

Fig. E.4 Beta Decay Curve, First Filter Paper of Filter Sampler at Station 22, Surface Shot.

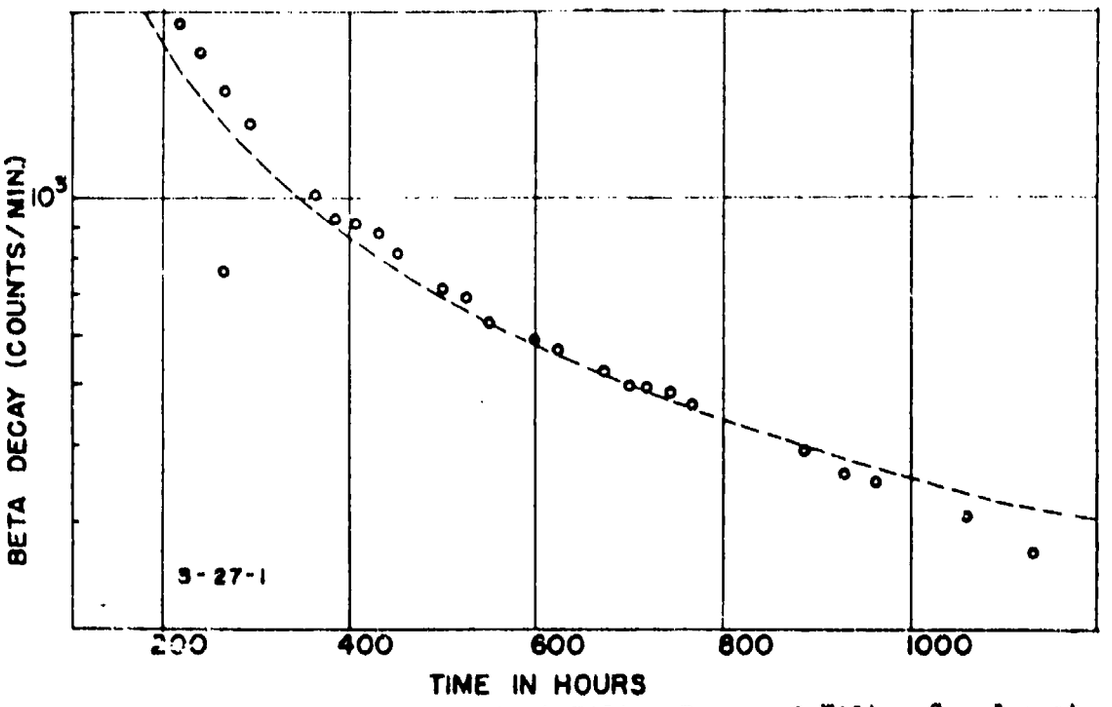

Fig. E.5 Beta Decay Curve, First Filter Paper of Filter Sampler at Station 27, Surface Shot.

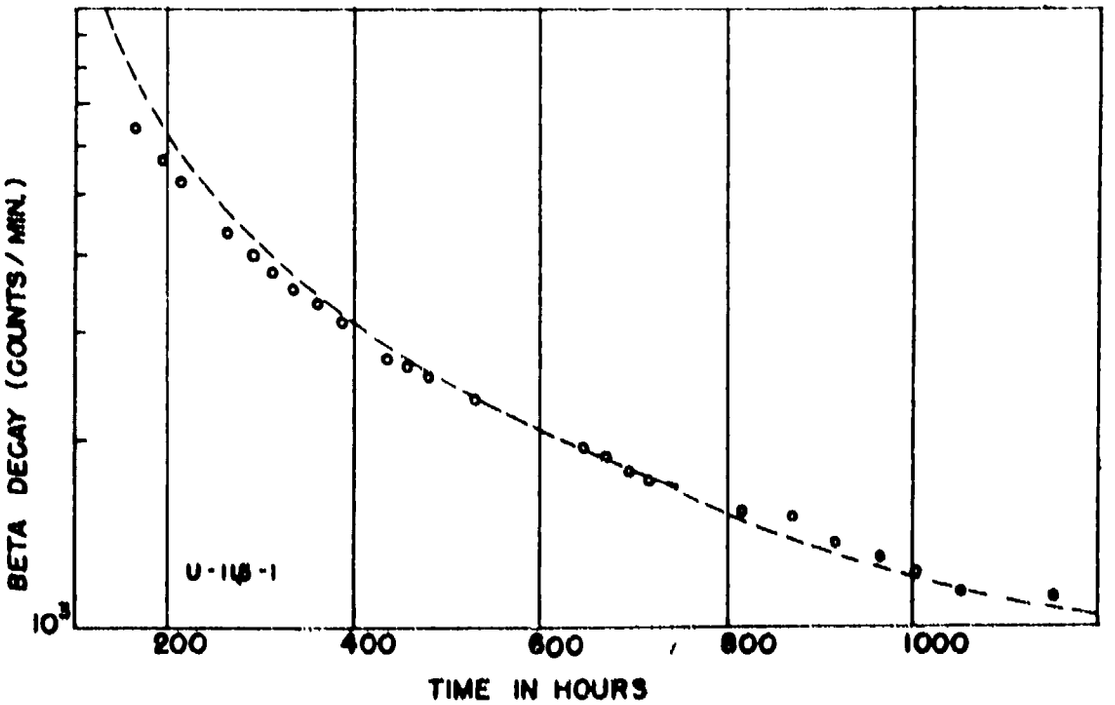

Fig. E.6 Beta Decay Curve, First Filter Paper of Filter Sampler at Station 115, Underground Shot.

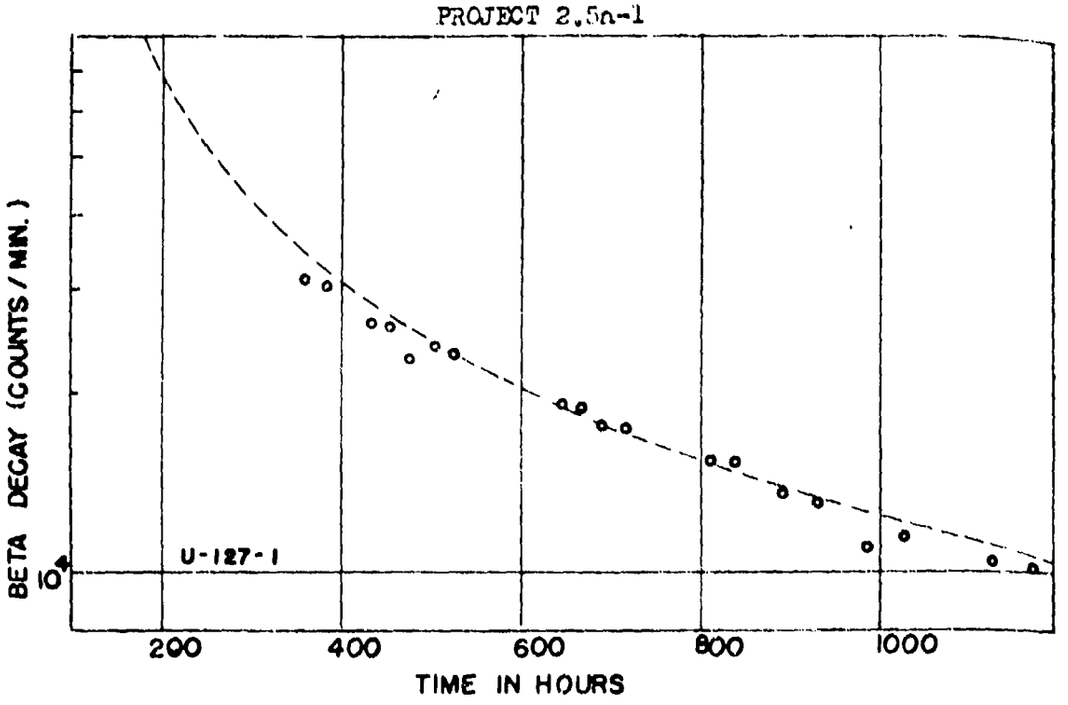

Fig. E.7 Beta Decay Curve, First Filter Paper of Filter Sampler at Station 127, Underground Shot.

It should also be mentioned that the upper limit of the size distribution curve is determined by the total number of particles which are measured. If 10,000 particles were measured instead of 1000, one could extend the distribution curve to slightly larger diameters.

We now define the size distribution function P:

$$P \equiv \frac{1}{N} \frac{dN}{dD} \qquad (E.3)$$

P is the probability of finding one particle of the population of N particles whose diameter is greater than D and less than D dD. Since we believe that the efficiency of recovery for particles larger than 4 microns is roughly constant, the slope (dP/dD) of our size distribution curve will be equal to the slope of the true size distribution within experimental errors. It will be convenient to define two new parameters:

$$\frac{1}{b} \equiv \frac{1}{P} \frac{dP}{dD} \qquad (E.4)$$

$$n \equiv \frac{dP/P}{dD/D} = \frac{D}{b} \qquad (E.5)$$

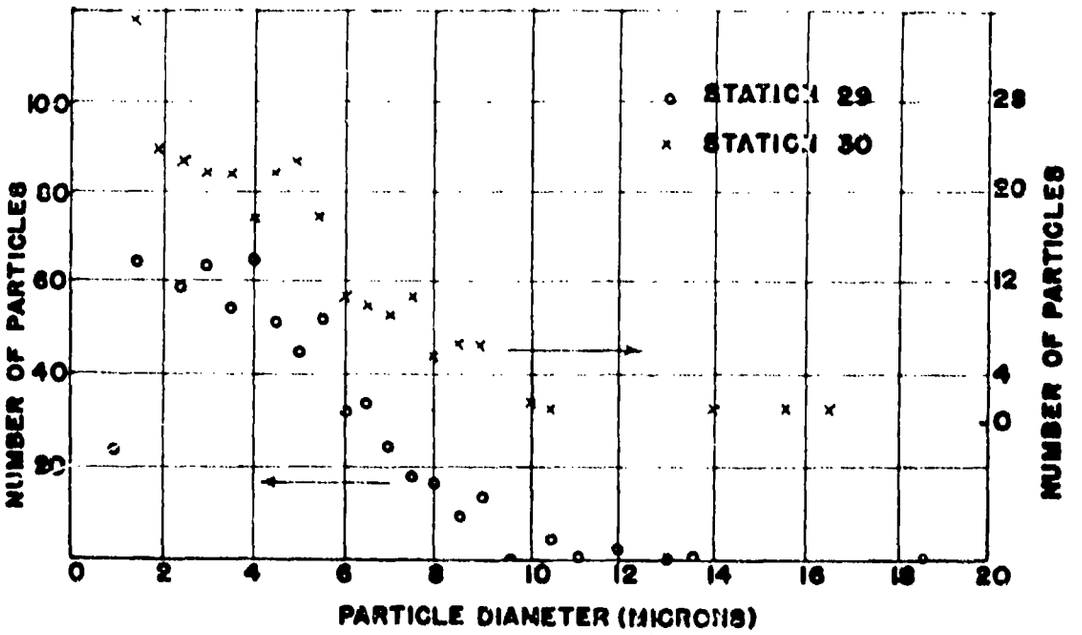

Fig. E.8 Particle Size Distribution of Radioactive Particles on First Filter Paper of Filter Samplers at Stations 29 and 30, Surface Shot.

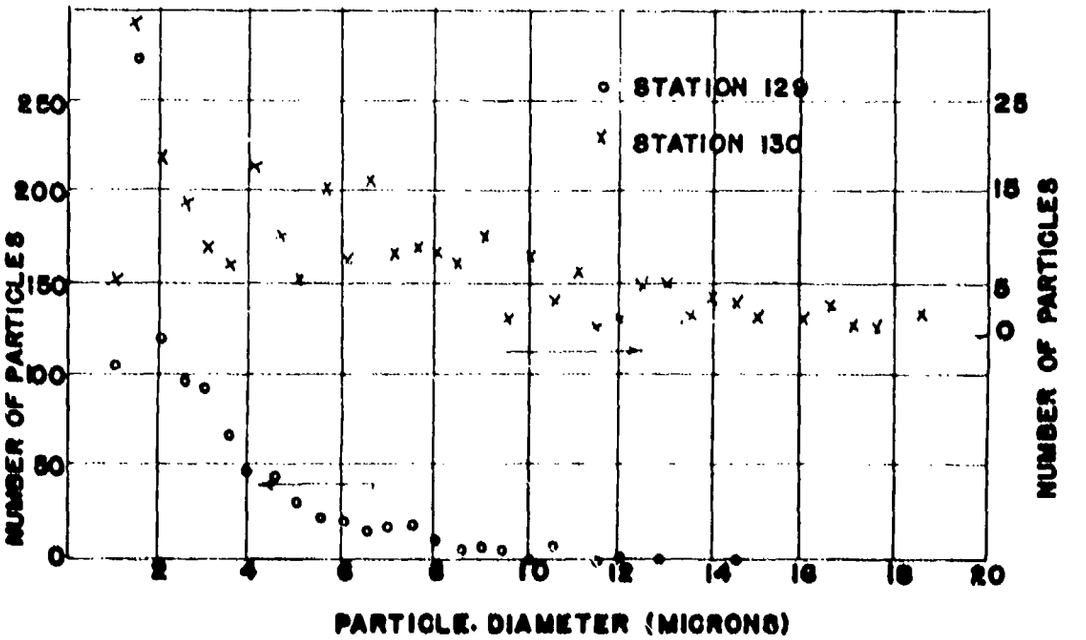

Fig. E.9 Particle Size Distribution of Radioactive Particles on First Filter Paper of Filter Samplers at Stations 129 and 130, Underground Shot.

PROJECT 2.5a-1

TABLE E.3

RADIOACTIVE PARTICLE SIZE DISTRIBUTION PARAMETERS

Filter Paper	b (microns)	n	Range of Sizes of Most Particles Found (in microns)
S-29M	2.8	2.8	3-11
S-30M	3.8	1.6	3-9
U-129M	2.4	1.4	2-6
U-130M	7.0	1.0	2-12
AFOAT Surface	3	2	3-9
" Underground	6	1.3	4-12

In general, the parameters b and n are functions of the diameter D; two special cases are of interest, however:

$$(P)_{b\ const} = (const)\ e^{-D/b} \qquad (E.6)$$

$$(P)_{n\ const} = (const)\ D^{-n} \qquad (E.7)$$

To determine b and n from the experiment, we notice that $\frac{1}{b}$ is given by the negative of the slope of a plot of log P vs D, and (-n) is the slope of the plot of log P vs log D. Drawing the best straight lines through the experimental points gives us our best estimates of n and b in the size range studied.

The experimental values of b and n are reported in Table E.3 where results obtained for two AFOAT Papers are also shown for comparison.

E.4.2 "Gross" Particles

At the suggestion of Col. Robbins the particle group attempted to find the size distribution of all particles collected on filters U-129X1 and U-107X1, not just the radioactive particles. Active portions of these filter papers were dispersed on glass slides and all particles observed under the microscope were measured for "diameter". In this case the definition of "diameter" is the longest observable dimension. For comparison purposes we also prepared "blanks". "Filter paper blanks" were simply smears of the collodion which was used for dispersal purposes.

The result of this work was that all three types of samples contained the same number of particles per unit area, and, as one would expect from this result, all three had the same size and color distribution. Our conclusion, then, is that we measured mostly laboratory dust, and that the standards of cleanliness necessary for this work are much higher than for radioactive particle work.

This work was repeated on AFOAT[ ]filter number U-13-B, which was 10 times as radioactive per unit area as ACC filter U-129X1. The result was again found to be negative.

In view of these disappointing results, the only result that can be quoted is an upper limit to the number of inactive particles present per radioactive particle. From the work done on AFOAT[ ]filter U-13-B, one can say that there are fewer than 10^4 nonradioactive particles per radioactive particle, where nonradioactive particles are defined as being optically detectable (1), and where radioactive particles are defined as being optically detectable and as having sufficient activity to produce a spot on photographic film. The work on the ACC filters would give higher upper limits, due to the fact that less debris was collected on them.

E.5 RADIOCHEMISTRY

E.5.1 Introduction

The original purpose of this part of the program was to establish the shape of the fission yield curve by radiochemical analyses for those elements occurring at several points of inflection of the curve. The elements chosen were Mo^{99}, Ba^{140}, Sr^{89}, Ag^{111}, Cd^{115}, and $Cs^{136-137}$. It was originally considered that an upward displacement of the curve in the neighborhood of Cd was indicative of the release of large numbers of neutrons, while horizontal displacements of the slopes of the curve (such as that including Ag) could be used to identigy the fissionable material. Although there is no reason to use chemical analysis to answer this latter question about our own bombs, it has always been recognized that the successful application of these tests to debris from foreign bombs would require that t ese tests be applied to bombs of known fissionable content.

A gradually increasing uncertainty has arisen because of the fractionation of activity associated with debris from explosions of atomic weapons. [_

An examination of the results presented in the tables that follow will show that fractionation in JANGLE occurred to such an extent that it is impossible to associate a counting ratio with a particular shot unless the origin of the sample is known. In addition to the samples supplied from stations set up as part of this contract, other samples from Air Force collections and an independent source have been analyzed and are reported in these results.

E.5.2 Experimental Details

The results that are incorporated here are counting rates of standard weighing forms of the elements involved, corrected for decay by extrapolation backward to the known time-zero for each shot. Although the decay curves are not included in this interim report, they have been carefully checked and in all cases (except two early experiments on Sr^{89}) have shown decay rates that correspond very closely to those recorded for each nuclide.

The counting rates have also been corrected to zero-thickness by comparison against precipitate-thickness curves that were determined as part of the preparation for this contract. It is hoped that the counting-rate ratios (e.g. the $\frac{Cd115}{Mo99}$ ratio) may be compared with the same ratios measured on the products of an irradiation of normal U_3O_8 by thermal neutrons. In this way, the results from different laboratories may be intercompared without tedious and vulnerable attempts to reduce counting rates to disintegration rates.

E.5.3 Precision of Results

The counting of samples was controlled by the standard statistical procedures used in radiochemistry. As a rule, the precision of the results is estimated to about 5%. In those cases where the counting rate was very low, there will be included in parenthesis immediately after the counting rate, the nine-tenths error converted to percentage of the counting rate. For example, the counting rate of Cd^{115} from sample S-16-L is recorded in Table E.4 as 66(23%). This means that the total number of counts per minute of Cd^{115} (extrapolated to time zero and corrected to zero thickness of precipitate) is 66, and that this number has one chance in ten of being in error by 20%.

Standard factors are taken (from a standard Bi^{210} source) on each counter each working day in this laboratory. Moreover, a careful check has been kept of the background during the last five months, and a shift of as much as 3 cpm would be cause for concern. This constancy of background has been achieved by placing 2-inch bricks of lead under the manual sample changers, thereby reducing to a small fraction those effects that come from other sources of radioactivity that are handled in the basement.

In Tables E.4 and E.5 are listed the extrapolated counting rates for the total sample of each element analyzed. Tests of the filters showed that there was virtually no activity on the second filter paper from each station. However, both first and second papers were treated by the standard dissolution procedures.

The standard practice of laboratories working on these elements is to record the ratio of the counting rate of each element to the Mo^{99}. These are also included in Tables E.4 and E.5.

E.5.4 Surface Shot (T_o is Nov. 191700)

The amount of activity collected at the four stations listed below was quite small:

Station	Gross B Count on Nov.24
S-13-L	151×10^3 cpm
S-14-L	53×10^3 cpm
S-15-L	64×10^3 cpm
S-16-L	165×10^3 cpm

As a result, the counting rates of Cd and Cs were so low that they have little significance.

E.5.5 Underground Shot (T_o is Nov. 292000)

The distribution of activity from this shot followed a very unexpected pattern. A heavy surge must have gone from ground-zero in the direction toward Station U-114, because the amount of activity collected there was many times greater than that collected at any of the other three stations included here. Except for this station, gross B activity collected at the other stations was comparable in amount to that collected on the surface shot.

In addition to the four samples from the ACC stations, activity was analyzed from a close-in Air Force paper. The paper was divided into three parts and the different elements analyzed; each one referred to Mo^{99}. It was assumed here that the distribution of activity due to each nuclide would be independent of that part of the paper taken for analysis. It is now thought (from other results) that this assumption is not always strictly true.

One other source of activity collected independently, was also analyzed, but the results of this analysis will be given in the final report because there is some uncertainty whether the sample (a particle resembling slag) contains debris from the surface on the underground shot.

Pages 182 183 blank

In Table E.5 are listed the results from the underground shot. These are presented in the same general pattern as those from the surface shot.

E.5.6 Discussion and Conclusions

The distinctive fact about these ratios is their variation. Although the precision of the measurements is sometimes low because the total amount of activity was low, there were several samples where the counting levels were high enough to make the maximum error less than 5%. In the underground shot, for example, the statistical errors on the samples from Station U-114-L and the Air Force paper were 1 or 2%. The great variations in the Ag/Mo and Cd/Mo ratios at these stations must be considered accurate to within 3 or 4 %. These results confirm the earlier evidence for fractionation, a term that this laboratory has until recently considered to be a scapegoat for difficulties arising in the course of the analysis.

Once the reality of fractionation has been established, the use of radiochemical results to establish fission-yield curves is seen to be highly vulnerable. There is, however, one interesting ratio that appears to be useful in identifying a shot. This ratio is the Ag^{111}/Cd^{115} ratio, and a survey of a considerable amount of data from former shots shows a remarkable consistency in the values of this ratio. In the case of JANGLE, we have the following Ag/Cd ratios:

	Station
Surface Shot	S-13-L
	S-16-L

The counting data on S-14L and S-15-L is not sufficiently precise to give a valid ratio.

	Station
Underground Shot	U-114-L
	U-115-L
	Air Force Paper J213B

When one considers the great variations in the Ag/Mo and Cd/Mo ratios in Tables E.4 and E.5, it would at first seem remarkable that the Ag/Cd ratios are as consistent as they are. But this is seen to be plausible (though not at all necessary), if one considers the relative volatilities of Pd, Ag and Cd oxides that are formed by the end of the first second in an atomic explosion. In fact, when we consider the periodic variation in

the volatility of oxides of the elements, we are led to make a hypothesis that will certainly be subjected to an exhaustive trial-namely, that fission-product ratios will be most consistent when they involve precursors and final radioactive daughters that have similar volatilities. This is a rather crude hypothesis, and it will likely be considerably refined. It ignores the influence of variations in the half-lives of the precursors as well as several other relatively abstruse points of nuclear physics. Certainly, the constancy of the Ag/Cd ratios is consistent with this hypothesis.

The solution to the problem of fractionation will require an integrated effort by chemists, physicists, and nuclear physicists engaged in this work. It is essentially an attempt to treat rationally the combination of events that can give rise to such variations in radiochemical distribution as those found in the analysis of Jangle debris. The program is being initiated in this laboratory because we realize that it is a problem of central importance in the analysis of atomic bomb debris and the interpretation of the results.

OPERATION JANGLE

PROJECT 2.5a-2

FALL-OUT PARTICLE STUDIES

by

I. G. Poppoff
P. D. LaRiviere
E. C. Evans III
C. E. Adams
J. W. Washkuhn
N. R. Wallace
J. V. Zaccor
S. K. Ichiki
N. H. Farlow
R. K. Laurino
R. R. Soule
E. A. Schuert

2 April 1952

U. S. NAVAL RADIOLOGICAL DEFENSE LABORATORY

SAN FRANCISCO 24, CALIFORNIA

ACKNOWLEDGMENTS

The authors are pleased to acknowledge the invaluable guidance and assistance by F. R. Holden, Associate Head of the Chemical Technology Division, U. S. Naval Radiological Defense Laboratory.

The editorial guidance provided by Jarvis Todd, Publications Editor, Chemical Technology Division, is gratefully acknowledged.

PROJECT 2.5a-2

CONTENTS

CONTENTS (Continued)

PROJECT 2.5a-2

ILLUSTRATIONS

ILLUSTRATIONS (Continued)

ILLUSTRATIONS (Continued)

PROJECT 2.5a-2

TABLES

PROJECT 2.5a-2

ABSTRACT

The chemical and physical properties and the distribution with time and area of the particulate matter dispersed by a surface and an underground atomic bomb detonation were investigated. Aerosol samplers, differential fall-out collectors, and fall-out trays were designed and developed. Sampling was conducted from ground based stations.

The following points were specifically investigated:

1. Median particle diameters of the gross and the radioactive material.
2. Radioactivity of the fall-out material as a function of particle size.
3. Composition of the fall-out and correlation with the source material.
4. Time and area distributions of the fall-out material.

The median particle sizes of the gross and radioactive materials were 0.2 μ and 1.4 μ respectively. The radioactive particles were glassy and had the same elemental composition as the source material except for the absence of carbon and boron. The bulk of the activity was found in the size fraction $> 20\ \mu$. The time distribution studies showed heavy initial concentrations transported by high altitude winds and followed by several secondary waves of material carried by surface winds. Area distributions were found to be determined by the extent of the base surge and wind profile.

CHAPTER 1

INTRODUCTION

1.1 OBJECTIVE

The purpose of this investigation was to study the physical and chemical characteristics and distribution of the particulate matter comprising the cloud and base surge resulting from underground and surface atomic bomb detonations. This information is important, from the point of view of military defense, as basic data necessary for the study and evaluation of internal hazards and decontamination problems.

In its study of the physical and chemical characteristics of particulate matter, the U. S. Naval Radiological Defense Laboratory (USNRDL) paid particular attention to the following points:

1. Gross particle size distributions.
2. Radioactive particle size distributions.
3. Activity as a function of particle size.
4. Identification and correlation of collected materials with source materials.

In the investigation of the distribution of particulate matter, consideration was given to its distribution with regard to both time and area.

1.2 BACKGROUND MATERIAL

The aerosol cloud produced by an atomic bomb detonation has been of interest ever since the first bomb at Alamogordo. Fall-out from this cloud was observed at one or two places in the United States and is said to have caused some difficulty by contaminating the raw material for photographic film packing. Measurements of the size of particles comprising the cloud were attempted at Operations CROSSROADS and SANDSTONE. These measurements, however, were not of sufficient refinement to provide reliable data.

Reliable data regarding chemical composition and physical properties become more and more necessary as research in contamination-decontamination measures and inhalation hazards progresses. Recent investigations at Operation GREENHOUSE have revealed that cloud samples taken under isokinetic

flow conditions show a much smaller median size[1] (approx 0.15 μ) than those previously taken under non-isokinetic conditions. They also revealed that, under certain meteorological conditions, the fall-out can be significant even from an air burst.[2]

It is now of interest to investigate the properties of the aerosol resulting from an underground and a surface burst since these are militarily possible situations. The conditions differ in many ways from an air burst situation. First of all, there is the tremendous mass of material involved. The controlling factor in the chemical composition of the carrier is the soil surrounding ground zero rather than the bomb constituents. Secondly, since drone operation was considered impracticable for this test, ground level sampling was used. Under these conditions, the velocities for isokinetic sampling were those of the surface winds rather than the air speed of drone aircraft. These two factors, namely, large amounts of material and low velocity sampling, allowed the use of a thermal precipitator sampler which is more ideally suited to electron micrographic analysis than either the electrostatic precipitator needed for high velocity sampling or the impactor instruments which discriminate against the smaller sizes. Large quantities of fall-out were collected easily under these conditions. Studies of activity as a function of particle size, fall-out as a function of time, and identification of carrier material were, therefore, more fruitful than for air bursts.

---

[1] J. P. Mitchell and T. C. Goodale, "Cloud Phenomena: Study of Particulate and Gaseous Matter", Greenhouse Report, Annex 6.1.

[2] C. E. Adams, F. R. Nolden, and N. R. Wallace, "Fall-out Phenomenology", Greenhouse Report, Annex 6.4.

CHAPTER 2

INSTRUMENTATION

2.1 AEROSOL COLLECTOR

2.1.1 Theory of Thermal Precipitation

It is known that if a hot body is suspended in a wind-free dust-laden atmosphere, a clear dust-free space a fraction of a millimeter wide is observed immediately surrounding the body. Theory explains this phenomenon by an interaction between the dust particle and the steep thermal gradient around the body which causes the particle to be accelerated from the body. If a cold (with respect to the body) surface is placed within the dust-free space, a particle passing between this hot body and the cold surface will be precipitated on the cold surface. This is essentially the way the thermal precipitator operates.

The dust-free space surrounding a hot body was first reported by Tyndall in 1870 and Rayleigh in 1882. This space was studied by Aitken and by Lodge and Clark in 1884. Empirical formulae for the width of the space as a function of pressure, excess temperature over the surrounding gas, shape, and convective heat loss, were determined by Miyake in 1935 and Watson in 1936. These formulae were of the form,[1]

$$A = L\theta H^{-0.38} \tag{2.1}$$

where A = thickness of dust-free space
H = convective heat loss
θ = temperature excess
L = constant,

and

$$A = kp^{-a} \tag{2.2}$$

where k = a proportionality constant
p = pressure
a = 0.61 to 1.0 depending upon the size and shape of the particle.

The convective heat loss in (2.1) equals $C^{1.25}$ where C is a constant which varies with the size, shape, and orientation of the body.

---

[1] H. H. Watson, Proc. Faraday Soc., XXXII (1936), 1073.

Cawood, in 1936, developed an expression for velocity based on the theory of molecular bombardment of a particle in a thermal gradient,[2] namely:

$$V = \frac{\frac{1}{2} P \frac{dT}{dx} \frac{L}{T} - \frac{RT}{N}}{6\pi\eta r} \times (\pi r^2)\left(1 + \frac{AL}{r}\right) \qquad (2.3)$$

where
- P = pressure
- $\frac{dT}{dx}$ = thermal gradient
- L = mean free path
- T = temperature
- r = radius of particles
- R = gas constant
- N = Avogadro's number
- A = constant
- η = viscosity.

Measurements of velocity agreed to within an order of magnitude.

A more successful approach has been to consider thermal repulsion as a radiometer phenomenon. As early as 1825, Fresnel noted the effect of radiation on a particle suspended in a gas. Since that time many investigators attempted to derive equations to explain the radiometer effect as observed with the classical vane radiometer. The first equation which successfully agreed with experimental observations was derived by A. Einstein in 1924, and was based on heat flow using a simplified model:[3]

$$F = -\frac{1}{2}(PL^2T)\frac{dT}{dx} \qquad (2.4)$$

where
- F = force per unit length of vane
- P = pressure of gas
- L = mean free path
- T = temperature of gas
- $\frac{dT}{dx}$ = thermal gradient.

Maxwell developed an equation in 1880 for the force on a radiometer vane in a high pressure atmosphere. Although this equation

---

[2] W. Cawood, Proc. Faraday Soc., XXXII (1936), 1068.

[3] A. Einstein, Z. Physik, XXVII (1924), 1.

was not even in qualitative agreement with experiment, a more rigorous derivation based on Maxwell's work was developed by Epstein[4] in 1929 and led to a satisfactory explanation. The equation given by Epstein is:

$$F = - \frac{9\pi a H_a}{2H_a + H_i} \frac{\eta^2}{T} \frac{dT}{dx} \qquad (2.5)$$

where H_a = heat conductivity of gas
H_i = heat conductivity of particle
a = radius of particle
η = viscosity of gas
ρ = density of gas.

Particles having diameters of several microns and below acquire terminal velocities in distances less than their diameters. These velocities are described by:

$$V = ZF \qquad (2.6)$$

where Z is the mobility of the particles. In a medium rendered inhomogeneous by a steep thermal gradient, Z is dependent upon the ratio L/a. Expressions for Z for three values of L/a follow, namely:

when L/a is small, $Z = (1 + A\,L/a)/6\pi\eta a$ (2.7)
when L/a is large, $Z = (A + B)\,L/6\pi\eta a^2$ (2.8)
and when L/a has an intermediate value, $Z = \frac{1 + L/a\,(A + Be^{-Ca/L})}{6\pi\eta a}$ (2.9)

where L = mean free path
A = 1.23
B = 0.41
C = 0.88

Equation (2.9) reduces to (2.7) and (2.8) in the appropriate regions.

Substituting equations (2.5) and (2.9) in (2.6), and using the well known expressions

$$\eta = 0.499\ \bar{V}L \qquad \text{and} \qquad \rho\bar{V}^2 = 8P/\pi$$

[4] P. S. Epstein, Z. Physik, LIV (1929), 537.

(where $\bar{V}$ is the average molecular velocity), the following general equation for the velocity of a particle in a thermal gradient is obtained:

$$V = -17.9 \frac{1}{2 + H_1/H_2} P \frac{L^2}{T} \frac{dT}{dx} \frac{1 \pm J/a\,(A \pm Be^{-Ca/L})}{6\pi\eta} \qquad (2.10)$$

This equation has been verified experimentally by Rosenblatt and La Mer.[5] The radiometer theory also predicts a "thermal creep" effect which should result in a streaming effect of the gas from the cold to the hot side of the particle. This was observed by Gerlach and Schutz in 1932. From this evidence it certainly appears that the phenomenon is explained by the radiometer theory.

The first thermal precipitator as such was described by Green and Watson in 1935. Since the repulsive force is dependent on particle size (2.5), the deposit is fractionated to some degree when precipitated. The smaller particles tend to be deposited first and the larger ones last. This is not suitable for electron microscope analysis since only a small area of the sample is observed in the field of view and a representative size distribution is not obtained. This defect was remedied by the development of an oscillating thermal precipitator at the Porton Laboratories. In this device the sample holder oscillates back and forth across the hot wire and the size fractionation is overcome by uniform mixing. Ideally, then, every point on the sample collector will receive the proper proportion of each size particle precipitated. An oscillating thermal precipitator of better design was developed by Wilson, Laskin, and Meier[6] at the University of Rochester. Their precipitator forms the basic unit of the USNRDL aerosol sampler used in Operation JANGLE.

2.1.2 Isokinetic Sampling

The general theory of isokinetic sampling is straightforward and reasonable. Simply stated, if sampling is done with a lineal flow identical to that of the aerosol stream, the streamlines will not be disturbed and the sample will be representative insofar as particle sizes are concerned. If sampling is done with a lineal flow exceeding that of the aerosol stream, the streamlines will converge toward the sampler inlet and the smaller particles will be favored in the sample. Conversely, if sampling is done with a lineal flow less than that of the aerosol stream,

---

[5] P. Rosenblatt and V. K. La Mer, Phys. Rev., LXX (1946), 385.

[6] R. Wilson, S. Laskin, and D. Meier, University of Rochester Quarterly Report, December 1949.

the streamlines diverge around the inlet and the larger particles are favored. This is explained by the fact that the smaller particles tend to follow the streamlines while the larger particles do not because of their greater inertia.

What is not well known, however, is to what extent the size distribution of the sample is affected by any given deviation from isokinetic conditions. The importance of isokinetic sampling has been mentioned by many authors though the restrictions which should be imposed on the air flow have never been clearly delineated. The calculations of the dependence of sampling on isokinetic conditions are difficult and laborious. They are now in progress at the USNRDL.

Experimental evidence is scanty at best. One experimentor has reported measurable differences in mass between samples collected under isokinetic conditions and those collected at sampling rates differing by five and ten miles per hour from that of the aerosol stream. However, his data and description of sampling conditions were not complete enough to evaluate his conclusions properly. It was found in sampling the radioactive aerosols at recent atomic bomb tests that samples taken at isokinetic conditions yielded particle size distributions significantly smaller than those collected at previous tests where the sampling velocities were less than the aerosol velocities. However, these data are applicable only to aircraft velocities.

2.1.3 Design Criteria

The aerosol sampler used in this investigation was designed to operate under the following conditions:

1. Expected wind velocity, 5 to 10 mph with a maximum anticipated afternoon wind of 35 mph.
2. Extreme temperature differences of approximately 20 to 80°F.
3. Dry atmosphere laden with wind blown dust.
4. Remote starting signal.

Furthermore, the sampler was designed to accomplish the following:

1. Collect samples isokinetically in the wind direction.
2. Collect samples in the size range of 0.02 to 8 μ diameter particles.
3. Collect samples directly onto electron microscope screens and microscope cover glasses.
4. Start from a remote starting signal and turn off when the sampling period was complete.

2.1.4 Description of Aerosol Collector

The aerosol sampling instrument is essentially a University of Rochester oscillating thermal precipitator in a housing designed to reduce the air velocity to a value approximating the inlet velocity of the thermal precipitator. A pump, operating at constant speed, is attached to the housing through a manifold to furnish air flow into the housing and, through a calibrated metering orifice, into the thermal precipitator. A wind-actuated rotary valve controls an external calibrated leak which, connected through the manifold, controls the flow into the sampler. The entire instrument is vaned and free to rotate in a complete circle so as to head always into the wind. A schematic cross sectional view is shown in Fig. 2.1.

The thermal precipitator is essentially the University of Rochester design (Fig. 2.2), but a slight modification was made in its over-all appearance by tapering the inlet to reduce turbulence. The wire assembly was also modified to incorporate spring tension and a slightly easier method of changing wires.

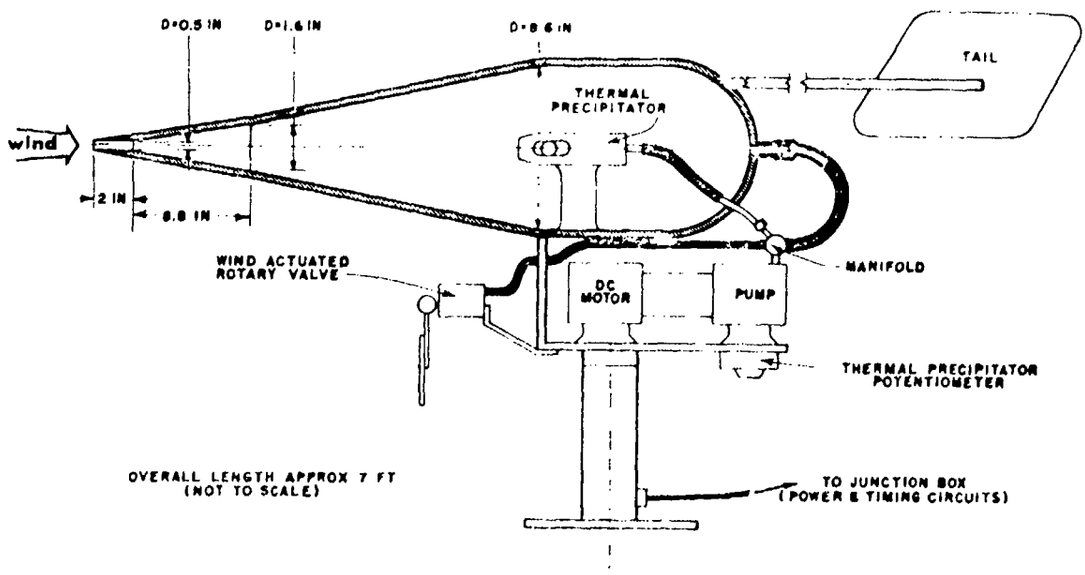

Fig. 2.1 Aerosol Sampler

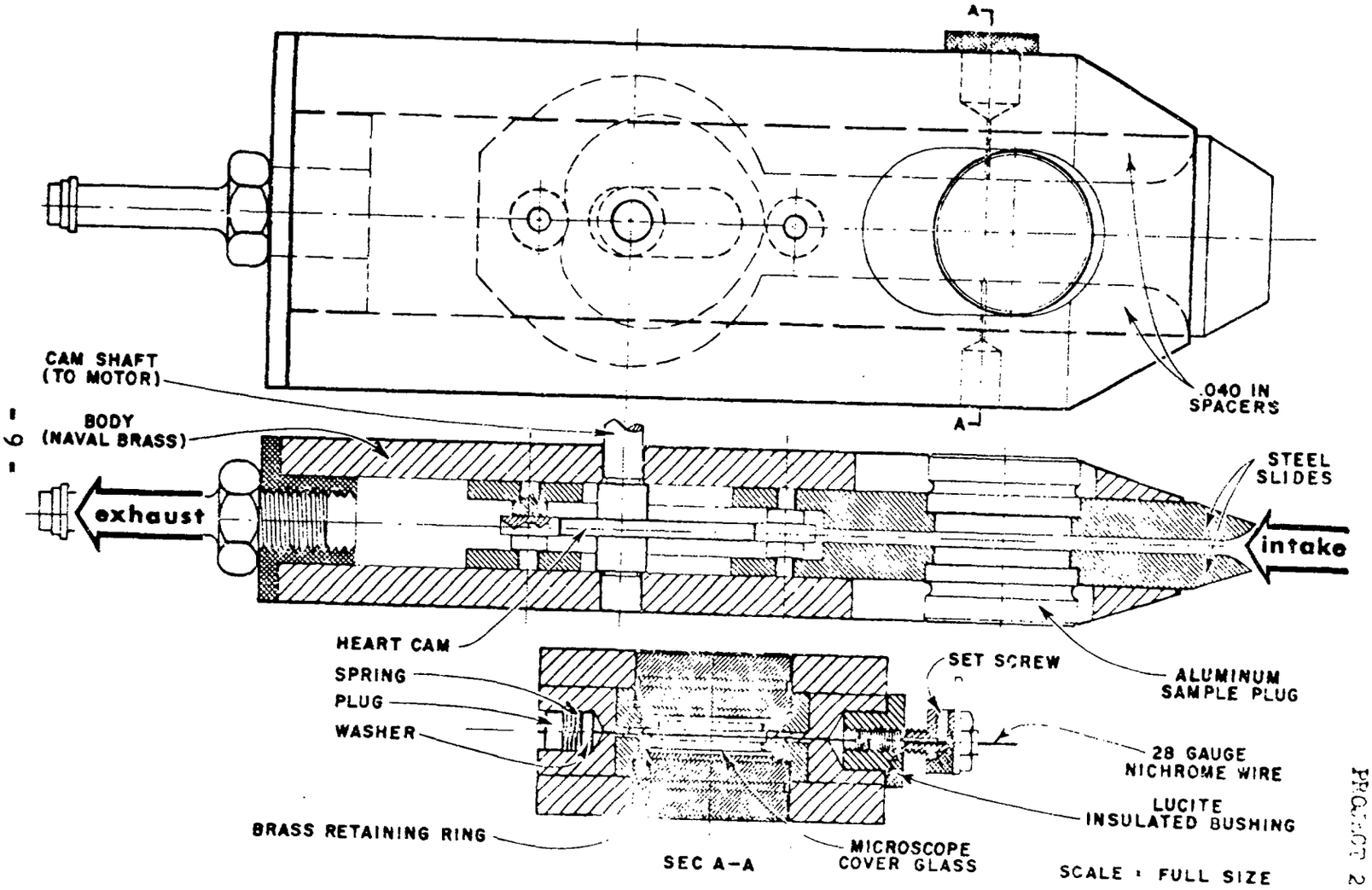

Fig. 2.2 Thermal Precipitator

PROJECT 2.5a-2

In this model, two steel slides, separated by a 0.040 in. brass spacer, travel back and forth at the rate of 0.6 cycles per minute. Between the slides is a stationary nichrome wire (28 gauge) mounted parallel to the plane of the slides and perpendicular to the direction of motion. Aluminum plugs with microscope cover glasses attached are inserted in the steel slides to that the glasses oscillate back and forth in the region of the wire. The oscillations are controlled by a 0.6-rpm d-c timing motor driving a heart cam which, in turn, drives the slides. The entire device is enclosed in a brass (Naval grade) housing.

An aerosol passing between the slides is precipitated onto the cover glasses opposite the hot wire. On one of the glasses is mounted an electron microscope screen. The flow rate through the precipitator is approximately 7 cc/min and the lineal velocity past the wire is approximately 2.4 fpm. The wire is heated by 2.5-amp dc which gives it a temperature of approximately 560°C. A condition of no leakage around the wire which still allows oscillation of the slides without lubrication is attained by keeping the tolerances to a few ten-thousandths of an inch. Such tolerances also apply to the positioning of the holes for the hot wire to prevent intermittent shorting. It was necessary to reduce the oscillation rate to less than one cycle per minute for most effective precipitation. Higher rates of oscillation decreased the collection efficiency to a large extent.

The diffuser housing was designed to sample isokinetically from the ambient airstream and to slow the aerosol down to the intake velocity of the thermal precipitator. The flow rate through the housing is such that the lineal flow at the tip is the same as the wind blowing past the nozzle. This lineal flow is reduced in two steps to that of the thermal precipitator:

Step 1, from V_o to $\frac{V_o}{10}$ through an ideal 7° diffuser section

Step 2, from $\frac{V_o}{10}$ to V_T through a second section more divergent than the preferred 7° angle. This was done to keep the precipitator within a reasonable size.

The housing is basically designed to sample from a 5 mph wind. The flow rate is modified to sample from winds up to 30 mph as indicated in Table 2.1.

TABLE 2.1

Theoretical Sampling Velocities[a]

Wind Velocity (mph)	Flow Rate through Housing (cfm)	Inlet Velocity (mph)
0 - 10	0.6	5
10 - 20	1.8	15
20 - 30	3.0	25

(a) At all velocities the sampler was within ± 5 mph of being isokinetic.

The wind gauge is a remodeled aircraft gas level gauge. A disk is substituted for the float and allowed to hang freely in the airstream. The wind impinging on the disk deflects the arm at an angle proportional to the velocity. This motion is transferred through a set of beveled gears to a rotary valve which is calibrated to allow the leakage in the manifold necessary to produce the housing flow rates listed in Table 2.1.

The pump is powered by a 24-v dc motor and has a maximum capacity of approximately 3.0 cfm. The manifold connected to the pump has inlets for main housing flow, the wind actuated valve, and thermal precipitator flow.

The timing unit consists basically of two timing motors:

1. A 4-hr motor which turns the unit off after a 3-hr sampling period,
2. A 5-min motor which closes the starting circuit of the differential fall-out collector five minutes after receiving the T - 5 min remote-starting pulse. This starting pulse actuates a relay which simultaneously starts the aerosol sampler (allowing at least a 5-min warm-up period), the 4-hr motor with a 3-hr turn-off cam, and the 5-min delay motor for the differential fall-out collector (DFO). This is all physically incorporated in a main junction box with cables running to the battery, remote-starting relay, differential fall-out collector, and the aerosol sampler.

Power requirements are furnished by a 24-v storage battery. The current drain is approximately 10 amp for three hours.

2.1.5 Evaluation

To evaluate properly the sample collected by this instrument, the following points had to be investigated before the field operation:

1. Collection efficiency as a function of particle size.
2. Collection efficiency as a function of heat conductivity

The investigations were not as thorough as desired because of the short time between the inception of the instrument and the manufacture of the field models. All the results indicated, however, that this would be a satisfactory instrument for the conditions which were expected to prevail.

2.1.5.1 Collection Efficiency as a Function of Particle Size

It has been generally conceded that, as nearly as can be determined, precipitation is complete for particles not exceeding 2 to 3 μ in diameter. It has been claimed by some and refuted by others that collections of particles up to 10 or 20 μ in diameter can be made with good efficiency. Since there seems to be no doubt about the sampling efficiency for particles less than 2 μ in diameter, and since Laskin and Lauterbach at the University of Rochester have tested this particular precipitator in the range 0 to 3 μ with NaCl aerosol, it was decided to check the upper end of the particle size spectrum.

By the expedient method of connecting two precipitators in series and observing collections on the second instrument, it was determined that there was complete precipitation of alumina particles in the range 0 to 2 μ.

To determine precipitation efficiency in the range 1 to 10 μ the cam was removed from the precipitator, so that all particles not precipitated would have clear passage, and a jet impactor (known to be very efficient for particles over 0.5 μ) was connected to the exhaust. Impactor samples were taken with the wire of the thermal precipitator cold and with the wire hot. The samples were counted and the numbers in each size group compared. The efficiencies given in Table 2.2 were determined in this manner:

TABLE 2.2

Collection Efficiency

Size (μ)	Efficiency (%)
1 - 4	100
4 - 6	99
6 - 10	98

2.1.5.2 Collection Efficiency as a Function of Heat Conductivity

Combining Epstein's equation (Equation 2.5) and Equation 2.6,

$$V = -Z\left(\frac{9\pi \, a \, H_a}{2H_a + H_1}\right)\frac{\eta^2}{\rho}\,\frac{1}{T}\frac{dT}{dX}\,, \qquad (2.11)$$

from which it is evident that the velocity of thermal repulsion is almost exactly inversely proportional to the heat conductivity of the material being precipitated. It was determined experimentally that a wire temperature sufficient to precipitate alumina was not at all adequate to precipitate dry NaCl. These results are shown in Table 2.3.

TABLE 2.3

Precipitation Temperatures

Material	Heat Conductivity (cal/cm/sec°C)	Temperature Necessary for Precipitation (°C)
Al_2O_3	0.01	280
NaCl	0.015	560

It is evident from Equation 2.11 that to impart the same velocity to NaCl and Al_2O_3 particles, thereby permitting the same collection efficiency, it is necessary to adjust the quantity $\left(\frac{1}{T}\frac{dT}{dX}\right)$. Considering the inaccuracy in determining the wire temperature

and the heat conductivity of the material, the agreement between calculated and observed values of the ratio $\left(\frac{1}{T}\frac{dT}{dX}\right)_{NaCl} \Big/ \left(\frac{1}{T}\frac{dT}{dX}\right)_{Al_2O_3}$ is good (calculated, 1.50; observed, 1.54).

Since a preliminary survey indicated that none of the material at the site would have heat conductivity greater than that of NaCl, a wire temperature of 560°C appeared sufficient to ensure good precipitation.

2.2 FALL-OUT COLLECTORS

In the past, fall-out collectors have suffered from two major deficiencies:

1. No separation of actual fall-out material from background windblown material (either inactive or redispersed active material).
2. No data have been gathered regarding time rate of fall-out.

Of the following instruments, the first one attempts to correct both of these deficiencies and the second attempts to remedy the first.

2.2.1 Description of Instruments

The differential fall-out collector (Fig. 2.3) consists of a circular Lucite disk approximately 25 in. in diameter partitioned into twenty sectors. A glass plate coated with carbowax is inserted in each sector providing a surface which is easy to work. On each glass plate is placed an electron microscope screen and a microscope cover glass. The disk powered by a spring-driven clock motor rotates for one period of revolution starting at T = 0. Two periods were used in the tests:

1. Twenty minutes for the near stations.
2. Two hours for the far stations.

The rotating disk is enclosed in an aluminum housing. Directly over the disk is an opening in the form of a sector of the disk and one-quarter its width. This opening is adjustable over a small range in azimuthal position so that collection can start at the beginning of a sector for convenience in analysis.

In operation, the collector is set in position and started by a triggering pulse from the thermal precipitator junction box. The disk revolves once and stops. During the operating period, it collects

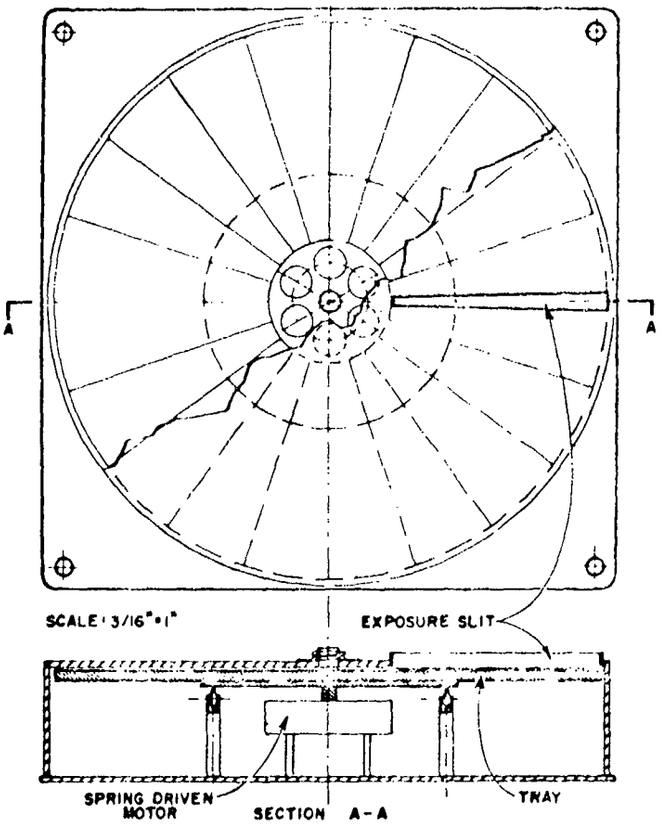

Fig. 2.3 Differential Fall-out Collector

fall-out in small increments through the opening in the housing. Background material is kept to a minimum because the sample is collected only during the fall-out period except for the first and last positions.

The fall-out collector tray consists of a 1-ft-square tray, a tray cover, and two clock-actuated mechanisms (Fig. 2.4).

The clocks are set so the tray will be exposed one hour before the shot and covered one hour after the shot. When the first clock-actuated mechanism triggers, it allows the tray to be pulled out from under the cover by a spring which is in the extended position before the mechanism is actuated. The tray remains exposed to the fall-out during the fall-out period. Then the other clock mechanism is actuated allowing the cover, which is also under spring tension, to slide over the tray. In this manner, much of the background material is excluded from the collection.

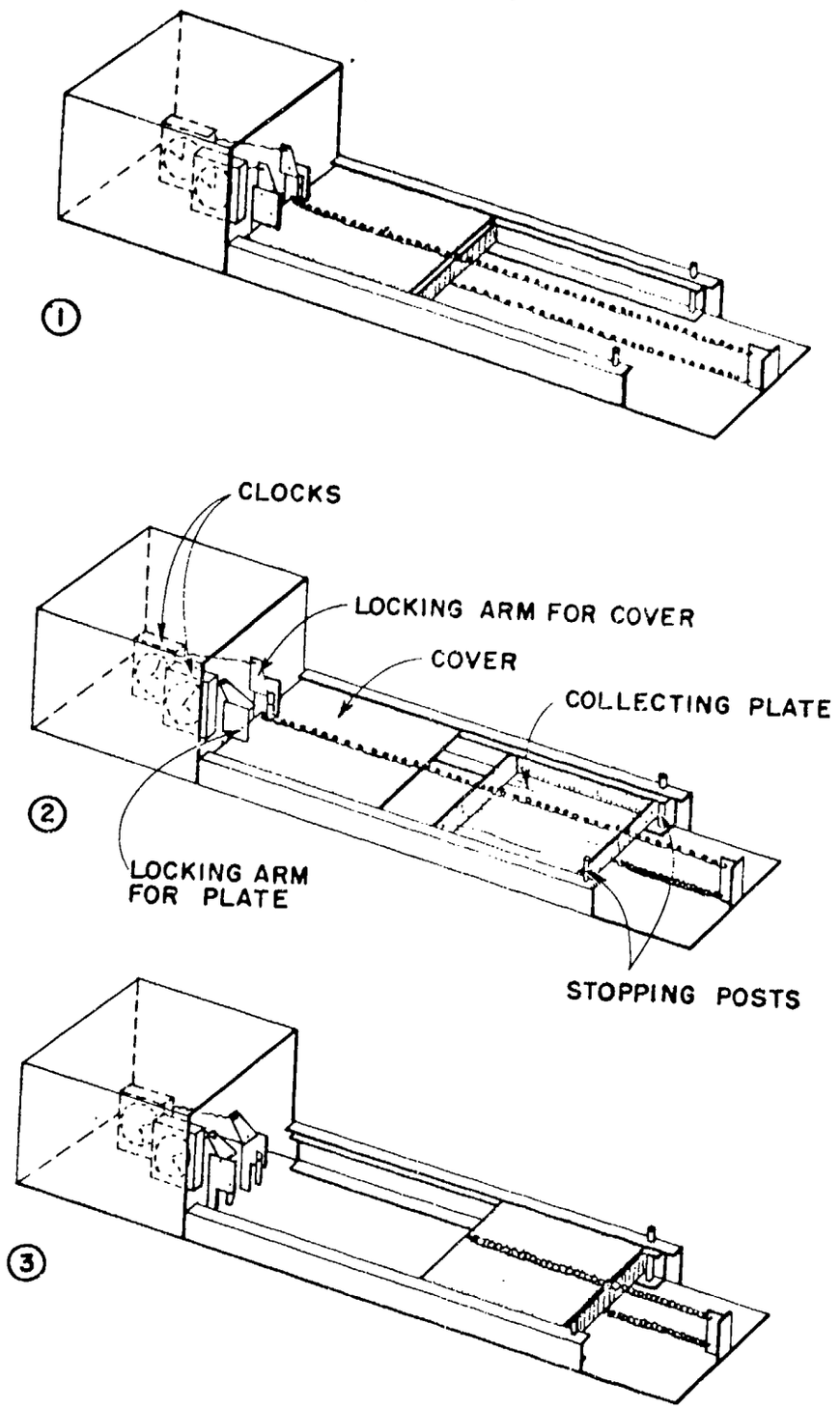

Fig. 2.4 Fall-out Tray

CHAPTER 3

FIELD OPERATIONS

3.1 AEROSOL COLLECTORS

A series of 7-ft towers located according to the pattern in Fig. 3.1 were provided by the Army Chemical Center for the installation of equipment. This pattern formed a sector straddling the expected wind direction and allowing for a maximum shift of 60° in either direction. The aerosol collectors were mounted on top of the towers near whose bases were situated junction boxes containing the timing motors. Near each junction box a starting relay, which was tied into the timing network, was installed and batteries were placed on the ground to supply the power. The batteries were furnished by the Evans Signal Laboratory.

The instruments were started by the remote starting signal (T-5 min) and stopped automatically three hours later. The samples were recovered as soon as it was possible for personnel to re-enter the area and were shipped by air to USNRDL.

During the operation of the instruments in the field, the following difficulties were encountered:

1. Failure to receive a starting signal.
2. Plugged needle valves.
3. Jammed precipitators.

Two stations (Nos. 129 and 130) failed to function apparently because galling of the brass ways caused the precipitator to jam. This failure invalidated the electron microscope analyses for these two stations. Autoradiographic analyses for Stations 129 and 130 were not invalidated since the entire field is counted when searching for active particles instead of the small portion employed in electron microscopy. Prior to the underground shot, metering orifices were substituted for the needle valves and operated satisfactorily.

3.2 DIFFERENTIAL FALL-OUT COLLECTORS

The differential fall-out collectors were situated on the ground and all but two were near enough to the towers with the aerosol collectors to be operated from its junction box. These two were located at the 2,000 yd range as shown in Fig. 3.1 and had their own timing units.

PROJECT 2.5a-2

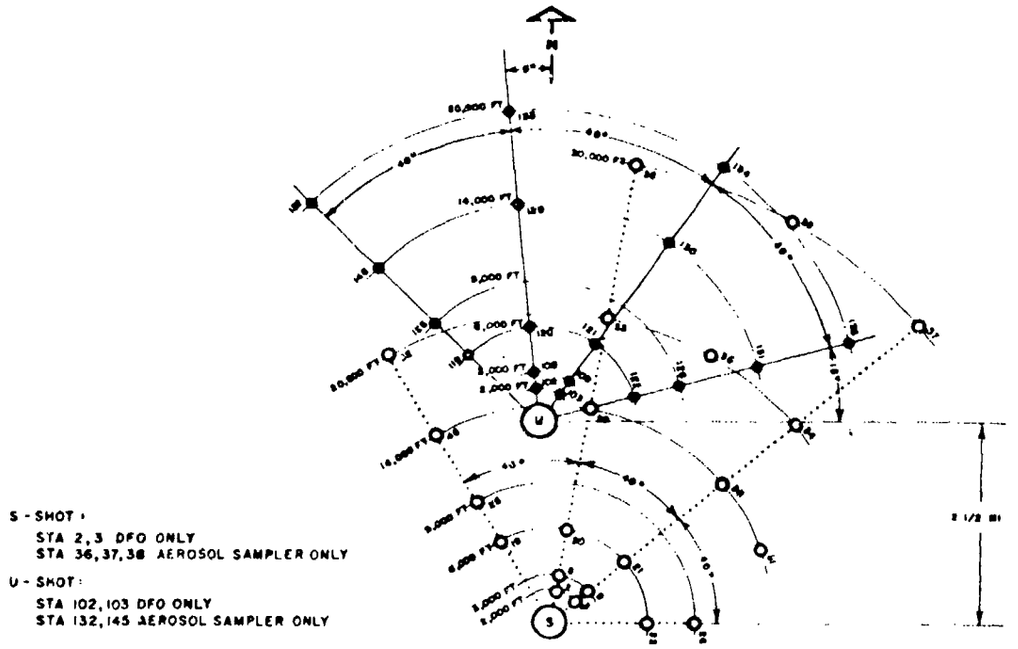

Fig. 3.1 Instrument Layout

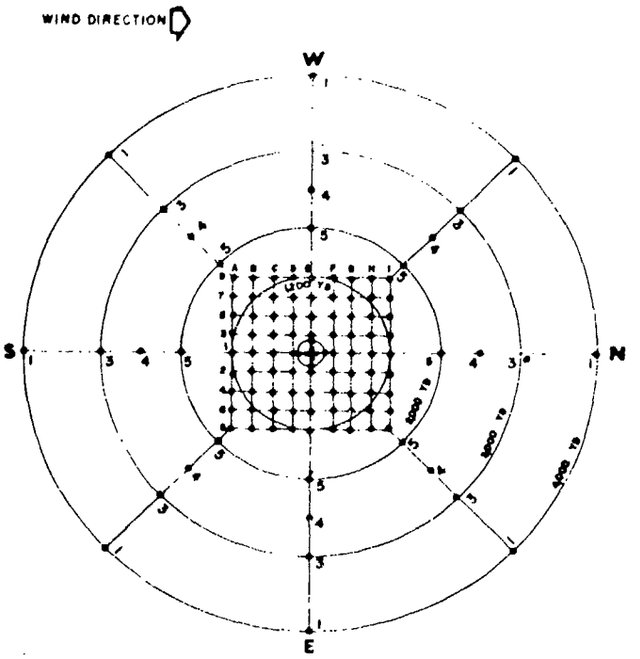

Fig. 3.2 Collector Plate Fall-out Pattern for Shots 1 and 2

The differential fall-out collectors were started by the remote starting signal (T-5 min) and turned themselves off after one complete revolution. The samples were recovered when it was safe for personnel to re-enter the area and shipped to USNRDL.

In the field operation of the differential collectors, the following difficulties were experienced:

1. Failure of the start-stop mechanism.
2. Dirty relay contacts.
3. Failure to receive a starting signal.

The start-stop mechanism consisted of a pin pushed against the balance wheel of the clock motor by a relay. This arrangement did not function perfectly and, consequently, some of these devices did not start and others did not stop at the completion of a single revolution. Dusty conditions which prevailed at the site made it very hard to keep all relay contacts sufficiently clean to assure their perfect operation.

In the area covered by the fall-out after the underground shot, one collector (No. 119) did not operate because it failed to receive a starting signal; collectors No. 109 and No. 121 failed because of conditions 1 and 2. Of the five collectors which were in the fall-out area after the surface shot, one (No. 8) failed to start and another (No. 2) stopped shortly after starting. The failure of No. 8 was presumably due to conditions 1 or 2, but no satisfactory reason was found for the failure of No. 2.

3.3 FALL-OUT TRAYS

The fall-out trays were located in the field as shown in Fig. 3.2. The clocks which actuated the trays were set to uncover them at T-1 hr and to cover them at T+1 hr.

As soon as it was safe to re-enter the area, the samples were measured in place for ionization intensity. A more careful measurement was made at the field laboratory and there the material was removed from the pans in a dry box and weighed. Samples were selected and sent back to the USNRDL for specific activity determination and sieve size grading.

One hundred and twelve instruments were installed for the surface shot. Of this number, the tray release failed on one, the lid release on fourteen, and both releases on five. Of the one hundred instruments which were installed for the underground shot, the lid releases failed on nineteen and both releases on one. A lid release failure does not necessarily invalidate the collection result unless high winds come up before they are retrieved.

CHAPTER 4

ANALYSIS AND RESULTS

4.1 CHARACTERISTICS OF FALL-OUT MATERIAL

4.1.1 Particle Size Distribution of Gross Sample

All the electron microscope grids from the thermal precipitators plus those differential fall-out grids which showed an activity above an arbitrary 500,000 c/m (using a special aluminum window, gas flow proportional counter) were scanned in an RCA EMU2B electron microscope with extended range lens. Limiting the initial scanning to grids from sectors with an activity count above a certain amount facilitates early discovery of grids with sufficient numbers of particles to obtain a size distribution.

If over 200 particles could be found on a grid, the particles were photographed at an electronic magnification of 2,700X. Then, in the case of the thermal precipitator grids, these particles were sized directly from the lantern slides with a Gaertner optical comparator. This method was selected only to eliminate the necessity of making prints. However, since there was frequently some difficulty in determining the boundaries of the particles, the plates from the grids of the differential fall-out collectors were photographically enlarged four times to give a total magnification of 10,800X and the particles were sized from the prints.

A few of the remaining grids with an activity count of less than 500,000 were picked at random and scanned to determine whether they too might not yield a sufficient number of particles to obtain a distribution. Although some particles were found, sufficient number for size distributions were not and, consequently, further scanning of these grids was discontinued.

Almost without exception, the grids were so sparsely populated with particles that a rigid geometric photographic sequence would have been impractical. Therefore, only those areas containing relatively large deposits of particles were photographed, the single particles being skipped whether large or small. Quantitatively, it would be hard to evaluate this bias, but qualitatively, it is known to shift the distribution in favor of the larger particles.

All diameters on both the micrographs and the lantern slides were measured as a projection of the maximum diameters on a common

axis. Since there is a certain amount of distortion inherent in the lenses of an electron microscope, particles are apparently elongated in a radial direction, those farthest from the electron beam axis being distorted the most. This again introduces a bias shifting the size distribution toward a higher median diameter, but the distortion amounts to less than 3 per cent and is, in fact, insignificant in comparison to the bias previously mentioned. It may be eliminated completely, however, by picking the aforementioned common axis of projection orthogonal to the radial line from the center of the micrograph through that of the particle being measured.

From past experience, it has been found that the magnification of the particular RCA EMU2B electron microscope used for these studies may vary as much as 10 per cent between grids since magnification is quite dependent on positioning and there are several relative positions which may be altered when grids are changed. This problem may be resolved only through recalibration of the microscope each time a new grid is introduced. This was not considered to be sufficiently worthwhile considering the poor yield of particles and the other bias already mentioned.

The particles appearing in the photographs were measured with a scale ruled in 0.5 mm divisions and the sizes recorded in intervals of 0.5 mm, from 0 to 10 mm; 1 mm, from 11 to 25 mm; 5 mm, from 25 to 50 mm; and 10 mm, from 50 to 100 mm. These apparent sizes were converted in turn to microns. In all the statistical treatments of the data, the upper limit of the size interval was used. These data were converted to cumulative percentage and plotted on logarithmic probability paper, (see Figs. 4.1 and 4.2). The best straight line between the twentieth and eightieth percentile ranks was used to determine the standard geometric deviation, σ_g, and the logarithmic probability median, d_g, frequently referred to herein as the median.

The particles were measured on a comparator which had a least count of 0.001 cm and tabulated in order of magnitude. The median size was then obtained by plotting the 20, 30, 40, 46, 54, 60, 70, and 80 per cent size on logarithmic probability paper. The best straight line between the points was used to determine the standard deviation, σ_g, and the logarithmic probability median d_g. This was in reality unnecessary since the 50 per cent size could be picked out of the tabulated data, but was done this way for the sake of uniformity.

Check recounts were made on some of the photographs by another observer and one is included in Table 4.1. The agreement is within 9 per cent, the difference being due not to disagreement over class interval, but rather to the decision as to what constitutes a particle. An estimated reliability for the diameter measurements is within the reported order of magnitude. This reliability does not warrant

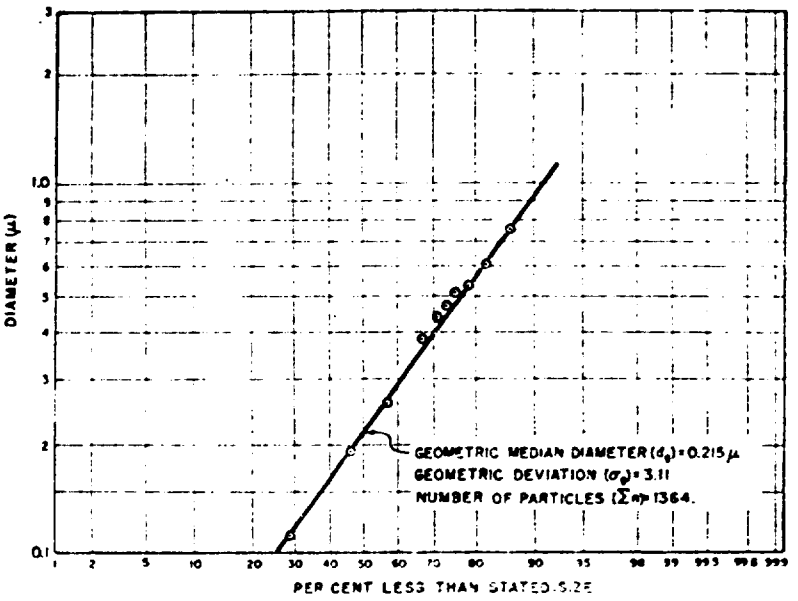

Fig. 4.1 Cumulative Size Distribution from Thermal Precipitator Electron Micrographs

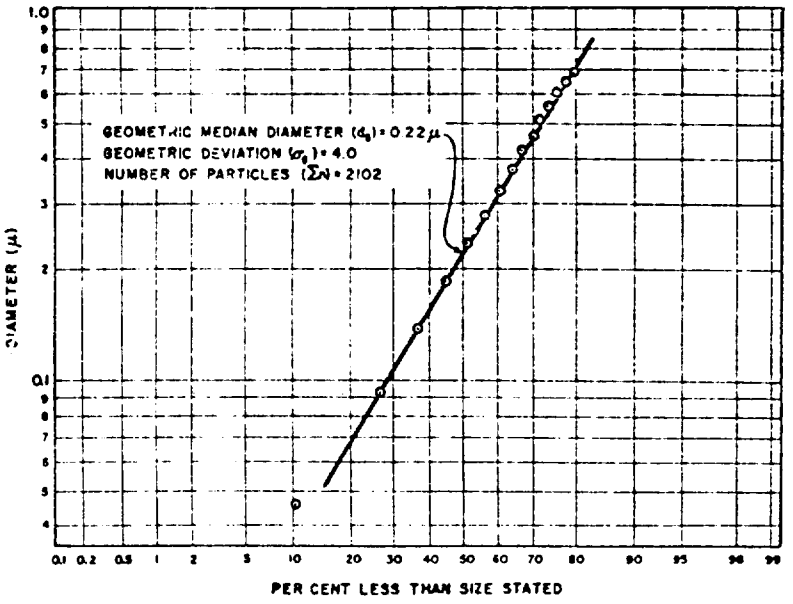

Fig. 4.2 Cumulative Size Distribution from Differential Fall-out Electron Micrographs

correlation of median diameter with distance or time from the atomic bomb detonation.

TABLE 4.1

Median Diameters of Gross Samples

Station	Distance from U-Zero (ft)	Median Diameter Thermal Precipitator (μ)	Median Diameter Differential Fall-out (μ)	Standard Deviation	Total No. Particles
103	2,000		0.36	3.0	550
108	3,000	0.37		3.2	310
109	3,000		0.26	4.4	453
120	6,000	0.22		2.4	712
120	6,000		0.12	3.1	386
120	6,000		0.10	3.7	469(a)
121	6,000	0.54		2.2	94
121	6,000		0.20	3.6	713
134	20,000	0.07		2.4	248
Cumulative Differential Fall-out			0.22	4.0	2,102
Cumulative Thermal Precipitator		0.22		3.1	1,364

(a) Check recount not included in cumulative totals.

4.1.2 The Size Frequency Distribution of Radioactive Particles

Autoradiography is a reliable and practical scheme of identification and measurement of radioactive particles. In order that no bias be introduced in the determination of the size frequency distribution of the particles, they should not be removed from the collection surface during the radioautographic process.

For this experiment, contrast radioautography was employed.[1] In contrast radioautography, the multitudes of grains are rendered

[1] J. P. Mitchell and T. C. Goodale, "Cloud Phenomena: Study of Particulate and Gaseous Matter", Greenhouse Report, Annex 6.1.

developable into a dense black spot about the radioactive source by the overexposure of photographic emulsion to beta particles. This method, however, presents four problems.

Exposure time: If the particles collected on the thermal precipitator were assumed to have diameters in the range 10 to 10^{-2} μ (maximum difference in diameters, 10^3 μ), their activity would vary on the order of 10^6 to 10^9 times depending on whether it is a function of the surface or the volume of the particle. Therefore, positive identification of all radioactive particles between 10 to 10^{-2} μ becomes rather difficult, especially if the concentration of particles per unit area is high.

Background fog: Most emulsions used in radioautography are quite sensitive to background fogging, a fact which makes identification of weaker autographs difficult.

Resolution of particles: Since the size of the silver grains in the emulsion is in the order of 0.3 μ, particle sizes of 0.5 μ diameter or smaller are quite difficult to distinguish from the silver grains.

Identification of highly active particles: An active particle, which might cause a dense autograph, may not be visible under the standard microscope due to the obstruction of under stage light by the dense silver grain spots.

4.1.2.1 Procedure

The circular microscope sampling slides (diameter 1.8 cm) from the thermal precipitator were removed and counted for radioactivity under an end-window halogen filled GM tube at constant geometry (approx 5 per cent). The background count remained fairly constant (approx 25 to 30 c/m) during the whole process.

The use of 4 x 5 in. Eastman Kodak NTB type stripping film, which has the emulsion on a thin cellulose ester base backed by a celluloid support, was selected because of its ease of handling and low susceptibility to background fog. The film (emulsion and cellulose ester base) was stripped from the celluloid support with a scalpel. The film was then cut into appropriate sizes (approx 2 x 2 cm) and placed on the sampling slide with the cellulose ester base side in contact with the particles. A warm glycerin jelly was used as the mounting medium, which, after hardening, permanently mounted the particles between the film and the sampling slide. The sampling slides were previously cemented with jelly on a larger cover slide (22 x 40 mm) for convenience in handling, (Fig. 4.3).

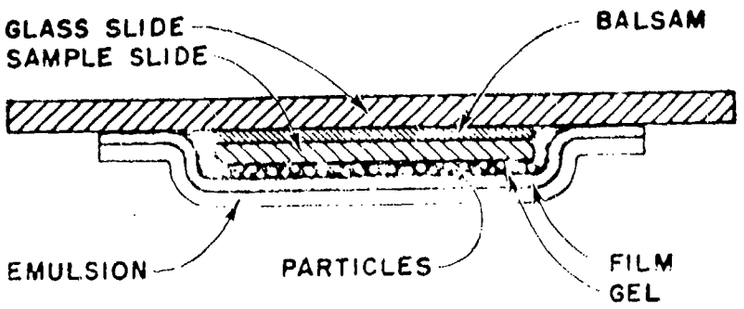

Fig. 4.3 Sectional View of Autoradiography Plate

It was determined empirically that the exposure time was related to radioactivity by the equation, $T = kA^{-1}$, where T equals exposure time in hours and A equals activity in counts per minute per unit area.

After exposing the films for a designated period of time, they together with the sampling and cover slides were developed in Kodak D-19 Developer at 68°F for 10 min, rinsed in running water for 5 min, fixed in Kodak Acid Fixer for 15 min, washed in running cold water for approximately 30 min, and then dried. At no time was separation of film from the glass slide containing particles necessary.

Measurements of particles were made under the standard microscope by placing the sample slide together with the film on the microscope stage (with slide facing the objective). This, in effect, oriented the plane of the sampling slide containing the particles above that of the film. In addition to the substage (Kohler type) illumination using a mercury vapor lamp with a blue filter(λ= 4,358 Å), an auxiliary vertical illuminator (either Bausch and Lomb (B and L) type or Leitz Ultrapak) was employed. The latter type illuminator rendered visible the active particles which were situated above their autographs. The small opaque particles (approx 0.5 μ) causing light radioautographs were easily distinguished. The cellulose ester base separating the emulsion from the particles was thick enough so that a slight adjustment of the focus distinguished the plane of the particles from the plane of the emulsion thus enabling the operator to differentiate the particles from the silver grains.

A total magnification of approximately 520X was obtained using a 43X B and L objective and a filar micrometer ocular.

The use of oil immersion type objectives for a higher magnification was not possible because of the thickness of the sampling slides. Therefore, particle sizes smaller than 0.5 μ could not be sized.[2]

4.1.2.2 Results

All data in this section refer to the underground shot and are summarized in Table 4.2 and Fig. 4.4.

Approximately 20 per cent of the autographs failed to reveal a particle, and consequently it was assumed that the particles responsible for those autographs were beyond the limit of detection. About one out of every four particles observed and measured was glassy, colorless, and transparent, indicating that any such particle whose index of refraction approached that of the gel medium (n = 1.50) might be undetectable, even though its diameter might be well above the limit of resolution.[3] Therefore, a resizing of the radioactive particles was made

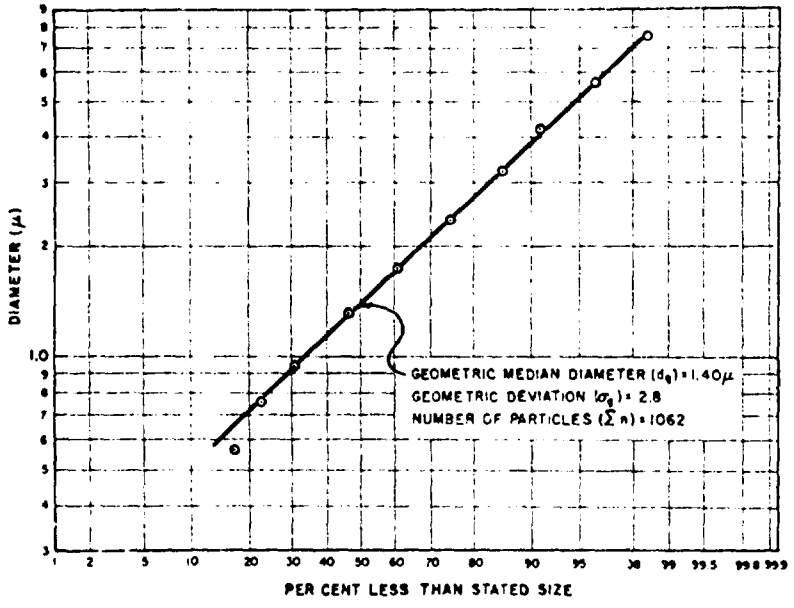

Fig. 4.4 Total Size Distribution of Radioactive Particles

[2] Theoretically, a smallest resolvable particle diameter using a blue filter and a 43X objective (Numerical Aperture, N.A. = 0.65) is

$$d = \frac{\lambda}{2 \sin 1} = \frac{\lambda}{2\ N.A.} = .35\ \mu.$$

[3] Foster and Schrenk, Bureau of Mines Paper R. I., (1938) p. 3368

TABLE 4.2

Particle Size Distribution and Radioactivity Concentrations of Thermal Precipitator Samples (Underground Shot)

Station No.	Distance from Zero Point (ft)	Geometric Median Diameter (μ)	Geometric Deviation (σ_g)	Total Number of Particles Counted[a]	A_5 (c/m)[b]	A_{100} (c/s)[c]	Volume Sampled (cc)	Activity[d] (μc/cc)	Concentration (Particles per Liter)
108	3,000	1.4	2.0	429	533	13,000	3,900	1.2×10^{-3}	250
recount using phase microscope		1.4	2.2	282					
120	6,000	1.3	2.4	488	451	10,800	4,000	1.0×10^{-3}	140
129	14,000	1.7	2.0	53	113	2,740	4,600	3×10^{-4}	26
130	14,000	1.6	1.5	92	81	1,950	6,640	2×10^{-4}	32
Average[e]		1.4	2.2	1,062					

(a) For total collector surface area of 1.78 sq cm.

(b) Counts per minute at 5 per cent geometry made at U + 35 hr.

(c) Counts per second at 100 per cent geometry extrapolated to U + 1 hr.

(d) Based on A_{100}.

(e) Weighted by the concentrations at the four stations.

with a phase microscope which was capable of revealing very small index differences.

The recount with the phase microscope on one sample decreased the number of invisible particles by about 50 per cent. The remaining blank autographs were assumed to contain small particles beyond the limit of detection. The newly detected particles were glassy in appearance and generally less than 1 μ in diameter. The frequency of those particles was such that a recalculation of the over-all size frequency distribution produced no appreciable change.

Approximately 50 per cent of all radioactive particles sized from the four samples were less than 1.5 μ in diameter. The data were obtained by plotting sizes versus accumulative percentages of frequency on log probability graphs. The 50 per cent size is designated as the geometric median diameter and the geometric deviation is the ratio, 84%-size/50%-size.

The concentration of radioactivity (μc/cc) and the concentration of active particles for the four stations were estimated from the radioactivity measurements and the number of particles sized. Since the exact volume of the cloud sampled was not known, an estimate was made by multiplying the total time (approx 120 min) the thermal precipitator was in operation by the average volume (cc) sampled per minute.

The collection efficiency of thermal precipitation was assumed to be 100 per cent. Also, the total volume sampled was assumed to be collected equally on the two sample plugs.

The values computed for each station are rough approximations and the activity and particle concentrations may be surmised to be the minimum values.

4.1.3 Activity as a Function of Particle Size

Activity as a function of particle size involves finding the activity associated with each particle size group. To establish this functional relation, some of the gross material deposited on the differential fall-out collector was divided into three size ranges, less than 2 μ, between 2 and 20 μ and greater than 20 μ. Each fraction was then counted to determine the per cent of total activity associated with each size group.

PROJECT 2.5a-2

4.1.3.1 Fractionation Procedure

The procedure for separating the particles collected by the differential fall-out collector into three size ranges is essentially the same, except for minor modifications, as that described by C. E. Adams, et al.,[4] in the analysis of fall-out particles collected at Operation GREENHOUSE. One or more sectors upon which most of the initial fall-out was deposited were selected from a differential fall-out tray and washed with distilled water into a clean photographic processing tray. The contents of the tray were washed again into a beaker. In each case, the washing was continued until the radiation level of the sector and, subsequently, of the tray was down to normal background. Part of the contents of the beaker was transferred to two 50 ml centrifuge tubes and was then centrifuged for 30 min at sufficient speed to precipitate all particles greater than 0.25 μ in diameter. The supernatant liquid was decanted and saved. The tubes were again filled from the beaker. This process was carried on until all particles greater than 0.25 μ had been concentrated in one 50 ml centrifuge tube. This precipitate was redispersed in an Alrosol[5]-water solution and ultrasonorated at 400 kc to break up agglomerates formed by the centrifugation.

The suspension of particles collected in this manner was allowed to settle through a distance of 9.5 cm for 2.5 min. In this time, particles of greater than 20 μ in diameter settled out. The remaining solution, in which were contained particles of 20 μ or less, was decanted into a beaker. The entire operation from redispersion to decantation was repeated three times on the precipitate in order to remove most of the particles of 20 μ or less which may have settled out with those of a diameter greater than 20 μ.

The medium size (2 to 20 μ) particles were separated from the small (less than 2 μ) particles by a method employing two concentric centrifuge tubes and a urea water solution. A 15-ml centrifuge tube with a hole in the end was fitted into a 50-ml centrifuge tube. The smaller tube was supported inside the larger by a cork through which the smaller tube extended and which fitted into the neck of the larger (Fig. 4.5). This double-layered tube was filled with 30 ml of a solution of urea in water (800 g of urea in 1,000 ml of water). About 1 ml of the aqueous suspension of particles was carefully placed on the surface of the urea water solution inside the smaller centrifuge tube. A medicine dropper was used to pour the particulate suspension down the side of the inner tube in order that no mixing might

---

[4] C. E. Adams, F. R. Holden, and N. R. Wallace, "Fall-out Phenomenology", Greenhouse Report, Annex 6.4.

[5] Dispersing agent manufactured by Alrose Chemical Company.

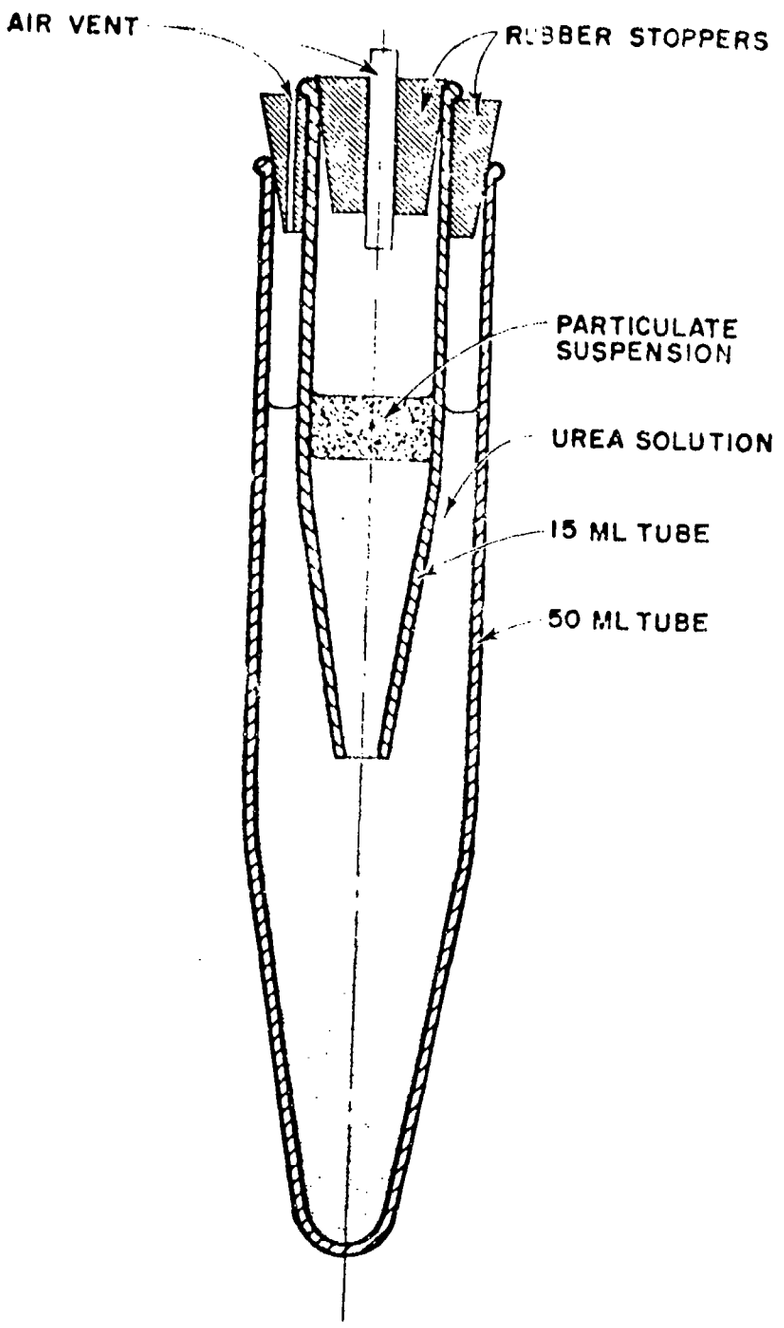

Fig. 4.5 Cross Section of Double Layered Tube

occur between the two liquids.

It was found empirically that, when the double-layered tube was centrifuged for 2.25 min at 1,100 rpm, the great majority of the particles less than 2 μ in diameter remained in suspension above the urea solution while most of the particles of diameter greater than 2 μ settled to the bottom of the larger tube. Particles of all sizes were distributed throughout the volume of the urea solution. The suspension of particles less than 2 μ was removed from the inner tube with an eye-dropper and the inner tube itself was removed from the outer. In this last operation, it was necessary to save the liquid from the inner tube intact for recycling. A cork with an air vent was placed in the 15 ml tube and the air vent was closed. It was then possible to remove the inner tube and spill its contents into another container. The urea solution in the 50 ml tube was decanted and the precipitate saved.

The entire suspension of particles less than 20 μ in diameter was fractionated by this method. Recycling of the contents of the inner tube consisted of precipitation of the particles by a 30-min centrifugation, redispersion in water with a small amount of Alrosol added and fractionation by means of the double-layered tube.

Although the group of particles lying in the size range between 0.25 and 20 μ had been separated into two fractions, each fraction was still contaminated with particles which belonged to the other. It was necessary, as in the case of the large fraction, to purify each group to remove outsized particles.

The intermediate fraction (2 to 20 μ) was purified by redispersing the fraction in 30 ml of a water-Alrosol solution, ultrasonorating the suspension to break up agglomerates and centrifuging it for 2.5 min at 1,100 rpm. The supernate, containing trace quantities of particles too small to be classified in the intermediate group was discarded. This procedure was repeated three times.

The fine fraction (less than 2 μ) was purified in the same way as was the intermediate fraction with the sole exception that the supernate was saved and the precipitate was discarded. The 120 ml of supernate accumulated during the purification process of the small fraction (0.25 to 2 μ) was centrifuged for 0.5 hr at sufficient speed to precipitate all the particles in that size range.

4.1.3.2 Weighing and Counting Procedure

At the completion of the fractionation process, each size group of particles was in the form of a wet residue on the

bottom of a 50 ml centrifuge tube. In order to weigh and count this material, it was necessary to transfer the separate fractions to microscope cover glasses which measured 0.875 by 0.875 in. and weighed approximately 0.2 g each. By adding small quantities of water to the residues in the tubes, it was possible to make thick sludges which could easily be transferred to the cover glasses with a spatula or a medicine dropper.

In order that each sample be of constant geometry, the material was placed on the cover glasses a little at a time so that the residues spread out into circles of fairly uniform diameters. Each deposit was allowed to dry before more material was added. The samples were oven dried and weighed. Since the weight of each dry cover glass was determined beforehand, the true weight of the sample was easily determined.

The intermediate and fine fractions from a single analysis were mostly of sufficiently small amount and formed such a hard, compact residue on the cover glasses that generally each could be contained on a single cover glass without danger of being shaken off the glass or of being so thick as to introduce self-absorption errors in the subsequent counting. This was not the case with the large fraction (greater than 20 μ) obtained from the underground shot wherein the size of individual particles was so large that they would roll off the cover glass or, if the entire fraction were placed on the cover glass, form such a mound of material that self-absorption effects would attain serious proportions.

For these reasons, each large fraction obtained from sectors exposed to the underground shot was weighed in its entirety in a watch glass and was then split up into about eight parts, each on an individual cover glass. Like the glass sectors used in the field, each cover glass was coated with a film of carbowax to keep the particles in place.

A gas flow proportional counter with a side window chamber built by the Instruments Branch of the USNRDL was capable of counting at a rate of 2×10^6 c/m without the need of correction factors. Since the most active individual cover glass sample had a counting rate of the order of 10^5 c/m, this counting system was well able to handle the material obtained from both bursts. This counter was not available for the counting of the surface shot samples. Therefore, an IDL 161-C scaler attached to an end window halogen filled tube in a lead castle was used for the counting of all surface shot fractions. The activity of the samples collected from the surface shot was so low that the limited counting rate of the latter system was no handicap. However, no comparison between the results obtained from the surface shot and those obtained from the sub-surface shot is possible except in

those cases where the results are independent of the counting system used.

4.1.3.3 Results

Tables 4.3 and 4.4 give the results of the analysis of the three size fractions from each of eight trays taken from both underground shot and surface shot. The trays are identified according to the station at which they were exposed.

TABLE 4.3

Radioactivity vs Particle Size for the Surface Shot Fall-out

Size Fraction (μ)	Count Corrected to S 24 Days (c/m)[a]	Counts per Unit Weight (c/m/g)[a]	Weight of Fraction (g)	Per Cent of Activity
Station 19, Sectors 12, 13				
Small, <2	8	2.1×10^3	0.0038	1.0
Medium, 2-20	32	1.5×10^3	0.0211	3.9
Large, >20	773	13.1×10^3	0.0590	95.1
Station 33, Sector 7				
Small, <2	0	0	0.0004	0
Medium, 2-20	0	0	0.0038	0
Large, >20	1,804	5.7×10^4	0.0316	100.0
Station 29, Sectors 2, 3, 4				
Small, <2	0	0	0	0
Medium, 2-20	75	1.5×10^4	0.0049	1.5
Large, >20	4,818	2.9×10^5	0.0168	98.5
Station 29, Sectors 14, 15				
Small, <2	80	1.0×10^5	0.0008	0.4
Medium, 2-20	1,259	3.0×10^5	0.0042	6.2
Large, >20	18,882	2.0×10^6	0.0094	93.4

(a) Corrected to 100 per cent geometry.

The selection of particular sectors from a tray was not random. A preliminary monitoring of the entire tray indicated which area was the most active and only those sectors which constituted

this area were removed for analysis. With the exception of Wheel 29, Sectors 14 and 15, the sectors chosen were those which contained the initial heavy fall-out.

TABLE 4.4

Radioactivity vs Particle Size for the Underground Shot Fall-out

Size Fraction (μ)	Count Corrected to U 20 Days (c/m)(a)	Counts per Unit Weight (c/m/g)(a)	Weight of Fraction (g)	Per Cent of Activity
	Station 102, Sector 8			
Small, <2	746,324	9.6×10^6	0.0078	1.0
Medium, 2-20	230,816	4.0×10^6	0.0582	3.0
Large, >20	7,304,565	9.4×10^6	0.7783	96.0
	Station 120, Sector 1			
Small, <2	38,825	11.8×10^6	0.0033	0.7
Medium, 2-20	256,611	6.5×10^6	0.0395	4.8
Large, >20	5,028,133	12.2×10^6	0.4119	94.5
	Station 133, Sectors 9, 10			
Small, <2	53,408	6.4×10^6	0.0083	0.5
Medium, 2-20	221,384	3.3×10^6	0.0676	1.9
Large, >20	11,088,397	12.6×10^6	0.8821	97.6
	Station 108, Sector 1			
Small, <2	109,377	9.9×10^6	0.0110	1.1
Medium, 2-20	269,395	4.8×10^6	0.0211	2.6
Large, >20	10,001,980	9.6×10^6	1.0382	96.3
	Station 129, Sectors 7, 8			
Small, <2	96,755	10.5×10^6	0.0092	1.0
Medium, 2-20	451,799	5.3×10^6	0.0859	4.8
Large, >20	8,952,487	12.0×10^6	0.7433	94.2

(a) Corrected to 100 per cent geometry.

Since the counting process extended over a period of several days, each count had to be corrected for decay. Gross decay curves determined from some of the same differential fall-out collectors used in this analysis were prepared by the Nuclear and Physical Chemistry Branch of the USNRDL. These curves were available for Stations 102, 103,

108, and 19. The three underground shot curves did not agree as to slope on log-log paper because of the inhomogeneity of the fall-out from place to place in the shot area. However, there was sufficient agreement among them in the region of U + 20 to about U + 60 days to validate the use of any one of the curves for correcting counts from any underground shot station for decay. The decay curve for Station 103 was used for adjusting all the counts because the experimental points determining it showed the least variation from the curve in the critical region (U + 20 to U + 60 days).

Because of the sparse fall-out resulting from the surface burst, only one fall-out collector, that at Station 19, was analyzed for gross decay. This curve was used for adjusting the surface shot counts to S + 24 days.

The underground shot samples were analyzed for radiochemical composition. The results are presented in Table 4.5. It is significant to note that there are definite differences in radiochemical content of the three size fractions. Since the fall-out material was dissolved before analysis, the inherent self-absorption errors present in the values of Tables 4.3 and 4.4 are greatly reduced.

TABLE 4.5

Variations of Product Activities with Three Size Fractions
68 Days after Bomb Detonation

Element	Activity					
	(c/m/mg soil)[a] x 10^{-3}			Per Cent of Total		
	Large (> 20 μ)	Medium (2 to 20 μ)	Small (< 2 μ)	Large (> 20 μ)	Medium (2 to 20μ)	Small (< 2 μ)
Rare Earth	19.1	4.46	4.70	67.3	76.0	79.2
Ba	0.675	0.375	0.385	2.4	6.4	6.5
Sr	0.436	0.298	0.288	1.5	5.1	4.86
Zr	6.24	0.442	0.234	21.9	7.5	3.95
Ru^{106}	0.236	0.0699	0.141	0.83	1.2	2.38
Ru^{103}	1.74	0.216	0.191	6.14	3.7	3.22
Total	28.43	5.861	5.939	100.07	99.9	100.11

(a) Corrected to 100 per cent geometry.

4.1.4 The Identification of Collected Material and Correlation with Source Material

In order to characterize the fall-out material chemically and determine the effect of the parent material on the physical and chemical characteristics of the radioactive fall-out, petrographic surveys, size distributions and certain analyses were made on both the parent and the fall-out material.

In the chemical identification of the material, the 0 to 2 fraction of the parent soil was separated and subjected to additional analysis in order to determine the clay constituent. A combination of x-ray diffraction, electron microscope, differential thermal analysis, and dehydration techniques was employed in this phase. The remaining bulk of the soil sample was investigated by petrographic microscopy, spectrochemical analysis and by standard Department of Agriculture size distribution determinations. The radioactive portion of the fall-out was examined petrographically and spectrochemically and the bulk fall-out material was sized in accordance with the Department of Agriculture method.

The soil samples from 0 to 6 ft were obtained with a shovel. The deeper core samples were procured from the U. S. Geological Survey. They were obtained with a churn drill and represented composite samples of 10 ft intervals in depth.

Additional standard soil tests which were made to further characterize the soil at this location are described in Appendix C.

4.1.4.1 Petrographic Analyses

The sand was sieved into various sizes and a preliminary microscopic examination was made of the sand in each sieve size. The size classes into which the sand was sieved are as follows:

Mesh (U.S.)	Size (mm)	
4	4.760	
8	2.380	(A)
16	1.168	
30	0.595	
50	0.297	
80	0.175	(B)
100	0.149	(C)
230	0.062	
pan	--	

The sand in three different size classes, designated (A), (B), and (C) above, was analyzed in detail. The sand between 2.380 and 1.168 mm, (A), was examined with the aid of a stereoscopic microscope. Each of the finer portions (B) and (C) was split with an Otto microsplit to approximately 1,000 grains of sand and of these approximately 300 were identified under the petrographic microscope. The composition of the sand is shown in Table 4.6.

TABLE 4.6

Petrographic Analysis of Sand

Constituent	Constitution of Fractions Retained on Sieves[a] % by Number (A)	(B)	(C)	Constitution of Whole Sample[b] % by Number
Quartzite	5.2	--	--	0.7
Limestone	0.2	--	--	0.1
Acid Volcanic	80.0	--	--	10.4
Caliche	1.6	--	--	0.2
Sandstone	2.4	--	--	0.3
Quartz	5.0	6.4	2.8	4.3
Schist	4.0	--	--	0.5
Pumice	0.2	--	--	0.1
Granite	0.2	--	--	0.1
Alkali Feldspar (orthoclase)	--	25.1	31.7	25.2
Lime-Alkali Feldspar (plagioclase)	1.2	17.4	15.3	14.1
Biotite	--	7.0	4.4	4.8
Chlorite	--	0.7	2.0	1.3
Volcanic Glass	--	6.4	3.2	3.9
Zircon	--	0.3	2.0	1.2
Altered Feldspar	--	33.4	37.8	31.3
Opaque Minerals	--	3.3	0.8	1.5
Rutile	--	--	trace	trace
Total	100.0	100.0	100.0	100.0

(a) Based on the examination of 300 particles in each sieve fraction.

(b) Based on grading of the sand and on the distribution of constituents by sieve fractions shown at the left above.

The sand between 2.380 and 1.168 mm (A) consists predominantly of acid volcanic grains, probably rhyolite, with minor amounts of pink quartzite, clear quartz, and ferruginous micaceous schist. Very small amounts of gray limestone, fine grained sandstone, granite, pumice, plagioclase feldspar, and caliche are also present. The colors of the acid volcanic grains include pink, red, violet, and pale yellowish-orange. The grains are soft and can be broken easily with slight pressure. Some of the volcanic granules are porphyritic and contain quartz and hornblende phenocrysts embedded in a dense groundmass. The quartz phenocrysts are short stubby hexagonal crystals terminated by equally developed pyramid faces; quartz of this type is known as "high" quartz or "beta" quartz and was probably formed above 573°C. The ferruginous micaceous schists are waferlike, soft, and foliated and break easily in a direction at right angles to the foliation. In color, they are gray, grayish red purple, and very dusky red purple.

The sand between 0.175 and 0.149 mm (B) consists principally of feldspar, with minor amounts of quartz, biotite, opaque minerals (probably magnetite), and volcanic glass. Very small amounts of chlorite and zircon are also present. Altered feldspar grains account for approximately 33 per cent of this portion of the sample and are seen to consist of aggregates of cryptocrystalline silica, sericite, clay particles, and parts of unaltered feldspar fragments. Many of the altered feldspar grains show myrmekitic patches. The comparatively fresh feldspar grains consist of orthoclase (some sanidine) and plagioclase. The composition of the plagioclase probably falls between albite and oligoclase, (Ab90An10), although measurements are difficult because twin planes, when present, are obscured by alteration products.

The sand between 0.149 and 0.062 mm (C) consists of the same minerals as the sand between 0.175 and 0.149 mm. Feldspar, in all stages of decomposition, is the major constituent.

Petrographic analysis of the fall-out material was made with a petrographic microscope. A number of radioactive fall-out particles from both the surface and underground shots were examined to determine their mineralogical compositions.

The particles smaller than 20 μ were first removed from the samples by repeated sedimentations. The larger particles were then dispersed in a dilute solution of gelatin in water and spread over Eastman Kodak nuclear track plates, type NTB. The plates were exposed for a day or two in a light-tight box and were then removed and developed. The radioactive particles were easily identified by the halo of blackened film around them. These particles were removed by first softening the gelatin with a drop of water and then picking up and transferring the particles, with forceps, to clean glass slides.

Most of the active particles examined were about 50 to 400 μ in diameter. The particles were composed exclusively of glass with varying amounts of included mineral fragments.

Approximately 1 to 4 per cent of the particles were glassy spheres ranging in size up to about 40 μ in diameter. Most of these spheres were transparent and were either colorless or a pale blue-green or amber color. Occasionally one was found which had a black, pitch-like appearance. A few of the glassy particles exhibited tear-drop shapes.

Most of the radioactive particles were irregularly shaped, white to gray colored, translucent to opaque, and had a superficial resemblance to the mineral grains with which they were mixed. However, upon crushing these particles they were found to be glass with some included small mineral grains. The opacity of the particles was due to many included bubbles and tube-like cavities. The mineral fragments included amount to 5 to 20 per cent by volume of the total particle, but were too small to be identified positively except in one instance in which a fragment was found to be quartz. However, the fragments had indices of refraction and birefringencies close to those of quartz and the feldspars. Since about 85 per cent of the soil near the shot points was composed of these minerals, it seems probable that most of the crystalline material included in the glass was quartz and feldspar. These fragments were angular and showed no signs of fusion. Apparently the vaporous material in the ball of fire condensed upon these fragments during the cooling stage of the cloud.

The number of radioactive particles was less than 1 per cent of the total number of grains on the plate. Judging from the sizes and intensities of the darkened areas of the film around the active particles, the intensity of radiation is apparently not proportional to the size of the particle.

4.1.4.2 Spectrochemical Analyses

The following samples were analyzed spectrochemically:

1. Soil, 0 to 3-in. level.
2. Soil, 17-ft level.
3. Fused glassy spheres from the surface shot.
4. Fused glassy spheres from the underground shot.
5. Irregular, translucent grains from the underground shot.

These results are presented in Table 4.7 and show a close correlation between the elemental composition of the soil and the active fall-out particles.

TABLE 4.7

Spectrochemical Analysis of Soil and Fall-out

Element	Soil Sample from Underground Site		Glassy Spheres		Irregular Translucent Grains Underground Shot
	0 to 3-in.[a]	17-ft	Surface Shot	Underground Shot	
Al	V.S.	V.S.	S	S	S
B	T	T	N.D.	N.D.	N.D.
Ba	T	T	T	T	T
C	W	W	N.D.	N.D.	N.D.
Ca	V.S.	V.S.	V.S.	V.S.	V.S.
Cr	T	T	T	W	W
Cu	T	T	W	W	W
Fe	S	S	S	S	S
Ga	T	W	N.D.	N.D.	N.D.
K	M	M	N.D.	W	W
Mg	V.S.	V.S.	S	S	S
Mn	M	M	W	W	W
Na	M	M	S	S	S
Ni	T	T	T	T	T
Si	V.S.	V.S.	V.S.	V.S.	V.S.
Sr	T	T	T	T	W
Ti	W	W	N.D.	W	W
V	T	T	N.D.	N.D.	N.D.
Zr	N.D.	T	T	T	T

(a) T = 0.001 - 0.01% W = 0.01 - .1% M = 0.1 - 1%
S = 1. - 10% V.S. = < 10% N.D. = Not Detected

4.1.4.3 Size-weight Distributions

A sieve and hydrometer analysis was made on soil samples from the underground shot site taken at the following depths: 0 to 3 in., 5 to 6 ft, and 17 ft. The sample from each depth was passed through sieves including, and coarser than, No. 4. A representative portion of the material passing the No. 4 sieve was oven dried and a 100 g of the dried fraction was slaked overnight in water. The soil was then dispersed in an electric mixer for about 10 min and then tested for

gradation of the fines by making up a 1 liter suspension in a cylinder and measuring the specific gravity of the suspension with a soil hydrometer. The suspension included gum arabic in solution as a deflocculating agent. After the hydrometer test, the same soil fraction was washed through a No. 270 mesh sieve, the retained material dried and a dry sieve analysis made. The complete analysis was computed from the results of preliminary screening, dry sieve analysis of soil retained on the No. 270 sieve, and the hydrometer test.

A size analysis was also done on both pre-test soil and fall-out by the pipette method essentially as used by the U. S. Department of Agriculture.[6] In this method, the sample passing a 2-mm sieve is treated with hydrogen peroxide, washed and filtered through a porcelain filter to remove organic matter. The sand is separated from the silt and clay by washing the dispersed sample through a 300 mesh sieve. Sodium metaphosphate is used as the dispersing agent. The sand fractions are separated by sieving and the 20-, 5-, and 2-μ fractions are obtained by sedimentation and pipetting. The oven-dry, organic-free sample weight is used as the base weight for calculating the percentages of the various fractions.

The method used differed from that described[6] in that a 2-mm rectangular-holed sieve was used instead of a 2-mm round-holed sieve; a Coors filter cylinder, porosity No. 5, was used instead of a Pasteur-Chamberlain filter of "F" fineness, and hand sieving was used instead of a mechanical shaker.

The results of the analyses are summarized in Tables 4.8 and 4.9 and in Figs. 4.6 and 4.7.

TABLE 4.8

Sieve and Hydrometer Analysis of Pre-test Soil Samples at Underground Shot Site

Size	Depth at Which Sample Taken		
	0 to 3 in.	5 to 6 ft	17 ft
	GRAVEL (per cent less than stated size)		
2-in.	--	100	--
1-in.	--	98	100

[6] V.J. Kilmer and L. T. Alexander, "Methods of Making Mechanical Analysis of Soils", Soil Science, LXVIII (1949), 15-24.

TABLE 4.8 (Continued)

Sieve and Hydrometer Analysis of Pre-test Soil Samples at Underground Shot Site

Size	Depth at Which Sample Taken		
	0 to 3 in.	5 to 6 ft	17 ft
	GRAVEL (per cent less than stated size)		
3/4-in.	100	97	98
1/2-in.	98	94	95
	SAND (per cent less than stated size)		
No. 4 Sieve	91	88	80
No. 10 Sieve	84	83	65
No. 30 Sieve	77	73	42
No. 60 Sieve	68	58	27
	SILT OR CLAY (per cent less than stated size)		
No. 270 Sieve	20	22	9
2 μ	5	7	1

4.1.4.4 Clay Analyses

The less than 2 μ fraction of the surface soil from surface shot zero was used for a clay analysis by X-ray diffraction. This fraction was obtained as follows: the material passing a 2-mm sieve was dispersed for 10 min with distilled water in a mechanical dispersion cup fitted with baffles. The suspension was then allowed to settle in a tall, straight-sided glass vessel until particles greater than 2 μ effective diameter had settled out beyond the desired depth. The suspension containing the less than 2 μ particles was siphoned off. The remaining material was again shaken with water and allowed to settle and then siphoned off. This process was repeated until the liquid appeared fairly clear after the required settling time. The suspension removed by siphoning was concentrated by means of the Coors porcelain filter and by supercentrifugation. After concentration the less than 2 μ material was dried with the aid of an infrared lamp, and ground to pass a 60-mesh sieve.

TABLE 4.9

Comparison of Particle Size Distribution (by Weight) of Pre-test Soil Samples and Fall-out Determined by Sieve and Pipette Analysis

Fraction	Soil[a]		UF1[b]		UG3[c]	
	Actual Per Cent	Cumulative Per Cent	Actual Per Cent	Cumulative Per Cent	Actual Per Cent	Cumulative Per Cent
SAND						
Very coarse 2-1 mm	30.58	99.27	37.79	99.38	28.84	100.54
Coarse 1-0.5 mm	8.81	68.69	9.45	61.59	8.80	71.70
Medium 0.5-0.25 mm	0.48	59.88	0.78	52.14	0.39	62.90
Fine 0.25-0.1 mm	27.52	59.40	22.43	51.36	7.28	62.51
Very fine 0.1-0.05 mm	11.25	31.88	9.86	28.93	14.10	55.23
SILT						
0.05-0.02 mm	8.58	20.63	7.02	19.07	19.60	41.13
20-5 μ	3.52	12.05	4.83	12.05	10.07	21.53
5-2 μ	2.67	8.53	1.93	7.22	4.17	11.46
CLAY						
2-1 μ	1.17	5.86	0.50	5.29	2.00	7.29
< 1 μ	4.69	4.69	4.79	4.79	5.29	5.29

(a) Soil samples taken 0-30 ft from U-zero.

(b) UF1 = Fall-out from the station 300 yd north of U-zero on north leg.

(c) UG3 = Fall-out from the station 600 yd north of U-zero and 300 yd west of north leg.

X-ray diffraction patterns were determined on this material untreated and after glycerol solvation. The results of this analysis are tabulated in Table 4.10.

The 3.34 and 3.04 Å lines indicate the presence of orthoclase and the 9.93, 4.47, 3.34, 2.58, 1.93, and 1.49 Å lines indicate the presence of a biotite-muscovite-hydrous mica-type mineral. The lack of a 17.7 Å line with glycerol solvation indicates absence of montmorillonite, and the lack of a 7.2 Å line indicates the absence of kaolinite.

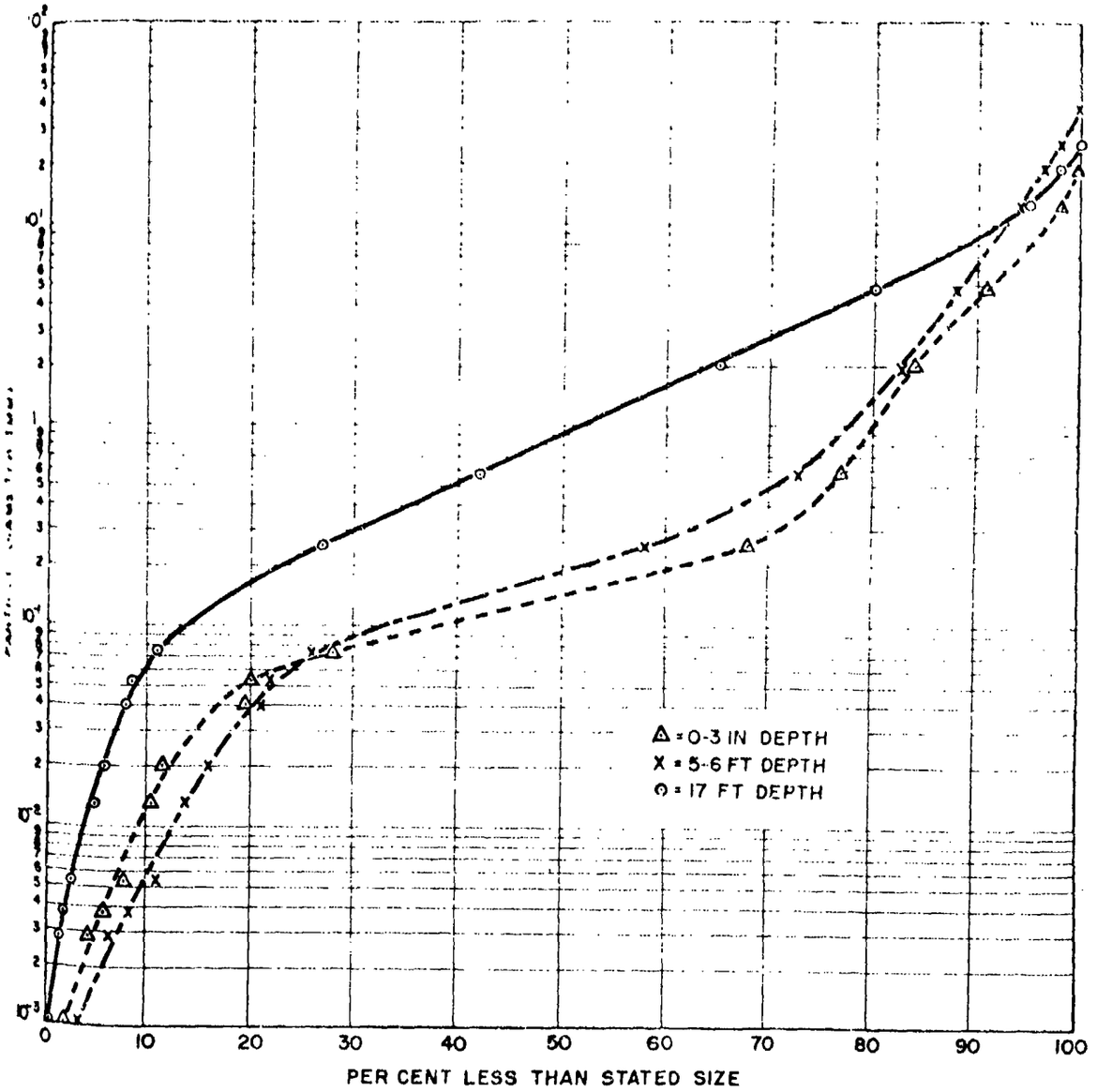

Fig. 4.6 Sieve and Hydrometer Analysis of Underground Site Pre-test Soil Samples

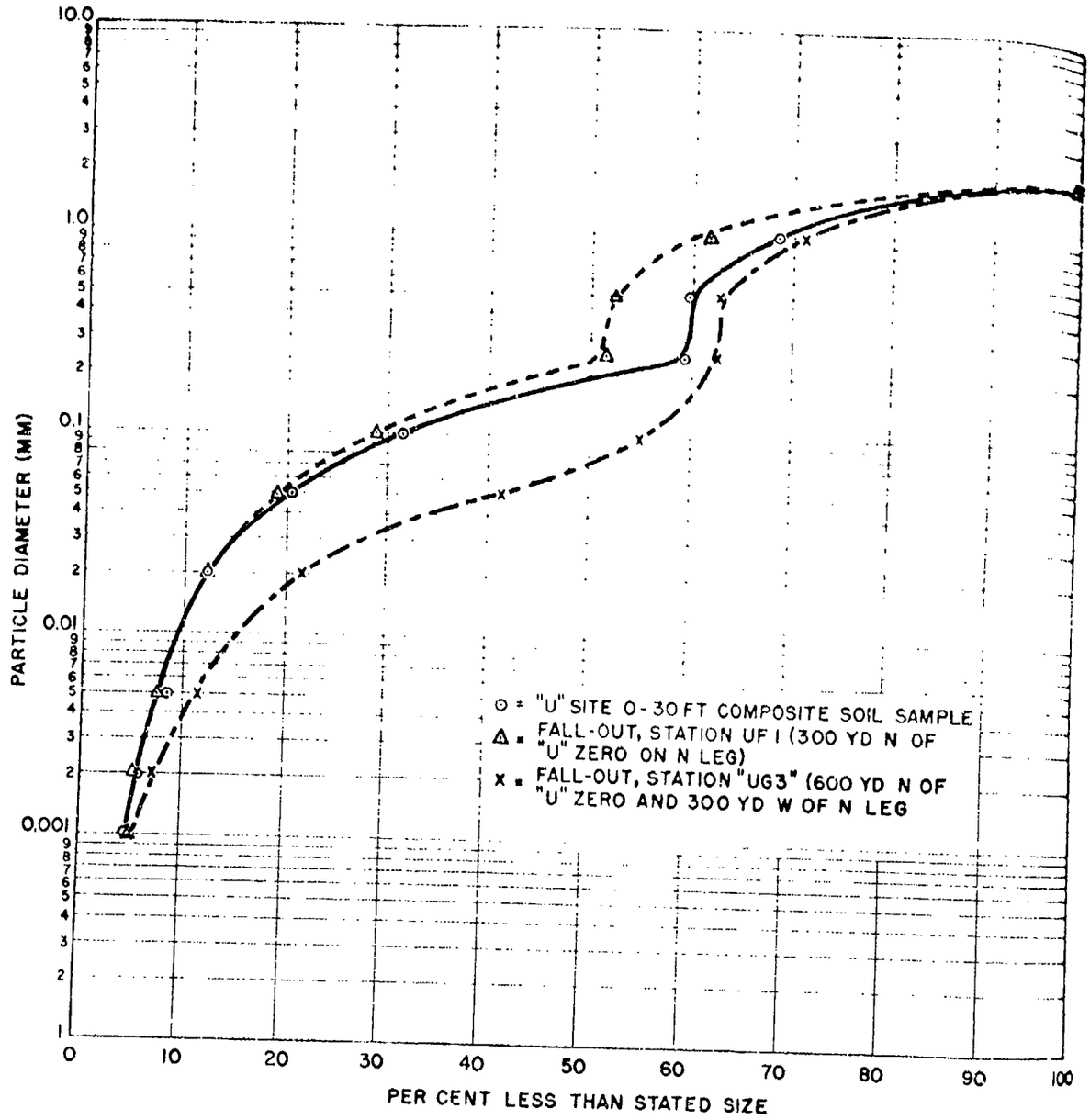

Fig. 4.7 Comparison of Particle Size Distribution of Soil and Fall-out by Pipette Analysis

TABLE 4.10

X-ray Diffraction Data

Wave Length (Å)	Intensity
9.93	Very Very Weak
4.47	Broad Strong
3.34	Strong
3.04	Strong
2.58	Broad Strong
2.28	Medium
2.125	Weak
2.090	Weak
1.93	Broad
1.907	Moderate
1.870	Moderate
1.814	Moderate
1.541	Very Weak
1.498	Strong
1.372	Weak
1.291	Weak

Differential thermal analysis is a useful technique in identifying the clay mineral fraction. The principle involved is that the release of water (which appears as endothermic breaks in the differential curves) at a temperature above 200°C takes place at a specific temperature for each mineral. The apparatus used in the analysis was described by Page.[7] The apparatus records the temperature at which a temperature change takes place in the sample relative to the temperature change in an anhydrous reference material (e.g., aluminum oxide) which is being heated at the same rate.

The endothermic break around 130°C on the differential analysis curve (Fig. 4.8) indicates the presence of hydrous mica or montmorillonite. The exothermic break at 800°C probably indicates a trace of chlorite. This analysis also confirms the absence of kaolinite.

Electron micrographs were made of the less than 2 μ fraction of the soil obtained from the 17-ft depth at the underground

[7] J. B. Page, "Differential Thermal Analysis of Montmorillonite", Soil Science, LVI (1943), 273-283.

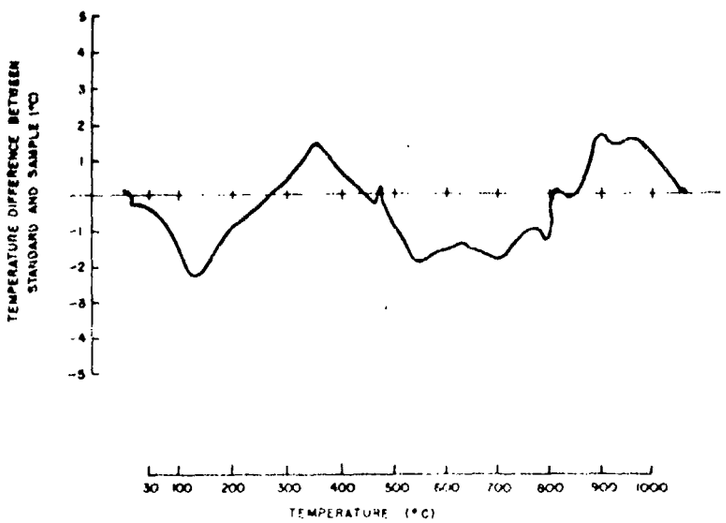

Fig. 4.8 Differential Thermal Analysis of Pre-test Soil (< 2 μ Fraction) from 17-ft Depth Underground Site

shot site. The less than 2 μ fraction was obtained by successive sedimentations as described above. Aliquots of the suspension removed by siphoning were dispersed by one of the following methods: addition of sodium metaphosphate plus sodium carbonate, ultrasonoration, and addition of sodium metaphosphate plus sodium carbonate after the colloid had been washed and filtered three times using water as the washing agent.

After any of the above treatments, the suspensions were placed overnight in a shaking machine at 120 oscillations per minute. After shaking, the suspensions were dispersed as an aerosol and collected on electron microscope grids and on optical slides using the oscillating thermal precipitator.

Positive identification of clay minerals with the electron microscope is not, at present, completely possible. However, in combination with other methods (chemical, optical, thermal, and X-ray) electron micrographs are helpful in establishing the presence or absence of certain clay types. In this instance, kaolinite was not found, confirming the results obtained by X-ray diffraction and thermal analysis. A trace of a mineral which resembled halloysite was found. The bulk of the material appeared to be primary mineral fragments rather than clay minerals.

A dehydration curve (Fig. 4.9) was run on the less than 2 μ fraction of soil from the 17-ft depth of the underground shot site. The data obtained from this curve were not specific or characteristic enough to permit identification of the clay components.

4.1.4.5 Discussion

The petrographic examination indicated that all the active particles were of a fused glassy material. The spectrochemical analyses showed that they were of the same elemental composition as the parent soil except that boron and carbon were missing. Their absence probably occurred because they are more readily volatilized.

The analyses of the less than 2 μ pre-test soil fraction by X-ray diffraction, differential thermal analysis, electron microscopy and dehydration indicated that this material had the following approximate composition: 30 to 50 per cent poorly crystalline hydrous mica type clay mineral, traces of chlorite and possibly halloysite, and finely divided primary mineral fragments.

The particle size distribution curves for the 0 to 30 ft pre-test sample and the UF1 and UG3 fall-out samples are remarkably similar in shape. Consideration of these curves seems to indicate that the effect of fracturing on particle size is minimal and that the decrease in median diameters is due mainly to a sedimentation effect. A detailed study of the greater than 2 mm fraction, necessary for the proper evaluation of the extent of fracturing in soil particles, was not made.

4.2 FALL-OUT DISTRIBUTION

4.2.1 Time Distribution of Fall-out

In investigating the time distribution of fall-out from the differential fall-out wheels, it was necessary to measure the radioactivity continuously around them beginning at the sectors exposed at shot time. To accomplish this a special housing and probe for the differential fall-out wheels were designed (Fig. 4.10). The housing was circular and a few inches larger in diameter than the wheels. It contained a turntable which could be rotated by a knob extending through the housing and engaging the turntable on its periphery. By means of a series of equally-spaced notches on the periphery the turntable could be repeatedly rotated one-eightieth of a revolution at a time.

The top of the housing was made removable for placing the differential fall-out wheels on the turntable. The housing completely

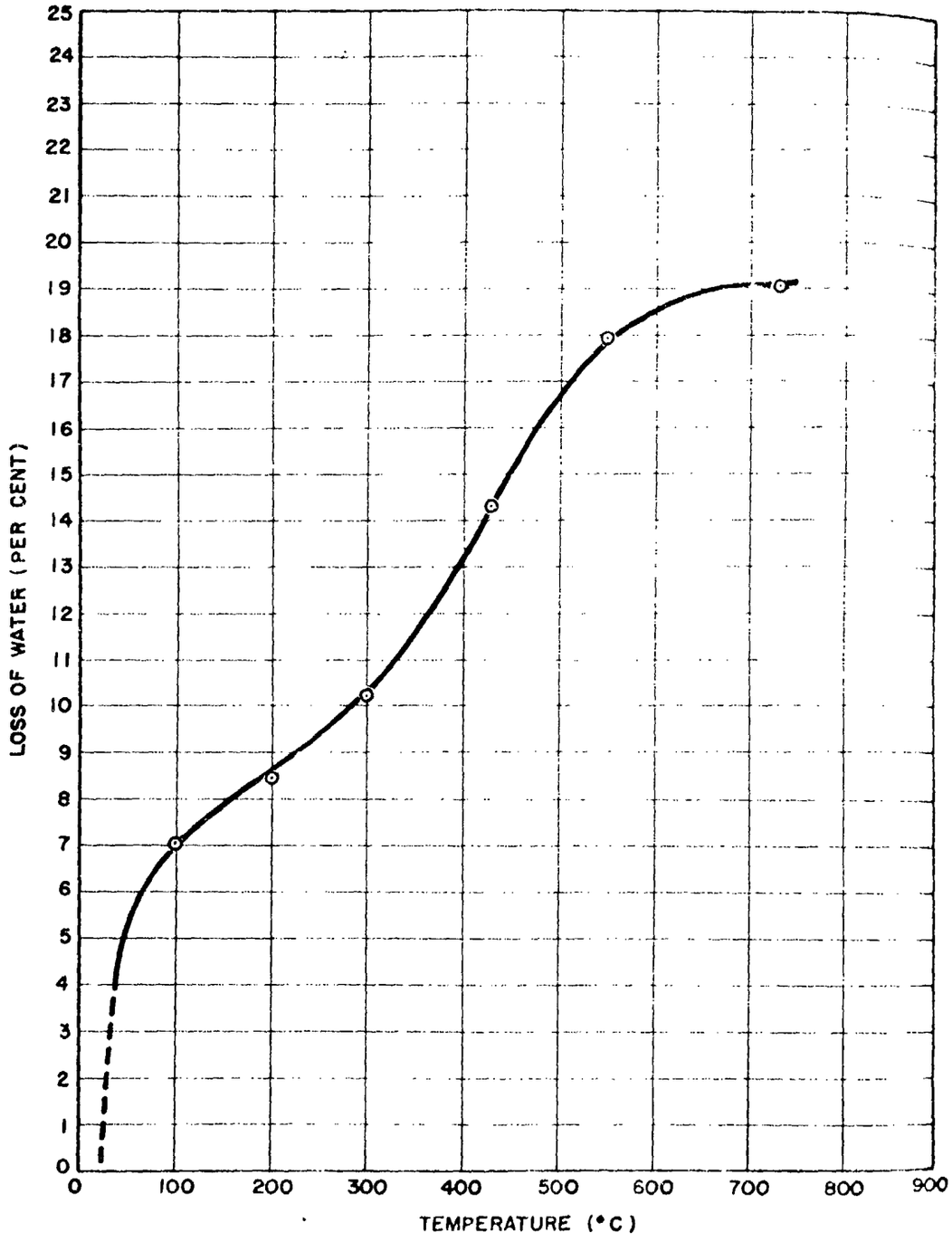

Fig. 4.9 Dehydration Curve

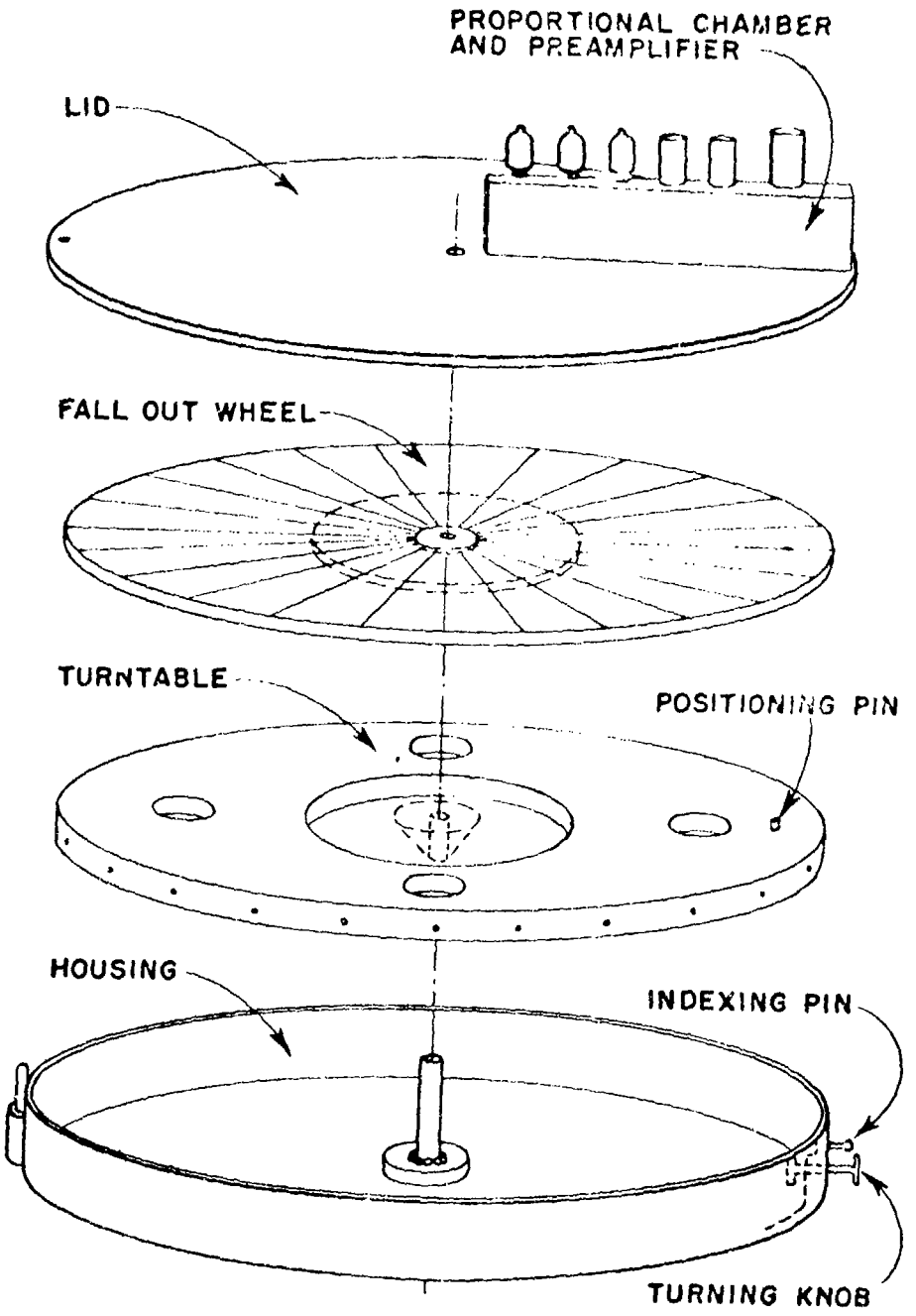

Fig. 4.10 Differential Fall-out Counting Apparatus

enclosed the turntable and wheel except for a radial section cut into the top for the probe. The window of the probe was 0.5 mil aluminum foil and rested 0.625 in. above the surface of the differential fall-out wheel. This window was 10 in. long and tapered in width from 0.25 in. near the center of the wheel to 1 in. at the periphery. The window was partially shielded by aluminum from all parts of the underlying differential fall-out wheel except for the sector directly beneath the window.

The probe was the gas-flow, proportional counting type that used a mixture of 90 per cent argon and 10 per cent carbon dioxide. A three-stage feedback pre-amplifier which fed into an Atomic Instrument Company scaler was built into the probe.

In the first step of the counting procedure, the top of the housing was removed and the wheel placed on the turntable with its starting mark directly beneath the probe window. The top of the housing and the probe were then replaced. By successively taking a 1 min count at each of the eighty positions around the wheel, a reliable measure of the relative distribution of the radioactivity was obtained. Because of the high level of radioactivity on some of the underground shot wheels, it was necessary to use a 1/16 in. aluminum absorber over the counting window.

From the relative distribution of the radioactivity around the wheels and the times of their rotation, graphs were constructed showing the variation of fall-out with time.

To make a qualitative comparison of the activity on the wheels at different stations, all the counting data were corrected for decay back to shot time plus 1 day by use of decay curves prepared from surface and underground shot fall-out samples by the Nuclear and Physical Chemistry Branch of the USNRDL. Attention is called to the fact that some of the wheels were counted with an absorber which makes it impossible to compare them directly with others counted without an absorber. Due to the heterogeneity of the fall-out samples, no unique correction factor was found which could be applied to the counts made with an absorber to compensate for the effect of the absorber.

It should be emphasized that the graphs are reliable only in indicating the time of maximum collection of radioactivity on the wheels. The width of the peaks on the graphs are exaggerated by the unabsorbed gamma radiation from the more radioactive sectors of the wheel which caused an increase in the counting rate of the adjacent sectors. Also, the magnitudes of the largest maxima are unreliable since the counting rates were so high that appreciable coincidence losses occurred.

Following the surface shot, the fall-out was distributed in a long narrow swath extending north from the shot point. The line of

differential fall-out collectors extending N10°E from the shot point fell within the edge of this fall-out area. Of these collectors only two received a significant amount of fall-out and operated satisfactorily. The data from these two Stations, Nos. 29 and 33, have been plotted and are shown in Figs. 4.11 and 4.12.

From Fig. 4.11, it is apparent that the radioactive fall-out reaching Station 29 arrived in two major waves. The duration of the first wave was apparently from approximately 8 to 23 min after shot time, and the second from about 60 to 100 min after shot time. Considering that the distance of this station was 14,000 ft from the shot point, it is evident that the initial fall-out must have traveled with an average horizontal speed of about 20 mph to reach the station in 8 min.

From an inspection of the graph for Station 33 (Fig. 4.12), it is seen that practically all the activity reached the station in one major wave which arrived about 10 min after the shot. Since Station 33 was located 20,000 ft from the shot point, the initial wave of fall-out must have been traveling with an average horizontal speed of about 23 mph.

Following the surface shot, the atomic cloud rose to a height of 11,000 ft above sea level. At this elevation, the wind had a velocity of about 40 mph, N20°E. The velocity of the surface wind was only 2 mph. It is evident that the fall-out material must have been transported by the high velocity winds aloft rather than by the surface winds to reach the outer stations in the observed time.

The complete absence at Station 33 of the second wave of fall-out, so well developed at Station 29, is surprising. However, during the laboratory examination of the fall-out samples from these stations, it was found that practically all the radioactivity in each sample was accounted for by a very few, intensely radioactive, glass spheres approximately 0.5 to 2 mm in diameter. Each of these spheres was sufficiently active to cause a maximum in the graphs. This meager number of radioactive particles in the fall-out introduces a large element of randomness into the fall-out distribution, which factor makes correlation between adjacent stations difficult. This difficulty was not encountered at the underground shot where each sample contained a large number of radioactive particles.

The apparent increase of activity at the end of the graph for Station 33 is typical of most of the graphs. It is caused by the unabsorbed radiation from the highly radioactive material on the first part of the wheel. This material increases the counting rate of the sector to which it is adjacent at the end of the run.

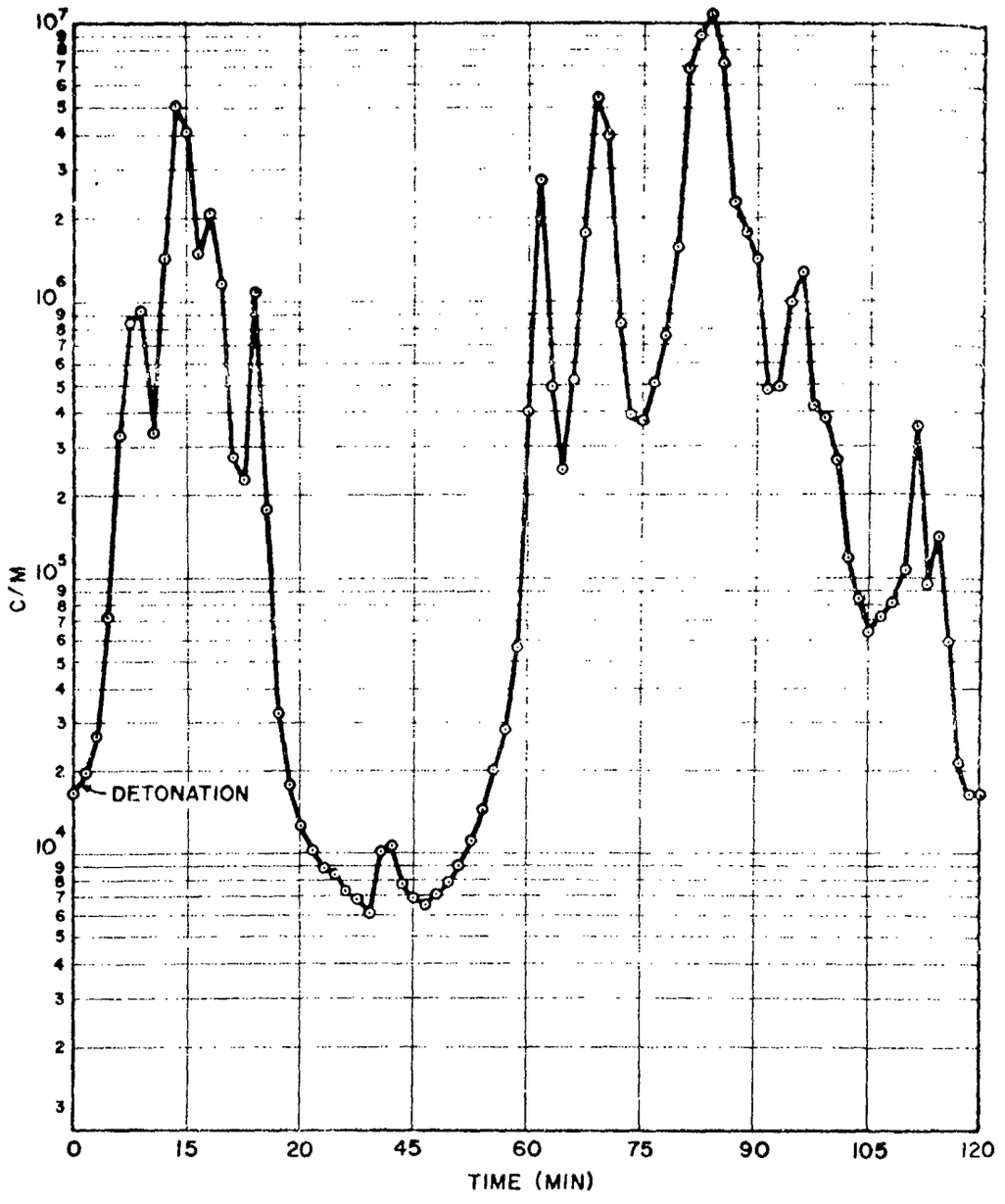

Fig. 4.11 Fall-out as a Function of Time, Station 29

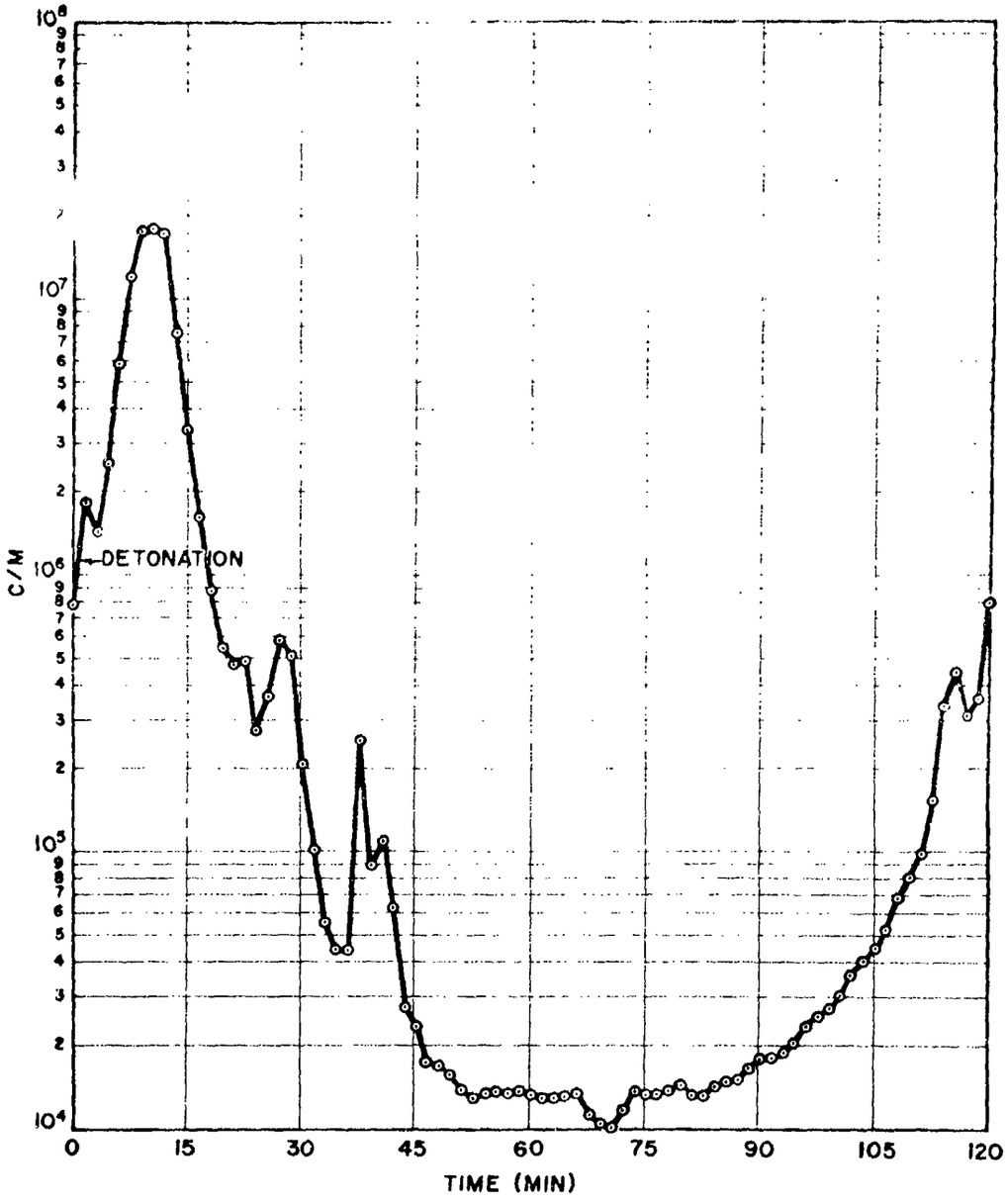

Fig. 4.12 Fall-out as a Function of Time, Station 33

The fall-out from the underground shot was distributed in a broad area extending generally NNE of the shot point. Included within this area were two lines of differential fall-out collectors extending N5°W and N35°E from the shot point. Data from the differential fall-out collectors located at Stations 102, 108, 129, 133, and 134 were successfully obtained: the resulting graphs are shown in Figs. 4.13 to 4.17.

From the graph for Station 102, it is seen that most of the activity apparently fell out in three waves which passed the station at about 0.5, 2, and 4 min following shot time. The fall-out at Station 108 apparently continued over a greater length of time, maximum fall-out occurring at about 1.25, 4, 8, and 10 min following shot time. Stations 102 and 108 were situated adjacent to each other at distances of 2,000 and 3,000 ft from the shot point, respectively. However, there is no apparent correlation between fall-out arrival times at the two stations. It is not possible to compute accurately the average horizontal velocity of the initial fall-out material from the shot point to these stations as the uncertainty in the starting times of the wheels varied from 10 to 30 sec, an appreciable fraction of the time which elapsed between the shot and the arrival of the first fall-out.

Stations 102 and 108 were located close enough to the shot point to be within the area affected by the base surge and throw-out from the shot. Photographs show material falling from the cloud into this area in streamers and irregular clumps. This probably accounts for the apparent irregularity and lack of correlation of the fall-out distribution for these two stations.

From the graphs for Stations 129 and 133, located 14,000 and 20,000 ft, respectively, from the shot point, it is seen that most of the radioactive fall-out arrived in one wave which reached Station 129 at approximately 7 min, and Station 133 at approximately 6 min, after shot time. Why the fall-out should reach the more distant station first is inexplicable. These arrival times indicate an average horizontal velocity of the fall-out material of 23 and 38 mph to Stations 129 and 133, respectively, from the shot point. The top of the cloud at the underground shot reached an elevation of approximately 9,000 ft above sea level. At this elevation, the wind velocity was about 21 mph in the direction N40°E (Stations 129 and 133 were N5°W from the shot point). At lower elevations the wind velocity was even less and decreased to 4.5 mph at the surface. While it seems possible the initial fall-out material could have been carried by the high winds and have arrived at Station 129 in about 7 min (giving an average velocity of 23 mph), it is highly unlikely the fall-out could have reached Station 133 in 6 min. This anomalous arrival time casts some doubt on the accuracy of the timing at Station 133.

The initial arrival time of the fall-out at Station 134 was not well defined.

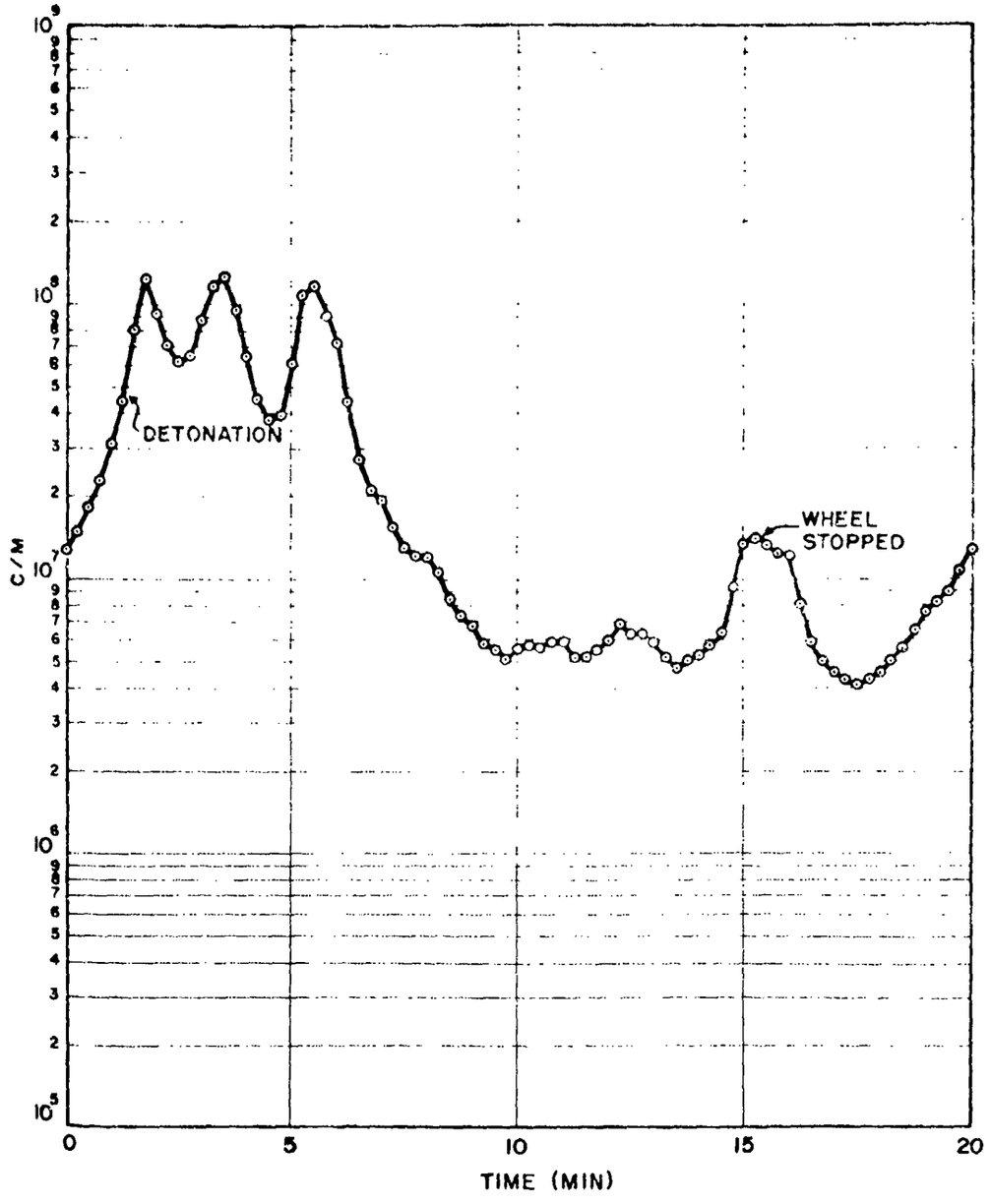

Fig. 4.13 Fall-out as a Function of Time, Station 102

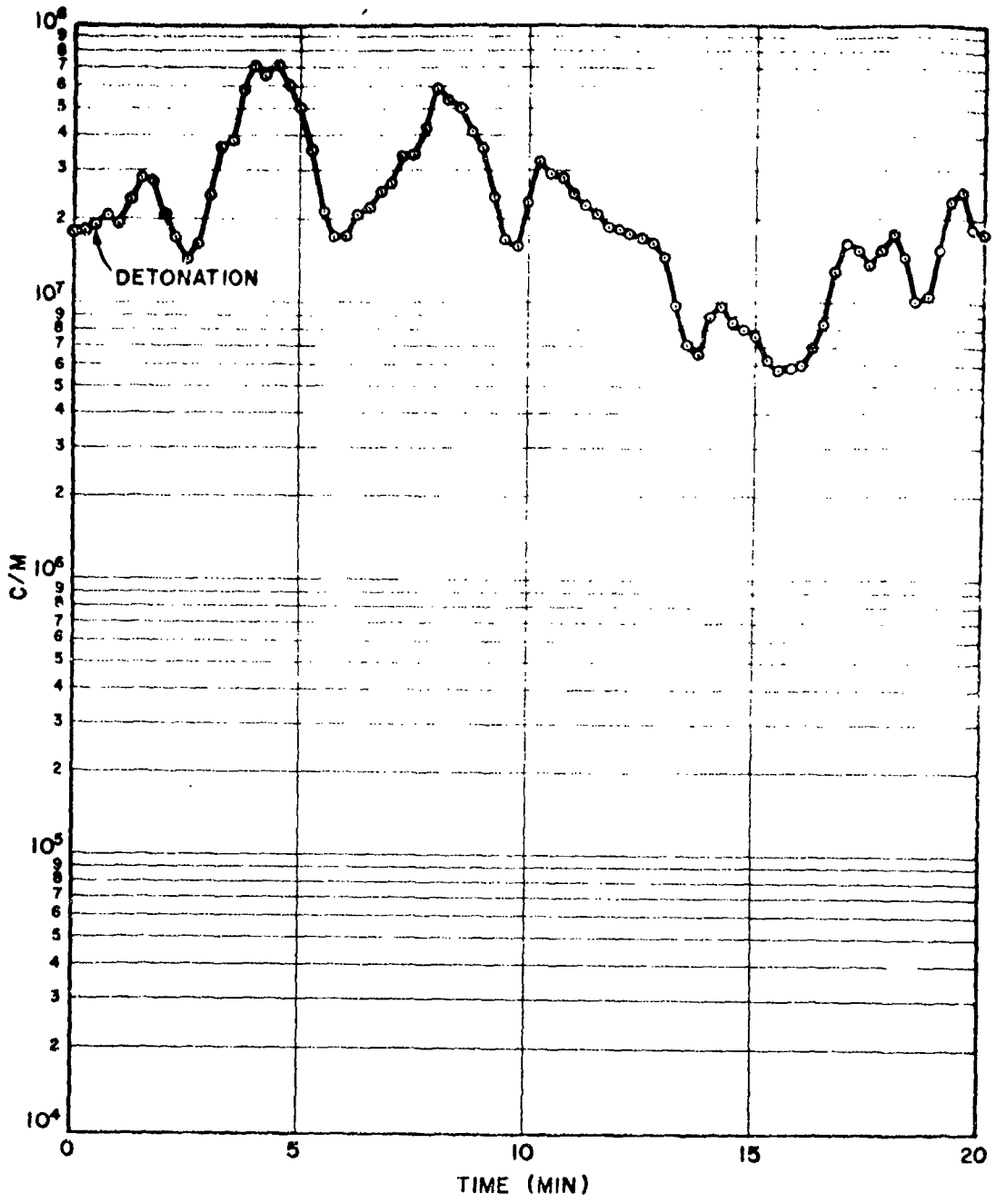

Fig. 4.14 Fall-out as a Function of Time, Station 108

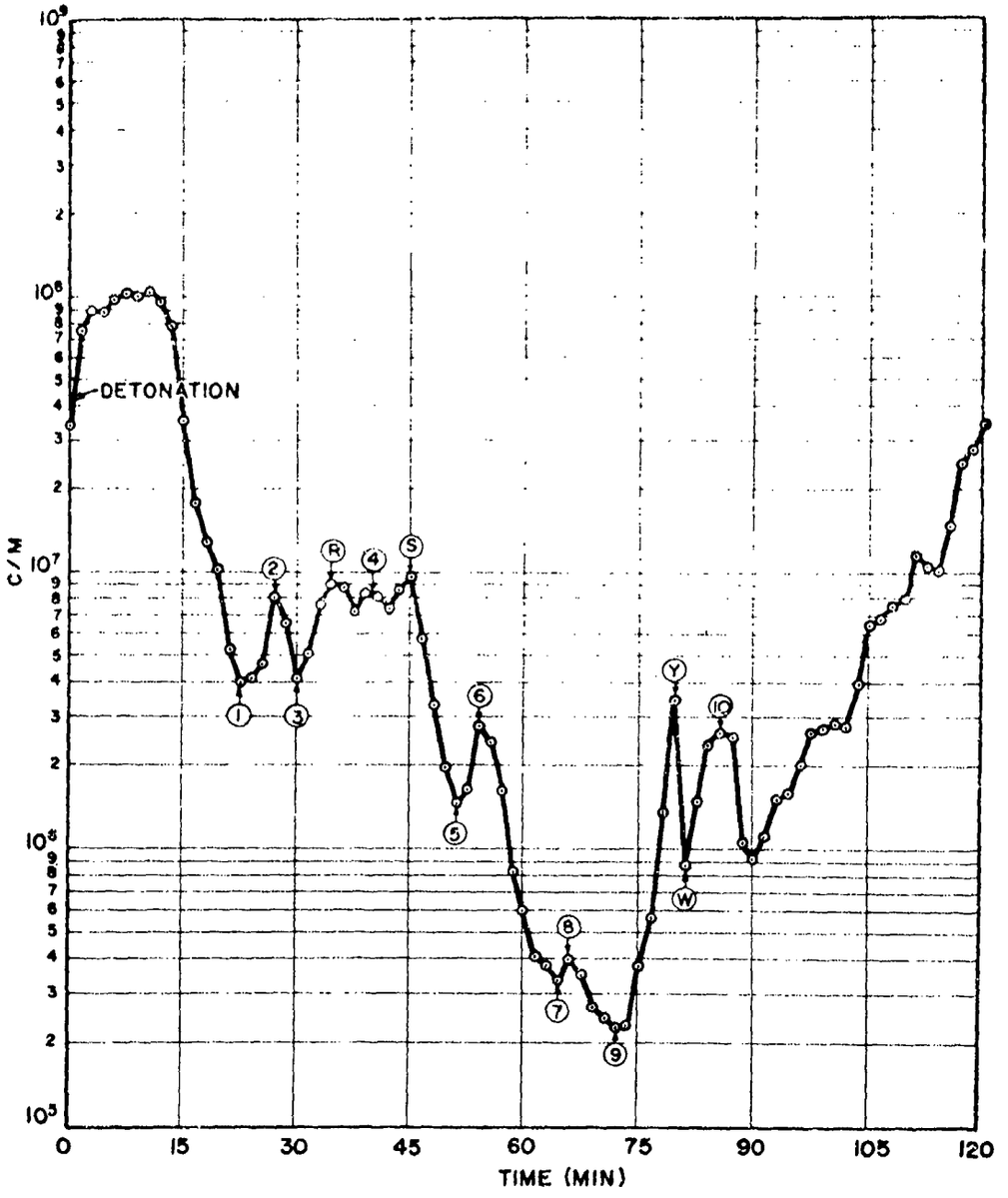

Fig. 4.15 Fall-out as a Function of Time, Station 129

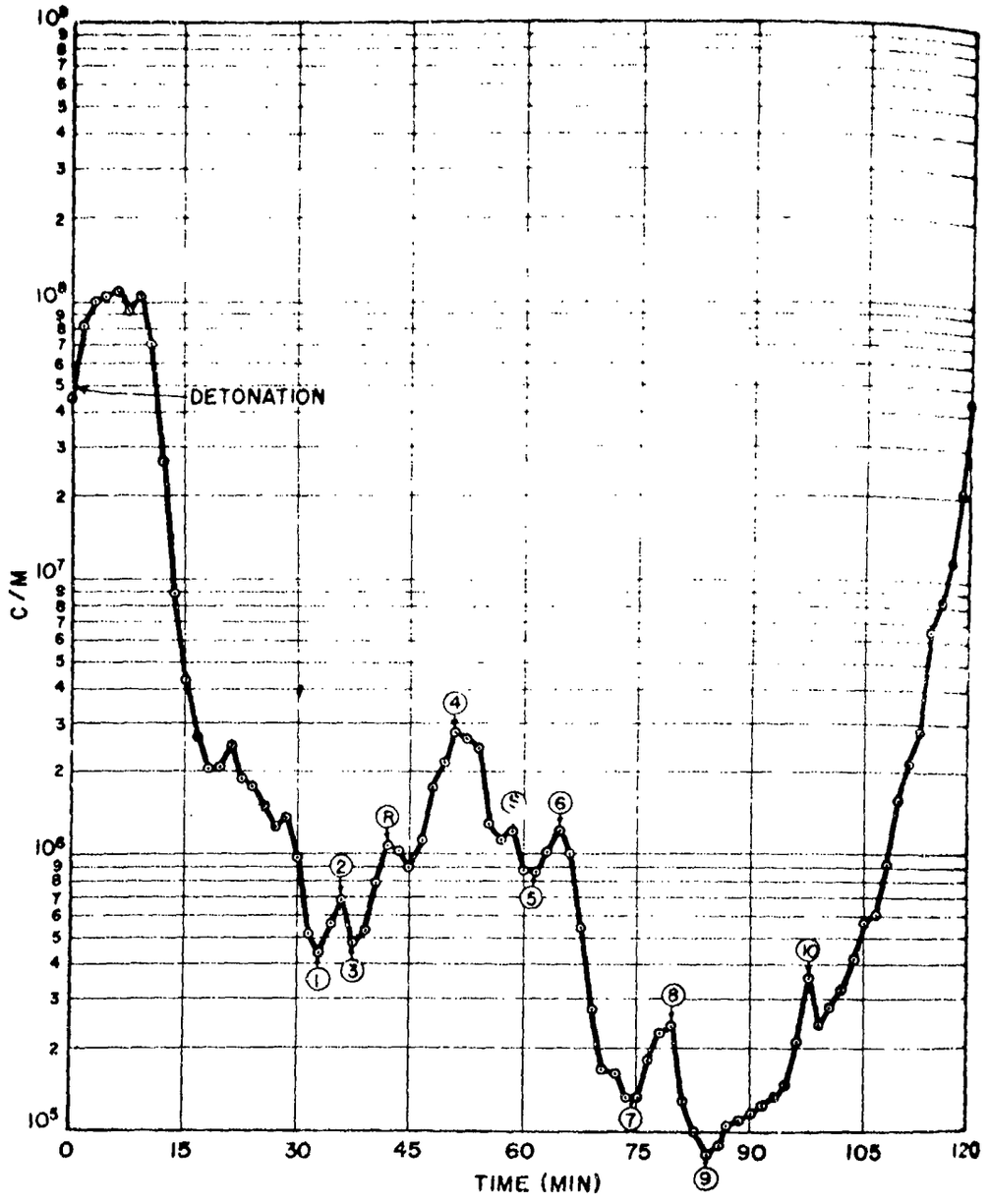

Fig. 4.16 Fall-out as a Function of Time, Station 133

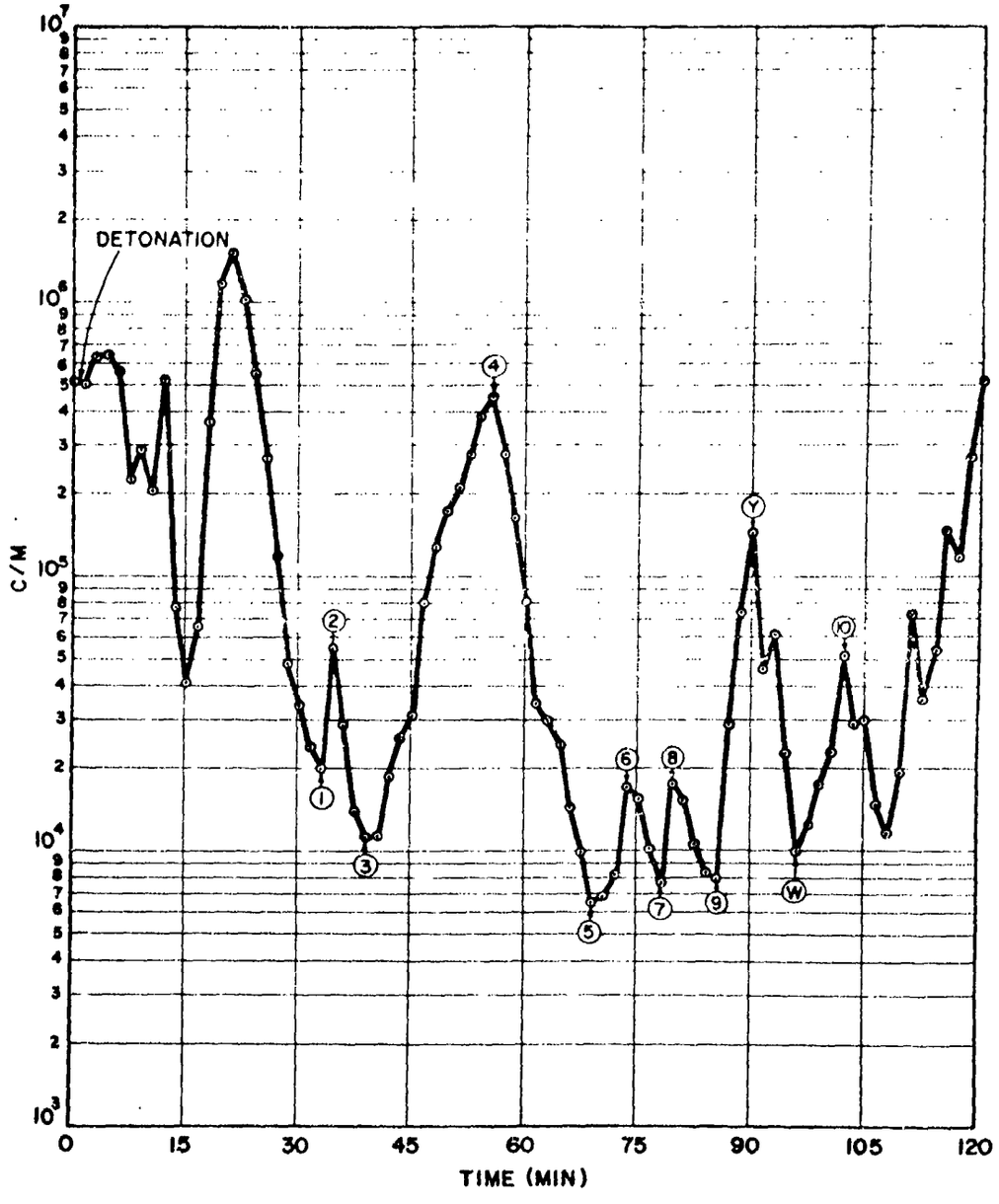

Fig. 4.17 Fall-out as a Function of Time, Station 134

A series of small fall-outs, indicated by minor maxima in the latter part of the graphs for Stations 129, 133, and 134, occurred following the passage of the main body of fall-out at Stations 129 and 133. There was apparently some pattern to these maxima which could be correlated fairly well between these stations. A few of the corresponding points on each curve have been indicated on the graphs by numbers 1 through 6. By measuring the differences of arrival times for each corresponding point at each station, and taking into account the geometrical arrangement of the stations, it is possible by simple trigonometry to calculate the horizontal speed and direction of travel of the radioactive material represented by these points. From these calculations, the velocity of the radioactive material is 4 to 6 mph in the direction N10°E to N30°E. The surface wind is reported as 4.5 mph in the direction N30°E. It seems probably that these secondary perturbations are due to radioactive material carried along by surface winds.

4.2.2 Area Distribution of Fall-out

The purpose of this study was to determine the pattern of fall-out from both the surface and underground explosions in terms of specific activity, weight, and particle size. To accomplish this purpose, over 100 collecting devices were placed around each test site. The array of stations and their designations are shown in Fig. 4.18. After each explosion field readings of the gamma intensity were taken at each station using the standard U. S. Army AN/PDR/T1B 3 ft from the ground. The material in the collectors was removed from those stations which experienced significant fall-out and taken to the field laboratory where readings of both the beta plus gamma and the gamma intensities were taken with a Beckman Ionization Chamber (M X-4) at a distance of 3 in. The former readings are referred to as Field Gamma Readings while the latter are referred to as Plate Beta plus Gamma Readings and Plate Gamma Readings.

Samples showing appreciable radiation intensity were shipped to the USNRDL where each sample was separated into fifteen size fractions by sieving, and the radiation intensity and the weight of each fraction measured. Because the moisture content of the samples was of the order of one per cent, its contribution to the weight was neglected. The counting was done with proportional gas-flow counters through a 200 mg aluminum absorber. The data obtained are given in Appendix D. Any interpretation given to these values other than their relationship to each other is meaningless.

Table 4.11 summarizes the measurements made at the test site. These measurements have been corrected to 1 hr after the respective explosions according to the standard formula $A_1 = A_2(t_1/t_2)^{-1.2}$.

TABLE 4.11

Field and Laboratory Measurements of Radiation Intensities from Fall-out Trays[a]

Station	Plate No.	Field Gamma Reading (mr/hr)	Plate Gamma Reading (mr/hr)	Plate Beta plus Gamma Reading (mr/hr)
SURFACE SHOT				
A	A-1	26		
	A-2			
	A-3	27		
	A-4			
	A-5	10		
	A-6			
	A-7	5		
	A-8			
	A-9	5		
B	B-1	210		
	B-2	160		
	B-3	160		
	B-4			
	B-5	51		
	B-6			
	B-7	26		
	B-8			
	B-9	8		
C	C-1	1,100		
	C-2	520		
	C-3	780		
	C-4			
	C-5	260		
	C-6			
	C-7	51		
	C-8			
	C-9	10		
D	D-1	26,000	3,500	12,000
	D-2	7,800		
	D-3	10,000		
	D-4	800		
	D-5	1,100		
	D-6			

TABLE 4.11 (Continued)

Field and Laboratory Measurements of Radiation Intensities from Fall-out Trays[a]

Station	Plate No.	Field Gamma Reading (mr/hr)	Plate Gamma Reading (mr/hr)	Plate Beta plus Gamma Reading (mr/hr)
SURFACE SHOT				
	D-7	190		
	D-8			
	D-9	32		
E	E-2	53,000	1,800	4,400
	E-3	76,000	2,700	16,000
	E-4	960		
	E-5	3,300		
	E-6			
	E-7	320		
	E-8			
	E-9	53		
F	F-1	540,000	71,000	390,000
	F-2	11,000		
	F-3	200,000	30,000	400,000
	F-4	500		
	F-5	2,500		
	F-6			
	F-7	340		
	F-8			
	F-9			
G	G-1	200,000	14,000	160,000
	G-2	3,300		
	G-3	460,000	39,000	
	G-4	100		
	G-5	16,000		
	G-6			
	G-7	330		
	G-8			
	G-9	112		
H	H-1	160,000	6,900	35,000
	H-2	1,300		
	H-3	340,000	47,000	530,000

TABLE 4.11 (Continued)

Field and Laboratory Measurements of Radiation Intensities from Fall-out Trays [a]

Station	Plate No.	Field Gamma Reading (mr/hr)	Plate Gamma Reading (mr/hr)	Plate Beta plus Gamma Reading (mr/hr)
SURFACE SHOT				
	H-4	60		
	H-5	67,000	9,100	92,000
	H-6			
	H-7	560		
	H-8			
	H-9	110		
I	I-1	88,000	1,400	2,900
	I-2	890		
	I-3	340,000	53,000	580,000
	I-4	10		
	I-5	89,000	10,000	75,000
	I-6			
	I-7	1,300		
	I-8			
	I-9	110		
N	N-2	110,000	11,000	79,000
	N-3	110,000	9,400	88,000
	N-4	110,000	14,000	92,000
	N-5	66,000	3,500	23,000
UNDERGROUND SHOT				
A	A-1			
	A-2			
	A-3	1,600		
	A-4			
	A-5			
	A-6			
	A-7			
	A-8			
	A-9			
B	B-1			
	B-2			
	B-3			
	B-4			

PROJECT 2.5a-2

TABLE 4.11 (Continued)

Field and Laboratory Measurements of Radiation Intensities from Fall-out Trays[a]

Station	Plate No.	Field Gamma Reading (mr/hr)	Plate Gamma Reading (mr/hr)	Plate Beta plus Gamma Reading (mr/hr)
UNDERGROUND SHOT				
	B-5	400		
	B-6			
	B-7	120		
	B-8			
	B-9	60		
C	C-1	10,000		
	C-2			
	C-3	4,000		
	C-4			
	C-5	1,000		
	C-6			
	C-7	200		
	C-8	360		
	C-9	75		
D	D-1	660,000	637,000	1,400,000
	D-2	210,000	25,000	160,000
	D-3	140,000	10,000	96,000
	D-4	7,600		
	D-5	3,100		
	D-6	1,800		
	D-7	510		
	D-8	510		
	D-9	360		
E	E-2	430,000	86,000	310,000
	E-3	250,000	Tray buried	
	E-4	130,000	5,800	140,000
	E-5	31,000	3,200	41,000
	E-6	3,000		
	E-7	1,800		
	E-8			
	E-9	220		
F	F-1	3,400,000	1,200,000	3,000,000
	F-2	1,300,000	170,000	1,400,000

TABLE 4.11 (Continued)

Field and Laboratory Measurements of Radiation Intensities from Fall-out Trays[a]

Station	Plate No.	Field Gamma Reading (mr/hr)	Plate Gamma Reading (mr/hr)	Plate Beta plus Gamma Reading (mr/hr)
		UNDERGROUND SHOT		
	F-3	360,000	75,000	560,000
	F-4	42,000	5,300	66,000
	F-5	29,000	2,900	37,000
	F-6	6,800	340	510
	F-7	4,100		
	F-8	1,700		
	F-9	260		
G	G-1	820,000	77,000	900,000
	G-2	420,000	74,000	790,000
	G-3	230,000	22,000	190,000
	G-4	51,000	3,800	34,000
	G-5	22,000	3,000	41,000
	G-6	15,000	170	860
	G-7	6,100		
	G-8	14,000		
	G-9	3,100		
H	H-1	610,000	74,000	640,000
	H-2	510,000	56,000	460,000
	H-3	220,000	45,000	600,000
	H-4	34,000	4,200	57,000
	H-5	41,000	4,600	78,000
	H-6	17,000	520	4,300
	H-7	10,000		
	H-8	5,100		
	H-9	2,400	1,400	20,000
I	I-1	410,000	62,000	720,000
	I-2	260,000	34,000	430,000
	I-3	1,000,000	120,000	1,400,000
	I-4	170,000	14,000	160,000
	I-5	140,000	21,000	240,000
	I-6	26,000	3,000	34,000
	I-7	10,000	1,700	28,000
	I-8	34,000	5,600	120,000
	I-9	5,100		

TABLE 4.11 (Continued)

Field and Laboratory Measurements of Radiation Intensities from Fall-out Trays[a]

Station	Plate No.	Field Gamma Reading (mr/hr)	Plate Gamma Reading (mr/hr)	Plate Beta plus Gamma Reading (mr/hr)
UNDERGROUND SHOT				
N	N-2	240,000	4,800	48,000
	N-3	270,000	21,000	410,000
	N-4	400,000	36,000	550,000
	N-5	340,000	29,000	530,000
NE	NE-1	340		
	NE-3	340		
	NE-4	1,700		
	NE-5	17,000	3,500	52,000
E'	E'-1			
	E'-3			
	E'-4			
	E'-5	500		
W	W-3	50		
	W-4	70		
	W-5	50		
NW	NW-5	820		

[a] Blanks in the columns indicate no measurable activity on the plate.

Comparison of columns 3 and 4 of Table 4.11 is significant only if the over-all counting efficiencies of the M X-4 at 3 in. and the T1B at 3 ft are considered. For a 1 ft-square sample, the ratio of these counting efficiencies is approximately 50, i.e., for a given sample the M X-4 at 3 in. indicates fifty times as great a value as the T1B at 3 ft. Therefore, the contribution of a square foot of sample to the general radiation field 3 ft above it is approximately equal to the plate reading (column 4, Table 4.11) divided by fifty.

Figures 4.19 and 4.20 show the field gamma readings and the plate gamma readings as a function of location for the surface explosion. Similarly, Figs. 4.21 and 4.22 show the field gamma and plate gamma values for the underground explosion. Field gamma readings were obtained primarily at the collector stations; however, extrapolation of lines beyond

the station array was accomplished by use of other sources, such as monitor's data and telemeter readings.

Figures 4.23 and 4.24, respectively, show the total mass distribution of the samples collected at the surface and underground explosions. Figures 4.25 through 4.28 show the distribution of total activity and of specific activity for both explosions. These graphs were plotted using the values shown in the tables in Appendix D. Figures 4.29 and 4.30 are graphs of the percentage of total station activity found in particles less than 74 μ for the two explosions. The mass distributions by particle size for the underground shot are shown in Figs. 4.31 to 4.34 and for the surface explosion in Figs. 4.35 to 4.38.

In the underground explosion a base surge formed as the main column began to settle back to earth. An estimation of the maximum extent of the base surge was made using binoculars containing a reticle. This visual estimation compared well with a well defined dust pattern later found on the ground in the cross wind direction. The dust pattern extended about 400 yd up wind from ground zero and about 750 yd cross wind in both directions. Down wind, the boundaries of the dust pattern were not clearly defined. In the up wind and cross wind directions, all of the contaminated material was found within the dust pattern; however, the radiation field extended well beyond the boundary of the pattern.

The particle size of the contaminant is significant in contamination-decontamination studies. For the surface explosion, no more than one per cent of the activity was found in the particles under 75 μ in diameter. The percentage of activity in the fraction under 75 μ was fairly constant and independent of the distance from ground zero. For the underground explosion the percentage of activity in the particles under 75 μ in diameter ranged from 0.5 to 40, and varied directly with the distance from ground zero.

The above observations suggest that it would be easier to decontaminate objects subjected to contamination from a surface burst than those contaminated by an underground burst; this was generally found to be true.

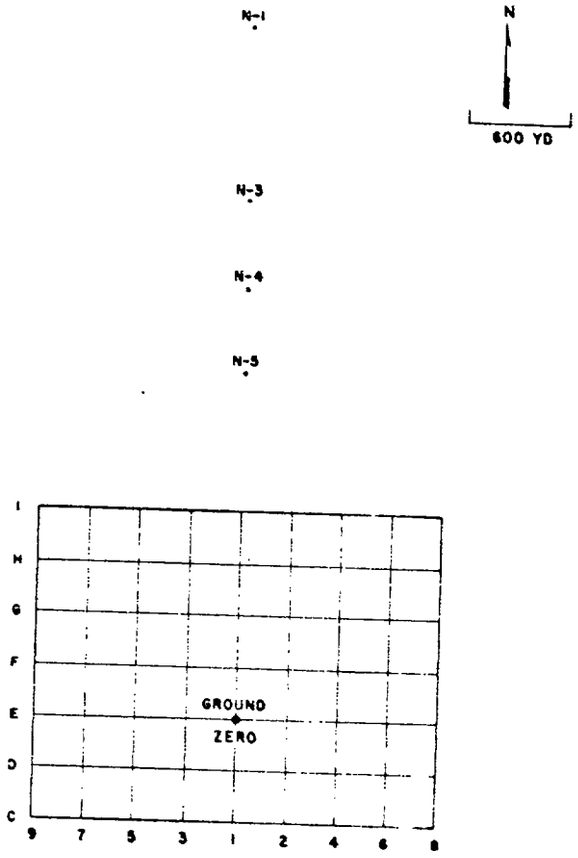

Fig. 4.18 Field Array Showing Stations within Area of Significant Fall-out

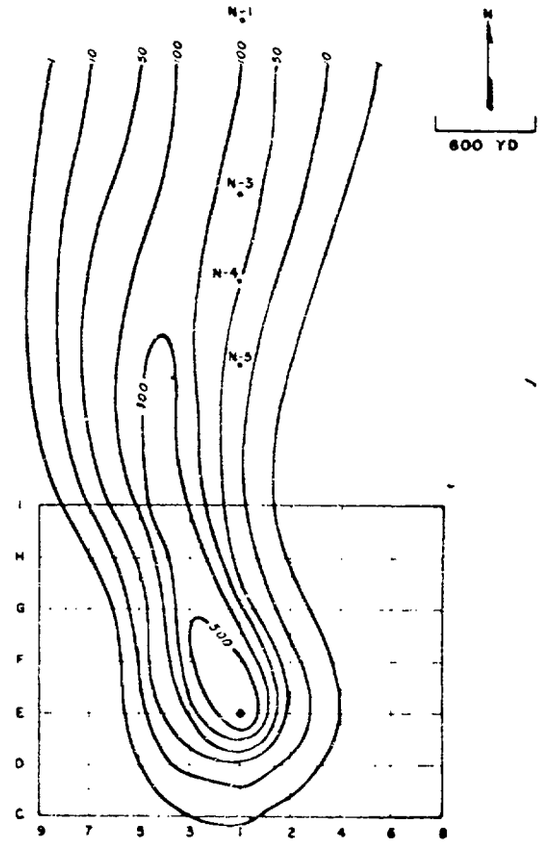

Fig. 4.19 Surface Explosion Field Gamma (H + 1 hr) in (r/hr)

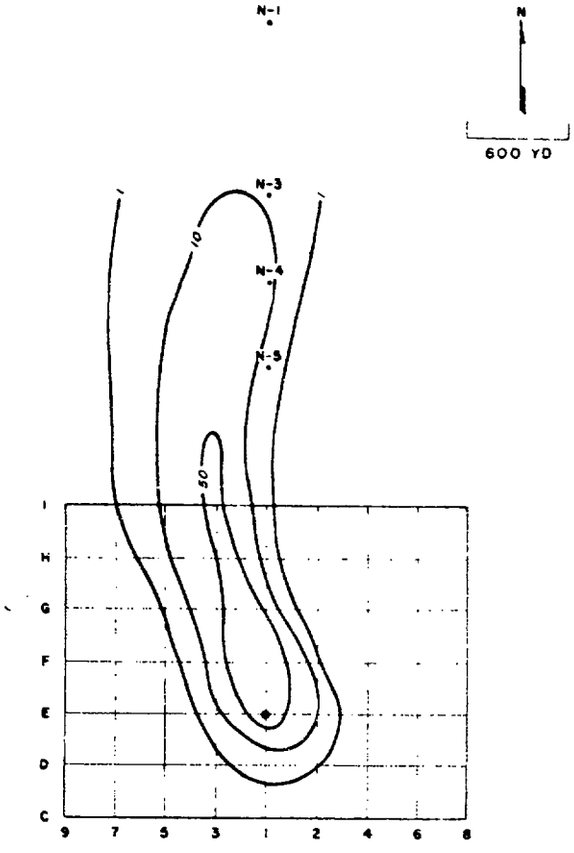

Fig. 4.20 Surface Explosion Plate Gamma (H + 1 hr) in (r/hr)

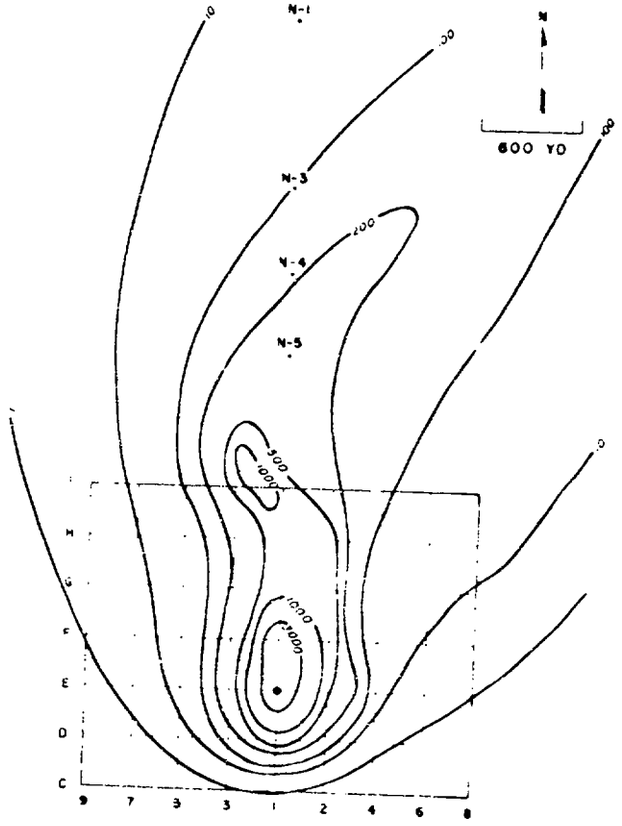

Fig. 4.21 Underground Explosion Field Gamma (H + 1 hr) in (r/hr)

PHOTO 2.5-3

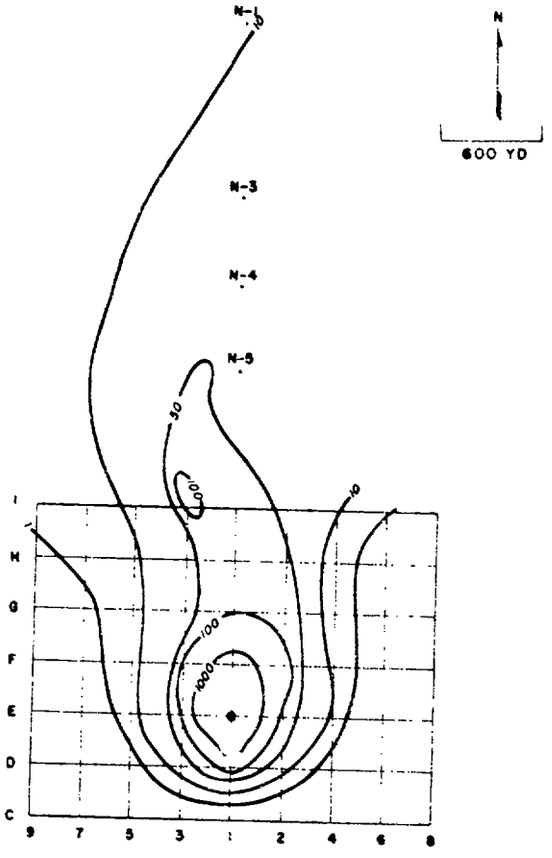

Fig. 4.22 Underground Explosion Plats Gamma (H + 1 hr) in (r/hr)

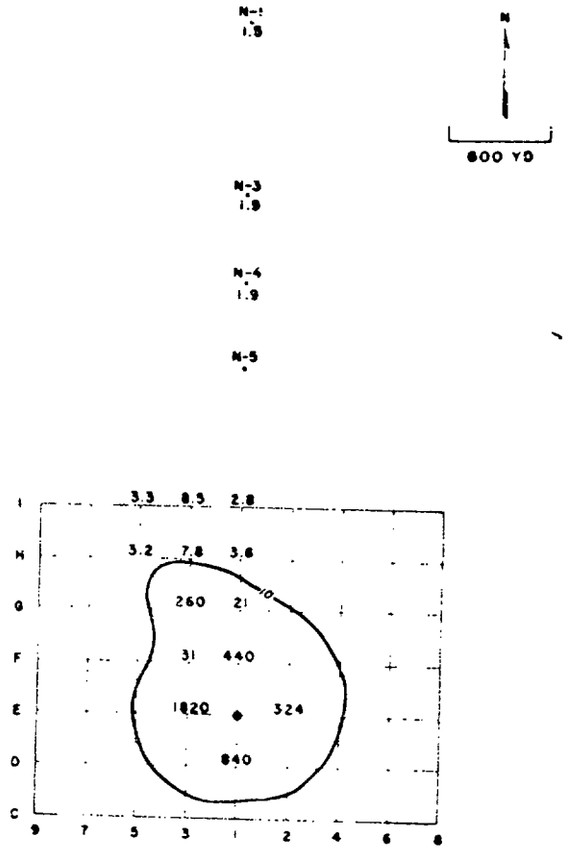

Fig. 4.23 Surface Explosion Total Mass Distribution (g/sq ft)

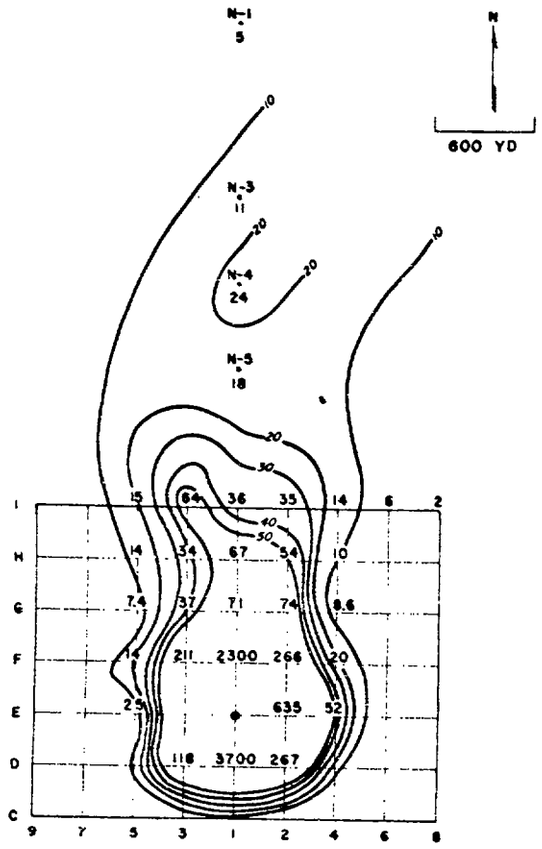

Fig. 4.24 Underground Explosion Total Mass Distribution (g/sq ft)

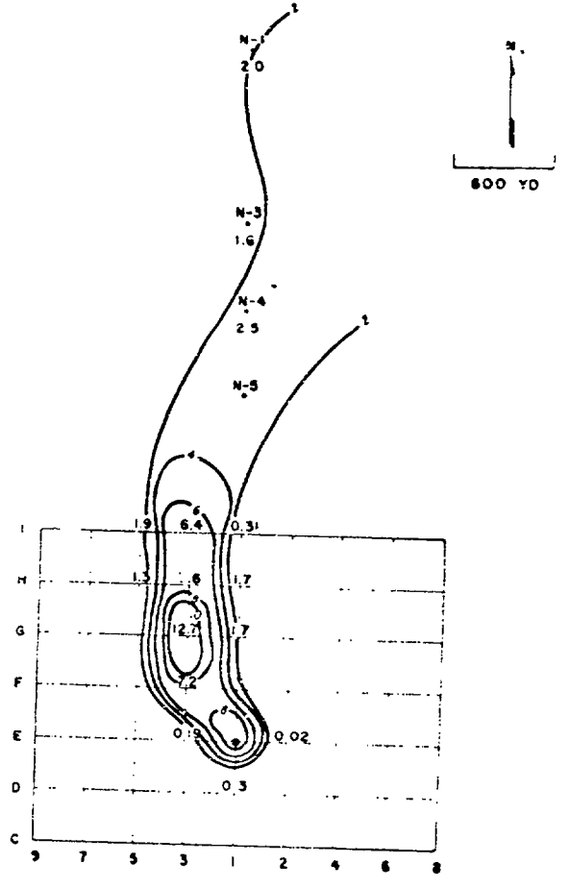

Fig. 4.25 Surface Explosion, Distribution of Total Activity (c/min/sq ft x 10^6)

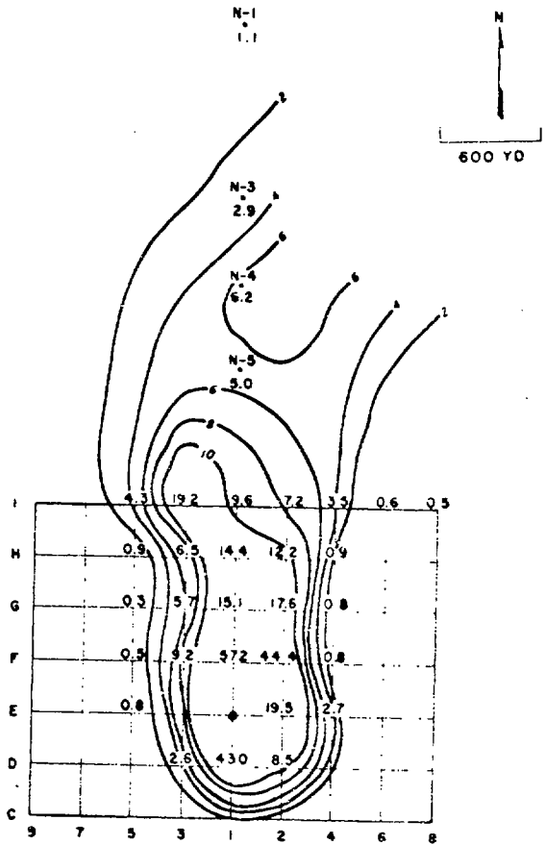

Fig. 4.26 Underground Explosion, Distribution of Total Activity (c/min/plate x 10⁶)

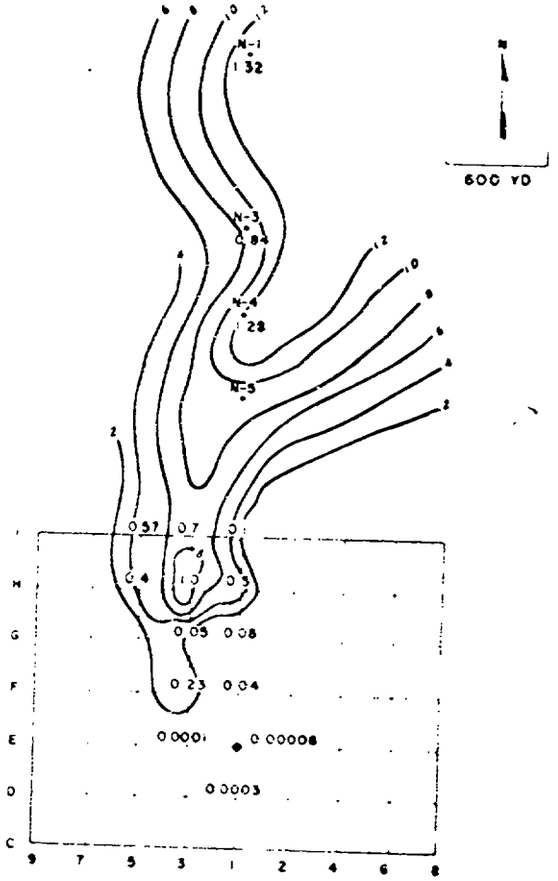

Fig. 4.27 Surface Explosion, Distribution of Specific Activity (c/min/g x 10⁶)

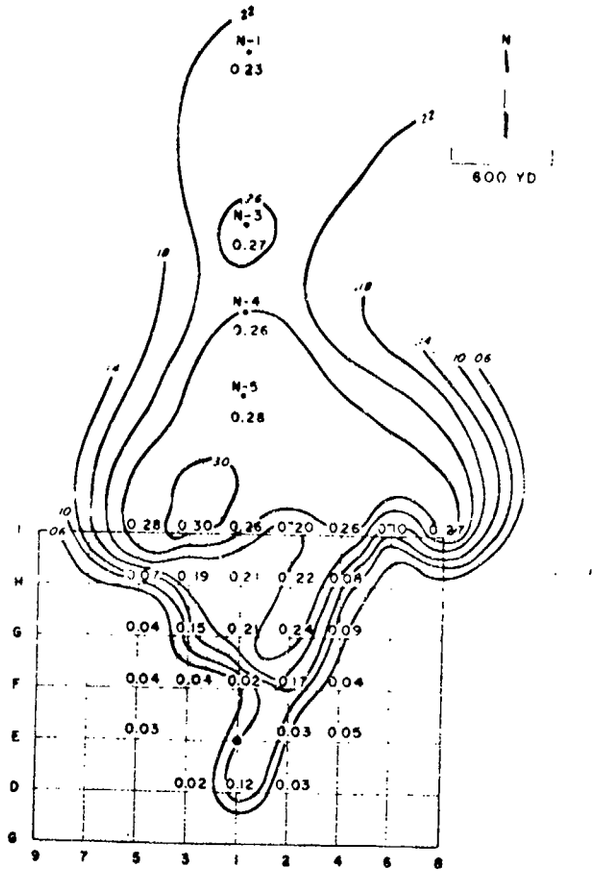

Fig. 4.28 **Underground Explosion, Distribution of Total Specific Activity (c/min/g x 10^6)**

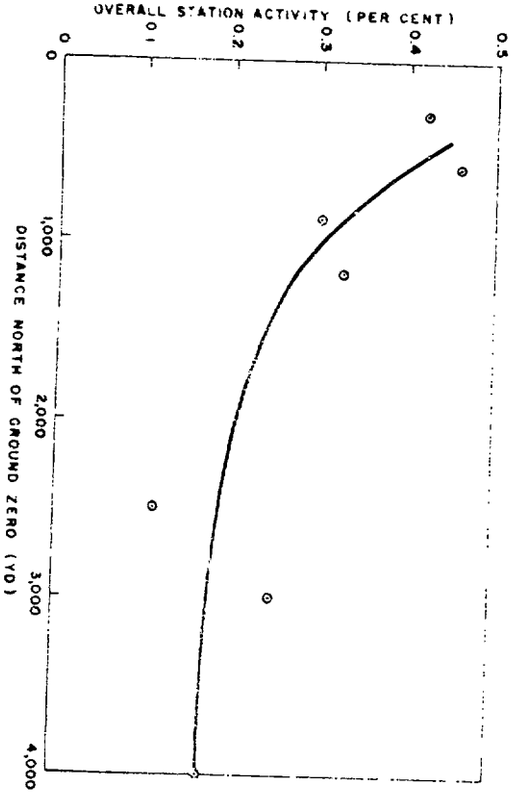

Fig. 4.29 Surface Explosion Percentage of Total Station Activity Found in 74 μ and Under Particulate

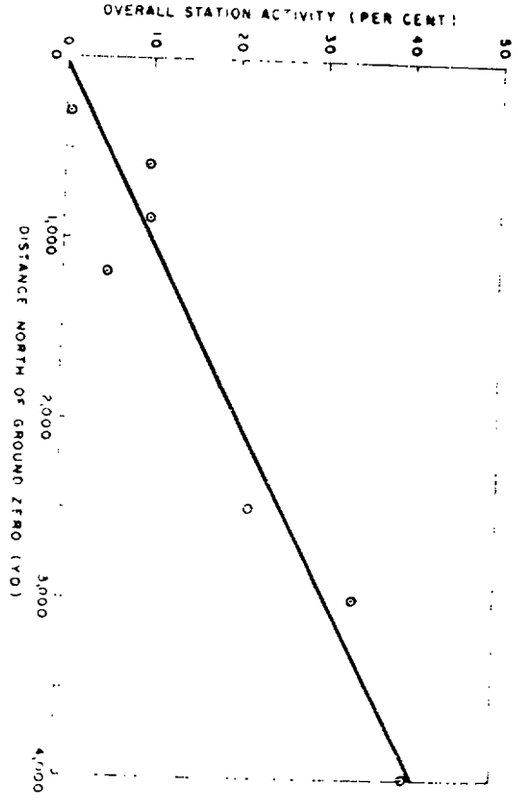

Fig. 4.30 Underground Explosion, Percentage of Total Station Activity Found in the 74 μ and under Particulate

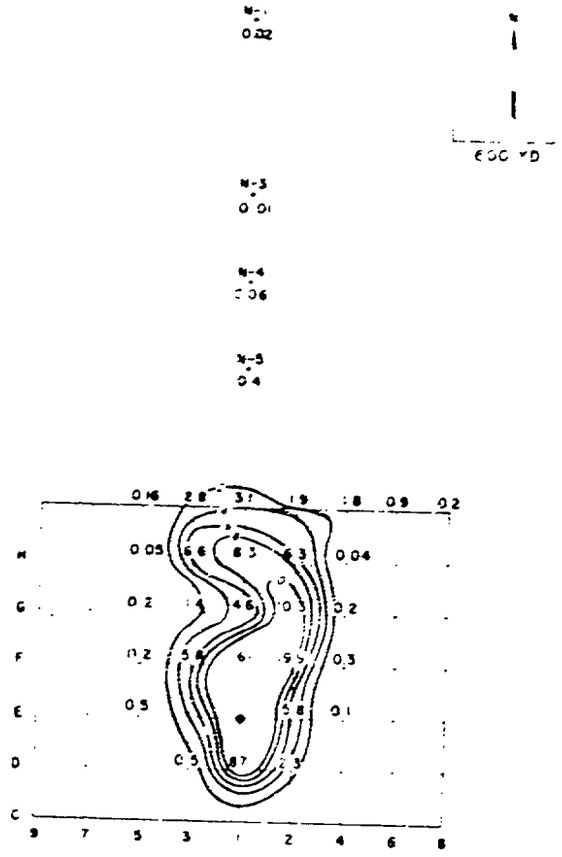

Fig. 4.31 Underground Explosion, Mass Distribution of 715 μ Fraction (g/sq ft)

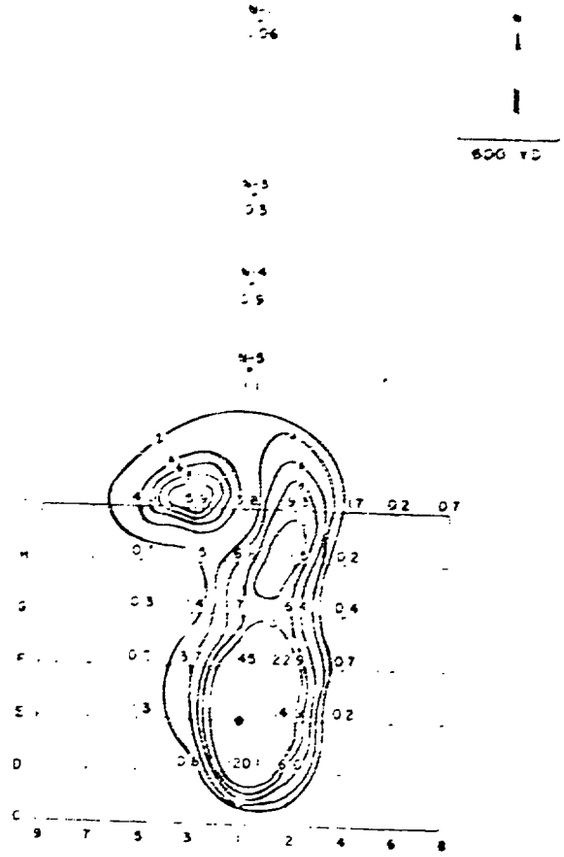

Fig. 4.32 Underground Explosion, Mass Distribution of 356 μ Fraction (g/sq ft)

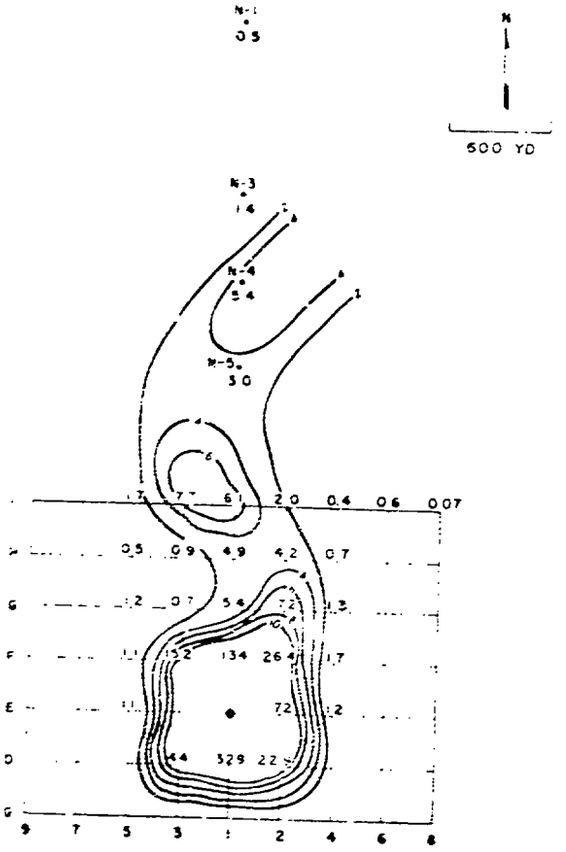

Fig. 4.33 Underground Explosion, Mass Distribution of 175 μ Fraction (g/sq ft)

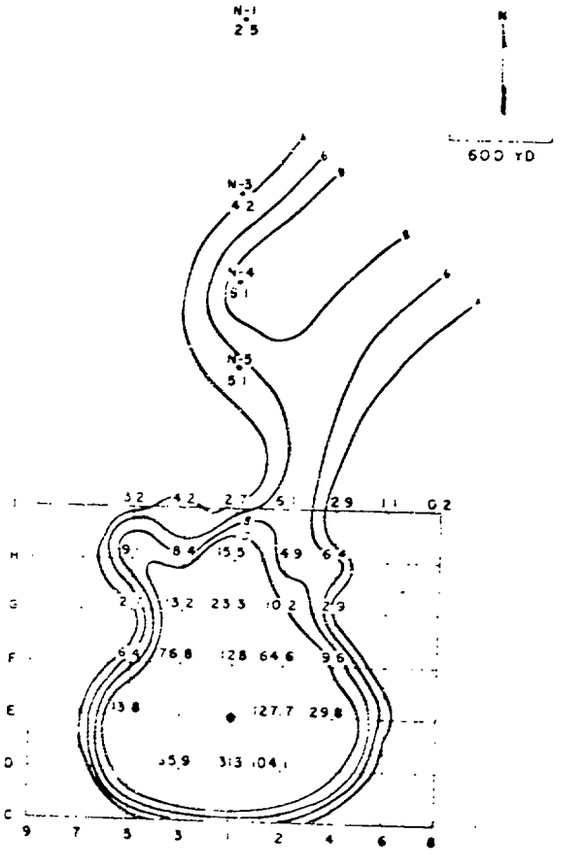

Fig. 4.34 Underground Explosion, Mass Distribution of 74 μ and under Fraction (g/sq ft)

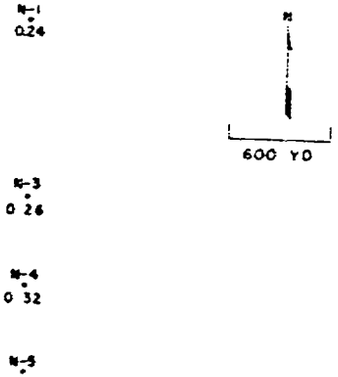

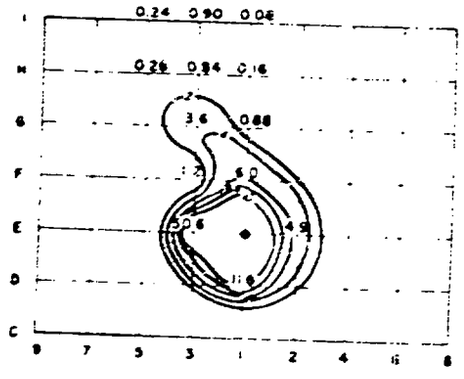

Fig. 4.35 Surface Explosion, Mass Distribution of 715 μ Fraction (g/sq ft)

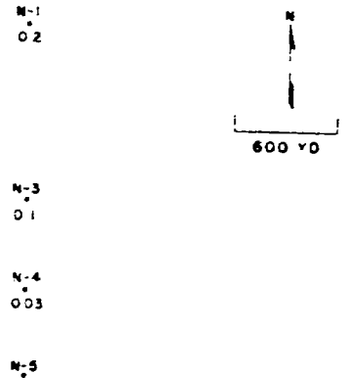

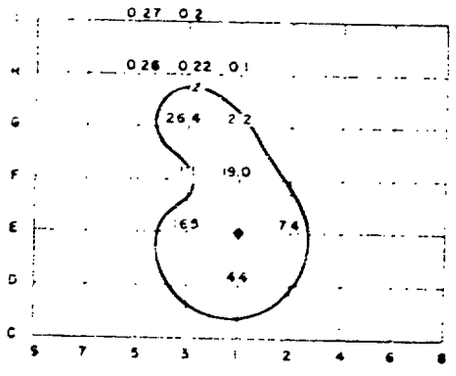

Fig. 4.36 Surface Explosion, Mass Distribution of 356 μ Fraction (g/sq ft)

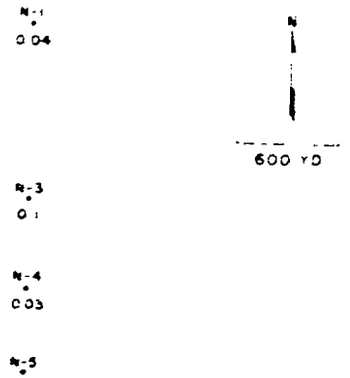

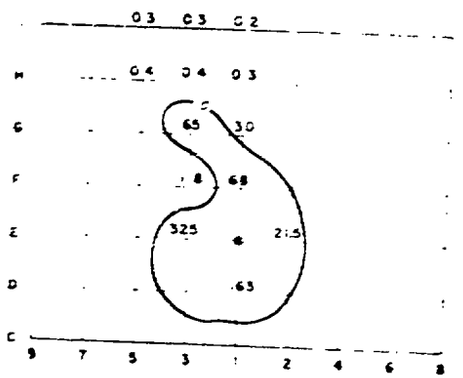

Fig. 4.37 Surface Explosion, Mass Distribution of 175 μ Fraction (g/sq ft)

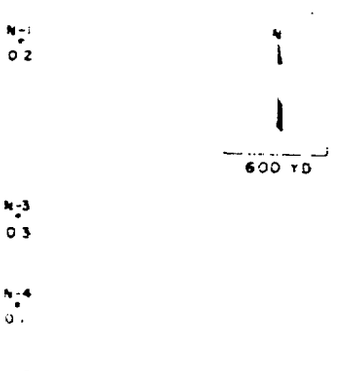

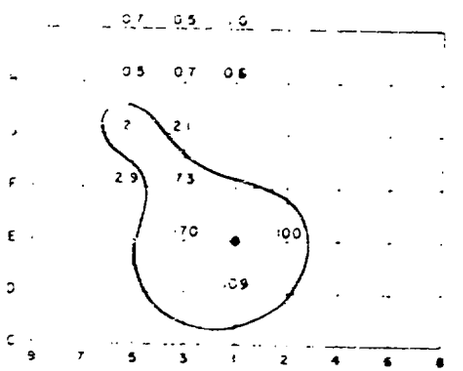

Fig. 4.38 Surface Explosion, Mass Distribution of 74 μ and under Fraction (g/sq ft)

CHAPTER 5

CONCLUSIONS

5.1 SUMMARY OF RESULTS

5.1.1 Particle Size Distributions

The weighted total collection median diameters and geometric deviations of particulate matter collected in the aerosol sampler and on the differential fall-out collector electron microscope grids are summarized in Table 5.1.

TABLE 5.1

Summary of Median Diameter Determinations

Sample	Geometric Median (μ)	Geometric Deviation
Gross Aerosol Sample EM Grids	0.22	3.1
Gross DFO EM Grids	0.22	4.0
Radioactive Fraction Aerosol Sample	1.4	2.2

All aerosol measurements are for the underground shot only. No samples were collected during the surface shot since the path of the cloud lay between two of the legs of the instrument layout and was not wide enough to contribute significantly to the aerosol collection.

In evaluating these results, it must be remembered that the particle size distributions obtained are always greatly influenced by both the collection and the analytical methods employed. At this time, there is no known method for sampling and analyzing aerosols with as wide a spread of particle size as was encountered in this investigation. The apparent difference in median particle diameter between the gross and radioactive samples was undoubtedly due to the difference in analytical

procedures. The radioactive particles were measured under an optical microscope with conditions limiting resolution to 0.5 μ while the gross samples were measured under the electron microscope whose limit of resolution is probably two orders of magnitude better. It has also been determined that size frequency distributions of the same sample made under different magnifications with the electron microscope show a decreasing median with increasing magnification. Two factors probably are responsible for this effect:

1. More small particles become visible with higher magnification.

2. Larger particles are automatically discriminated against when their apparent dimensions approach that of the viewing area.

As an example, it was noted that the maximum sizes recorded for the aerosol samples were 8 μ when measured optically and 1.5 μ when measured on electron micrographs.

Another factor to consider is the bias contributed by the sampling instruments. For instance, thermal precipitators will not collect particles much greater than 8 μ. As stated previously the DFO electron microscope grids were not covered with carbowax as were the glass sectors, and when they were collected it was observed that they looked much "cleaner" than the surrounding area. With the DFO collector, differences in surface conditions resulted in poor collection efficiencies for particles larger than a few microns in diameter.

It can be shown by an independent measurement, however, that the values in Table 5.1 are not as greatly biased by the inefficiencies of collection for large particles as might be assumed. Consider the particle size distribution of the fall-out sample labeled UG3 in Section 4.1.4. This distribution covers the entire range of particle sizes from the class interval 0 to 1 μ to the class interval 1 to 2 mm. It was obtained by plotting the weights of the particle size fractions separated by a combination of sieve and sedimentation methods. If this distribution be converted to one in terms of numbers of particles per size fraction, which is the manner in which the direct measurement data are usually presented, the interesting result of a median particle diameter less than 1 μ is found. In making this conversion, the per cent by weight, Pw, of the particles in a given class interval divided by the cube of their diameter was taken as a measure, N, of the number of particles in the interval (see Table 5.2).

Table 5.2 shows that the size fraction below 1 μ represents approximately 95 per cent of all the particles by number. It seems then that the measurements made from the electron micrographs are not greatly biased by the collection method but rather by the analytical method, and

TABLE 5.2

Comparison of Size-weight and Size-frequency Distributions
for Fall-out Sample UG3

Class Interval Size (mm)	Particle Diam., d (μ)	d^3	Size-weight Distribution		Size-frequency Distribution		
			Per Cent by Weight, Pw	Cumulative Per Cent by Weight (%)	Number of Particles, $N = \frac{Pw}{d^3}$	Per Cent by Number	Cumulative Per Cent by Number (%)
1.0 - 2.0	2,000	0.8×10^{10}	28.8	100.6	36.0×10^{-10}	--	--
0.5 - 1.0	1,000	1.0×10^{9}	8.8	71.8	8.8×10^{-9}	--	--
0.25 - 0.5	500	1.25×10^{8}	0.4	63.0	0.32×10^{-8}	--	--
0.1 - 0.25	250	1.56×10^{7}	7.3	62.6	4.68×10^{-7}	--	--
0.05 - 0.1	100	1.0×10^{6}	14.1	55.3	14.1×10^{-6}	0.00025	--
0.02 - 0.05	50	1.25×10^{5}	19.6	41.2	15.7×10^{-5}	0.0028	100.0
0.005 - 0.02	20	0.8×10^{4}	10.1	21.6	12.6×10^{-4}	0.0226	99.9996
0.002 - 0.005	5	1.25×10^{2}	4.2	11.5	3.36×10^{-2}	0.602	99.977
0.001 - 0.002	2	8.0	2.0	7.3	0.25	4.475	99.375
0.001	1	1.0	5.3	5.3	5.3	94.90	94.90

could conceivably be smaller than reported. This hypothesis becomes more credible when it is noted that, no matter how sensitive is the method of detection used, the mode of the size frequency distribution curve always crowds the minimum particle size interval. The standard procedure of plotting logarithms of particle diameters attempts to compensate for this effect.

Another interesting result of the radioactive particle measurements is the estimate of the concentrations of airborne radioactivity contributed by the 0 to 8 μ particles. Since this particle size range is important from the point of view of inhalation hazard, this estimate may furnish an indication of the seriousness of the problem with an underground detonation. The values given in Section 4.1.1 are actually averaged over the first 3 hr by virtue of the fact that the instruments operated during this period. The actual concentrations in the cloud are difficult to evaluate. However, the time differential data of Section 4.2.1 indicate that the heavy concentrations arrived at most of the stations within a few minutes and were of minutes duration. Therefore, the computed concentrations, which varied from 2×10^{-4} μ-curie/cc at Station 108 to 2×10^{-3} μ-curie/cc at Station 130, are minimum values. The actual cloud concentrations could easily be one or two orders of magnitude higher. It should be noted that even the minimum values are many times greater than the present AEC tolerance for mixed fission products concentration, which is 10^{-9} μ-curie/cc.

5.1.2 Activity as a Function of Particle Size

The percentage of the total activity and the relative specific activities of three size fractions of the fall-out material are summarized in Table 5.3.

TABLE 5.3

Summary of Activity vs Particle Size

Size of Fraction (μ)	Surface Shot		Underground Shot	
	Activity (%)	Activity per Unit Weight	Activity (%)	Activity per Unit Weight
0 - 2	0 - 1	0 - 0.1	0.5 - 1	6 - 10
2 - 20	0 - 6	0 - 0.3	2 - 5	3 - 6
> 20	93 - 100	0.01 - 2.0	94 - 96	9 - 12

Obviously the bulk of the activity of the fall-out material is contained in the greater-than-20 μ size fraction. It was observed in the surface shot samples that the bulk of the activity in the >20 μ fraction could be traced to a few large glassy particles as shown in Sections 4.1.3, 4.1.4, 4.2.1, and 4.2.2. Even though the spread of particle sizes of the active material was greater in the underground shot samples, the active particles still represented a small fraction of the total collection. (See Section 4.1.4.1.)

Measurements on the activity per unit weight are given in arbitrary units because they are only useful for comparison. It is noted that for the underground shot these activities are all of the same order of magnitude.

Since the total amount of material collected during the surface shot was small, the reliability of the measurements made is not as good as that for the underground shot.

5.1.3 Composition of Fall-out Material and Correlation with Source Material

Although it is difficult to summarize the results presented in Section 4.1.4 in more concise form, certain general conclusions may be presented.

Both the particle size and the composition of the gross fall-out samples are remarkably similar to the original materials. Analyses of the results indicate that little fracturing of soil grains occurred. It appears that the diminishing median size as a function of distance from zero (Section 4.2.2) is due mainly to sedimentation rather than the fracturing of larger particles.

The radioactive fall-out material apparently consisted solely of glassy spheres and glassy grains. The glassy particles were intensely radioactive. Only one or two accounted for all the radioactivity on some of the surface shot DFO sectors.

The elemental composition of the radioactive particles was identical to that of the parent soil with the exception of carbon and boron whose compounds are easily volatilized as compared to compounds of the other elements present. Apparently, the radioactive material was formed by an intimate mixing of fission products and vaporized material. There were indications that the mixing was not homogeneous insofar as fission products were concerned. The following observations during the analysis of the fall-out samples substantiate the possibility of inhomogeneous mixing:

1. Gross decay curves of samples from different stations were not identical.

2. The ratio of radioactivity measurements with and without absorbers were widely different from station to station, and from sector to sector in the individual DFO collectors.

3. Radiochemical analyses of the three fall-out size fractions show different ratios of fission products in the fractions, particularly for Zr, Ba, and Ru.

In comparing these data with those from air bursts, it seems that the particle size of the radioactive material may depend primarily on the concentration of source material in the fireball, and secondarily on its particle size. At Operation GREENHOUSE the concentration of source material was much smaller than at this operation, and the particle sizes were also smaller. Further, some of the radioactive fall-out material at GREENHOUSE consisted of coarse inert coral grains which had been swept into the cloud and upon which small radioactive spheres had adhered.[1] Upon such evidence the particle size of the soil involved at this operation could be expected to affect the size of the active airborne material. This secondary effect was, however, not observed.

5.1.4 Fall-out Distribution

5.1.4.1 Time Distribution

The results of the time distribution of fall-out studies seem erratic at first glance. It is regrettable that mechanical difficulties and timing circuit failures resulted in poor coverage. However, the two collections from the surface shot and the five from the underground shot, yield certain conclusions regarding fall-out.

The first heavy wave of fall-out on the surface shot arrived at Stations 29 and 33 sometime between 8 and 10 min after shot time. To arrive at that time the material must have been transported by the high velocity winds aloft. A second wave which arrived at Station 29 approximately 60 min after shot time was not detected at Station 33.

A well-defined heavy fall-out was experienced in the first few minutes following the underground shot. The fall-out on areas near the shot probably originated from material in the lower part of the stem of the cloud, in the base surge, and from throw-out. This

---

[1] C. E. Adams, F. R. Holden, and N. R. Wallace, "Fall-out Phenomenology", Greenhouse Report, Annex 6.4.

fall-out started almost immediately after the shot and persisted for approximately 5 to 10 min.

The fall-out which occurred at more distant areas probably originated from material in the higher regions of the cloud, which was rapidly carried afar by the upper winds. This fall-out arrived at a point 3 miles from ground zero in about 7 min, and persisted for about 10 min.

Following the heavy initial fall-out there were repeated minor amounts of fall-out decreasing greatly in quantity and apparently traveling along the ground with the velocity of the surface wind. These minor fall-outs persisted for at least 2 hr following the shot, and probably came in part from material of the earlier heavy fall-out which had been stirred up and carried along by the surface wind.

5.1.4.2 Area Distribution

The area distribution of the fall-out is best given by Figs. 4.20 and 4.22, which show the radiation fields, and by Figs. 4.23 and 4.24, which show the mass distribution of material, after the surface and underground shots. It seems evident that the up wind and cross wind dimensions near ground zero are determined by the extent of base surge, and the down wind pattern by the wind profile at and following time zero.

In the surface explosion, the bulk of the activity was found associated with glass spheroids. At stations close to ground zero larger spheroids predominated, while at remote stations they were smaller and more numerous. The direct relationship of frequency with distance, and the inverse relationship of size with distance, were most pronounced.

In contrast, the activity resulting from the underground explosion was found distributed throughout the gross fall-out. The radioactive particles could not be distinguished visually except for some partially fused rocks and large clinkers found near ground zero. Some of these clinkers were several inches long. The size fraction containing the greatest percentage of activity was dependent on the location of the collector since activity was found in all particle sizes and the percentage weight of any size fraction was a function of its distance from ground zero. Thus at the station 4,000 yd north of ground zero, 40 per cent of the over-all activity was found in the fraction of 74 μ and under (Fig. 4.30), while at the station 300 yd from ground zero less than 1 per cent of the over-all activity was found in the fraction $\gtrless$ 74 μ.

The specific activity for the surface explosion increased with distance out to the limits of the experimental array. This increase indicated the influence of the larger number of small spheroids at distant stations compared to the smaller number of large fused particles close to ground zero. Although the specific activity increased with distance, the total activity at any one station decreased with distance. Therefore, the larger quantity of fall-out at short distances overwhelmed the higher specific activity at distant stations.

For the underground explosion, the specific activity also increased with distance from ground zero. However, for both shots the rate of increase was slight beyond 2,500 yd.

The stations located 300 yd from ground zero, in both the surface and underground explosions, had by far the highest percentage of total fall-out along with the lowest specific activities. Apparently there was very little mixing of radioactive particles and inert soil at these close stations.

Several isolated areas of heavy fall-out can be located on Figs. 4.27 and 4.28 for surface and underground explosions, respectively. These areas indicate true fall-out with specific activities much higher than those found at the 300 yd stations.

5.2 CONCLUSIONS

1. The median particle diameter of the gross airborne material was measured as approximately 0.2 μ.
2. The median particle diameter of the radioactive particles was measured as approximately 1.4 μ.
3. The 0 to 8 μ fraction contributed at least 2×10^{-5} μ-curie/cc to the airborne radioactivity concentrations.
4. The bulk of the radioactivity was contained in the larger than 20 μ diameter particles.
5. Inhomogeneity in radiochemical content was noted in the fall-out collection.
6. Size distribution and mineral content of the fall-out material were similar to that of the parent material with the size distribution varying with distance from zero.
7. The radioactive particles were observed to be glassy and have the same elemental composition as the soil except that boron and carbon were missing.
8. The time distribution studies showed heavy initial concentrations transported by high altitude winds followed by several secondary waves of material transported by surface winds.

9. Area distributions were found to be determined by the extent of the base surge and the wind profile.

5.3 RECOMMENDATIONS

The following recommendations are offered for those who may undertake similar investigations in the future:

1. For size-frequency distribution studies, instruments which discriminate against the larger particle sizes are preferable to those which discriminate against smaller particle sizes. For size-weight distribution studies, the reverse is true.
2. Since the actual particle concentrations are low, high volume samplers are indicated for better statistical sampling.
3. Since it is impossible to collect the entire particle size spectrum with one instrument, it is suggested that the radioactivity concentrations contributed by the smaller particle sizes (less than 5 μ) be investigated since these are more important in investigating inhalation hazards and decontamination problems.
4. A more rugged differential fall-out collector which is cheap and simple enough to allow wide coverage should be developed.
5. The sampling of airborne particles by means of ground based sampling stations is extremely inefficient because of the large number of instruments and man hours needed for good coverage. A more reasonable approach would use a remote controlled airborne sampler which could be directed into the cloud after it is formed and thereby guarantee a collection. In this way, expensive instruments and manpower would not be wasted on stations not yielding useful information. Development of a sampler which can be transported in a small guided missile is suggested since large drone aircraft are too cumbersome. Even though the individual instrument cost would be higher, the price per usable sample would be much lower and manpower would be conserved.

APPENDIX A

PERSONNEL LOGISTICS

A.1 ROSTER OF PERSONNEL

A project of this magnitude requires the services of a large number of personnel of diversified skills. The following list is an attempt to credit all the people who took part in this work. The task could not have been accomplished without each contribution.

U. S. Naval Radiological Defense Laboratory.

C. E. Adams, Chemist, Chemical Physics Branch. Supervision of fall-out analysis. Preparation of the section on time distribution of fall-out. Petrographic survey of fall-out material.

T. H. Anderson, Chemist, Research Engineering Branch. X-ray diffraction analysis.

D. W. Berte, Electronics Engineer, Instruments Branch. Design of differential fall-out counting equipment.

M. Brownell, Toolmaker, Shops Branch. Fabrication of successful prototype of thermal precipitator. Inspection of production models.

W. Buser, Machinist, Shops Branch. Progress of instrument fabrication. On-site repairs.

H. Chan, Chemist, Applied Research Branch. Analysis of fall-out samples.

P. A. Covey, Electronics Engineer, Instruments Branch. Fabrication of gas flow proportional chamber and counting apparatus.

E. C. Evans, III, Physicist, Chemical Physics Branch. Supervision of on-site operations.

N. H. Farlow, Chemist, Chemical Physics Branch. Participated in aerosol sampler development, on-site installation and calibration of instruments, and fall-out analysis.

F. A. French, Chemist, Chemical Physics Branch. Participated in on-site instrument installation and calibration.

T. C. Goodale, Chemist, Assistant Chief, Chemical Physics Branch. Participated in on-site operations.

A. E. Greendale, Chemist, Nuclear and Physical Chemistry Branch. Preparation of gross decay curves from fall-out material.

P. Harris, Microscopist, Research Engineering Branch. Preparation of electron micrographs.

J. W. Hendricks, Mathematician, Chemical Physics Branch. On-site instrument installation and calibration.

M. Honma, Chemist, Analytical and Standards Branch. Spectrochemical analysis of soil and fall-out samples.

S. K. Ichiki, Physicist, Chemical Physics Branch. On-site instrumentation. Preparation of section on size distribution of radioactive particles.

W. Imhoff, Physicist, Chemical Physics Branch. Participated in particle size analysis of aerosol samples.

P. D. LaRiviere, Physicist, Chemical Physics Branch. Supervision of particle radioautography. On-site instrument installation and calibration.

R. Laurino, Chemist, Military Evaluations Branch. Participation in on-site and laboratory phases of fall-out study.

F. Mason, Mechanical Engineer, Design Branch. Supervision of engineering design of sampling instruments.

N. Morabe, Materials Branch. On-site materiel procurement.

J. D. O'Connor, Chemist, Analytical and Standards Branch. Spectrochemical analysis of soil and fall-out samples.

J. N. Pascual, Chemist, Analytical and Standards Branch. Exchange capacity determinations on soil samples.

W. W. Perkins, Chemist, Applied Research Branch. Analysis of fall-out samples.

I. G. Poppoff, Physicist, Chemical Physics Branch. Technical coordinator. Design and development of aerosol sampler and differential fall-out collector. Preparation of Chapters 1, 2, 3, and 5 of this report.

J. T. Quan, Chemist, Chemical Physics Branch. On-site instrument installation and calibration. Participation in particle size analysis.

E. A. Schuert, Physicist, Applied Research Branch. Development of fall-out trays. On-site instrumentation. Preparation of fall-out distribution portion of this report.

J. A. Seiler, Chemist, Analytical and Standards Branch. Radiochemical analysis.

W. Shipman, Chemist, Analytical and Standards Branch. Radiochemical analysis of fall-out samples.

R. R. Soule, Physicist, Applied Research Branch. Design and development of fall-out trays. Participation in on-site operations. Co-author of fall-out distribution section of this report.

H. Steiner, Physicist, Chemical Physics Branch. Calibration of differential fall-out counting apparatus.

N. Vogel, Mechanical Engineer, Shops Branch. Supervision of fabrication of field instruments.

N. R. Wallace, Physicist, Chemical Physics Branch. Development of differential fall-out collector. On-site instrumentation. Preparation of section on activity as a function of particle size.

J. W. Washkuhn, Industrial Hygienist, Chemical Physics Branch. Supervision of analysis of soil samples. On-site instrumentation. Preparation of section on identification of collected material and correlation with source material for this report.

J. P. Wittman, Physicist, Chemical Physics Branch. On-site instrument installation and calibration. Radioactivity measurements on differential fall-out.

J. V. Zaccor, Physicist, Chemical Physics Branch. Thermal precipitator development. On-site instrumentation. Preparation of section on size distribution of gross samples for this report.

University of California

I. Barshad, Division of Soils. Differential thermal analysis of clay fraction of soil. Assistance in the interpretation of other data on clay fraction.

PROJECT 2.5a-2

California Department of Public Health

L. Schmelzer, Chemist, Bureau of Adult Health. X-ray diffraction analysis of clay fraction of soil samples.

U. S. Geological Survey

A. M. Piper, Geologist, Portland, Oregon, Office. Data on caliche layer at site.

J. L. Poole, Geologist, Carson City, Nevada, Office. Soil sample collection.

U. S. Army Corps of Engineers

C. B. Palmer, J. G. Zeitlen, C. E. Bettinger, and C. V. McNicol, South Pacific Division Laboratory. Physical, chemical, and petrographic analysis of soil samples.

PROJECT 2.5a-2

APPENDIX B

GRAPHS (PARTICLE DIAMETER VS PER CENT LESS THAN STATED SIZE)

B.1 SIZE FREQUENCY DISTRIBUTIONS OF GROSS SAMPLES FOR INDIVIDUAL STATIONS

These graphs supplement Section 4.1.1. (See Figs. B.1 to B.9.)

B.2 SIZE FREQUENCY DISTRIBUTION OF RADIOACTIVE SAMPLES FOR INDIVIDUAL STATIONS

These graphs supplement Section 4.1.2. (See Figs. B.10 to B.13.)

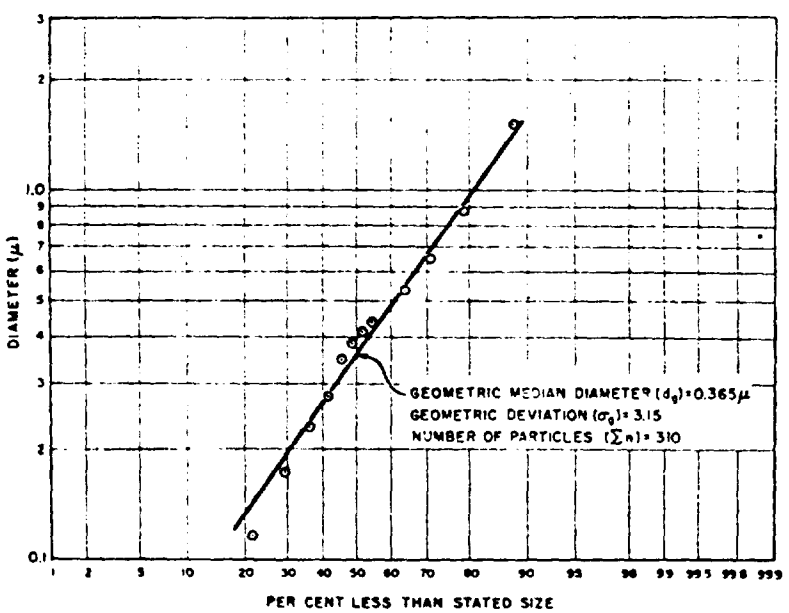

Fig. B.1 Thermal Precipitator Collection, Electron Microscope Analysis, Station 108

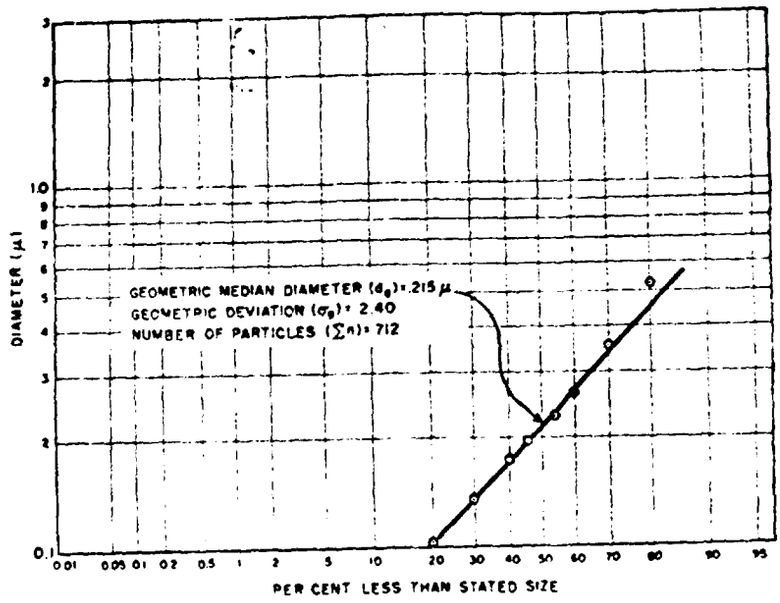

Fig. B.2 Thermal Precipitator Collection, Electron Microscope Analysis, Station 12

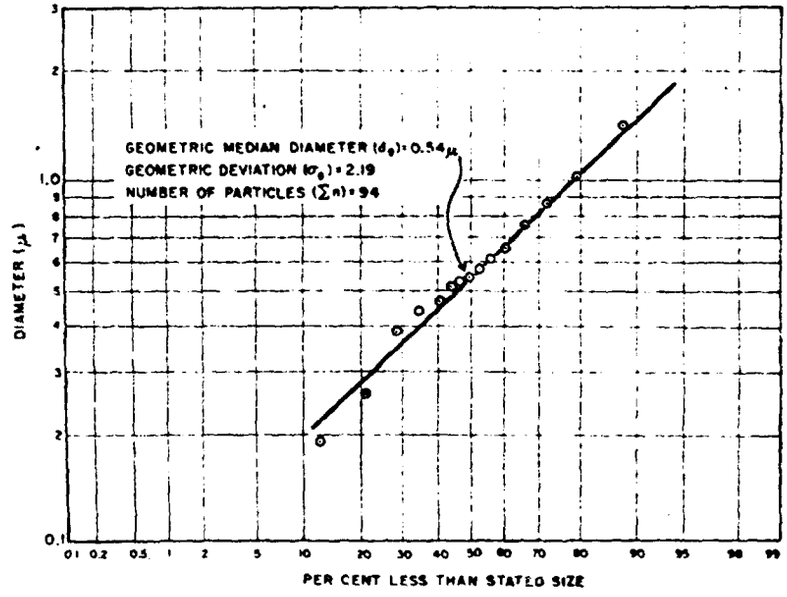

Fig. B.3 Thermal Precipitator Collection, Electron Microscope Analysis, Station 121

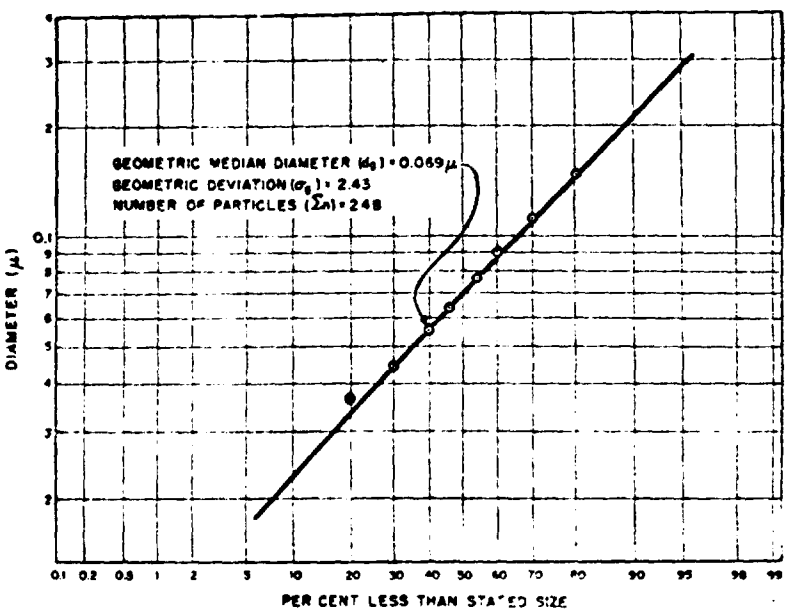

Fig. B.4 Thermal Precipitator Collection, Electron Microscope Analysis, Station 134

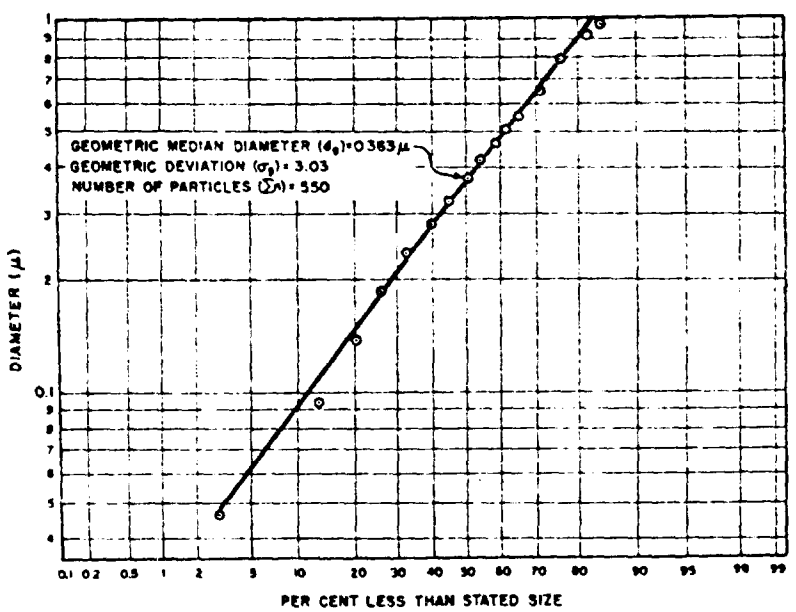

Fig. B.5 Differential Fall-out Collection, Electron Microscope Analysis, Station 103, Segment 16

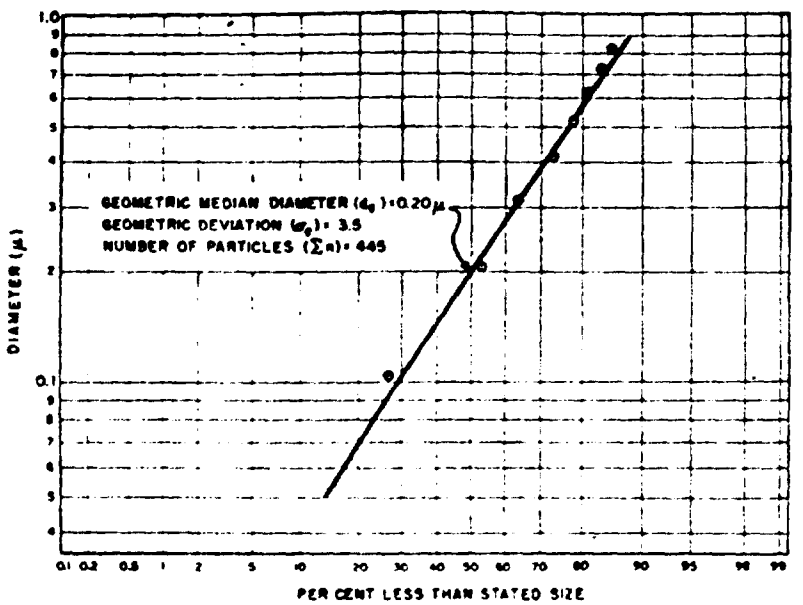

Fig. B.6 Differential Fall-out Collection, Electron Microscope Analysis, Station 108, Segment 17

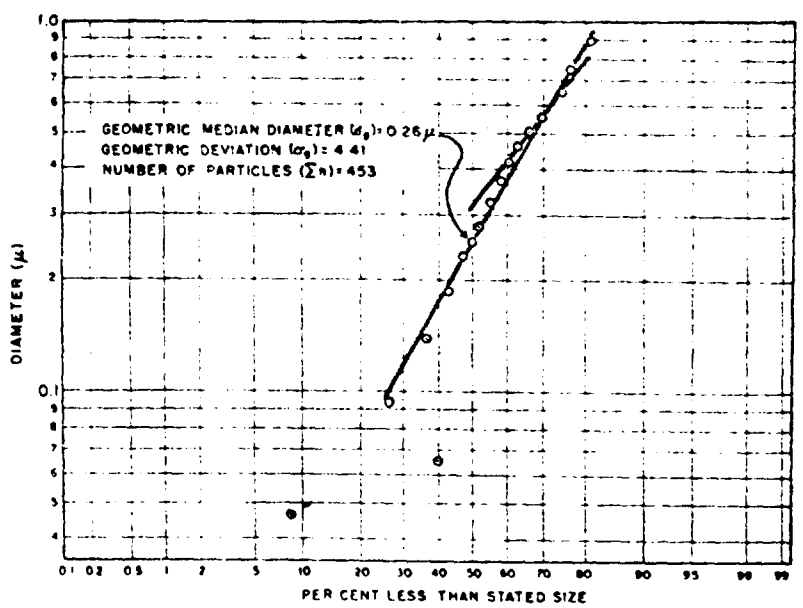

Fig. B.7 Differential Fall-out Collection, Electron Microscope Analysis, Station 109, Segment 5

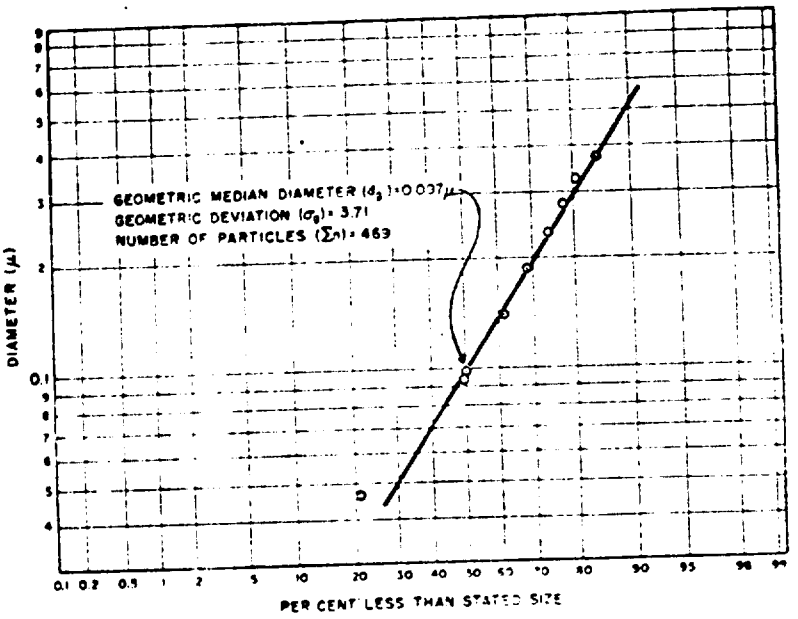

Fig. B.8 Differential Fall-out Collection, Electron Microscope Analysis, Station 120, Segment 2

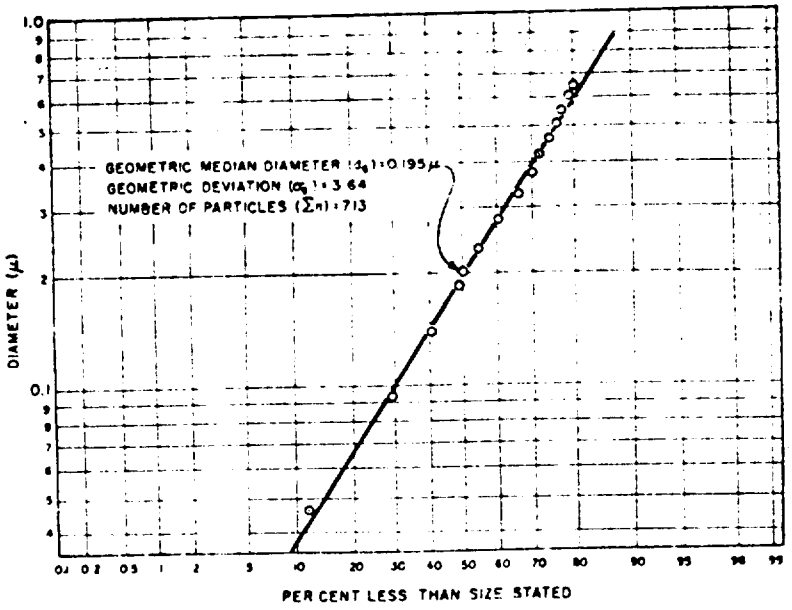

Fig. B.9 Differential Fall-out Collection, Electron Microscope Analysis, Station 120, Segment 13

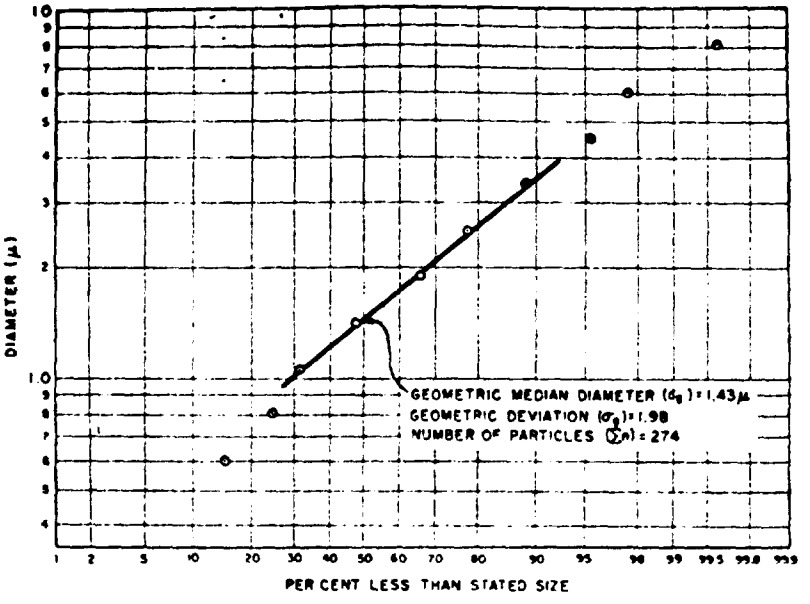

Fig. B.10 Size Distribution of Radioactive Particles, Station 108

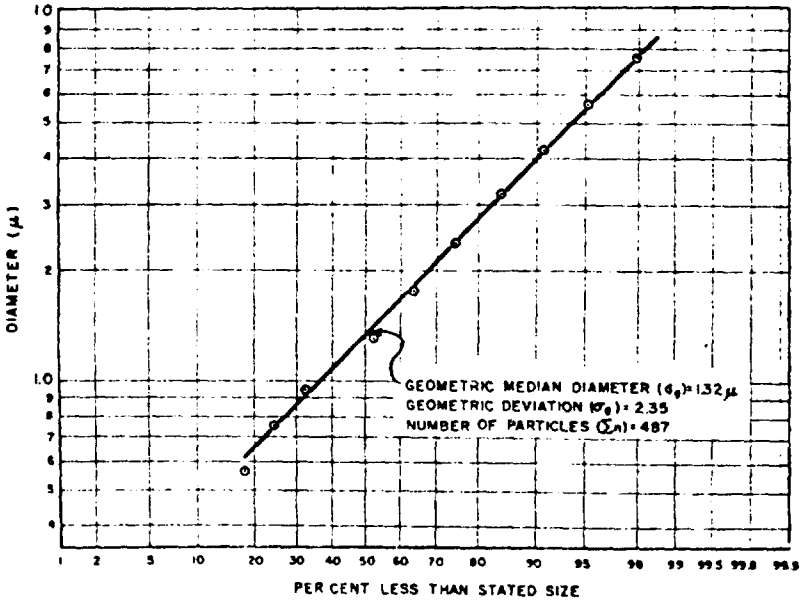

Fig. B.11 Size Distribution of Radioactive Particles, Station 120

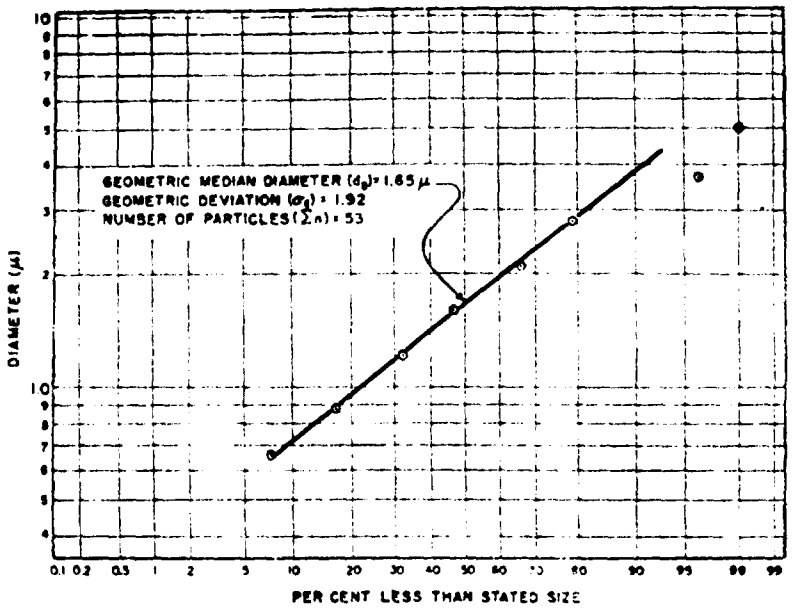

Fig. B.12 Size Distribution of Radioactive Particles, Station 129

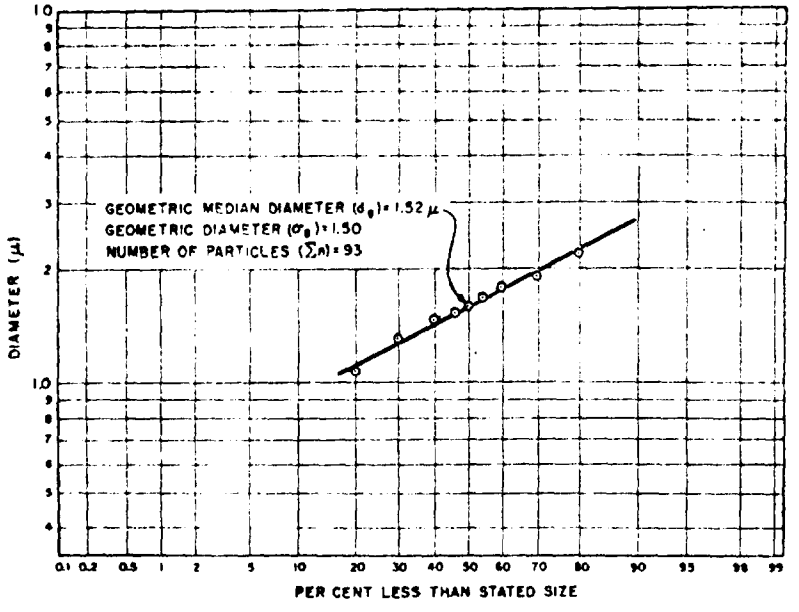

Fig. B.13 Size Distribution of Radioactive Particles, Station 130

APPENDIX C

ADDITIONAL SOIL ANALYSIS

C.1 EXPLANATION

The following soil analyses were made to characterize more fully the soil at the Yucca Flat test site. These tests supplement those discussed in Section 4.1.4.

C.1.1 Physical Tests

Atterberg Limits. Liquid and plastic limits were determined in general accordance with the A.S.T.M. Designations D423-39, "Standard Method of Test for Liquid Limit of Soils", and D424-39, "Standard Method of Test for Plastic Limit and Plasticity Index of Soils".

Specific Gravity. This was found by the pycnometer method, using evacuation to free the soil of adsorbed air.

Compaction. Since the soils were non-plastic, it was considered acceptable to test the materials in an air-dry condition as a measure of their behavior. Both the maximum and minimum densities were obtained on the material passing through a No. 4 sieve. For maximum density determinations, the soil was compacted into a 1/30-cu ft mold (4 in. in diameter) by twenty-five blows of a 10 lb-hammer dropped 18 in. on to each of five layers in the mold. The striking face of the hammer was 3.875 in. in diameter so that the soil was confined during the compaction. The minimum densities were found by pouring the soil loosely into the same mold with no compaction.

Field Moisture Equivalent. This was determined by the method given in A.S.T.M. Designation D425-39, "Standard Method of Test for Field Moisture Equivalent of Soils".

Centrifugal Moisture Equivalent. The method used was that given in A.S.T.M. Designation D425-39, "Standard Method of Test for Centrifuge Moisture Equivalent of Soils".

Field Density. The density was determined on a small piece of caliche by the "waxed chunk" method in which the soil chunk is waterproofed with a coating of wax and then weighed in water to determine its volume. After removing the wax, the material is oven dried and its dry weight per unit volume determined. The field density of the caliche was 100 lb per cu ft and its moisture content was 2.9 per cent.

The physical test results are summarized in Table C.1.

TABLE C.1

Physical Test Results of Pre-test Soil Samples at the Underground Site

Sample	Liquid Limit Per Cent	Plasticity[a] Index	Specific Gravity -4 Mesh	Compaction Min.	Compaction Max.	Moisture Equivalent Per Cent Field	Moisture Equivalent Per Cent Centrifugal
0-3 in.	21 (Plastic Limit = 22)	0	2.60	79 (Air-dry Moisture = 1.5%)	106	21	4.6
5-6 ft	20 (Plastic Limit = 21)	0	2.59	76	104	21	6.4
17 ft	Unobtainable (Non-plastic)		2.61	92 (Air-dry Moisture = 1.2%)	117	22	5.0

(a) As defined in A.S.T.M. Designations D424-39, "Standard Method of Test for Plastic Limit and Plasticity Index of Soils".

The liquid limit, plastic limit and plasticity index values indicate that the soil is either non-plastic or just barely plastic. The moisture equivalent values indicate that the moisture holding capacity is quite low. The compaction values indicate that the soil, as it exists in the field (with the exception of the caliche material), is not in a compacted condition.

C.1.2 Chemical Tests

Base-exchange Capacity. The capacity was determined on soil samples from the 0 to 3-in., 5 to 6-ft, and 17-ft levels from the underground shot site and on a caliche sample from the Operation BUSTER site. The samples were crushed to pass a No. 30 sieve and the analyses made according to the method of the American Association of Agricultural

Chemists.[1] In their method, the sample is saturated with ammonium acetate solution followed by an alcohol wash. The sample is then transferred to a distillation flask and distilled in the presence of sodium hydroxide, the ammonia distillate is received in HCl with methyl orange indicator. When distillation is complete, the solution is made distinctly alkaline with NaOH and back-titrated to the first yellow with HCl.

Exchange capacity was also determined on the less than 2 μ fraction and on the sand fraction of soil from the 17-ft level of the underground shot site. The less than 2 μ fraction was prepared as previously described under the X-ray diffraction and dehydration curve paragraphs. The sand fraction was prepared as follows: the total soil sample was placed in a casserole with water and triturated with the thumbs to free the sand from adhering silt and clay. The suspended silt and clay was removed by decantation. Trituration and decantation were repeated until the sand was free of silt and clay.

The exchange capacity of the less than 2 μ and the sand fractions were determined by Peech's method.[2] In this method the sample is leached with ammonium acetate solution followed by an alcohol wash. The sample is then transferred to a Kjeldahl flask and distilled. The distillate is received in standard acid with methyl red indicator and the excess acid titrated with sodium hydroxide.

The values obtained for exchange capacity were somewhat unusual for a sandy textured soil of this type. (See Table C.2.) In general, base exchange capacity is usually associated with the clay (less than 2 μ) fraction of soil. In this instance the exchange capacity of the sand fraction can probably be assigned to the weathered feldspars. The exchange capacity of the less than 2 μ fraction is probably essentially due to the hydrous mica and the weathered feldspars.

Chemical Analyses. These analyses were made by methods of the American Association of Agricultural Chemists.[3] The results are reported on the material passing a No. 4 sieve with the exception of the caliche sample where the total sample was used. The silica, iron, and aluminum were determined on fused samples and are reported as per cent of

---

[1] Official and Tentative Methods of Analysis of the Association of Official Agricultural Chemists (6th ed; Washington: Association of Official Agricultural Chemists, 1945).

[2] Michael Peech, "Determination of Exchangeable Cations and Exchange Capacity of Soils - Rapid Micromethods Utilizing Centrifuge and Spectrophotometer", Soil Science LIX (1945), 25-38.

[3] Op. cit.

TABLE C.2

Base Exchange Capacity

Sample	Exchange Capacity in Milli-equivalents NH_4/100 g of Sample
0 to 3-in. (crushed to pass through a 0.590 mm mesh)	24
5 to 6-ft (crushed to pass through a 0.590 mm mesh)	23
17-ft (crushed to pass through a 0.590 mm mesh)	18
Caliche (crushed to pass through a 0.590 mm mesh)	15
Sands (2.0 to 0.002 mm)	49.2
Less than 2 μ	41.3

dry weight of soil. The carbonates and organic carbon were determined on material crushed to pass a No. 100 sieve and the results are reported as per cent of dry weight.

The composition of the pre-test soil samples as obtained by chemical analysis is given in Table C.3.

TABLE C.3

Chemical Analysis of Pre-test Soil Samples

Component	Sample			
	0 to 3 in.	5 to 6 ft	Caliche	17 ft
Silica %	68.8	65.2	47.7	69.6
Fe and Al Oxides (R_2O_3) %	17.1	16.8	9.8	16.1
Iron Oxide (Fe_2O_3) %	2.9	3.0	2.0	(a)
Total Carbonates %	0.55	2.92	19.17	1.00
Organic Carbon %	0.16	(a)	(a)	(a)

(a) Not determined.

APPENDIX D

FALL-OUT DISTRIBUTION DATA SHEETS

D.1 EXPLANATION

The first letter in the station designator indicates the type of explosion, S and U for surface and underground, respectively. The remainder of the designator locates the station with respect to ground zero (Fig. 3.1).

The values of activity and activity per unit weight have been rounded off to two significant figures.

STATION S-D-1

Size of Fraction (μ)	Weight of Fraction (g)	Percentage of Total Weight	Activity (c/m)	Activity per Unit Weight (c/m/g)
5600 and over	50.7	6.05	0	0
5180	19.2	2.29	0	0
4040	36.2	4.32	1,600	45
2845	19.6	2.34	0	0
2006	17.4	2.07	140,000	7,600
1420	11.2467	1.34	13,000	1,200
1015	12.2000	1.45	27,000	2,200
715	11.6341	1.39	20,000	1,800
503	17.5224	2.09	12,000	700
356	43.8799	5.23	0	0
250	90.4	10.78	20,000	220
175	163.4	19.49	12,000	75
125	141.2	16.84	0	0
90	94.0	11.21	10,000	110
74 and under	109.7	13.08	9,000	84
Totals	834.4	100	2.77×10^5	Average Activity per Unit Weight 3.3×10^2

STATION S-E-2

Size of Fraction (μ)	Weight of Fraction (g)	Percentage of Total Weight	Activity (c/m)	Activity per Unit Weight (c/m/g)
5600 and over	37.9344	11.68	0	0
5180	10.0736	3.10	0	0
4040	16.2792	5.01	320	20
2845	13.4892	4.15	0	0
2006	8.9508	2.76	68	8
1420	7.0307	2.17	4,700	640
1015	5.8228	1.79	4,300	750
715	4.8688	1.50	780	160
503	5.5238	1.70	1,000	190
356	7.4143	2.28	750	100
250	12.6942	3.91	2,300	180
175	21.5552	6.64	2,900	130
125	36.7063	11.30	2,300	73
90	37.4725	11.54	0	0
74 and under	98.8966	30.46	0	0
Totals	324.7	100	2×10^4	Average Activity per Unit Weight 61

STATION S-E-3

Size of Fraction (μ)	Weight of Fraction (g)	Percentage of Total Weight	Activity (c/m)	Activity per Unit Weight (c/m/g)
5600 and over	85.3508	4.68	0	0
5180	26.1658	1.43	600	23
4040	41.0856	2.25	0	0
2845	30.4581	1.67	0	0
2006	27.9737	1.53	0	0
1420	24.1475	1.32	0	0
1015	33.3190	1.83	1,600	49
715	50.6013	2.77	0	0
503	100.0645	5.49	2,800	28
356	165.3572	9.07	104,000	630
250	220.4256	12.09	17,000	80
175	324.7897	17.81	46,000	140
125	259.4	14.22	10,000	40
90	215.9	11.84	0	0
74 and under	166.7	9.14	5,000	30
Totals	1,823.7	100	1.92×10^5	Average Activity per Unit Weight 1.05×10^2

STATION S-F-1

Size of Fraction (μ)	Weight of Fraction (g)	Percentage of Total Weight	Activity (c/m)	Activity per Unit Weight (c/m/g)
5600 and over	26.1	5.95	0	0
5180	9.4	2.14	300	32
4040	13.6	3.10	390	28
2845	8.7	1.98	1,400,000	160,000
2006	6.5606	1.49	3,800,000	570,000
1420	6.2968	1.44	4,500,000	720,000
1015	6.8677	1.57	3,700,000	540,000
715	6.1773	1.41	2,200,000	410,000
503	8.6389	1.97	700,000	81,000
356	19.1641	4.37	320,000	16,000
250	48.3806	11.03	150,000	3,200
175	68.3316	15.58	75,000	1,100
125	85.5	19.49	54,000	630
90	51.8814	11.83	29,000	560
74 and under	73.0264	16.65	71,000	980
Totals	438.6	100	1.72×10^7	Average Activity per Unit Weight 3.92×10^4

STATION S-F-3

Size of Fraction (μ)	Weight of Fraction (g)	Percentage of Total Weight	Activity (c/m)	Activity per Unit Weight (c/m/g)
5600 and over	9.7	30.98	1,300,000	140,000
5180	1.6576	5.29	0	0
4040	1.9642	6.27	580,000	150,000
2845	1.5429	4.93	230,000	150,000
2006	1.3747	4.39	1,100,000	820,000
1420	1.2353	3.95	880,000	710,000
1015	1.2171	3.89	870,000	710,000
715	1.2200	3.90	1,100,000	920,000
503	1.0232	3.27	670,000	650,000
356	1.1362	3.63	87,000	77,000
250	1.3621	4.35	54,000	40,000
175	1.8060	5.77	28,000	15,000
125	1.7851	5.70	22,000	12,000
90	1.3854	4.42	9,700	7,000
74 and under	2.8994	9.26	17,000	6,000
Totals	31.3	100	7.2×10^6	Average Activity per Unit Weight 2.27×10^5

PROJECT 2.5a-2

STATION S-G-1

Size of Fraction (μ)	Weight of Fraction (g)	Percentage of Total Weight	Activity (c/m)	Activity per Unit Weight (c/m/g)
5600 and over	0	0	0	0
5180	0	0	0	0
4040	1.5404	7.39	280,000	180,000
2845	0.6130	2.94	170,000	280,000
2006	0.8026	3.85	480,000	600,000
1420	0.7123	3.42	190,000	280,000
1015	0.7100	3.41	190,000	280,000
715	0.8810	4.23	150,000	180,000
503	1.5185	7.59	76,000	50,000
356	2.2285	10.69	26,000	12,000
250	2.9976	14.38	23,000	7,800
175	2.9925	14.36	14,000	4,900
125	2.3726	11.38	10,000	4,500
90	1.4174	6.80	5,400	3,800
74 and under	2.0566	9.87	8,000	3,900
Totals	20.8	100	1.7×10^6	Average Activity per Unit Weight 8.16×10^4

STATION S-G-3

Size of Fraction (μ)	Weight of Fraction (g)	Percentage of Total Weight	Activity (c/m)	Activity per Unit Weight (c/m/g)
4040 and over	2.7480	1.07	510,000	180,000
2845	1.3618	0.53	790,000	580,000
2006	1.4744	0.57	2,600,000	1,700,000
1420	1.6545	0.64	1,300,000	810,000
1015	2.2714	0.88	1,700,000	760,000
715	3.5772	1.39	2,500,000	700,000
503	9.1523	3.56	2,000,000	220,000
356	26.4	10.26	740,000	28,000
250	59.3	23.05	72,000	1,200
175	64.7	25.15	62,000	970
125	44.3	17.22	65,000	1,400
90	19.3	7.50	31,000	1,600
74 and under	20.5	7.97	72,000	3,500
Totals	257.3	100	1.27×10^7	Average Activity per Unit Weight 4.94×10^4

PROJECT 2.5a-2

STATION S-H-1

Size of Fraction (μ)	Weight of Fraction (g)	Percentage of Total Weight	Activity (c/m)	Activity per Unit Weight (c/m/g)
4040 and over	0.3453	9.49	180,000	530,000
2845	0.1899	5.22	290,000	1,500,000
2006	0.4848	13.33	230,000	490,000
1420	0.2042	5.61	310,000	1,500,000
1015	0.2128	5.85	300,000	1,400,000
715	0.1653	4.54	260,000	1,600,000
503	0.0682	1.88	46,000	680,000
356	0.0887	2.44	29,000	320,000
250	0.1526	4.20	18,000	110,000
175	0.2516	6.92	9,000	37,000
125	0.3824	10.51	6,000	17,000
90	0.3343	9.19	3,000	8,000
74 and under	0.7569	20.81	5,000	6,000
Totals	3.6	100	1.7×10^6	Average Activity per Unit Weight 4.72×10^5

STATION S-H-2

Size of Fraction (μ)	Weight of Fraction (g)	Percentage of Total Weight	Activity (c/m)	Activity per Unit Weight (c/m/g)
4040 and over 2845 2006 1420 1015 715 503 356 250 175 125 90 74 and under	THIS STATION NOT RECOVERED			
Totals				Average Activity per Unit Weight

PROJECT 2.5a-2

STATION S-H-3

Size of Fraction (μ)	Weight of Fraction (g)	Percentage of Total Weight	Activity (c/m)	Activity per Unit Weight (c/m/g)
4040 and over	0.5239	6.70	230,000	450,000
2845	0.4744	6.06	680,000	1,400,000
2006	1.0537	13.48	1,100,000	1,100,000
1420	0.8938	11.43	970,000	1,000,000
1015	0.8816	11.28	1,400,000	1,500,000
715	0.8381	10.72	1,400,000	1,600,000
503	0.5475	7.00	1,100,000	2,000,000
356	0.2237	2.86	430,000	1,800,000
250	0.2918	3.73	55,000	180,000
175	0.4073	5.21	29,000	70,000
125	0.5305	6.79	18,000	34,000
90	0.4116	5.27	11,000	26,000
74 and under	0.7376	9.44	18,000	25,000
Totals	7.8	100	7.6×10^6	Average Activity per Unit Weight 9.71×10^5

STATION S-H-5

Size of Fraction (μ)	Weight of Fraction (g)	Percentage of Total Weight	Activity (c/m)	Activity per Unit Weight (c/m/g)
4040 and over	0.0409	1.28	0	0
2845	0.0773	2.43	96,000	1,200,000
2006	0.2045	6.42	220,000	1,100,000
1420	0.2024	6.36	210,000	1,000,000
1015	0.2297	7.21	190,000	840,000
715	0.2587	8.13	300,000	1,100,000
503	0.2663	8.36	33,000	120,000
356	0.2618	8.22	130,000	520,000
250	0.2677	8.41	70,000	260,000
175	0.2741	8.61	21,000	75,000
125	0.3315	10.41	10,000	30,000
90	0.2366	7.43	4,000	18,000
74 and under	0.5322	16.72	6,000	11,000
Totals	3.2	100	1.3×10^6	Average Activity per Unit Weight 4.14×10^5

PROJECT 2.5a-2

STATION S-I-1

Size of Fraction (μ)	Weight of Fraction (g)	Percentage of Total Weight	Activity (c/m)	Activity per Unit Weight (c/m/g)
4040 and over	0.3326	11	0	0
2845	0.0227	.80	0	0
2006	0.0935	3.31	103,000	1,000,000
1420	0.0867	3.07	41,000	470,000
1015	0.0765	2.71	51,000	660,000
715	0.0818	2.90	79,000	970,000
503	0.0517	1.83	25,000	490,000
356	0	0	0	0
250	0.1270	4.50	2,500	19,000
175	0.2132	7.55	2,200	10,000
125	0.3987	14.12	830	2,800
90	0.3685	13.05	500	1,400
74 and under	0.9710	34.38	970	1,000
Totals	2.8	100	3.06×10^5	Average Activity per Unit Weight 1.08×10^5

STATION S-I-3

Size of Fraction (μ)	Weight of Fraction (g)	Percentage of Total Weight	Activity (c/m)	Activity per Unit Weight (c/m/g)
4040 and over	0.9732	11.38	400,000	410,000
2845	0.9269	10.84	260,000	280,000
2006	1.3433	15.71	1,200,000	920,000
1420	1.2578	14.71	900,000	710,000
1015	1.1453	13.40	1,300,000	1,100,000
715	0.8925	10.44	1,200,000	1,300,000
503	0.3442	4.03	660,000	1,900,000
356	0.2010	2.35	140,000	690,000
250	0.2274	2.66	92,000	400,000
175	0.2576	3.01	58,000	220,000
125	0.3027	2.54	40,000	130,000
90	0.2148	2.51	15,000	71,000
74 and under	0.4618	5.40	23,000	49,000
Totals	8.5	100	6.4×10^6	Average Activity per Unit Weight 7.49×10^5

PROJECT 2.5a-2

STATION S-I-5

Size of Fraction (μ)	Weight of Fraction (g)	Percentage of Total Weight	Activity (c/m)	Activity per Unit Weight (c/m/g)
4040 and over	0	0	0	0
2845	0.0684	2.04	84,000	1,200,000
2006	0.2429	7.24	130,000	530,000
1420	0.2846	8.48	250,000	870,000
1015	0.2614	7.79	370,000	1,400,000
715	0.2371	7.06	370,000	1,500,000
503	0.2444	7.28	260,000	1,000,000
356	0.2739	8.16	320,000	1,100,000
250	0.2423	7.22	49,000	200,000
175	0.2663	7.93	15,000	56,000
125	0.3213	9.57	5,000	17,000
90	0.2537	7.56	2,000	7,900
74 and under	0.6604	19.67	3,000	5,000
Totals	3.4	100	1.9×10^5	Average Activity per Unit Weight 5.66×10^5

STATION S-N-1

Size of Fraction (μ)	Weight of Fraction (g)	Percentage of Total Weight	Activity (c/m)	Activity per Unit Weight (c/m/g)
4040 and over	0.0118	0.78	0	0
2845	0.0063	0.42	0	0
2006	0.0595	3.96	24,000	400,000
1420	0.1038	6.91	150,000	1,400,000
1015	0.1543	10.28	260,000	1,600,000
715	0.2366	15.76	360,000	1,500,000
503	0.2855	19.02	630,000	2,200,000
356	0.1571	10.46	490,000	3,100,000
250	0.0438	2.92	32,000	730,000
175	0.0457	3.04	7,000	150,000
125	0.0782	5.21	4,500	57,000
90	0.0891	5.80	2,000	23,000
74 and under	0.2295	15.29	3,300	14,000
Totals	1.5	100	1.98×10^6	Average Activity per Unit Weight 1.32×10^6

PROJECT 2.5a-2

STATION S-N-3

Size of Fraction (μ)	Weight of Fraction (g)	Percentage of Total Weight	Activity (c/m)	Activity per Unit Weight (c/m/g)
4040 and over	0	0	0	0
2845	0.0614	3.19	25,000	410,000
2006	0.1068	5.54	150,000	1,400,000
1420	0.1655	8.59	170,000	1,000,000
1015	0.2394	12.43	290,000	1,200,000
715	0.2653	13.77	520,000	1,900,000
503	0.2471	12.83	380,000	1,500,000
356	0.0973	5.05	58,000	590,000
250	0.0776	4.03	0	0
175	0.0997	5.18	0	0
125	0.1605	8.33	7,000	45,000
90	0.1400	7.27	3,000	23,000
74 and under	0.2659	13.80	4,000	14,000
Totals	1.9	100	1.6×10^6	Average Activity per Unit Weight 3.42×10^5

STATION S-N-4

Size of Fraction (μ)	Weight of Fraction (g)	Percentage of Total Weight	Activity (c/m)	Activity per Unit Weight (c/m/g)
4040 and over	0.1229	6.38	10,000	81,000
2845	0.1575	8.17	180,000	1,200,000
2006	0.2176	11.29	130,000	610,000
1420	0.3789	19.66	430,000	1,100,000
1015	0.4003	20.77	690,000	1,700,000
715	0.3207	16.64	670,000	2,100,000
503	0.0872	4.52	250,000	2,900,000
356	0.0323	1.68	26,000	800,000
250	0.0316	1.64	20,000	640,000
175	0.0301	1.56	11,000	350,000
125	0.0353	1.83	7,000	180,000
90	0.0288	1.49	3,000	100,000
74 and under	0.0838	4.35	3,000	35,000
Totals	1.9	100	2.5×10^6	Average Activity per Unit Weight 1.28×10^6

PROJECT 2.5a-2

STATION U-D-1

Size of Fraction (μ)	Weight of Fraction (g)	Percentage of Total Weight	Activity (c/m)	Activity per Unit Weight (c/m/g)
4040 and over	1173.3	31.65	340,000,000	290,000
2845	152.5	4.11	40,000,000	260,000
2006	125.2	3.38	1,000,000	8,400
1420	105.9	2.86	9,400,000	89,000
1015	96.2	2.59	7,900,000	82,000
715	87.2	2.35	5,000,000	58,000
503	96.2	2.59	2,700,000	28,000
356	120.1	3.24	3,000,000	25,000
250	179.6	4.84	3,700,000	20,000
175	329.4	8.88	3,900,000	12,000
125	591.9	15.97	5,500,000	11,000
90	336.6	9.08	5,000,000	15,000
74 and under	313.1	8.45	6,000,000	20,000
Totals	3,707.2	100	4.3×10^8	Average Activity per Unit Weight 1.16×10^5

STATION U-D-2

Size of Fraction (μ)	Weight of Fraction (g)	Percentage of Total Weight	Activity (c/m)	Activity per Unit Weight (c/m/g)
4040 and over	8.7477	3.28	0	0
2845	1.1638	0.44	1,500	1,200
2006	1.3789	0.52	1,000	690
1420	1.2351	0.46	1,100	960
1015	1.6954	0.63	1,400	860
715	2.2653	0.85	83,000	37,000
503	3.3673	1.26	63,000	18,000
356	5.9562	2.23	90,000	15,000
250	11.2264	4.20	130,000	11,000
175	22.9	8.58	340,000	14,000
125	52.5	19.66	760,000	14,000
90	50.4	18.88	1,100,000	22,000
74 and under	104.1	38.99	5,800,000	56,000
Totals	267.0	100	8.5×10^6	Average Activity per Unit Weight 3.19×10^4

PROJECT 2.5a-2

STATION U-D-3

Size of Fraction (μ)	Weight of Fraction (g)	Percentage of Total Weight	Activity (c/m)	Activity per Unit Weight (c/m/g)
4040 and over	13.3	11.26	1,000	76
2845	1.8218	1.54	900	480
2006	1.9661	1.66	1,000	520
1420	1.1693	0.99	1,000	1,000
1015	0.6969	0.59	13,000	19,000
715	0.5297	0.45	45,000	84,000
503	0.6610	0.56	49,000	75,000
356	0.7779	0.66	32,000	41,000
250	0.5864	0.50	8,000	14,000
175	4.3825	3.71	32,000	7,000
125	11.1543	9.44	0	0
90	15.2	12.87	170,000	11,000
74 and under	65.9	55.78	2,200,000	33,000
Totals	118.1	100	2.6×10^6	Average Activity per Unit Weight 2.16×10^4

STATION U-E-2

Size of Fraction (μ)	Weight of Fraction (g)	Percentage of Total Weight	Activity (c/m)	Activity per Unit Weight (c/m/g)
4040 and over	43.7	6.88	10,000	240
2845	5.5272	0.87	2,800	500
2006	4.9565	0.78	49,000	10,000
1420	4.4729	0.70	127,000	28,000
1015	5.0070	0.79	490,000	99,000
715	5.8166	0.92	420,000	72,000
503	9.4205	1.48	280,000	30,000
356	14.8875	2.34	540,000	36,000
250	29.4	4.63	1,100,000	39,000
175	72.0	11.33	3,000,000	42,000
125	168.8	26.56	5,100,000	30,000
90	143.9	22.64	3,800,000	27,000
74 and under	127.7	20.09	4,200,000	33,000
Totals	635.5	100	1.9×10^7	Average Activity per Unit Weight 3.07×10^4

PROJECT 2.5a-2

STATION U-E-4

Size of Fraction (μ)	Weight of Fraction (g)	Percentage of Total Weight	Activity (c/m)	Activity per Unit Weight (c/m/g)
4040 and over	8.5	16.46	0	0
2845	0.1821	0.35	0	0
2006	0.2671	0.52	330	1,200
1420	0.1859	0.36	17,000	93,000
1015	0.2163	0.42	16,000	76,000
715	0.1387	0.27	16,000	110,000
503	0.1951	0.38	15,000	77,000
356	0.2378	0.46	8,000	33,000
250	0.4043	0.78	8,000	19,000
175	1.2013	2.33	23,000	18,000
125	3.9539	7.66	79,000	20,000
90	6.3514	12.30	197,000	31,000
74 and under	29.8	57.71	2,300,000	78,000
Totals	51.6	100	2.7×10^6	Average Activity per Unit Weight 5.23×10^4

STATION U-E-5

Size of Fraction (μ)	Weight of Fraction (g)	Percentage of Total Weight	Activity (c/m)	Activity per Unit Weight (c/m/g)
4040 and over	0.2448	0.97	170	650
2845	0.2219	0.88	130	620
2006	0.3894	1.55	11,000	27,000
1420	0.4392	1.75	520	1,200
1015	0.4912	1.95	740	1,500
715	0.4872	1.94	0	0
503	0.7351	2.92	29,000	39,000
356	1.3482	5.36	73,000	54,000
250	1.0272	4.08	16,000	15,000
175	1.1019	4.38	5,900	5,400
125	2.1627	8.59	39,000	18,000
90	2.6885	10.68	41,000	15,000
74 and under	13.8254	54.94	610,000	44,000
Totals	25.2	100	8.28×10^5	Average Activity per Unit Weight 3.29×10^4

PROJECT 2.5a-2

STATION U-F-1

Size of Fraction (μ)	Weight of Fraction (g)	Percentage of Total Weight	Activity (c/m)	Activity per Unit Weight (c/m/g)
4040 and over	472.8	20.35	210,000,000	450,000
2845	182.8	7.87	29,000,000	160,000
2006	194.3	8.36	37,000,000	190,000
1420	195.3	8.41	24,000,000	120,000
1015	186.1	8.01	59,000,000	310,000
715	161.5	6.95	62,000,000	380,000
503	157.5	6.78	55,000,000	340,000
356	145.3	6.26	37,000,000	250,000
250	135.1	5.82	29,000,000	220,000
175	134.6	5.79	11,000,000	84,000
125	140.0	6.03	5,100,000	42,000
90	89.8	3.87	2,400,000	27,000
74 and under	127.8	5.50	3,300,000	26,000
Totals	2,322.9	100	5.72×10^8	Average Activity per Unit Weight 2.4×10^5

STATION U-F-2

Size of Fraction (μ)	Weight of Fraction (g)	Percentage of Total Weight	Activity (c/m)	Activity per Unit Weight (c/m/g)
4040 and over	3.3035	1.24	980	290
2845	0.9143	0.34	100,000	110,000
2006	1.8508	0.70	120,000	68,000
1420	4.6327	1.74	1,000,000	220,000
1015	11.9555	4.49	2,300,000	190,000
715	19.9	7.48	6,300,000	310,000
503	26.6	10.00	8,000,000	300,000
356	22.9	8.61	7,600,000	330,000
250	21.2	7.97	4,600,000	220,000
175	26.4	9.92	4,200,000	160,000
125	34.9	13.12	2,600,000	76,000
90	26.9	10.11	1,500,000	58,000
74 and under	64.6	24.28	5,500,000	85,000
Totals	266.1	100	4.44×10^7	Average Activity per Unit Weight 1.67×10^5

PROJECT 2.5a-2

STATION U-F-3

Size of Fraction (μ)	Weight of Fraction (g)	Percentage of Total Weight	Activity (c/m)	Activity per Unit Weight (c/m/g)
4040 and over	20.2	9.56	1,800,000	93,000
2845	5.2857	2.50	60,000	11,000
2006	4.2823	2.03	160,000	38,000
1420	4.8067	2.27	490,000	100,000
1015	6.8973	3.26	810,000	110,000
715	5.7741	2.73	700,000	120,000
503	5.1388	2.43	300,000	60,000
356	3.6646	1.73	160,000	43,000
250	6.5417	3.10	210,000	32,000
175	15.1759	7.18	400,000	26,000
125	29.1	13.77	600,000	20,000
90	27.6	13.06	610,000	22,000
74 and under	76.8	36.35	2,700,000	36,000
Totals	211.3	100	9.2×10^6	Average Activity per Unit Weight 4.35×10^4

STATION U-F-4

Size of Fraction (μ)	Weight of Fraction (g)	Percentage of Total Weight	Activity (c/m)	Activity per Unit Weight (c/m/g)
4040 and over	0.6491	3.20	190	330
2845	0.1237	0.61	190	680
2006	0.1367	0.67	620	4,600
1420	0.3382	1.67	7,800	23,000
1015	0.2638	1.30	2,200	8,200
715	0.3179	1.57	27,000	85,000
503	0.5128	2.52	21,000	41,000
356	0.6936	3.41	15,000	21,000
250	1.0585	5.21	25,000	24,000
175	1.6974	8.36	58,000	34,000
125	2.5312	12.46	63,000	24,000
90	2.4303	11.96	88,000	36,000
74 and under	9.5591	47.06	530,000	55,000
Totals	20.3	100	8.4×10^5	Average Activity per Unit Weight 4.15×10^4

PROJECT 2.5a-2

STATION U-F-5

Size of Fraction (μ)	Weight of Fraction (g)	Percentage of Total Weight	Activity (c/m)	Activity per Unit Weight (c/m/g)
4040 and over	0.6129	4.42	120	160
2845	1.1189	8.06	38	34
2006	0.2036	1.47	100	530
1420	0.1769	1.27	200	1,000
1015	0.1974	1.42	1,700	8,500
715	0.1910	1.38	2,200	11,000
503	0.2198	1.58	3,100	14,000
356	0.2370	1.71	8,600	36,000
250	0.6272	4.52	68,000	100,000
175	1.1210	8.08	55,000	49,000
125	1.2173	8.77	36,000	29,000
90	1.3961	10.06	22,000	15,000
74 and under	6.5565	47.25	320,000	48,000
Totals	13.9	100	5.2×10^5	Average Activity per Unit Weight 3.73×10^4

STATION U-G-1

Size of Fraction (μ)	Weight of Fraction (g)	Percentage of Total Weight	Activity (c/m)	Activity per Unit Weight (c/m/g)
4040 and over	0.2949	0.41	32,000	110,000
2845	0.5986	0.84	71,000	110,000
2006	1.0627	1.49	110,000	100,000
1420	2.6099	3.65	390,000	150,000
1015	4.1889	5.86	840,000	200,000
715	4.6448	6.50	1,600,000	350,000
503	3.2886	4.60	1,600,000	510,000
356	7.1085	9.94	3,500,000	500,000
250	6.9080	9.66	2,400,000	350,000
175	5.4111	7.57	1,100,000	210,000
125	5.5647	7.78	760,000	130,000
90	6.5215	9.12	790,000	120,000
74 and under	23.2949	32.58	1,500,000	64,000
Totals	71.5	100	1.51×10^7	Average Activity per Unit Weight 2.11×10^5

PROJECT 2.5a-2

STATION U-G-2

Size of Fraction (μ)	Weight of Fraction (g)	Percentage of Total Weight	Activity (c/m)	Activity per Unit Weight (c/m/g)
4040 and over	1.7718	2.40	290,000	160,000
2845	0.6630	0.90	65,000	98,000
2006	1.0324	1.40	300,000	290,000
1420	2.9804	4.04	960,000	320,000
1015	7.1868	9.75	2,500,000	350,000
715	10.2980	13.96	3,000,000	290,000
503	9.7554	13.23	2,700,000	280,000
356	6.3939	8.67	1,900,000	300,000
250	6.9348	9.40	2,200,000	320,000
175	7.2329	9.81	1,500,000	210,000
125	5.5682	7.55	830,000	140,000
90	3.7442	5.08	240,000	66,000
74 and under	10.1811	13.81	750,000	74,000
Totals	73.7	100	1.76×10^7	Average Activity per Unit Weight 2.39×10^5

STATION U-G-3

Size of Fraction (μ)	Weight of Fraction (g)	Percentage of Total Weight	Activity (c/m)	Activity per Unit Weight (c/m/g)
4040 and over	1.7139	4.58	82,000	48,000
2845	0.5873	1.57	200,000	340,000
2006	1.7084	4.56	150,000	90,000
1420	2.4961	6.67	1,200,000	510,000
1015	3.7540	10.03	1,100,000	300,000
715	4.3961	11.75	710,000	160,000
503	2.8517	7.62	870,000	300,000
356	1.3673	3.65	290,000	210,000
250	0.8846	2.36	140,000	150,000
175	0.7089	1.89	51,000	72,000
125	1.4272	3.81	60,000	42,000
90	2.2913	6.12	57,000	25,000
74 and under	13.2403	35.38	670,000	50,000
Totals	37.4	100	5.71×10^6	Average Activity per Unit Weight 1.53×10^5

PROJECT 2.5a-2

STATION U-C-4

Size of Fraction (μ)	Weight of Fraction (g)	Percentage of Total Weight	Activity (c/m)	Activity per Unit Weight (c/m/g)
4040 and over	0.1258	1.46	0	0
2845	0.1394	1.62	52	370
2006	0.0864	1.00	63	720
1420	0.1247	1.45	10,000	81,000
1015	0.1583	1.84	34,000	210,000
715	0.2083	2.42	38,000	180,000
503	0.2547	2.95	40,000	150,000
356	0.3618	4.20	16,000	45,000
250	0.7068	8.20	100,000	150,000
175	1.3414	15.56	200,000	150,000
125	1.2448	14.44	130,000	100,000
90	0.9306	10.79	60,000	64,000
74 and under	2.9373	34.07	160,000	56,000
Totals	8.6	100	8.11×10^5	Average Activity per Unit Weight 9.41×10^4

STATION U-C-5

Size of Fraction (μ)	Weight of Fraction (g)	Percentage of Total Weight	Activity (c/m)	Activity per Unit Weight (c/m/g)
4040 and over	0.0757	1.03	0	0
2845	0.0321	0.43	12	370
2006	0.1193	1.62	3,000	25,000
1420	0	0	0	0
1015	0.1344	1.82	13,000	99,000
715	0.1572	2.13	210	1,300
503	0.2033	2.75	4,800	23,000
356	0.2891	3.92	6,000	21,000
250	0.5036	6.82	3,000	59,000
175	1.1576	15.69	73,000	62,000
125	1.2362	16.75	54,000	44,000
90	0.8010	10.85	26,000	33,000
74 and under	2.6705	36.19	150,000	58,000
Totals	7.4	100	3.08×10^5	Average Activity per Unit Weight 4.17×10^4

PROJECT 2.5a-2

STATION U-H-1

Size of Fraction (μ)	Weight of Fraction (g)	Percentage of Total Weight	Activity (c/m)	Activity per Unit Weight (c/m/g)
4040 and over	0.1133	0.17	41,000	360,000
2845	0.2464	0.37	59,000	240,000
2006	0.7392	1.10	530,000	720,000
1420	2.6174	3.90	770,000	290,000
1015	6.7002	9.98	1,200,000	180,000
715	8.2896	12.35	1,900,000	230,000
503	7.2583	10.81	2,000,000	280,000
356	6.8590	10.22	2,000,000	300,000
250	7.1128	10.60	2,000,000	290,000
175	4.9080	7.31	1,200,000	240,000
125	3.9185	5.84	550,000	140,000
90	3.2287	4.81	310,000	97,000
74 and under	15.1491	22.57	1,400,000	94,000
Totals	67.1	100	1.44×10^7	Average Activity per Unit Weight 2.14×10^5

STATION U-H-2

Size of Fraction (μ)	Weight of Fraction (g)	Percentage of Total Weight	Activity (c/m)	Activity per Unit Weight (c/m/g)
4040 and over	0	0	0	0
2845	0.0389	0.07	59	1,500
2006	0.0881	0.16	23,000	260,000
1420	0.5196	0.96	260,000	510,000
1015	2.0952	3.85	640,000	300,000
715	6.3069	11.60	2,000,000	320,000
503	11.8245	21.75	3,400,000	280,000
356	11.4916	21.14	1,100,000	150,000
250	8.5757	15.78	2,000,000	240,000
175	4.1961	7.72	920,000	210,000
125	2.1369	3.93	420,000	190,000
90	2.1658	3.98	360,000	160,000
74 and under	4.9147	9.04	860,000	170,000
Totals	54.4	100	1.22×10^7	Average Activity per Unit Weight 2.24×10^5

PROJECT 2.5a-2

STATION U-H-3

Size of Fraction (μ)	Weight of Fraction (g)	Percentage of Total Weight	Activity (c/m)	Activity per Unit Weight (c/m/g)
4040 and over	1.1	3.25	38	35
2845	0.1114	0.33	100,000	950,000
2006	0.3367	0.99	220,000	660,000
1420	0.9674	2.86	540,000	550,000
1015	3.3636	9.93	1,200,000	370,000
715	6.6661	19.68	1,600,000	240,000
503	6.0104	17.74	1,300,000	220,000
356	1.5434	4.56	400,000	260,000
250	0.7935	2.34	140,000	180,000
175	0.8573	2.53	40,000	46,000
125	1.6272	4.80	74,000	45,000
90	2.0967	6.19	98,000	46,000
74 and under	8.4033	24.80	640,000	77,000
Totals	33.8	100	6.55×10^6	Average Activity per Unit Weight 1.93×10^5

STATION U-H-4

Size of Fraction (μ)	Weight of Fraction (g)	Percentage of Total Weight	Activity (c/m)	Activity per Unit Weight (c/m/g)
4040 and over	0	0	0	0
2845	0	0	0	0
2006	0.0156	0.15	1,400	89,000
1420	0.0490	0.47	23,000	460,000
1015	0.0366	0.35	16,000	440,000
715	0.0494	0.48	7,800	150,000
503	0.0673	0.65	19,000	290,000
356	0.1611	1.55	21,000	130,000
250	0.2659	2.56	33,000	120,000
175	0.7256	6.98	95,000	130,000
125	1.3842	13.32	120,000	87,000
90	1.2287	11.82	68,000	55,000
74 and under	6.4104	61.67	450,000	70,000
Totals	10.4	100	8.59×10^5	Average Activity per Unit Weight 8.26×10^4

PROJECT 2.5a-2

STATION U-H-5

Size of Fraction (μ)	Weight of Fraction (g)	Percentage of Total Weight	Activity (c/m)	Activity per Unit Weight (c/m/g)
4040 and over	0.2201	1.59	0	0
2845	0.0713	0.51	0	0
2006	0.0716	0.52	79	110
1420	0.0366	0.26	93	250
1015	0.0675	0.49	1,300	19,000
715	0.0486	0.35	6,100	127,000
503	0.1911	1.38	75,000	390,000
356	0.7186	5.18	180,000	260,000
250	0.5099	3.68	84,000	160,000
175	0.4744	3.42	35,000	74,000
125	1.0869	7.84	46,000	42,000
90	1.2502	9.02	36,000	29,000
74 and under	9.1137	65.75	470,000	52,000
Totals	13.9	100	9.51×10^5	Average Activity per Unit Weight 6.86×10^4

STATION U-I-1

Size of Fraction (μ)	Weight of Fraction (g)	Percentage of Total Weight	Activity (c/m)	Activity per Unit Weight (c/m/g)
4040 and over	0	0	0	0
2845	0.0553	0.15	8,900	200,000
2006	0.1474	0.40	120,000	800,000
1420	0.3439	0.94	150,000	500,000
1015	1.1798	3.22	660,000	600,000
715	3.0737	8.40	1,000,000	400,000
503	5.8027	15.85	1,200,000	200,000
356	3.7923	10.36	910,000	400,000
250	8.8855	24.27	2,100,000	400,000
175	6.1377	16.76	1,700,000	400,000
125	2.7196	7.43	660,000	300,000
90	1.7928	4.90	450,000	300,000
74 and under	2.6806	7.32	450,000	200,000
Totals	36.6	100	9.6×10^6	Average Activity per Unit Weight 2.63×10^5

PROJECT 2.5a-2

STATION U-I-2

Size of Fraction (μ)	Weight of Fraction (g)	Percentage of Total Weight	Activity (c/m)	Activity per Unit Weight (c/m/g)
4040 and over	0	0	0	0
2845	0.0240	0.07	72	3,100
2006	0.0820	0.23	3,000	36,000
1420	0.1713	0.49	64,000	370,000
1015	0.6724	1.92	322,000	480,000
715	1.9444	5.54	0	0
503	7.6191	21.71	2,200,000	290,000
356	9.3277	26.57	1,900,000	200,000
250	3.5009	9.97	700,000	200,000
175	1.9995	5.70	420,000	210,000
125	1.9443	5.54	330,000	170,000
90	1.6837	4.80	230,000	130,000
74 and under	6.1388	17.49	920,000	140,000
Totals	35.1	100	7.2×10^6	Average Activity per Unit Weight 2.05×10^5

STATION U-I-3

Size of Fraction (μ)	Weight of Fraction (g)	Percentage of Total Weight	Activity (c/m)	Activity per Unit Weight (c/m/g)
4040 and over	0.0358	0.06	0	0
2845	0.0515	0.08	0	0
2006	0.2483	0.38	91,000	360,000
1420	0.3639	0.56	190,000	540,000
1015	0.9356	1.45	460,000	490,000
715	2.7694	4.28	1,100,000	400,000
503	11.5631	17.87	3,200,000	280,000
356	15.8999	26.11	4,300,000	270,000
250	14.0179	21.66	4,900,000	350,000
175	7.7255	11.94	2,300,000	300,000
125	3.3997	5.25	710,000	210,000
90	3.4536	5.34	770,000	220,000
74 and under	4.2497	6.57	900,000	210,000
Totals	64.7	100	1.92×10^7	Average Activity per Unit Weight 2.97×10^5

PROJECT 2.5a-2

STATION U-I-4

Size of Fraction (μ)	Weight of Fraction (g)	Percentage of Total Weight	Activity (c/m)	Activity per Unit Weight (c/m/g)
4040 and over	0	0	0	0
2845	0.0235	0.17	3,200	130,000
2006	0.0801	0.59	34,000	420,000
1420	0.1176	0.86	87,000	740,000
1015	0.5744	4.20	220,000	390,000
715	1.8385	13.45	940,000	500,000
503	4.5306	33.15	1,300,000	290,000
356	1.7441	12.76	300,000	170,000
250	0.2739	2.00	38,000	140,000
175	0.4339	3.17	62,000	140,000
125	0.5121	3.75	41,000	80,000
90	0.6085	4.45	49,000	81,000
74 and under	2.9299	21.44	390,000	135,000
Totals	13.7	100	3.55×10^6	Average Activity per Unit Weight 2.59×10^5

STATION U-I-5

Size of Fraction (μ)	Weight of Fraction (g)	Percentage of Total Weight	Activity (c/m)	Activity per Unit Weight (c/m/g)
4040 and over	0	0	0	0
2845	0	0	0	0
2006	0	0	0	0
1420	0.0412	0.27	1,900	47,000
1015	0.0521	0.35	4,600	89,000
715	0.1639	1.09	94,000	610,000
503	1.9397	12.88	931,000	480,000
356	4.0100	26.63	1,100,000	280,000
250	1.5826	10.51	420,000	260,000
175	1.7136	11.38	450,000	260,000
125	1.4228	9.45	300,000	210,000
90	0.8899	5.91	110,000	130,000
74 and under	3.2419	21.53	340,000	100,000
Totals	15.1	100	4.27×10^6	Average Activity per Unit Weight 2.83×10^5

PROJECT 3.5a-2

STATION U-I-6

Size of Fraction (μ)	Weight of Fraction (g)	Percentage of Total Weight	Activity (c/m)	Activity per Unit Weight (c/m/g)
4040 and over	0	0	0	0
2845	0	0	0	0
2006	0.0357	0.58	37,000	1,100,000
1420	0.0746	1.21	59,000	790,000
1015	0.3180	5.15	170,000	540,000
715	0.9210	14.94	210,000	220,000
503	0.6739	10.92	100,000	150,000
356	0.2270	3.68	4,100	20,000
250	0.4195	6.80	5,500	13,000
175	0.6467	10.48	4,900	7,700
125	0.9835	15.94	8,200	8,300
90	0.7820	12.68	5,200	6,600
74 and under	1.0870	17.62	12,000	11,000
Totals	6.2	100	6.28×10^5	Average Activity per Unit Weight 1.02×10^5

STATION U-I-8

Size of Fraction (μ)	Weight of Fraction (g)	Percentage of Total Weight	Activity (c/m)	Activity per Unit Weight (c/m/g)
4040 and over	0	0	0	0
2845	0	0	0	0
2006	0.1095	5.57	16	140
1420	0.0275	1.40	15,000	550,000
1015	0.0394	2.00	20,000	520,000
715	0.2003	10.19	150,000	760,000
503	0.2591	13.18	97,000	370,000
356	0.7442	37.85	200,000	270,000
250	0.1701	8.65	27,000	160,000
175	0.0718	3.65	1,200	16,000
125	0.0885	4.50	1,000	11,000
90	0.0912	4.64	1,000	12,000
74 and under	0.1647	8.38	3,100	19,000
Totals	2.0	100	5.24×10^5	Average Activity per Unit Weight 2.66×10^5

PROJECT 2.5a-2

STATION U-N-1

Size of Fraction (μ)	Weight of Fraction (g)	Percentage of Total Weight	Activity (c/m)	Activity per Unit Weight (c/m/g)
4040 and over	0	0	0	0
2845	0.0073	0.15	0	0
2006	0	0	0	0
1420	0	0	0	0
1015	0	0	0	0
715	0.0203	0.42	200	10,000
503	0.0174	0.36	2,000	120,000
356	0.0596	1.22	21,000	350,000
250	0.1981	4.06	59,000	290,000
175	0.5110	10.48	190,000	330,000
125	0.7952	16.31	220,000	280,000
90	0.7498	15.38	175,000	230,000
74 and under	2.5163	51.62	450,000	170,000
Totals	4.9	100	1.1×10^6	Average Activity per Unit Weight 2.27×10^5

STATION U-N-3

Size of Fraction (μ)	Weight of Fraction (g)	Percentage of Total Weight	Activity (c/m)	Activity per Unit Weight (c/m/g)
4040 and over	0	0	0	0
2845	0	0	0	0
2006	0	0	0	0
1420	0	0	0	0
1015	0	0	0	0
715	0.0136	0.12	130	10,000
503	0.0393	0.36	15,000	380,000
356	0.3103	2.83	114,000	360,000
250	0.5453	5.89	190,000	300,000
175	1.4116	12.89	460,000	330,000
125	2.4892	22.73	690,000	270,000
90	1.7908	16.35	440,000	240,000
74 and under	4.2523	38.83	980,000	230,000
Totals	11.0	100	2.91×10^6	Average Activity per Unit Weight 2.66×10^5

PROJECT 2.5a-2

STATION U-N-4

Size of Fraction (μ)	Weight of Fraction (g)	Percentage of Total Weight	Activity (c/m)	Activity per Unit Weight (c/m/g)
4040 and over	0	0	0	0
2845	0	0	0	0
2006	0	0	0	0
1420	0	0	0	0
1015	0.0164	0.06	550	33,000
715	0.0653	0.27	18,000	280,000
503	0.2488	1.03	99,000	390,000
356	0.9017	3.72	340,000	380,000
250	2.9043	11.97	900,000	310,000
175	5.4063	22.52	1,700,000	320,000
125	4.7592	19.63	1,200,000	270,000
90	1.8838	7.77	400,000	210,000
74 and under	8.0627	33.25	1,300,000	170,000
Totals	24.2	100	6.24×10^6	Average Activity per Unit Weight 2.57×10^5

STATION U-N-5

Size of Fraction (μ)	Weight of Fraction (g)	Percentage of Total Weight	Activity (c/m)	Activity per Unit Weight (c/m/g)
4040 and over	0.0046	0.02	0	0
2845	0.0126	0.07	0	0
2006	0.0178	0.10	0	0
1420	0.0298	0.17	0	0
1015	0.1200	0.67	61,000	500,000
715	0.4032	2.24	140,000	360,000
503	1.0520	5.83	290,000	280,000
356	1.0929	6.06	360,000	330,000
250	2.1153	11.73	760,000	360,000
175	3.0855	17.10	970,000	310,000
125	3.3095	18.35	930,000	280,000
90	1.6026	8.88	310,000	190,000
74 and under	5.1297	28.44	820,000	150,000
Totals	18.0	100	4.70×10^6	Average Activity per Unit Weight 2.76×10^5

OPERATION JANGLE

PROJECT 2.5a-3

RADIOCHEMICAL STUDIES OF LARGE PARTICLES

by

Roy D. Maxwell

April 1952

ARMY MEDICAL SERVICE GRADUATE SCHOOL
Washington 12, D. C.

Reproduced Direct from Manuscript Copy by
AEC Technical Information Service
Oak Ridge, Tennessee

PROJECT 2.5a-3

CONTENTS

ILLUSTRATIONS

CHAPTER 2 TECHNIQUES AND OBSERVATIONS

CHAPTER 3 STATISTICAL STUDY

TABLES

CHAPTER 2 TECHNIQUES AND OBSERVATIONS

CHAPTER 3 STATISTICAL STUDY

PROJECT 2.5a-3

ABSTRACT

A study has been made of fall-out particles from both the surface and the underground shots at Operation JANGLE. Particles were collected upon trays placed downwind five to ten miles from point zero. The size, radioactivity present including decay, and chemical composition of the particles were determined. The method of mechanical separation of the radioactive particles from the non-active material gave a preference for large sizes. However, the findings indicate that particles as large as five hundred microns fall as far as ten miles from the point of detonation.

CHAPTER 1

INTRODUCTION

1.1 BACKGROUND

Fall-out of radioactive particles from the cloud after an atomic bomb has been detonated at or near the ground is a well known and much studied phenomena. Since the first shot at TRINITY, it has been known that particulate matter falls over a rather wide area. For the most part the collection of this material has been confined to air sampling devices. After the first shot at Operation GREENHOUSE it was noted that rather high levels of activity were encountered on the inhabited islands. Soil samples were collected and by tedious methods of mechanical separation of the radioactive material, the average size was found to be above 50 microns. Prior to this time most investigators felt that the largest quantity of radioactivity falling out from a cloud after an atomic bomb were particles of 5 microns or less. Thus, with the opening of the proving ground in Nevada, it was desirable to ascertain the true conditions which would exist after the contaminating burst.

A small amount of radioactivity was encountered at the Control Point building after one of the BUSTER shots and here, as at GREENHOUSE, samples of soil were collected and a few particles were isolated. These particles were approximately 500 microns in diameter and had the appearance of fused soil. They contained radioactivity, either absorbed in the particle or mechanically held after the cooling process. The samples hereafter discussed were collected after the surface and underground shots from the JANGLE operation.

CHAPTER 2

TECHNIQUES AND OBSERVATIONS

2.1 SAMPLE COLLECTION

Inasmuch as it was necessary to adhere rather closely to the agreed wind requirements for shot time, the sampling points were selected several weeks prior to the shots. These areas were determined by the Army Chemical Center, under the direction of Lt. Col. Robbins. Among the equipment at the station points selected was a 7-foot steel tower. In order to ascertain that the material collected was true fall-out, wooden trays were made measuring approximately 2 feet wide and 3 feet long with a one-half inch border protruding above the surface so that any material falling onto the tray would not be blown off. Then at D-1, a section of thin plastic material was placed on the surface of each tray and anchored in such a way that the wind would not cause it to whip. The trays were then placed on the above mentioned towers. Personnel of Project 2.5a-1 went forward to collect these trays as soon as the radiological situation would permit. In most cases this was within three days. The area covered by the sampling points extended out to 14 miles. Some radioactivity was found on several of the collecting trays and particularly on those immediately downwind. The points from 5 to 10 miles in both the surface and underground shots gave the highest total reading for the radioactivity collected.

2.2 ISOLATION TECHNIQUE

The method used for isolating the radioactive particles is more applicable to the larger particles, although any amount of activity which could be detected was investigated. A small amount of the soil and/or fall-out particles from the tray was placed on a microscope slide and distributed rather evenly over the surface. The slide was then placed on the table approximately one inch under the counter tube and surveyed. A No. 263 G. M. Field Counter was used in some instances, but for the most part a more sensitive Nuclear Instrument and Chemical Corporation Laboratory Survey Model was used. The thin window was covered by a piece of aluminum one-eighth of an inch thick with a hole in the center one-fourth of an inch in diameter. This served to somewhat collimate the beta activity. If, as the tube crossed the area, a particle or particles gave an increased number of counts, the material was isolated and placed on another slide. The operation was continued

until such time as only one particle showing activity remained of those originally removed for study. After ascertaining that only one particle was present to give the reading on the Survey Meter, the particle was mounted under cellophane tape or placed in a small droplet of quick drying plastic. Several hundred particles were isolated by this method and approximately 250 of these were carefully examined.

2.3 PHYSICAL OBSERVATIONS

Approximately 250 particles were mounted; of these, 150 were isolated from the surface shot and 100 from the underground shot. Photographs were made of particles from each shot, four of each being presented in Figures 2.1 through 2.8. It will be noted that the eye piece micrometer is clearly indicated. The scale for one division equals 15 microns, or a total of 750 microns for the micrometer. The photographs were made by using reflected light rather than transmitted light in order to bring out as much of the character of the material as possible.

It was found that many of the particles from the surface shot were smooth, round and bead-like in appearance of varying transparency, showing continuity of material resembling glass. In a private communication from Dr. Charles Williams, the author was informed that the index of refraction of the particles was 1.572 - 1.578, which is typical of the index of refraction of glass. Photographs of typical spherical particles recovered from the surface shot appear in Figures 2.1 and 2.2. An interesting irregularity associated with a spherical particle is shown in Figure 2.3.

Some particles from the surface shot and all from the underground shot were irregular in shape and somewhat opaque in appearance. No attempt is made to describe each particle isolated but an indication of size variation and extreme irregularity of shape of these particles is illustrated in Figures 2.4 - 2.8. The particles appeared to be fused earth with adhering small metallic points and imbedded black specks. These points and specks varied from sub-micron size up to fifteen microns, with the majority from one-half to two microns in size. Observations made in the course of activity measurements indicated that the greater the number of these black specks the greater the activity.

2.4 CHEMICAL ANALYSIS

It was highly desirable to know the elements present in these particles in quantities large enough to be chemically analyzed.

Fig. 2.1 Surface Shot Particle

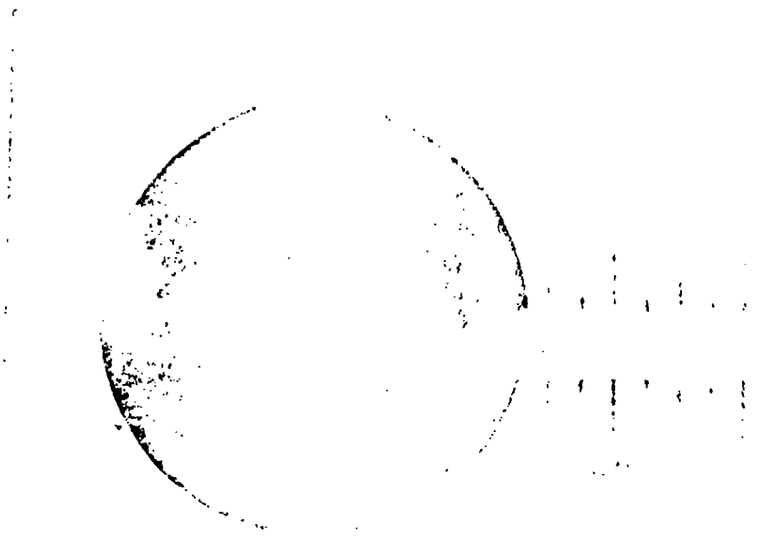

Fig. 2.2 Surface Shot Particle

Fig. 2.3 Surface Shot Particle

Fig. 2.4 Surface Shot Particle

Fig. 2.5 Underground Shot Particle

Fig. 2.6 Underground Shot Particle

Fig. 2.5 Underground Shot Particle

Fig. 2.6 Underground Shot Particle

Fig. 2.7 Underground Shot Particle

Fig. 2.8 Underground Shot Particle

However, because of the critical nature of the experiment it was deemed advisable to have a complete spectrographic analysis made. With this in mind ten particles from the surface shot and ten from the underground event were analyzed at the National Bureau of Standards and a report of the findings is given in Tables 2.1 and 2.2. Elements not detected in any of the particles examined include the following: Ag, As, Be, Bi, Cb, Cd, Co, In, Mo, Ni, Ta, Th, U, V, Zn, Zr.

There appear to be no significant differences in the composition of the individual large particles collected from the fall-out of either shot. Furthermore, the chemical composition of large active particles is the same as that of the original soil (See report of Project 2.8, Operation JANGLE) except for minor constituents which were not looked for in both analyses.

TABLE 2.1

Chemical Composition of Surface Shot Particles*

Slide No.	Size in Microns	Major Constituents over 10% 1 - 10% (listed in order of concentration)	Minor Impurities less than 0.1% listed in alphabetical order
110	450	Si Al Fe Ca Mg	Ba Cu Mn Na Pb Sn Sr Ti -
113	495	Si Al Fe Ca Mg	Ba Cu Mn Na Pb Sn Sr Ti -
105	395	Si Al Fe Ca Mg	Ba Cu Mn Na Pb Sn Sr Ti -
100	465	Si Al Fe Ca Mg	Ba Cu Mn Na Pb Sn Sr Ti -
82	465	Si Al Fe Ca Mg	Ba Cu Mn Na Pb Sn Sr Ti Cr
75	480	Si Al Fe Ca Mg	Ba Cu Mn Na Pb Sn Sr Ti Cr
72	525	Si Al Fe Ca Mg	Ba Cu Mn Na Pb Sn Sr Ti Cr
47	375	Si Al Fe Ca Mg	Ba Cu Mn Na - - Sr Ti -
73	510	Si Al Fe Ca Mg	Ba Cu Mn Na Pb Sn - - -
71	525	Si Al Fe Ca Mg	- Cu - Na - - - - -
91	465	Si Al Fe Ca Mg	- Cu - Na - - - - -
108	360	Si Al Fe Ca Mg	- Cu - Na - - Sr - -
103	480	Si Al Fe Ca Mg	- Cu Mn Na - - - - -
90	495	Si Al Fe Ca Mg	- Cu Mn Na Pb Sn - - -

* These analyses, made on individual particles, need not necessarily agree with chemical analyses made on pre-shot gross soil samples.

PROJECT 2.5a-3

2.5 RADIOCHEMICAL MEASUREMENTS

In an attempt to ascertain whether there was any difference in the radioactive substances adhering to the fused mass, 25 of the more active particles collected from each shot were used for studying the beta decay rate. It was found that the decay curves, plotted on log-log paper, were very characteristic and were in every way similar regardless of the size of the particle used. While there is a slight variation from the surface shot to the underground shot, there was no marked deviation in the decay characteristics between individual particles collected for either shot. This report does not give all the data collected, but one representative set of data is given for each of the two shots. In addition to the representative decay data which appear in Tables 2.3 and 2.4 and as curves C and D in Figure 2.9, the decay data for gross crater lip samples is presented as curves A and B in Figure 2.9 for comparison. The crater lip sample data was furnished by Dr. Charles Maxwell of the National Institutes of Health. The reader is referred to the report of Project 2.6c-1 for further information on the physical and chemical nature of crater lip samples. A comparison of these data shows that the activity is not selective as might first be thought.

TABLE 2.2

Chemical Composition of Underground Shot Particles

Slide No.	Size in Microns	Major Constituents over 10% 1 - 10% (listed in order of concentration)	Minor Impurities less than 0.1% listed in alphabetical order
114	1050 x 750	Si Al Fe Ca Mg	Ba Cu Mn Na Pb Sn Sr Ti Cr
93	540 x 665	Si Al Fe Ca Mg	Ba Cu Mn Na Pb Sn Sr Ti Cr
95	450 x 665	Si Al Fe Ca Mg	Ba Cu Mn Na Pb Sn Sr Ti Cr
70	525 x 360	Si Al Fe Ca Mg	Ba Cu Mn Na Pb Sn Sr Ti Cr
115	625 x 225	Si Al Fe Ca Mg	Ba Cu Mn Na Pb - Sr Ti -
101	180 x 375	Si Al Fe Ca Mg	- Cu Mn Na Pb - - - -
78	550 x 400	Si Al Fe Ca Mg	Ba Cu Mn Na Pb Sn Sr Ti ?Cr
86	600 x 600	Si Al Fe Ca Mg	- Cu Mn Na -? - - - -
60	1075	Si Al Fe Ca Mg	-? Cu Mn Na Pb - - - -
59	375 x 375	Si Al Fe Ca Mg	Ba Cu Mn Na Pb - Sr - -
38	225 x 300	Si Al Fe Ca Mg	Ba Cu Mn Na Pb - -? - -
29	1050 x 300	Si Al Fe Ca Mg	Ba Cu Mn Na Pb? Sn - -? -
52	275 x 225	Si Al Fe Ca Mg	Ba Cu Mn Na Pb Sn - Ti -

PROJECT 2.5a-3

Radioactive analysis was not carried out because it was not considered to be within the scope of this study. However, every particle isolated was very carefully studied with respect to the amount of total activity present. The counting geometry was determined by using a cobalt standard in the same relative position to the thin window Geiger tube used. Table 2.5 and Table 2.6 give the complete analysis as found, including the size of the particle, the activity found, the size in cubic millimeters, and the activity present at the end of one hour, using the decay curve for crater lip samples, Figure 2.9, Curves A and B. The size in cubic millimeters was determined by using the 4/3 R3 formula for the spheres, and for the irregular particles the long axis was multiplied by the square of short axis. This was assumed to be within the limits of error and certainly within the limits of the method of examination. All particles from both series are included.

TABLE 2.3

Beta Decay Data for Surface Particle

Hour	Day	Hours After Zero	Counts per Second
1330	21 November	52	467
1945	21 November	59	417
0930	22 November	72	342
1045	23 November	98	247
1930	23 November	106	223
0945	24 November	121	197
2200	24 November	133	164
1030	25 November	145	144
2130	25 November	156	130
1130	26 November	170	112
2000	26 November	179	104
1000	27 November	193	91
1030	28 November	217	74
0830	29 November	239	63.5
1015	30 November	265	51
0830	1 December	287	45
1045	2 December	314	37.8
1000	3 December	336	33.5
1345	11 December	533	12.3
1715	19 December	728	12.2
1545	26 December	895	10.3
1515	2 January	1062	8.3

TABLE 2.4

Beta Decay Data for Underground Particle

Hour	Day	Hours After Zero	Counts per Second
1830	30 November	30.5	406
0645	1 December	43	325
1830	1 December	54	247
0930	2 December	71	188
1915	2 December	79	167
1030	3 December	94	143
1830	3 December	102	128
0900	4 December	117	110
1100	6 December	167	64
1330	7 December	191.5	49
1000	8 December	212	39.6
0815	10 December	260	26.2
0930	11 December	285	22
0900	12 December	309	18.2
1345	14 December	362	14
1315	17 December	433	9
1315	19 December	481	8.1
0945	21 December	536	7.1
1430	26 December	658	5.0
1545	28 December	685	4.5
1600	2 January	826	3.6
1445	4 January	872	3.4

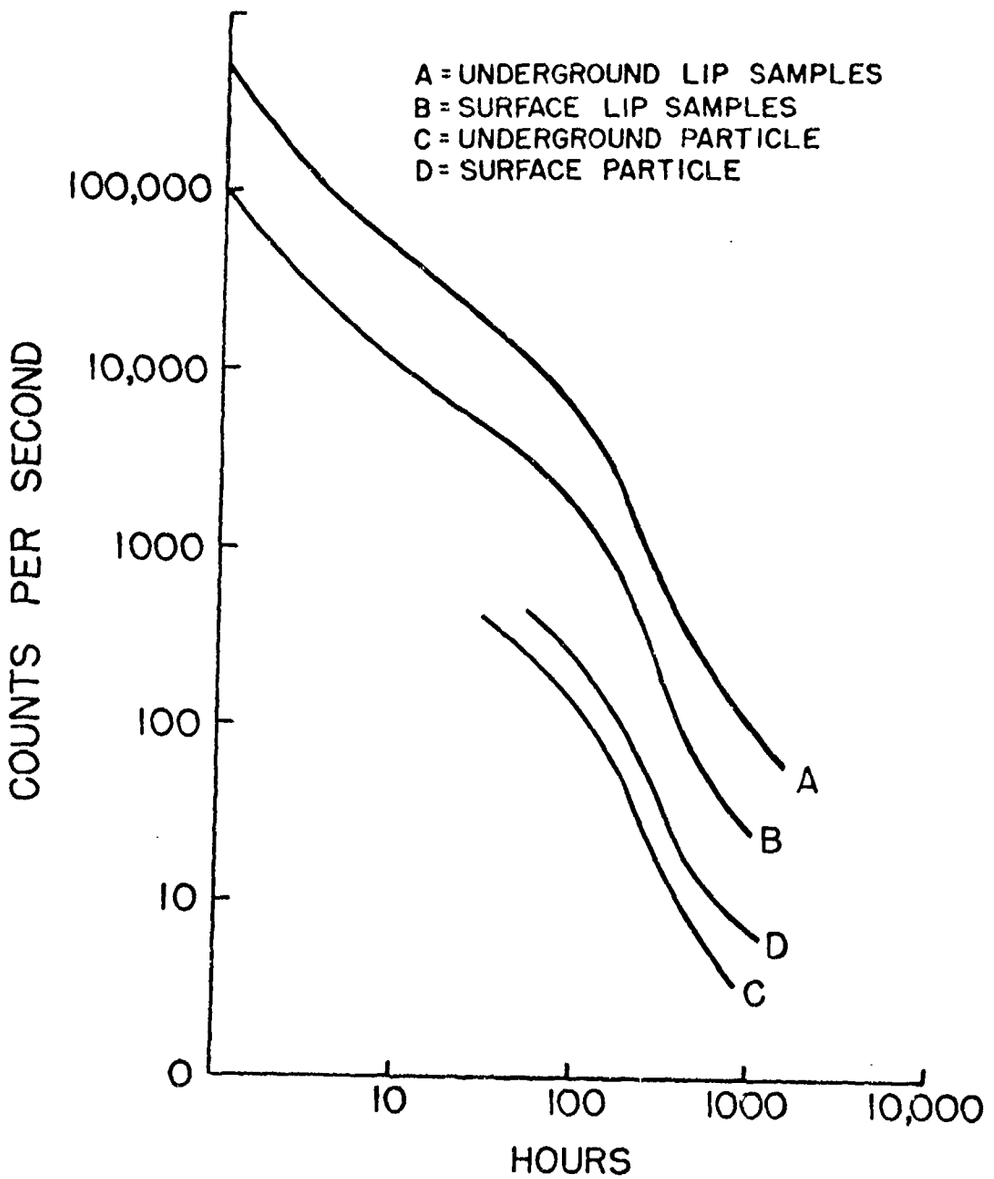

Fig. 2.9 Beta Decay Curves

TABLE 2.5

Activity Data for Surface Shot Particles

No.	Size In Microns*	Counts Per Second	Size In mm^3**	mc x 10^{-5}	mc x 10^{-5} / mm^3	Extrapolated to One Hour mc/particle ***
Readings made on 23 November 1951						
1	450 x 450 x 450	118.0	0.0915	122.0	1330.0	0.08
2	650	380.0	0.140	394.0	2810.0	0.262
3	450	104.0	0.0472	108.0	2290.0	0.07
4	600	280.0	0.108	290.0	2690.0	0.191
5	425	400.0	0.042	415.0	9800.0	0.274
6	450 / 373 / 150	330.0	0.095	342.0	3600.0	0.228
7	1140 x 495	70.0	0.280	72.5	259.0	0.047
8	450	94.0	0.0483	97.5	2000.0	0.065
9	465	72.0	0.0523	74.5	1410.0	0.049
10	315 / 550	280.0	0.111	290.0	2615.0	0.192
11	465	160.0	0.0523	167.0	3180.0	0.11
12	450	19.7	0.0478	20.2	423.0	0.013
13	495 x 200	165.0	0.0695	171.0	2450.0	0.113
14	345	66.0	0.0223	68.5	3060.0	0.045
15	375	180.0	0.0282	187.0	6630.0	0.123
16	450	88.0	0.048	91.0	1900.0	0.06
17	555	47.0	0.0895	48.8	547.0	0.0316
18	500	112.0	0.0655	116.0	1780.0	0.077
19	1100 x 450	197.0		203.0	910.0	0.134
20	495	350.0	0.0617	362.0	5860.0	0.238
21	500	220.0	0.066	228.0	3440.0	0.151
22	330	57.0	0.0189	59.0	3110.0	0.039
23	450	197.0	0.0484	204.0	4220.0	0.135
24	480	75.0	0.058	78.0	1340.0	0.052
25	330	12.0	0.02	12.4	624.0	0.008
26	330	72.0	0.02	74.5	3700.0	0.049
27	465	81.0	0.052	84.0	1610.0	0.055
28	375	16.5	0.0286	17.1	600.0	0.011
29	400	112.0	0.0336	116.0	3460.0	0.077
30	450 / 105	306.0	0.09	317.0	3510.0	0.209
31	480	120.0	0.0578	124.0	2150.0	0.082
32	550	304.0	0.0872	315.0	3590.0	0.208
33	450	210.0	0.0480	217.0	4500.0	0.143
34	375	80.0	0.029	83.0	2850.0	0.055
35	480	170.0	0.058	176.0	3040.0	0.115
36	495	140.0	0.063	145.0	2310.0	0.095
37	420	98.0	0.039	101.0	2590.0	0.067

TABLE 2.5 (Cont.)

No.	Size In Microns*	Counts Per Second	Size In mm^3**	mc x 10^{-5}	mc x 10^{-5} / mm^3	Extrapolated to One Hour mc/particle ***
38	850	42.0	0.322	43.5	135.0	0.038
39	540	308.0	0.082	320.0	3900.0	0.211
40	400	47.0	0.0336	49.0	1450.0	0.032
41	450 x 480 / 200 x 150	270.0	0.0713	280.0	3920.0	0.185
42	480	250.0	0.0585	259.0	4330.0	0.171
43	525	83.0	0.0755	86.3	1140.0	0.056
44	495	147.0	0.063	152.0	2410.0	0.10
45	750 x 225	19.7	0.0466	20.2	435.0	0.013
46	525	187.0	0.075	193.0	2580.0	0.127
47	375	32.0	0.0286	34.0	1180.0	0.021
48	450	193.0	0.0480	199.0	4150.0	0.131
49	600	148.0	0.113	153.0	1360.0	0.101
50	390	110.0	0.0311	114.0	3670.0	0.075
51	630	133.0	0.138	134.0	1000.0	0.103
52	450	86.0	0.0480	89.0	1800.0	0.068
53	730	210.0	0.206	214.0	1040.0	0.104
54	850 x 975	450.0	0.375	465.0	1240.0	0.358
55	375 / 600 x 75	39.0	0.0324	40.5	1250.0	0.031
56	375 x 300	13.3	0.0336	13.8	403.0	0.01
57	600	185.0	0.113	193.0	1700.0	0.148
58	375	145.0	0.0286	150.0	5270.0	0.113
59	750	530.0	0.211	540.0	2560.0	0.41
60	645 / 250	300.0	0.16	312.0	1940.0	0.236
61	400 / 100 / 150	35.0	0.0505	36.3	720.0	0.028
62	300 x 225	3.2	0.0152	3.6	232.0	0.002
63	2 mm x 1.2 mm	1100.0	2.88	1140.0	400.0	0.87
64	180 x 225	1.3	0.0072	1.4	195.0	0.001
65	700 x 375	10.0	0.098	11.2	112.0	0.008
66	300 x 225	2.1	0.0153	2.2	143.0	0.0016
67	330 x 400	3.3	0.0435	3.4	78.0	0.002
68	450 x 600	10.0	0.122	10.2	83.0	0.0077
9	450 x 600	118.0	0.122	120.0	985.0	0.091
	Readings made 27 November 1951					
70	525	116.0	0.0755	120.0	1590.0	0.1665
71	525	47.0	0.0755	48.8	648.0	0.0876
72	510	54.0	0.0696	55.8	801.0	0.0772
73	540	116.0	0.079	120.0	1520.0	0.1665

TABLE 2.5 (Cont.)

No.	Size In Microns	Counts Per Second	Size In $\frac{mc}{mm^3}$ **	mc x 10^{-5}	$\frac{mc \times 10^{-5}}{mm^3}$	Extrapolated to One Hour mc/particle ***
74	480	30.0	0.058	31.2	540.0	0.0434
75	480	50.0	0.058	51.8	890.0	0.0718
76	525	36.0	0.0755	37.2	495.0	0.0514
77	409	75.0	0.036	77.5	2160.0	0.1075
78	270	18.6	0.015	19.2	1280.0	0.1548
79	465	114.0	0.052	113.0	2170.0	0.1568
80	450	114.0	0.048	113.0	2360.0	0.1568
81	465	149.0	0.052	154.0	2960.0	0.216
82	495	72.5	0.0617	74.5	1210.0	0.1025
83	525	184.0	0.0755	190.0	2500.0	0.263
84	480	69.0	0.0588	71.5	1210.0	0.0989
85	435	23.2	0.0441	24.0	545.0	0.0333
86	465	52.0	0.052	53.7	1030.0	0.0743
87	495	76.0	0.064	78.5	1220.0	0.1088
88	465	46.0	0.052	47.7	915.0	0.066
89	450	72.5	0.048	75.0	1560.0	0.104
90	465	114.0	0.052	118.0	2270.0	0.163
91	400	32.4	0.036	33.5	925.0	0.0464
92	395	31.2	0.0327	32.3	1000.0	0.0448
93	420	38.6	0.0384	40.0	1040.0	0.0554
94	510	66.0	0.070	68.5	980.0	0.095
95	400	11.3	0.036	11.7	325.0	0.0162
96	465	160.0	0.052	166.0	3180.0	0.231
97	435	48.0	0.043	49.6	1150.0	0.0688
98	465	130.0	0.052	135.0	2600.0	0.1875
99	465	61.0	0.052	63.3	1220.0	0.0875
100	465	137.0	0.052	142.0	2730.0	0.197
101	300	47.0	0.0143	48.7	3310.0	0.0675
102	480	173.0	0.057	179.0	3160.0	0.248
103	420	55.0	0.039	57.0	1460.0	0.08
104	395	22.8	0.0323	23.6	725.0	0.0328
105	360	30.6	0.0243	31.8	1310.0	0.0441
106	345	27.8	0.0218	27.9	1320.0	0.0386
107	360	20.8	0.0244	21.6	885.0	0.030
108	345	44.5	0.0218	46.2	2110.0	0.064
109	450	61.0	0.0483	63.2	1310.0	0.0875
110	420	83.5	0.0384	86.5	2300.0	0.125
111	465	57.0	0.0523	59.0	1130.0	0.082
112	495	84.5	0.065	87.0	1340.0	0.121
113	435	20.0	0.0403	20.5	510.0	0.0284
114	480	85.0	0.058	88.0	1510.0	0.122
115	300	32.0	0.0143	33.2	2320.0	0.046

PROJECT 2.5a-3

TABLE 2.5 (Cont.)

No.	Size In Microns*	Counts Per Second	Size In mm^3**	mc x 10^{-5}	$\frac{mc \times 10^{-5}}{mm^3}$	Extrapolated to One Hour mc/particle***
116	2 mm	570.0	8.00	580.0	74.0	0.804
117	5 mm x 2 mm	43.0	20.00	44.0	2.0	0.061
118	27C x 150	41.0	0.061	42.0	690.0	0.058
119	3 mm x 1.7mm	120.0	6.70	123.0	18.4	0.17
120	525	250.0	0.0765	259.0	3390.0	0.369
121	575	105.0	0.0282	109.0	3860.0	0.151
122	750 x 450	92.0	0.0635	95.0	1490.0	0.131
123	750 x 600	10.7	0.145	11.0	76.0	0.0152
124	750 x 300	83.0	0.068	85.0	1250.0	0.117
125	2 mm x 450	240.0	0.405	248.0	615.0	0.344
126	600 x 275	10.0	0.0455	11.0	242.0	0.0152
127	300 x 450	23.0	0.045	24.0	510.0	0.0322
128	3 x 300(0)	105.0	0.042	109.0	2600.0	0.151
129	135 / (180 x 75)	3.5	0.0053	3.6	260.0	0.005
130	660 x 480	405.0	0.0149	409.0	2740.0	0.566
131	525(0) x 165	188.0	0.098	190.0	1970.0	0.264
132	330 x 105	58.0	0.02	60.0	3000.0	0.083
133	480 x 150	94.0	0.12	96.0	800.0	0.133
134	105	5.5	0.0055	5.6	1000.0	0.0076
135	600 x 185	236.0	0.143	240.0	1660.0	0.332
136	700	482.0	0.18	486.0	2700.0	0.674
137	1.5 mm x 400	300.0	0.24	310.0	1290.0	0.430
138	600 x 300	3.0	0.054	3.1	575.0	0.0043

* Two types of particles are included in this list. Those with only one value shown are spherical glass beads. The remaining particles showing two dimensions are irregular.

** The size of the spheres was calculated by $4/3\pi R^3$. The size of the irregularly shaped particles was found by multiplying the long axis by the short axis squared. The latter was considered to be a sufficiently close approximation.

*** The first 69 were read on 23 November - H plus 109 hours. The value here for interpolation was 104,000/1560 x mc. The next 69 were measured at 1930 on 27 November - H plus 180 hours. The factor used was 104,000/750 x 138.6 x mc.

TABLE 2.6

Activity Data for Underground Shot Particles *

No.	Size In Microns**	Counts Per Second	Size In mm^3***	mc x 10^{-5}****	$\frac{mc \times 10^{-5}}{mm^3}$	Extrapolated to One Hour mc/particle*****
1	675 x 375	212	0.095	90	950	0.055
2	525 x 1100	282	0.3	120	400	0.072
3	540 x 375	123	0.076	56	750	0.0342
4	900 x 300	127	0.081	54	665	0.033
5	1050 x 300	475	0.095	200	1900	0.122
6	535 x 660	244	0.190	108	560	0.0665
7	790 x 375	192	0.111	82.5	750	0.0504
8	750 x 330	254	0.081	103	1260	0.0625
9	375 x 480	625	0.068	266	3900	0.1625
10	800 x 540	345	0.233	104	445	0.0635
11	1150 x 390	171	0.175	72.5	425	0.0443
12	1100 x 375	175	0.155	74	475	0.0452
13	750 x 240	215	0.043	85	1970	0.0518
14	225 x 300	85.5	0.0155	36	2320	0.022
15	700 x 980	445	0.274	188	685	0.115
16	900 x 480	1080	0.208	450	2160	0.274
17	750 x 500	195	0.187	82.5	440	0.0503
18	750 x 525	176	0.208	74.5	360	0.0454
19	500 x 675	510	0.167	212	1260	0.129
20	675 x 1200	625	0.545	265	485	0.1615
21	300 x 750	435	0.0675	185	2740	0.113
22	525 x 525	310	0.145	131	900	0.08
23	225 x 255	33	0.0114	14	1220	0.0085
24	300 x 255	30	0.0153	12.6	820	0.007
25	150 x 525	73	0.0118	30.8	2600	0.0188
26	450 x 450	57.6	0.091	24.2	267	0.0148
27	185 x 300	14.2	0.0103	6	580	0.0036
28	275 x 225	47.2	0.014	20	1430	0.0122
29	275 x 450	92	0.031	38.8	1250	0.0237
30	210 x 345	8	0.015	3.36	245	0.002
31	270 x 270	29	0.0197	12.5	620	0.0076
32	540 x 540	7.2	0.157	3.04	194	0.0018
33	525 x 600	1.7	0.145	0.72	5	0.0004

Table 2.6 (cont.)

No.	Size In Microns**	Counts Per Second	Size In mm^3***	mc x 10^{-5}****	$\frac{mc \times 10^{-5}}{cm^3}$	Extrapolated to One Hour mc/particle*****
34	600 x 800	9.7	0.278	4.12	11.7	0.0025
35	375 x 375	21.7	0.0525	9.2	175	0.0056
36	1075	10.6	1.23	4.45	3.6	0.0027
37	600 x 375	38.2	0.28	16.2	58	0.0098
38	375 x 525	10	0.064	4.23	66	0.0026
39	200 x 150	18.3	0.045	7.75	172	0.0047
40	195 x 225	20.2	0.085	8.5	100	0.0052
41	550 x 550	42.5	0.167	18	108	0.011
42	700 x 480	58	0.160	24.6	153	0.015
43	600 x 400	37.8	0.096	16	167	0.0097
44	450 x 425	150.4	0.19	51	268	0.031
45	600 x 525	19.5	0.165	8.3	50.5	0.005
46	525 x 360	135	0.067	57	850	0.035
47	525 x 300	208	0.124	88	700	0.054
48	480 x 525	97	0.120	41	332	0.025
49	575 x 360	28	0.05	11.8	276	0.017
50	350 x 300	25.4	0.03	10.7	358	0.0065
51	750 x 550	110	0.226	46.6	204	0.028
52	225 x 225	150	0.0115	63.5	5560	0.039
53	510 x 375	34	0.071	14.4	204	0.009
54	550 x 400	54	0.087	22.8	262	0.014
55	450 x 300	120	0.04	50.6	1260	0.031
56	800 x 600	30	0.288	12.7	44.3	0.0077
57	525 x 500	35	0.132	14.8	112	0.009
58	1125 x 900	12.5	0.92	5.3	5.7	0.003
59	450 x 390	120	0.0085	50.7	742	0.031
60	825 x 450	140	0.167	59.5	355	0.036
61	750 x 375	100	0.105	42.3	400	0.026
62	600 x 600	2.9	0.216	0.123	0.5	0.00007
63	600 x 525	100	0.195	42	216	0.0256
64	570 x 375	39	0.080	16.5	206	0.01
65	750 x 400	50	0.12	21.1	176	0.0129
66	480 x 800	3	0.185	0.128	0.7	0.00008
67	330 x 375	83	0.041	35	850	0.0214
68	375 x 375	108	0.053	45.5	840	0.0275
69	540 x 665	800	0.175	338	1930	0.206
70	300 x 450	3	0.045	0.127	2.8	0.00007
71	800 x 675	3	0.362	0.127	0.35	0.00007
72	1500 x 450	84	0.264	35.4	134	0.022

PROJECT 2.5a-3

TABLE 2.6 (Cont.)

No.	Size In Microns**	Counts Per Second	Size In mm^3***	mc x 10^{-5}****	$\frac{mc \times 10^{-5}}{mm^3}$	Extrapolated to One Hour mc/particle*****
73	630 x 300	140.0	0.057	59.00	1030.00	0.036
74	510 x 150	14.0	0.0115	5.90	515.00	0.0036
75	180 x 225	7.6	0.0073	3.20	438.00	0.0019
76	180 x 375	71.0	0.012	30.40	254.00	0.0185
77	av. 150	9.0	0.0034	3.80	1150.00	0.0023
78	150 x 540	80.0	0.012	33.80	282.00	0.0206
79	235 x 180	10.5	0.0076	4.45	585.00	0.0027
80	375 x 210	50.0	0.0167	21.20	1270.00	0.0129
81	225 x 330	3.8	0.0167	1.60	95.00	0.0097
82	120 x 150	39.0	0.0041	16.50	4000.00	0.01
83	450 x 750	218.0	0.152	92.00	605.00	0.056
84	525 x 820	286.0	0.226	121.00	535.00	0.074
85	450 x 725	63.0	0.142	26.60	186.00	0.016
86	525 x 525	2.0	0.145	0.85	0.57	0.0005
87	450 x 750	226.0	0.152	96.00	630.00	0.058
88	950 x 600	7.1	0.332	2.96	9.00	0.0018
89	1050 x 750	224.0	0.590	95.00	160.00	0.058
90	625 x 225	76.0	0.316	32.20	102.00	0.0196
91	525 x 525	48.0	0.145	20.20	139.00	0.0123
92	600 x 750	490.0	0.270	208.00	770.00	0.127
93	400 x 225	55.0	0.203	23.20	114.00	0.014
94	800 x 345	508.0	0.095	216.00	2260.00	0.132
95	325 x 495	42.0	0.052	17.80	342.00	0.0108

* All readings were made beginning at 1500 hours on 2 December, which was H plus 75.

** The size was measured on the longest axis and an average of shortest. The particles were very irregular.

*** The size in cubic millimeters was found by assuming that the particle was somewhat rectangular and thus the long axis was multiplied by the square of short axis.

**** The geometry of the counter was such that $\frac{\text{counts per sec} \times 5.13 \times 10^{-5}}{12.1} = mc \times 10^{-5}$.

***** The data used to extrapolate to one hour was furnished by Dr. C.L. Maxwell and is shown elsewhere in this report. The factor is 500,000/8200 = 61. Then 61 x mc = value at one hour.

CHAPTER 3

STATISTICAL STUDY

3.1 INTRODUCTION

In order to assess the trend in activity variation with particle size the data collected on the size and activity of the individual particles (Tables 2.5 and 2.6) was presented to the statistician at the Army Medical Service Graduate School. The procedure and results of this examination are presented in the following paragraphs.

TABLE 3.1

Mean Activity versus Particle Volume, Spherical Particles*

Volume Interval	Number Contributing Measurements	Mean Activity		Range	
Cubic mm		Curies x 10^{-8}		Curies x 10^{-8}	
		Mean	Standard Error	Low	High
0-0.01	0	--	--	--	--
0.01-0.02	3	48.6	15.3	12.4	74.5
0.02-0.03	6	89.9	24.7	17.1	187.0
0.03-0.04	4	95.0	13.6	49.0	116.0
0.04-0.05	9	160.1	36.5	20.2	415.0
0.05-0.06	7	136.9	23.8	74.5	259.0
0.06-0.07	5	200.6	39.7	116.0	362.0
0.07-0.08	2	139.6	37.9	86.3	193.0
0.08-0.09	3	227.9	73.2	48.8	320.0
0.09-0.10	0	--	--	--	--
0.10 or larger	8	245.2	52.5	43.5	540.0

* See Figure 3.1 for graphical representation

3.2 SPHERICAL PARTICLES

The data analyzed consisted of the diameter and the measured radiation, in curies, originating from a number of spherical particles collected from the surface detonation. The measure of size of the particle was arbitrarily chosen as volume which was calculated directly from the data. Two groups of spherical particles, grouped by the day on which the activity measurements were made, were studied. The volume range of the particles was chiefly below 0.10 cubic millimeters and an arbitrary class interval of 0.01 cubic millimeters, starting from the base of zero volume, was set up. All particles larger than 0.10 cubic millimeters were placed in a single class. The mean, standard error and the range were calculated from the frequency distributions for each interval and are presented in Tables 3.1 and 3.2. The correlation coefficients and regression lines based on the data were also investigated. (See Figures 3.1 and 3.2).

TABLE 3.2

Mean Activity versus Particle Volume, Spherical Particles*

Volume Interval	Number Contributing Measurements	Mean Activity		Range	
Cubic mm		Curies x 10^{-8}		Curies x 10^{-8}	
		Mean	Standard Error	Low	High
0-0.01	0	--	--	--	--
0.01-0.02	3	33.7	7.0	19.2	48.7
0.02-0.03	4	31.9	4.5	21.6	46.2
0.03-0.04	8	45.5	8.8	11.7	88.5
0.04-0.05	6	57.5	12.9	20.5	113.0
0.05-0.06	15	98.2	12.1	31.2	179.0
0.06-0.07	4	73.9	5.8	55.8	87.0
0.07-0.08	6	97.4	21.4	37.2	190.0
0.08-0.09	0	--	--	--	--
0.09-0.10	0	--	--	--	--
0.10 or larger	0	--	--	--	--

* See Figure 3.2 for graphical representation

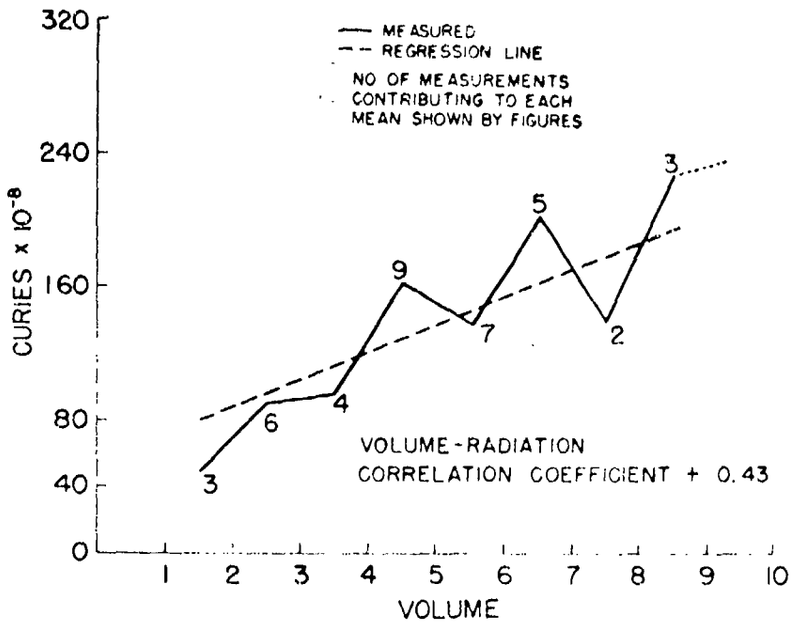

Fig. 3.1 Mean Activity Versus Particle Volume (23 November Activity)

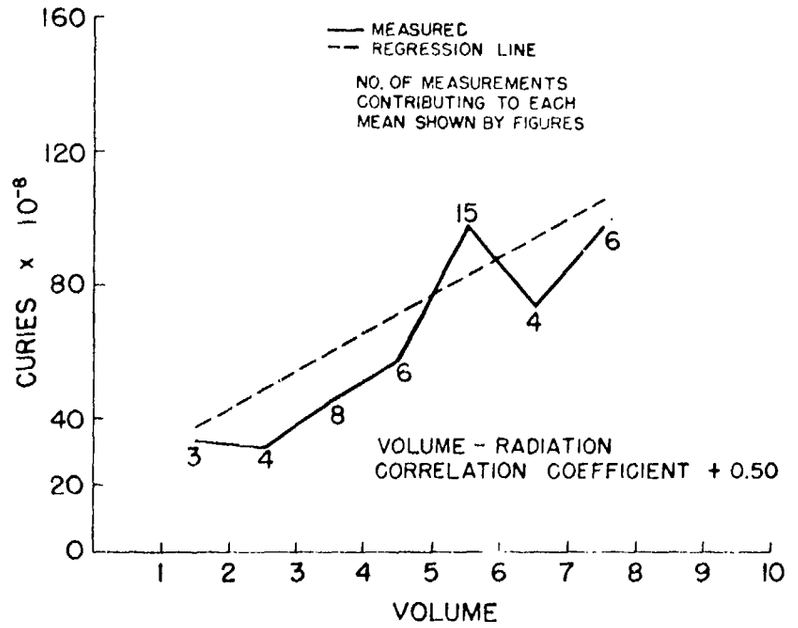

Fig. 3.2 Mean Activity Versus Particle Volume (27 November Activity)

In general, the intensity of radiation was shown to vary directly with the volume of the particle, since the volume-radiation correlation coefficients in both groups of spherical particles were significantly greater than zero. There was considerable random fluctuation in the quantity radiation per unit volume within the range of volumes studied, and no significant trend of that quantity was demonstrable.

3.3 IRREGULAR PARTICLES

A number of irregular particles were also analyzed on the same lines of inquiry using a prolate spheroid to express the volume since the length and width of the particles were the only dimensions recorded. The results gave an indication of a volume-radiation correlation similar to that observed with the spherical particles but the variation encountered was very wide and there was some doubt whether the group represented a random sample.

CHAPTER 4

DISCUSSION AND CONCLUSIONS

4.1 DISCUSSION

It is not, nor has it ever been, the contention of the author that all fall-out particles are large. However, it has been definitely proven that a large quantity of activity may be found in large particles in areas removed from the immediate zero point in a terrain similar to the one in Nevada and under wind conditions which prevailed at the time of the shots. Some of the activity may be due to small airborne particles which may be a health hazard when inhaled. This does not mean that there is no health hazard in the large particles because, as indicated from the data, many of these individual particles have as much as 0.1 to 0.2 millicuries at the end of one hour after the shot has occurred. The hazard would then be that of external radiation and not inhalation. Inasmuch as the particles isolated were within a radius of fourteen miles, with the majority between five and ten miles away from zero point, the activity on the ground in the general vicinity mentioned would be due to the large particles and not to the smaller ones. At distances greater than this, namely 20 to 50 miles, no statement can be made. It would appear, however, that with larger bombs and higher winds, particles of 50 microns could be carried to this distance and fall out within a period of two hours. It is not believed that these large particles are carried much beyond this point, although this is strictly the author's own viewpoint.

It is of interest to cite two instances which serve to substantiate the finding that a great amount of the activity in nearby fall-out areas is due to particles large enough to lend themselves to this method of separation. The first instance was a boot worn by a man who went into the area 14 miles from zero point and which upon his return to the laboratory was found to be highly contaminated. By surveying the boot with the No. 263 Field Survey Instrument the majority of the activity was found to be on the sole. A pen knife was used to take the adhering material off the sole and it was noted that the activity went with the removed soil. Three particles were isolated and more than 80 percent of the activity was carried in these three particles.

The second item of interest was a water can which had been in the field approximately three miles from ground zero for the surface shot of JANGLE. This can had become moistened in some way prior to shot time, and dirt had adhered to it. It was brought to the laboratory

Best Available Copy

and approximately 10 grams of dirt were scraped off. This dirt was found to contain a considerable amount of activity. The 10 grams were divided in half and very carefully studied by the technique mentioned above. Thirty-eight particles were isolated from one 5 gram portion and placed in a container. The No. 263 G. M. instrument with the beta window open was placed approximately 2 inches above the sample. A reading of 19 mr. per hour was obtained. The remainder of the soil from the same portion contained 0.3 mr. per hour. Thus it can be seen that about 90 percent of the activity was carried on these thirty-eight particles. All of them were greater than 150 microns in diameter and none was greater than 400 microns. Twenty-two of the largest particles carried 85 percent of the above mentioned activity, while the remaining sixteen particles contained the remaining 15 percent.

4.2 CONCLUSIONS

It has been shown with this method of sample collecting of fall-out particles due to an atomic detonation that:

(1) Particles of 300 to 700 microns in size may be found as far as 14 miles downwind from zero point.

(2) There does not appear to be any selectivity of specific radioactive isotopes on large particles of the size range reported.

(3) There seems to be at least a trend, from statistical analysis, that the larger particles carry a larger amount of activity.

(4) Specifically for the surface shot, a very large fraction of the total fall-out activity is carried by particles above 100 microns out to distances of 10 miles downwind.

(5) Significant differences of the physical properties of particles were found for the surface and underground shots. Fused spherical particles were found in considerable number only after the surface shot.

Best Available Copy

OPERATION JANGLE

PROJECT 2.8

ANALYSIS OF TEST SITE AND FALL-OUT MATERIAL

by

L. T. Alexander, J. M. Blume
and M. E. Jefferson

1 March 1952

Bureau of Plant Industry, Soil
and Agricultural Engineering

Agricultural Research Administration
United States Department of Agriculture

PROJECT 2.8

PREFACE

The work reported herein was undertaken at the request of the Division of Biology and Medicine of the Atomic Energy Commission. Questions were raised regarding the possible agricultural hazard of fall-out material from surface and underground explosions of atomic weapons. It was decided that a study would be made of the sites of the surface and underground shots and of fall-out material at various distances from the sites. Collection of the material for study of the sites was made by L. T. Alexander. Dr. Andrews agreed to arrange for collection of the fall-out material. Major John d' H. Hord made these collections and arranged for shipment of the material to Washington. Dr. N. E. Tolbert of the Division of Biology and Medicine, Atomic Energy Commission, contributed very greatly to the planning and execution of the project.

PROJECT 2.8

CONTENTS

ILLUSTRATIONS

PROJECT 2.8

TABLES

CHAPTER 2 RESULTS

PROJECT 2.8

ABSTRACT

A study was made of the chemical and physical composition of the sites of the surface and underground shots of JANGLE operation prior to test date. Subsequent to the tests, collections of fall-out material were made. Some physical characterizations have been made of these fall-out materials. Measurement of radioactivity indicates that the fall-out within a four mile distance from zero had an activity of about 10 curies per ton. The fall-out at one-half mile north was more than 1,000 tons per square mile while 63 tons fell at four miles northeast. Fall-out at four miles northeast was somewhat more radioactive per ton than at one-half mile north. Gradation of the material was dependent on distance from zero. Preliminary studies of the uptake of radioactivity from fall-out material mixed with different soils indicate a very high uptake of a beta emitting element of approximately 50 days half-life. The element is thought to be strontium 89. The amount taken up from a soil low in calcium is of a magnitude that might constitute a hazard to agriculture.

CHAPTER 1

COLLECTION OF SAMPLES

1.1 PRE-TEST

Soil samples were collected 17 and 18 September 1951 at JANGLE underground site, JANGLE surface site, and to a limited extent at BUSTER tower shot site. Except for the small fraction used in the analyses, these two to four pound samples are held at the Beltsville Laboratory of the Division of Soil Management and Irrigation Agriculture. Additional tests can be made on the whole soil or on any fraction of it if this seems desirable.

1.2 POST TEST

Post test fall-out sample collections were made at H plus 72 hours for the JANGLE surface shot and at H plus 48 hours for the JANGLE underground shot. The 3/8 inches of rain that occurred between the time of the surface shot and the sample collection made collection difficult and caused loss of some sample from the 52-inch x 70-inch suspended oil cloths. Decantation of the water in 24-inch diameter tubs used for collecting close-in samples caused some loss of the finer fraction of these samples. No water was encountered in collection of fall-out material from the underground shot except for the station 8 miles northeast of shot site. Collection of fall-out material from the underground shot is considered satisfactory except for the possibility that wind action may have removed fall-out from some collection oil cloths.

1.3 SITE FIELD DATA

Location of exact sampling positions and comments on the locations are given in the following paragraphs.

1.3.1 JANGLE Underground Shot Site

The samples through 10 feet in depth were taken in a pit 150 feet north of exact zero. Depths from 10 feet through 16 feet were from an excavation 350 feet east and a bit north of exact zero. The sample at 22 feet was taken at exact zero. This location is in an area of alternating layers of sandy and gravelly material that

has been formed by outwash from the surrounding mountains or hills as alluvial fans. The site is relatively coarse textured as compared to most inhabited and agricultural regions. The amount of material that is fine enough to remain in suspension in the atmosphere for any long period of time without comminution is a small fraction of the total. There are no very hard pans or cemented layers at this site to the depth examined. Cementing material where present is calcium carbonate.

1.3.2 JANGLE Surface Shot Site

At this site samples were obtained from a small pit dug 100 feet west and a few feet south of exact zero and from rotary drilling at Station 7 which is 642 feet south of exact zero. This site is similar, as regards mode of formation, to the surface shot site but is more uniform in particle size distribution. The most striking difference between this site and the underground site is the presence here of a hard calcium carbonate horizon called "caliche" extending from two to four feet in depth. The cemented materials are similar to those above and below except for the cementing matrix of calcium carbonate. This layer is so hard that a heavy crowbar rebounds upon striking it. This site also had a very loose surface mulch (zero to 3 inches) of loose material with somewhat higher percentage of silt than the horizons beneath. Efforts were being made to stabilize this layer at the time of sampling prior to the tests. Unstabilized it blows into the air very readily.

1.3.3 BUSTER Tower Shot Site

The samples were taken in an undisturbed area 150 feet west of the tower. The depth from zero to 6 inches was very loose and powdery. The content of silt is higher than that at the JANGLE surface site but has less clay. These two sites, when undisturbed should be quite similar with regard to ease of movement of surface material by air blast. All sites were dry except for a small amount of moisture just above the "caliche" layer at the JANGLE surface shot site.

PROJECT 2.8

CHAPTER 2

RESULTS

2.1 PHYSICAL DATA ON PRE-TEST SAMPLES

Methods used are recognized standard procedures for soil analyses. Because of the time required and expense involved all determinations were not made on all samples. Where this was the case, enough determinations were made to give the trend or value desired. Additional determinations can be made if needed.

2.1.1 Particle Size Distribution JANGLE Underground Test Site

The samples of soil material were sieved on 2- and 6-mm (actually 5.6-mm square meshes) sieves for separation into fine earth, fine gravel, and coarse gravel. The results are given in Table 2.1. Although there is present considerable quantities of gravel-size particles, the less than 2-mm fraction predominates.

A more detailed particle-size distribution analysis of the fraction less than 2-mm in diameter seemed desirable from two standpoints: first it is only this fraction that can be carried appreciable distances without comminution and second, it is desirable that the test site material be compared in texture with soil material found in other places. For agricultural purposes it is the less than 2-mm fraction only that is analyzed in detail. Table 2.2 gives the data of this analysis.

2.1.2 Particle Size Distribution JANGLE Surface Test Site

The corresponding data for the JANGLE surface shot are given in Tables 2.3 and 2.4.

This site is more homogeneous than the underground test site. This is particularly true with respect to the particle size distribution of the fine earth below a depth of two feet. The finer fractions, silt and clay, are somewhat higher than in case of the underground site.

PROJECT 2.8

TABLE 2.1

JANGLE Underground Shot Site Size Fractions of Whole Material at Various Depths*

Depth	Diameter in Millimeters		
	Less than 2	2 to 6	6 and Up
Feet	Percent	Percent	Percent
0 - 1	82	10	8
1 - 2	81	9	10
2 - 3	84	4	12
3 - 4	66	21	13
4 - 5	72	14	14
5 - 6	83	7	10
6 - 7	84	9	7
8 - 9	81	5	14
9 - 10	58	19	23
10 - 11	49	17	34
11 - 12	82	11	7
15 - 16	47	17	36
22	73	16	11

* The distribution of particle sizes reflects the layering of the horizons at the site.

PROJECT 2.8

TABLE 2.2

JANGLE Underground Shot Site Size Fractions of Fine Earth (less than 2-mm diameter) at Various Depths

Depth	Size Class and Diameter of Particles (in mm.)						
	Very coarse sand 2-1	Coarse sand, 1-0.5	Medium sand, 0.5-0.25	Fine sand, 0.25-01	Very fine sand 0.1-0.05	Silt 0.05-0.002	Clay <0.002
Feet	Percent	Percent	Percent	Percent	Percent	Percent	Percent
0 - 1	6.3	11.0	9.2	27.8	23.4	12.8	9.5
1 - 2	9.2	12.4	9.5	27.4	23.4	11.5	6.6
2 - 3	10.3	17.7	13.0	27.7	19.0	7.9	4.4
3 - 4	29.2	37.3	11.5	9.4	3.4	5.1	4.1
4 - 5	18.2	29.3	16.7	19.6	7.4	4.5	4.3
5 - 6	4.4	11.6	13.1	32.4	20.4	12.9	5.2
6 - 7	6.6	16.5	12.5	31.0	17.7	11.2	4.5
8 - 9	11.3	22.5	16.7	25.7	9.4	6.0	8.4
9 - 10	15.6	25.0	15.8	23.4	8.7	4.3	7.2
10 - 11	13.0	23.1	15.0	24.2	9.9	6.9	7.9
11 - 12	10.2	15.4	11.9	26.2	12.1	13.9	10.3
15 - 16	11.7	21.5	16.2	27.2	10.4	7.4	5.6
22	9.6	17.0	12.3	28.0	17.4	10.7	5.0

* The contents of clay and silt are much less than are normal in most inhabited regions of the world. The changes in distribution of the various fractions again reflect the vertical heterogeneity of the site.

PROJECT 2.8

TABLE 2.3

Size Fractions of Whole Material at Various Depths
JANGLE Surface Shot Site

Depth	Diameter in Millimeters		
	Less than 2	2 to 6	6 and Up
	Percent	Percent	Percent
0 - 5"	61	15	24
5 - 11"	48	23	29
11" - 2'	78	10	12
2' - 4'	49	20	31
4'	66	15	19
6'	80	9	11
8'	83	7	10
10'	84	8	8
12'	77	11	12
15'	65	16	19
20'	76	15	9
25'	79	12	9
30'	73	19	8

PROJECT 2.8

TABLE 2.4

Size Fractions of Fine Earth (less than 2-mm diameter) at Various Depths
JANGLE Surface Shot Site

Depth	Size Class and Diameter of Particles (in mm.)						
	Very coarse sand 2-1	Coarse sand, 1-0.5	Medium sand, 0.5-0.25	Fine sand, 0.25-0.1	Very fine sand 0.1-0.05	Silt, 0.05-0.002	Clay, <0.002
	Percent	Percent	Percent	Percent	Percent	Percent	Percent
0 - 5"	3.8	4.6	6.7	35.8	25.9	17.7	5.5
5 - 11"	8.4	10.0	11.9	36.0	14.6	10.9	8.2
11 - 24"	3.1	5.6	9.5	38.1	22.0	12.7	9.0
24 - 48"	9.3	13.9	14.2	30.1	12.6	12.0	7.9
4'	7.8	13.7	14.6	27.4	11.8	14.8	9.9
6'	6.3	13.1	14.4	29.2	11.7	15.7	9.6
8'	5.0	12.6	15.2	34.0	14.8	11.9	6.5
10'	7.1	13.4	14.4	31.6	14.2	12.5	6.8
12'	4.7	11.0	15.8	35.6	12.9	13.8	6.2
15'	9.5	14.6	14.3	30.5	12.9	12.7	5.5
20'	8.4	12.1	11.7	31.1	12.7	14.7	9.3
25'	6.9	12.3	11.8	29.1	16.2	15.5	8.2
30'	5.2	11.2	12.7	30.3	17.6	14.5	8.5

PROJECT 2.8

2.1.3 Particle Size Distribution BUSTER Tower Shot Site

For purposes of comparison, data are presented for two samples from the BUSTER tower shot site.

TABLE 2.5

Size Fractions of Whole Material at Two Depths
BUSTER Tower Shot Site

Depth	Diameter in Millimeters		
	Less than 2	2 to 6	6 and Up
Inches	Percent	Percent	Percent
0 - 6	73	16	11
6 - 18	64	24	12

TABLE 2.6

Size Fractions of Fine Earth (less than 2-mm diameter) at Two Depths
BUSTER Tower Shot Site

Depth	Size Class and Diameter of Particles (in mm.)						
	Very coarse sand 2-1	Coarse sand, 1-0.5	Medium sand, 0.5-0.25	Fine sand, 0.25-0.1	Very fine sand, 0.1-0.05	Silt, 0.05-0.002	Clay, <0.002
Inches	Percent	Percent	Percent	Percent	Percent	Percent	Percent
0 - 6	10.0	10.9	6.6	17.5	22.5	26.5	6.0
6 - 18	17.0	19.7	11.0	19.8	14.1	11.6	6.8

PROJECT 2.8

2.1.4 Air Elutriation Data

The particle-size distribution data on the less than 2-mm soil material presented in Sections 2.1.1 to 2.1.3 were obtained by ultimate dispersion in water by use of dispersing agents and use of agitation. Since the soil materials at the sites are dry and are blown into the air without liquid dispersion, it was thought desirable to know the degree of dispersion in air as the materials exist at time of the explosion. By means of the Roller Air Elutriator the data shown in Table 2.7 were obtained. For comparison the ultimate dispersion data are given for the same samples in the last column.

TABLE 2.7

Comparison of Dispersion in Air and in Liquid of Samples from Various Depths at Three Sites

JANGLE and BUSTER

Sample Site	Depth	Size Fractions by Air Elutriation			Material 0 - 50 microns by complete dispersion in liquid.
		Size Fraction Diameter Microns	Percent Found	Cumulative Percent	
Tower	0 - 6"	0-10	14.6	14.6	
		10-20	2.8	17.4	
		20-40	17.0	34.4	32.5
	6 - 18"	0-10	11.7	11.7	
		10-20	2.1	13.8	
		20-40	5.3	19.1	18.4
Underground	0 - 1'	0-10	16.0	16.0	
		10-20	1.9	17.9	
		20-40	5.0	22.9	22.3
	21 - 22'	0-10	9.3	9.3	
		10-20	2.9	12.2	
		20-40	5.9	18.1	15.7
Surface	0 - 5"	0-10	11.3	11.3	
		10-20	1.6	12.9	
		20-40	7.0	19.9	23.2
	5 - 11"	0-10	14.4	14.4	
		10-20	1.0	15.4	
		20-40	3.7	19.1	19.1
	11 - 24"	0-10	18.6	18.6	
		10-20	1.7	20.3	
		20-40	5.0	25.3	21.7

While an exact comparison of particle sizes is not possible from the data obtained, it is seen that essentially all of the particles below 50 microns in diameter are unaggregated. This gives an explanation for the very dusty nature of the sites in spite of the fact that they are composed of relatively coarse textured materials. In most areas of the country the fine fractions of the soil are aggregated to a considerable extent.

2.2 CHEMICAL DATA ON PRE-TEST SAMPLES

Chemical data were obtained on selected samples from JANGLE underground and surface shot sites. Total analyses by a fusion procedure were made on these selected samples from each site. Calcium carbonate, pH, and soluble salts were determined on all samples. Additional determination can be made if needed.

2.2.1 Total Analyses of Selected Samples

The chemical composition of materials in the immediate blast area and in the neutron cloud is important in determining the induced radioactivity in the fall-out material. Since the finer fractions of the soil is carried further than the coarse, it was decided to analyze the coarse and fine fractions separately. These analyses are given in Table 2.8.

The outstanding difference between the underground and surface shot sites is in the higher content of calcium in the latter. The sodium and potassium content of the coarse fraction of samples from the surface shot is much lower than the corresponding material from the underground site. Sodium and potassium contents of the fine earth fraction from the two sites are essentially the same. The large ignition losses on samples from the surface shot site reflect loss of carbon dioxide from calcium carbonate. Low values for iron, SiO_2 etc. result from dilution by the large amount of calcium carbonate.

TABLE 2.8

Chemical Composition of Fine and Coarse Fraction of Material from Selected Horizons of JANGLE Underground and Surface Shots

Compound	JANGLE - Underground Shot						JANGLE - Surface Shot					
	5 to 6 ft.		10 to 11 ft.		22 ft.		0 to 5 in.		11 to 24 in.		10 ft.	
	Fine	Coarse	Fine	Coarse	Fine	Coarse	Fine	Coarse	Fine	Coarse	Fine	Coarse
K_2O	3.32	4.04	3.09	2.61	3.50	3.75	3.04	0.90	3.13	0.95	2.98	0.98
Na_2O	2.19	1.19	1.93	1.02	2.24	1.94	2.10	0.27	1.98	0.34	2.09	0.54
CaO	2.60	2.37	4.26	7.52	2.39	2.12	7.99	44.52	9.50	39.09	11.10	38.17
MgO	0.91	0.78	0.85	1.22	1.21	0.80	1.35	1.10	1.32	1.09	1.36	1.08
SiO_2	69.72	70.94	68.50	65.21	68.00	69.79	60.65	11.76	59.39	18.99	57.70	20.84
Fe_2O_3	2.92	2.96	2.93	3.18	3.26	3.64	2.78	1.29	2.56	1.57	2.17	1.39
Al_2O_3	13.98	12.91	12.96	10.66	14.88	13.86	12.88	3.32	11.92	5.36	11.36	4.95
TiO_2	0.46	0.44	0.41	0.43	0.53	0.43	0.37	0.21	0.42	0.23	0.29	0.22
MnO	0.04	0.07	0.04	0.07	0.05	0.06	0.05	0.05	0.04	0.06	0.03	0.04
P_2O_5	0.13	0.12	0.09	0.10	0.15	0.11	0.14	0.19	0.05	0.15	0.05	0.13
Ignition Loss	4.41	3.58	5.64	7.78	5.38	2.91	8.90	35.96	10.47	31.70	12.29	31.07
Total	100.68	99.49	100.70	99.88	101.59	99.55	100.25	99.71	100.78	99.62	101.42	99.51
SO_3	0.35	0.09	0.03	0.08	0.03	0.14	0.03	0.14	0.03	0.09	0.05	0.10

Fine - fine earth less than 2-mm in diameter
Coarse - material greater than 2-mm in diameter

PROJECT 2.8

2.3 AMOUNT AND CHARACTERISTICS OF FALL-OUT

Although the fall-out materials are quite radioactive, some determinations have been made. More detailed examinations will be made as time and radiation levels permit. Enough determinations have been made to indicate the possible hazard of the fall-out material to agricultural and residential areas near the site of an explosion of the underground type.

2.3.1 Fall-out From Surface Shot

Between the time of placing of the tubs and cloths and the time of the shot, some tubs were stolen. This made some predetermined stations missing for this shot and limited the number of collections for the underground test. Table 2.10 gives the weights of fall-out material.

TABLE 2.10

Surface Shot Fall-out Material

Location	Receptacle	Grams/sq ft	Pounds/acre	Tons/sq mi
1 Mi E	Tub	0.430	41.3	13.2
1/2 Mi E	Tub	0.366	35.1	11.2
1/2 Mi N	Tub	3.06	294.	94.0
1 Mi N	Tub	1.80	173.	55.3
1 Mi N	Cloth	0.016	-	-
2 Mi N	Tub	5.14	494.	158.0
2 Mi N	Cloth	0.022	-	-
4 Mi N	Tub	0.923	88.6	28.4
4 Mi N	Cloth	0.530	-	-
6 Mi N	Cloth	0.258	-	-
10 Mi N	Cloth	0.004	-	-

PROJECT 2.8

As mentioned previously the rain that fell subsequent to the test greatly interfered with sample collections. Amounts found can only be regarded as minimal values. It is not known how much sample material was lost in run off from the cloths nor how much radioactivity was dissolved in the water decanted.

2.3.2 Fall-out from Underground Shot

Conditions were more favorable for collection of fall-out material from the underground test. There was no precipitation except for the 8-mile northeast station where a small amount was collected on the oil cloth. The data are given in Table 2.11.

TABLE 2.11

Underground Shot Fall-out Material

Location	Receptacle	Grams/sq ft	Pounds/acre	Tons/sq Mi
1 Mi E	Tub	0.003	0.3	0.1
1/2 Mi E	Tub	0.579	55.6	17.8
1/2 Mi W	Tub	1.15	110.4	35.3
1 Mi W	Tub	0.19	18.2	5.8
2 Mi W	Cloth	None	None	None
1/2 Mi N	Tub	37.50	3601.	1152.
1 Mi N	Tub	23.52	2259.	723.
2 Mi N	Cloth	2.88	277.	88.5
4 Mi N	Cloth	0.015	1.4	0.5
4 Mi NE	Cloth	2.04	196.	62.7
8 Mi NE	Cloth	0.24	23.0	7.4

The fall-out pattern fits well with the observed slight shift of the cloud to the west and then the movement to the east of north. The largest amount of material collected was the 37.5 grams per square foot at one-half mile north of zero. The very low value found at four miles north seems open to question in view of the relatively large quantity found at four miles northeast. It seems probable that this sample may have been partially lost by wind action. It is doubtful that the suspended cloth is a satisfactory means of collecting fall-out under conditions of the test.

2.3.3 Particle Size Distribution of Fall-out

A dry-sieve analysis was made of the four largest samples of fall-out material from the underground test. The results are shown in Table 3.12.

TABLE 2.12

Particle Size Distribution of Fall-out Material from Four Stations - JANGLE Underground Shot

Distance From Zero	Size Class and Diameter of Particles (in mm)					
	Very coarse sand 2-1	Coarse sand 1-0.5	Medium sand 0.5-0.25	Fine sand 0.25-0.1	Very fine sand 0.1-0.05	Silt & Clay <0.05
	Percent	Percent	Percent	Percent	Percent	Percent
1/2 Mi N	5	44	26	6	11	8
1 Mi N	0	3	23	51	11	12
2 Mi N	0	0	1	44	45	10
4 Mi NE	0	0	0	38	60	2

The fall-out material is rather nicely sized according to distance from the zero point. A more precise evaluation of the particle size distribution of these materials will be made when they can be more easily handled. This will be done by suspension in water. The clay fraction less than 2 microns in diameter will also be determined.

PROJECT 2.8

2.3.4 Radioactivity of Fall-out Material from Underground Shot

Because most of the radioactivity in the fall-out material was concentrated in fused coatings on occasional mineral grains it was considered necessary to have samples of about 0.1 gram or larger in order for them to be representative. Three samples each were weighed from the fall-out from one-half mile north and from four miles northeast on 12 December 1951. At this time the activity was so great that these samples could only be counted with equipment available through 276 mg/cm^2 aluminum filters. Under these conditions samples ranging from 0.0985 gram to 0.3599 gram gave counts per gram ranging from 20.3 to 21.7 for the fall-out from one-half mile north and from 22.4 to 24.4 for material from four miles northeast. Under conditions of the measurements beta radiation of 0.6 Mev or less would be lost.

In order to count the samples with no filter and with a range of filters, the counting geometry shown in Figure 2.1 was used. In this assembly a Ra D+E standard (NBS 500 disintegrations per second) gave a corrected rate of 0.58 counts per second. This setup was used to obtain the half-life data shown in Figure 2.2.

On 21 February 1952 samples from four miles northeast and from one-half mile north were counted in a hemispherical, 2π geometry, proportioned flow counter. The data in disintegrations per second per gram of material corrected for decay to D+28 days are given in Table 2.13 along with data obtained by use of the setup shown in Figure 2.1.

TABLE 2.13

Radioactivity of Fall-out Material

Sample	End Window Counter	Proportional Counter
1/2 mile north	320,000 d/s/g	423,000 d/s/g
4 miles northeast	432,000 d/s/g	530,000 d/s/g

Disintegrations on the order of 4.3×10^5 corresponds to 11 curies per ton of fall-out material. The radioactivity of the fall-out material from four miles northeast was found to be five percent soluble in water in 18 hours. A solution of rare earth salts in 1 N HCl dissolved 26 percent of the activity under similar conditions.

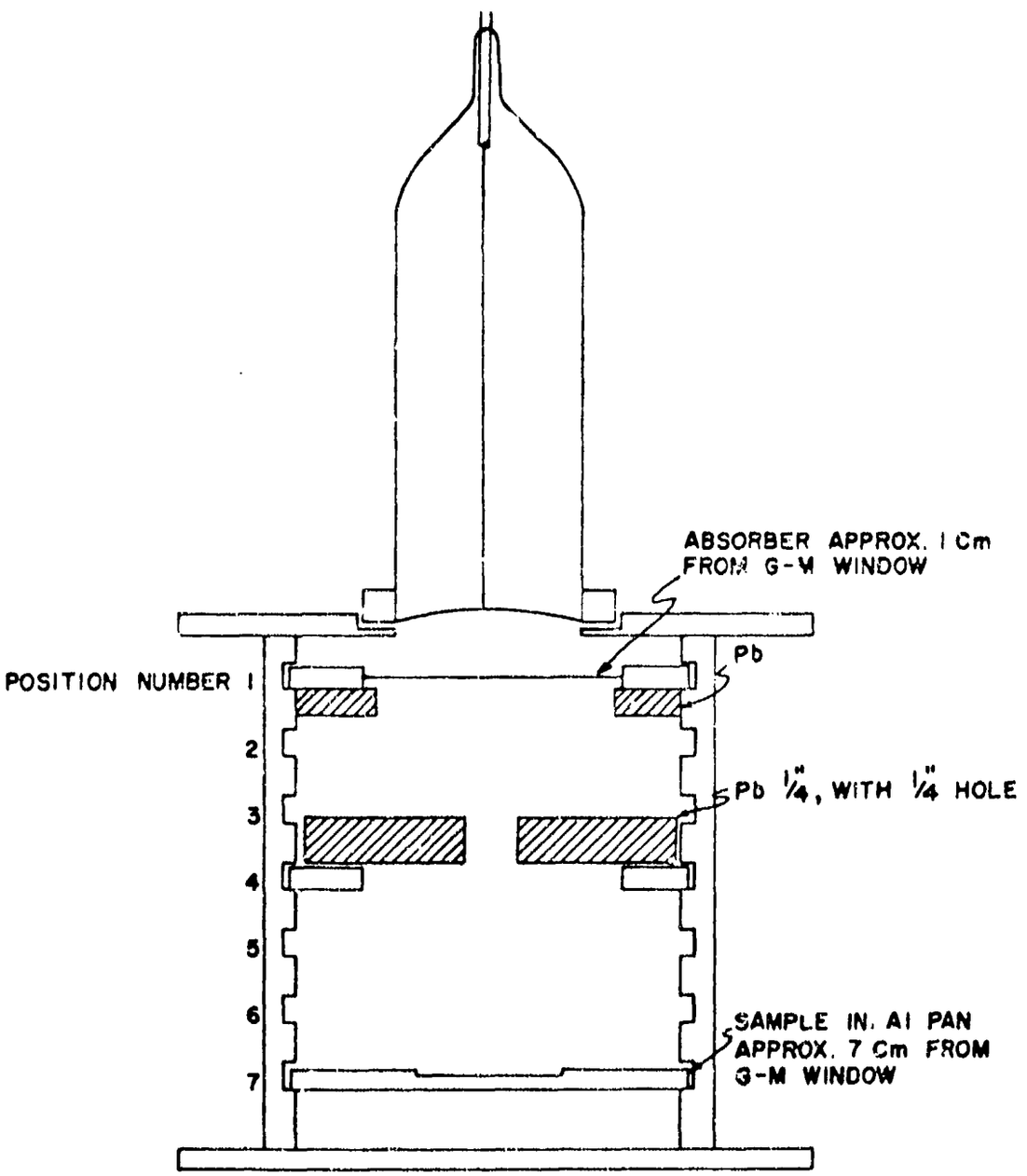

Fig. 2.1 Geometry of End Window Counting Tube and Lead Shield

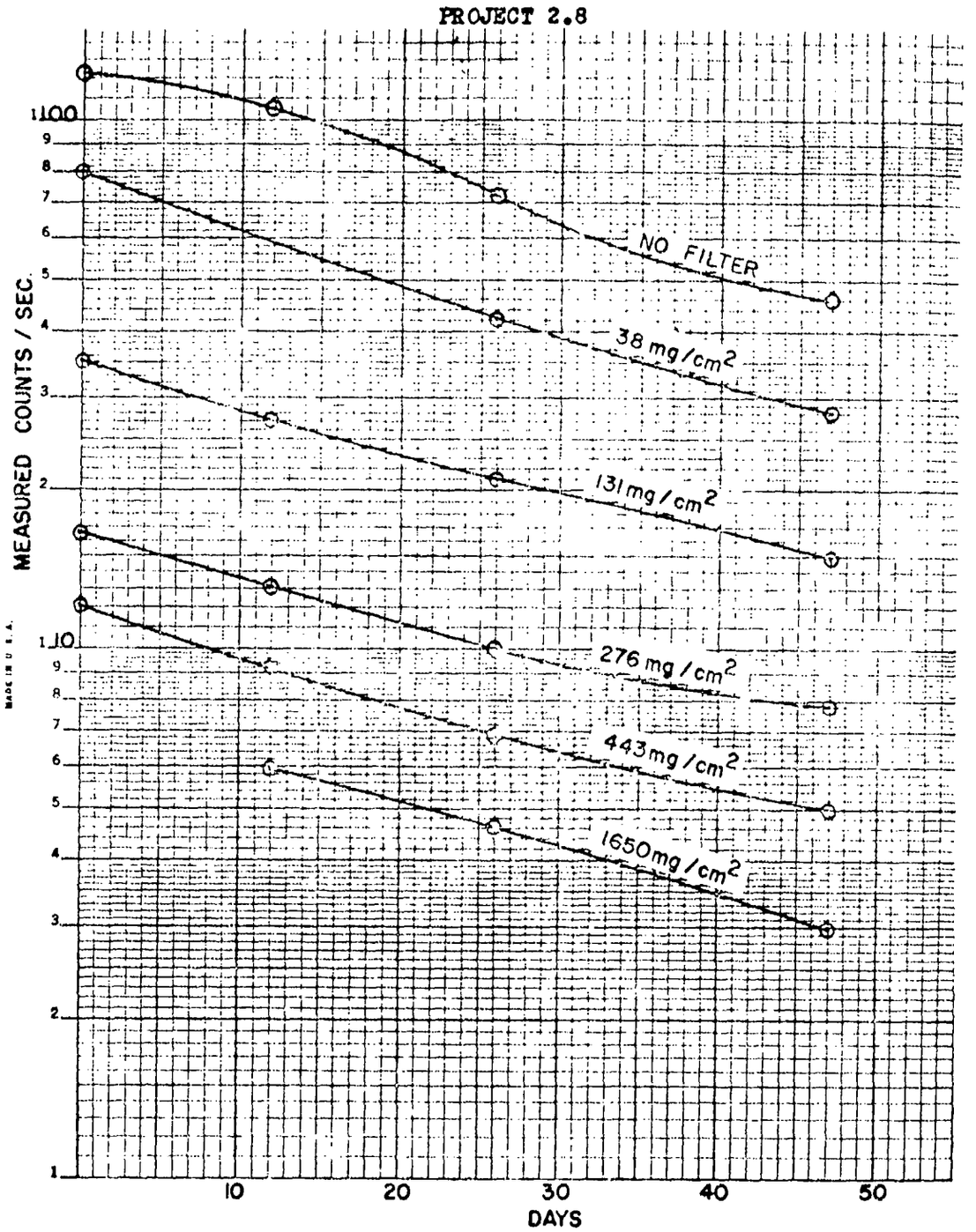

Fig. 2.2 Absorption Data on Fall-out Material from 4 Miles Northeast - Underground Shot

PROJECT 2.8

2.3.5 Uptake of Radioactivity by Plants

Fall-out material from four miles northeast was mixed with Evesboro sandy-loam soil from Prince Georges County, Maryland and with Chester loam from Montgomery County, Maryland for studies on the uptake of radioactivity by barley plants. Fall-out material was mixed with 2700 grams of soil in a pot of 6 inches diameter on 3 January 1952. The barley plants were harvested on 28 January following germination and growth in a light chamber. The plants were ashed and counted in a proportional counter on 21 February 1952. The data are shown in Table 2.14.

TABLE 2.14

Uptake of Activity by Barley Seedlings from Fall-out Material Four Miles Northeast - JANGLE Underground Shot

Soil	Grams Fall-out per Pot	Dry Weight (1) of Plants Grams	Ash Weight Grams	Disintegrations(2) per sec/gm ash
Evesboro	7.5	2.22	0.25	7750
Evesboro	0.75	2.47	0.29	1150
Chester	7.5	3.78	0.44	270
Chester	0.75	3.82	0.46	45

(1) Barley planted 3 January 1952, harvested 28 January 1952. Weight of soil 2700 grams. Pot diameter, 6 inches.

(2) Counted in Nuclear Measurements Corporation proportional counter 21 February 1952. Corrected to 1 February 1952.

The characteristics of the plant ash indicate that the activity is almost wholly due to strontium 89 with a half-life of about 50 days. Mass absorption of the plant ash is given in Table 2.15.

This table also gives some half-life measurements on the plant ash. These latter data are plotted in Figure 2.3.

PROJECT 2.8

TABLE 2.15

Plant Ash from Evesboro Soil with 0.75 gram Fall-out Material
*Mass Absorption (counted through 2.8 mg/cm^2 end window tube)

Aluminum Filter (mg/cm^2)	cps
0.0	20.95
13.0	19.10
27.5	17.55
38.3	16.13
77.8	12.13
87.3	10.92
131.	7.94
170.	5.48
219.	3.59
276.	2.04
359.	0.80

*Estimated maximum approximately 1.1-1.4 Mev.

TABLE 2.16

Half-life Measurements on Plant Ash

Days	cps
0 (2/1/52)	45.50
7	41.32
14	36.74
18	35.13
24	32.56
42	25.18

Estimated half-life 46-56 days.

PROJECT 2.8

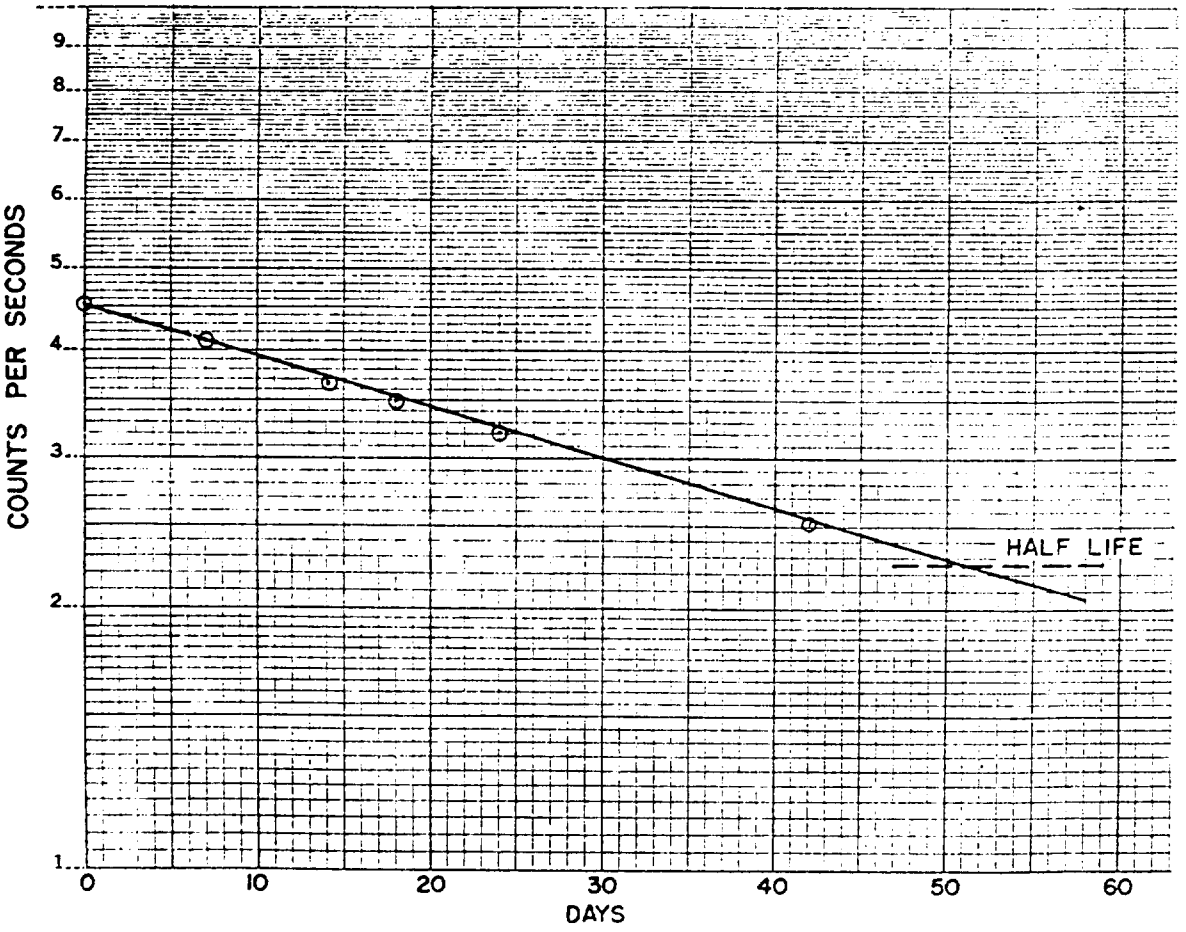

Fig. 2.3 Half-Life Measurements on Plant Ash

The activity of the ash of the plants represents a sizeable percentage of the total activity added to the soil when one considers the short duration of the experiment. The following tabulation shows the data as calculated from the activity of the ash and that of the added material.

TABLE 2.17

Uptake of Activity from Fall-out Material by Barley Seedlings

Soil and Fall-out Material Added	Percent of Activity taken up by Plants
Evesboro - 7.5 grams	0.10
Evesboro - 0.75 gram	0.17
Chester - 7.5 grams	0.006
Chester - 0.75 gram	0.01

The big difference between uptake of the activity from the two different soils indicates the dependence of uptake of strontium on the level of exchangeable calcium in the soil. The Evesboro soil is very low in this element while the Chester is a good fertile agricultural soil with relatively high calcium status. Treatment of fall-out areas with moderate to heavy applications of high calcium limestone might be an effective method of reducing plant uptake of radioactive strontium from acid soils. On calcareous soils little uptake would be expected. A great deal of research will be required to establish the effectiveness of such a treatment and the hazards due to plant uptake and subsequent ingestion of the plants by animals or people.

END

DTIC